JOHANNES GUTENBERG UNIVERSITÄT MAINZ

MAX PLANCK INSTITUTE FOR POLYMER RESEARCH

Controlled drug delivery by lignin nanocarriers for sustainable plant protection

Dissertation

zur Erlangung des akademischen Grades eines

„Doctor rerum naturalium“

des Fachbereichs Chemie, Pharmazie und Geowissenschaften (FB09)

der Johannes Gutenberg-Universität Mainz

vorgelegt von

Sebastian Johannes Beckers

geboren in Aachen

Dekan: Univ.-Prof. Dr. Tobias Reich

Erster Gutachter: PD. Dr. Frederik R. Wurm

Zweiter Gutachter: Prof. Dr. Holger Frey

Die vorliegende Arbeit wurde in der Zeit von Januar 2017 bis zum April 2020 am Max-Planck-Institut für Polymerforschung sowie dem Institut für Organische Chemie der Johannes Gutenberg-Universität Mainz unter Anleitung von PD Dr. Frederik R. Wurm im Arbeitskreis von Prof. Dr. Katharina Landfester angefertigt.

Hiermit versichere ich, die vorliegende Arbeit selbstständig und ohne Benutzung anderer als der angegebenen Hilfsmittel angefertigt zu haben. Alle Stellen, die wörtlich oder sinngemäß aus Veröffentlichungen oder anderen Quellen entnommen sind, wurden als solche eindeutig kenntlich gemacht. Diese Arbeit ist in gleicher oder ähnlicher Form noch nicht veröffentlicht und auch keiner anderen Prüfungsbehörde vorgelegt worden.

Sebastian Johannes Beckers Essen, 21.06.2020

Danksagung

Besonders danke ich **PD Dr. habil. Frederik Wurm** für die Möglichkeit in seiner Arbeitsgruppe promovieren zu dürfen. Dank zahlreicher wissenschaftlicher Diskussionen, vielen kreativen Ideen und seiner Liebe für guten Wein, blicke ich nun auf drei erfolgreiche und spannende Jahre zurück, an die ich mich in Zukunft gerne erinnern werden. Seine Unermüdlichkeit an seinen Zielen festzuhalten, war mir stets eine Inspiration.

Bei **Prof. Dr. Katharina Landfester** bedanke ich mich für die Möglichkeit meine Doktorarbeit in ihrem Arbeitskreis durchführen zu dürfen und für die anregenden Gespräche.

Ich bedanke mich auch bei unserem großartigen Team aus erfahrenen Technikern und Laboranten. Besonderer Dank gilt dabei **Sabrina Brand, Christine Rosenauer, Michael Steiert, Beate Müller, Elke Muth, Katja Klein, Gunnar Glasser, Christoph Siebert und Sandra Seywald** für die Analyse zahlreicher, komplexer Proben, Übernahme von Synthesen sowie hilfreicher Diskussionen. Bei **Stefan Schuhmacher** bedanke ich mich zudem für die professionelle Illustration meiner Ergebnisse. Für ihre Unterstützung bin ich allen sehr dankbar.

Ebenfalls möchte ich mich bei **meinen Kollegen** für zahlreiche Denkanstöße, eine produktive Arbeitsatmosphäre im Labor, den Gruppenzusammenhalt und natürlich viele lustige Mittagspausen bedanken. Insbesondere danke ich **Stefan Peil** für die erfolgreiche Zusammenarbeit während seiner Masterarbeit. Ich werde mich stets gerne an die gemeinsame Zeit am MPI-P erinnern.

Großen Dank gilt ebenfalls meinen Kollegen aus der Biologie **Dr. Jochen Fischer (IBWF)** und **Dr. Andreas Kortekamp (DLR)**, welche mir stets geduldig mit Rat und Tat bei biologischen Fragenstellungen rund um Botanik und Pilzen zur Seite standen. Unsere Zusammenarbeit im Weinberg hat mir stets viel Freude bereitet. Für gelungene und sehr ergiebige Kooperationen bedanke ich mich ebenfalls bei **Xander Staal** (Radboudumc, Niederlande) sowie bei meinen **BioRescue**-Partnern **Dr. Irantzu Alegria** (CENER, Spanien) und **Prof. Petri Ihalainen** (Metgen Oy, Finnland). Dankbar bin ich ebenfalls **Antes Weinbau Service** für die zur Verfügung gestellten Testpflanzen.

Mein größter Dank gilt jedoch **meiner Familie** die während des Studiums und der Promotion verständnisvoll und unerschütterlich an meiner Seite standen. Für ihren Rückhalt bin ich unbeschreiblich dankbar. Ihr seid die Besten!

Für meine Familie

“Irgendwann in deinem Leben wirst du merken wer wichtig ist,

wer es nie war, und wer es immer sein wird.”

Zusammenfassung

Das pflanzliche Biopolymer Lignin ist nachwachsend, biologisch abbaubar und steht der Industrie in großen Mengen als Rohstoff zur Verfügung. Trotz seines enormen Potentials als nachhaltige Ressource findet es bis heute kaum wirtschaftliche Anwendung. Insbesondere für die Landwirtschaft stellt Lignin jedoch einen attraktiven Rohstoff dar. Diese Dissertation zeigt, wie Lignin- und Lignocellulose-verwandte Verbindungen zur Formulierung von Agrochemikalien verwendet werden können. Das Ziel der Studien war die Entwicklung von Nanoträgerdispersionen, die als umweltfreundliche Wirkstoffdarreichungssysteme im Pflanzenschutz verwendet werden können. Die Herstellung der Formulierungen erfolgte unter Verwendung des Miniemulsionsansatzes.

Kapitel 1 und **2** geben dem Leser einen Überblick über die Hintergründe und die erreichten Forschungsergebnisse dieser Arbeit. Anschließend führt **Kapitel 3** in die theoretischen Grundlagen der Stabilität von Emulsionen ein und erklärt die strukturellen Merkmale des Lignins, sowie die Anwendung von Nanomaterialien im Pflanzenschutz.

Kapitel 4 beschreibt die erste kurative und protektive Behandlung der weltweit auftretenden Weinrebenstammkrankheit Esca durch Injektion einer Nanoträgerdispersion in den Rebstamm. Die Nanoformulierung wurde durch kovalente Vernetzung von methacryliertem Kraft Lignin in einer Öl-in-Wasser-(O/W-)Miniemulsion hergestellt und konnte mit dem hydrophoben Fungizid Pyraclostrobin beladen werden. Nur im Falle einer Esca-Infektion erfolgte der Abbau der Ligninmatrix durch ligninolytische Enzyme des pathogenen Esca-Pilzes und induzierte die Freisetzung des Fungizids. *In-vitro*-Experimente bestätigten die spezifische antimykotische Aktivität der Formulierung. Zudem bewies eine mehrjährige Feldstudie die kurative und protektive Wirkung der entwickelten Nanoformulierung gegen Esca.

Kapitel 5 gibt einen Einblick in die strukturellen Unterschiede verschiedener technischer Lignintypen (Kraft Lignin, Organosolv Lignin, Ligninsulfonat) und beschreibt die Funktionalisierung mit reaktiven Methacrylatgruppen durch Veresterung mittels Methacrylsäureanhydrid. Die Methacrylierung von Kraft Lignin wurde hinsichtlich Sicherheit, Kosten und Nachhaltigkeit optimiert, um eine Produktion im großtechnischen Maßstab zu ermöglichen. Je nach Löslichkeit der methacrylierten Ligninderivate wurden zwei unterschiedliche Strategien auf Basis einer O/W-Miniemulsion zur Herstellung von Ligninnanoträgern entwickelt: Das hydrophobe methacrylierte Kraft Lignin wurde in einem dispergierten Chloroformtröpfchen durch verschiedene Reaktivverbindungen vernetzt wohingegen das wasserlösliche und oberflächenaktive methacrylierte Ligninsulfonat an der Tropfengrenzfläche umgesetzt wurde.

Kapitel 6 beschreibt einen neuartigen Bioraffinerieprozess der im Rahmen des Projekts "BioRescue" entwickelt wurde. Ziel des Projektes war die Erschließung von sogenannten "Spent Mushroom Substrate" (SMS) – einem Biomasseabfall, der in Millionen Tonnen während der Pilzproduktion generiert wird – als „grüne“ Ressource zur Gewinnung von Naturstoffen wie Lignin. Das SMS wurde entweder einer thermochemischen Behandlung unterzogen, die eine kohlenhydratangereicherte Flüssigkeitsfraktion ergab, oder einer Organosolv-Extraktion, die Lignin als Hauptbestandteil enthielt. Aus den letztgenannten Extrakten gelang die Herstellung enzymatisch abbaubarer Ligninnanoträger durch Grenzflächenpolymerisation mit Toluoldiisocyanat (TDI) in einer inversen Miniemulsion. Die Kohlenhydratfraktion enthielt oberflächenaktive Phenolglykoside, die auf ihre Nutzbarkeit als biobasierte Tenside untersucht wurden.

In Kapitel 7 entwickelten wir beladene Nanoträger aus dem Polysaccharid Xylan, das neben Lignin einen Hauptbestandteil der Lignocellulose darstellt. Die Xylannanoträger wurden durch Grenzflächenvernetzung mit TDI in einer inversen Miniemulsion gewonnen und konnten mit dem Fungizid Pyraclostrobin beladen werden. Da Xylan pflanzlichen Ursprungs ist und aus preisgünstigen Biomasseabfällen wie Maiskolben gewonnen werden kann, stellt es neben Lignin einen nützlichen Rohstoff zur Herstellung nachhaltiger Formulierungen in der Landwirtschaft dar.

Kapitel 8 zeigt die Synthese bioabbaubarer Monomere mit struktureller Verwandtschaft zu den Monolignoldimeren β-O-4-Arylether und Phenylcoumaran. Im Gegensatz zu natürlichem Lignin, dessen Struktur stark von seinem pflanzlichen Ursprung sowie der genutzten Extraktionsmethode abhängt, können diese synthetischen Verbindungen strukturell wohl definiert gewonnen und so leichter zu Herstellung "Lignin-basierter" Werkstoffe genutzt werden. In diesem Kapitel wurden die Monomere in die Schale eines TDI-basierten Nanoträgers eingearbeitet wo sie als enzymatisch abbaubare "Sollbruchstellen" in der Polyurethanmatrix fungieren.

Kapitel 9 beschreibt die erste Untersuchung von Transport und Stabilität polymerer Nanoträgern in Pflanzen. Bis heute ist der Verbleib polymerer Nanomaterialen *in planta* ungeklärt, da die meisten Polymerpartikel aufgrund biologischer Größenbarrieren nach Applikation auf Wurzel oder Blattwerk nicht in die Pflanze gelangen können. Eine Nanoträgerinjektion direkt in das Leitungsgewebe wie in Kapitel 4 verwendet, ermöglicht es jedoch diese natürliche Hürde zu umgehen. Wir haben daher die Bedingungen innerhalb der Pflanze nach der Injektion durch Holzextrakte simuliert und die Wechselwirkung zwischen Holzsap und verschiedenen Polymernanopartikel basierend auf Polystyrol, Lignin oder PLGA untersucht. Anschließend wurde die Verteilung von Fluorid- oder Schwermetall-markierten

Nanoträger durch das Leitungsgewebe von Weinstecklingen verfolgt. Zur Lokalisierung dienten ^{19}F-MRI oder Elementaranalyse.

Table of Contents

1 Motivation and Outline

Efficient agriculture is essential to ensure the food supply for a rapidly growing global population. Therefore, yearly farmers spray million tons of agrochemicals to enhance plant growth and to protect the crops against insects, fungi, or bacteria. Although advanced formulations were developed over the last years, hurmful agrochemicals still threaten the ecosystem, contaminate crop and kettle and might be taken up by the consumer.[1] Additional to pesticides or fertilizers, current formulations contain numerous additives that enable an efficient distribution and performance on the field but also release plastic particles into the environment. Thus, recently, the European Chemical Agency (ECHA) restricted "the use of intentionally added microplastic particles to consumer or professional use products of any kind"[2] and initiated the search for innovative delivery systems for agrochemicals composed of sustainable materials .

The objective of this thesis was therefore to develop **eco-friendly strategies for the formulation of pesticides**, which **use bio-based and biodegradable resources**, guaranteeing safe and easy handling as well as a **targeted drug delivery to minimize the required pesticide dosage**.

In agriculture, convential liquid formulations are based either on solutions or on dispersions containing drug-loaded particles with sizes in the makro- to micrometer range.[3, 4] A more sustainable alternative offers drug delivery by nanotechnology with a release on-demand as heavily researched for biomedical applications (e.g. for the treatment of cancer). Such "nanocarrier" systems are designed to respond to external stimuli that come along with the infection and thereby trigger the release of loaded therapeutics.[5, 6] Due its biodegradability combined with a high abundancy and a plant origin, especially lignin is an ideal carrier material for drug delivery in agriculture. Therefore, most recently, our group prepared degradable nanocarriers from methacrylated Kraft lignin, which could be loaded with versatile hydrophobic drugs.[7, 8] The nanocarriers were generated by covalent crosslinking in a O/W-miniemulsion and were injected into the trunk of grapevine plants as a treatment against the fungal grapevine trunk disease Esca (Chapter 4). As we observed a significant reduction of the disease symptoms, we further optimized the lignin methacrylation regarding safety, costs, and sustainability to allow a large-scale production and to simplify the registration of the nanocarriers as an agricultural formulation (Chapter 5; part 1). The developed protocol was not only suitable for the functionalization of Kraft lignin but could be transferred to lignin sulfonate as well. As both lignin types differed strongly regarding their solubility properties though, methacrylated lignin sulfonates were not crosslinked inside the dispersed phase but at the droplet-interface yielding nanocarriers with core-shell structure that can be loaded with drugs (Chapter 5, part 2).

To encapsulate hydrophilic drugs, nanocarriers were prepared by W/O-miniemulsion. Our group already proved that degradable lignin nanocarriers can be obtained by interfacial crosslinking of commercially available lignin sulfonate with toluene diisocyanate (TDI) in an inverse system.[9] To investigate if this concept can be expanded to other biodegradable, lignocellulose-related feedstock, we prepared TDI-crosslinked nanocapsules from lignin-enriched extracts isolated from a biomass waste referred as “spent mushroom substrate” (Chapter 6) and from xylan, which occurs naturally in high percentage in hemicellulose (Chapter 7). The challenge of the latter two starting materials is their structural complexity and heterogeneity. Therefore, two potentially degradable lignin binding motifs were synthesized and incorporated as potential “breaking points” in the polyurethane shell (Chapter 8).

The produced nanodispersions might be used as sustainable drug delivery systems in agriculture. However, due to biological size barriers of roots and leaves, most polymeric nanomaterials cannot enter the plant. A trunk injection of a nanocarrier dispersion as used in chapter 4 can overcome this problem and might allow the distribution through the vascular tissue. However, for optimal performance, the interaction between nanocarrier and plant must be understood. Therefore, chapter 9 presents the first investigation regarding colloidal stability and transport of polymeric nanomaterials after injection into a plant.

2 Abstract

Lignin is a renewable, abundant and biodegradable biopolymer and therefore a potential “green” resource to produce sustainable materials.[10] In this thesis, nanocarriers were produced from lignin and lignocellulose-related materials using the miniemulsion approach. The dispersions are of high interest as eco-friendly drug delivery systems in agricultural formulations.

Chapter 4 describes the first curative and protective treatment of the worldwide occurring grapevine trunk disease Esca by trunk injection of nanocarrier dispersions. The nano-formulation was prepared by covalent crosslinking of methacrylated Kraft in an O/W-miniemulsion and could be loaded with the hydrophobic fungicide pyraclostrobin. Only in case of an Esca infection, ligninolytic enzymes, secreted by the Esca-associated fungi degraded the lignin matrix and induced the release of the fungicide. *In vitro* experiments confirmed the specific antifungal activity of the formulation. A field studied further proved that the nanoformulation can be used as protective and curative Esca treatment.

Chapter 5 gives an inside into the structural differences of several technical lignins (Kraft lignin, Organosolv lignin, lignin sulfonates) and describes the attachment of reactive methacrylate functional groups by esterification with methacrylic anhydride. The methacrylation of Kraft lignin was optimized regarding safety, costs, and sustainability to allow a large-scale production. Depending on the solubility of the methacrylated lignin derivatives, two different formulation strategies based on an O/W-miniemulsion were applied: The hydrophobic methacrylated Kraft lignin was crosslinked inside a dispersed chloroform droplet by different crosslinking agents or the highly water-soluble and surface-active methacrylated lignin sulfonate was crosslinked at the droplet interface.

Chapter 6 describes a novel bio-refinery strategy developed as one part of the “BioRescue” project to valorize “spent mushroom substrate” (SMS) – a biomass waste generated in million tons during the mushroom production. SMS was subjected either to a thermochemical treatment yielding a carbohydrate-enriched liquid fraction or to an Organosolv extraction solubilizing mainly lignin. From the latter extracts, enzymatically degradable nanocarriers were prepared by interfacial crosslinking with toluene diisocyanate (TDI) in an inverse miniemulsion. The carbohydrate fraction contained surface-active phenolic glycosides, which were investigated as bio-based surfactants.

In **Chapter 7**, xylan was utilized as shell material for nanocarriers. Xylan nanocarriers were produced by interfacial crosslinking with TDI in inverse miniemulsion. The nanocarriers were loaded with the broad-spectrum fungicide pyraclostrobin. Xylan can be obtained from

lignocellulose and might be a useful feedstock to prepare sustainable formulations in agriculture.

Chapter 8 focuses on the synthesis of the lignin substructures β-O-4-aryl ether and phenylcoumaran. Unlike, natural lignin whose structure depends strongly on plant origin and extraction method, these molecularly defined compounds allow a straightforward preparation of “lignin-based” materials with potentially controlled biodegradation profiles. As both “monomers” are microbial degradable binding motifs of lignin, they were incorporated into the shell of nanocarriers using an inverse miniemulsion approach. Here, they might act as “breaking proints” degrading only in the presence of ligninolytic fungi.

Chapter 9 presents the first investigation regarding the transport and stability of polymeric nanocarriers in plants. Up to date, the fate of polymeric nanocarriers *in planta* has not been investigated yet, as the most polymer particles cannot enter the plant when applied via roots or leaves due to biological size barriers. However, a nanocarrier injection directly into the vascular tissue as presented in chapter 4 can overcome this problem. We mimicked the *in planta* conditions after injection by wood extracts and investigated the interaction of plant-based solutes with the interface of polystyrene, lignin, and poly(lactic-*co*-glycolic acid) (PLGA) nanocarriers prepared by miniemulsion polymerization. We further tracked the distribution of fluoride- and heavy metal-labeled nanocarriers through the vascular tissue of grapevines cuttings by ^{19}F-MRI or elemental analysis of heavy-metal-labeled nanocarriers.

Graphical Abstract: **Pesticide-loaded nanocarriers for a sustainable agriculture**

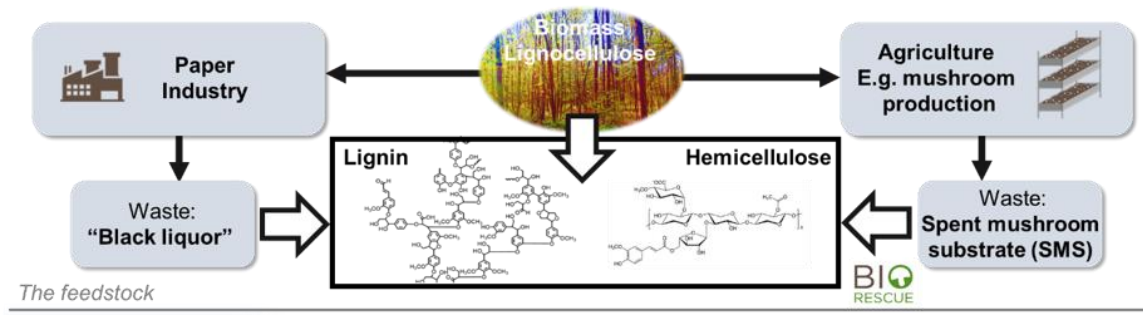

The feedstock

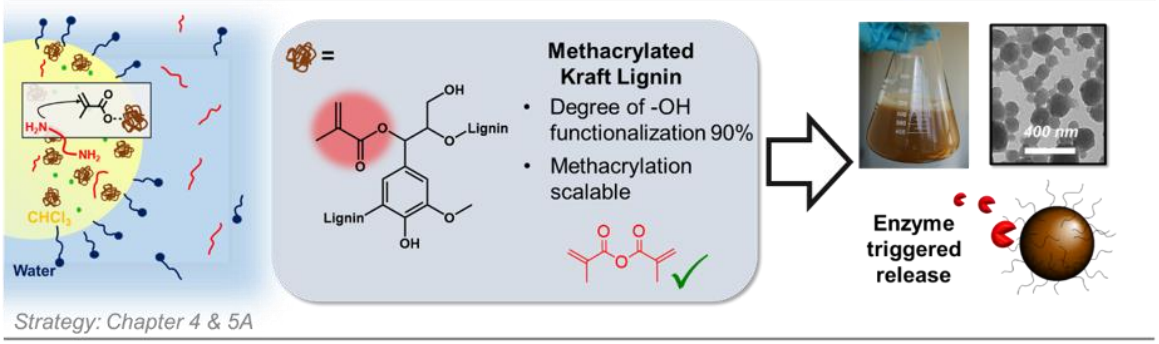

Strategy: Chapter 4 & 5A

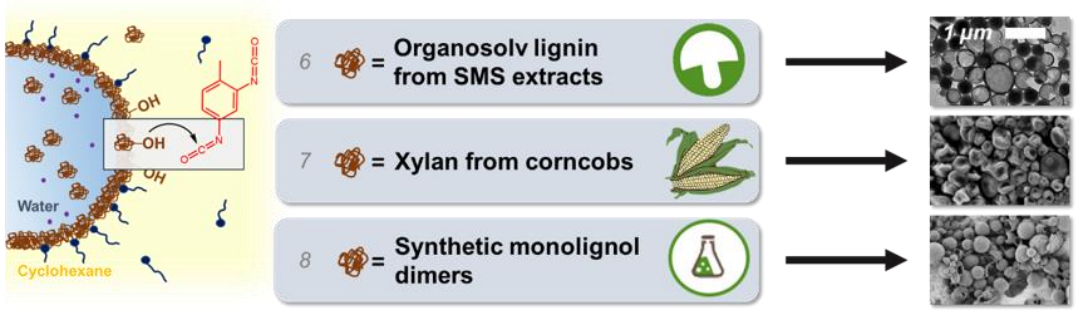

Strategy: Chapter 6,7 & 8

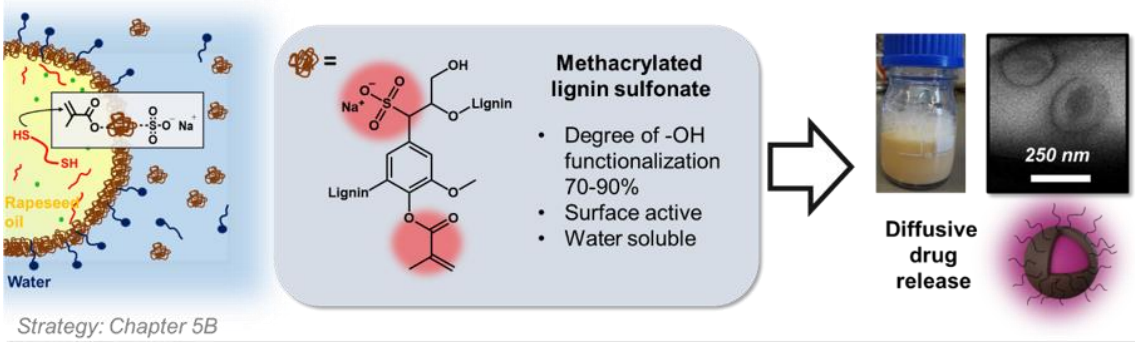

Strategy: Chapter 5B

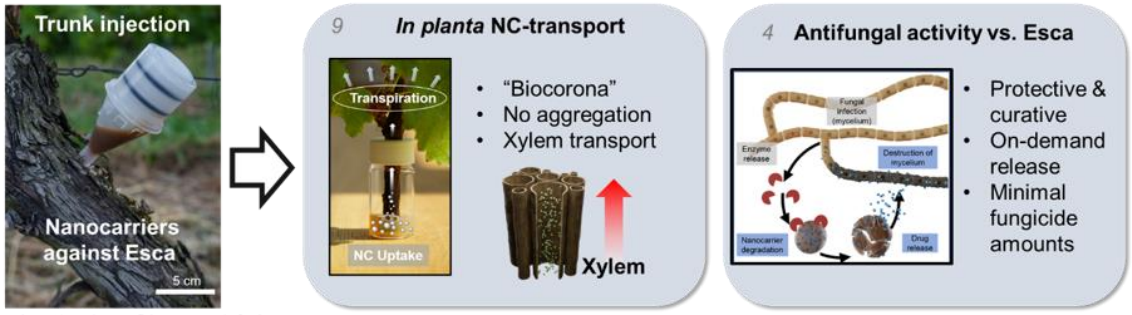

Application: Chapter 4 & 9

3 Introduction

The objective of this thesis is the development of lignin-based nanocarrier dispersions as sustainable pesticide formulations for plant protection. As the nanocarriers were prepared using the miniemulsion approach; the following chapter gives in inside in the physics of emulsions and explains their stabilization by surfactants. Afterwards, the structural properties of lignin are presented and the valorization as a “green” feedstock for chemicals and (nano-)materials is discussed. Finally, the utilization of nanotechnology in plant protection is described.

3.1 Emulsions

Emulsions are omnipresent in our daily life. Many groceries such as milk, butter, mayonnaise but also cosmetics, pharmaceuticals or cleaning agents are stable emulsions.[11, 12] These hetero-phase systems consist of two unmixable liquids, in which one is finely distributed in isolated droplets, i.e. the “dispersed phase”, whereas the other forms the so-called “continuous phase”. In the simplest case, the two phases are water and a hydrophobic oil. Depending on the ratio of both liquids, we distinguish between oil-in-water- (= O/W, direct) or water-in-oil- (W/O, inverse) emulsions. Additionally, there are more complex multiple systems such as W/O/W-double emulsions consisting of a continuous water phase, in which droplets of a W/O-emulsion are finely dispersed.[11, 13]

Most emulsions are generated by mechanical processes, which can be performed either continuously or batch-wise. In industry, especially rotor-stator systems are used, which form through shear forces stable emulsions consisting of comparably large droplets with a broad size distribution.[13] If smaller droplets with a more defined size are required, high-pressure homogenizers offer a powerful alternative. During the process, a high-pressure pump compresses a pre-emulsion in a first step. Afterwards, the generated pressure is relieved by conducting the fluid through a homogenization valve. The high shear forces generated during this process finally yield emulsions with small and finely distributed droplets. In this thesis, a homogenizer of the company ‘microfluidics’ was used. The so-called ‘Microfluidizer’ (Model: LM10) can build a pressure of up to 1546 bar and induces the droplet breakup by high shear forces generated in a Z-shaped homogenization valve.[14, 15]

Next to rotor-stator systems and high-pressure homogenizers, ultrasound can be used for emulsion preparation. The method is frequently used on the lab-scale. During sonication, a local pressure gradient is generated inside the droplet causing deformations, which can finally

lead to a breakup. Likewise, capillary waves or cavitations are discussed in the literature as mechanisms leading to droplet formation.[16]

3.1.1 Interfacial tension and surfactants

The interface is the boundary layer between two unmixable phases. The term “surface” is used if one of these phases is gaseous. Within a liquid, attractive forces interact between molecules evenly in all directions. As there is less interaction between the liquid phase and the air molecules at the surface, a force remains vertical to the interface directing inside the liquid (Figure 3.1). In consequence, molecules at the surface have higher potential energy, which is named “surface energy”. To minimize this energy, liquids form spherical droplets as they have the lowest surface to volume ratio.[11, 17]

The same happens at the interface between unmixable liquids. Considering this, energy in the form of work is needed to emulsify a hetero-phase system since molecules must be transferred from the inside of the liquid to the interface. The work *dW* required to expand the interface for an area *dA* is proportional to the interfacial tension γ:[11]

Equation 3.1 $$dW = \gamma \cdot dA$$

The interfacial tension is a system-specific constant, which can be measured for example by ring tensiometry or by the spinning drop approach. The addition of interfacially active substances like surfactants reduces the interfacial tension and simplifies the emulsification process. This is essential to prepare a stable emulsion. Therefore, the properties of surfactants are introduced in the next paragraph.[11, 17]

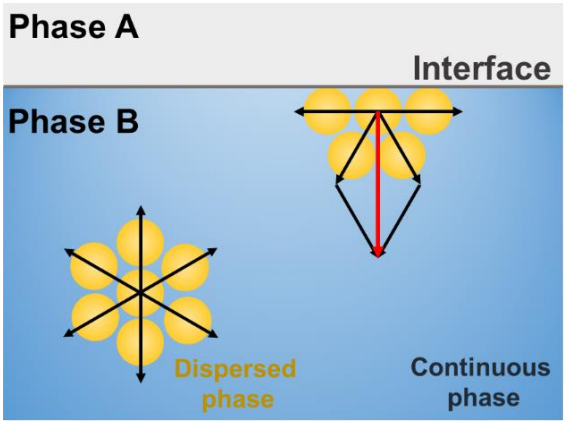

Figure 3.1: Vectoral definition of the surface tension.[17]

Surfactants have an amphiphilic molecular structure, composed of a hydrophilic head group and hydrophobic tail. Due to their amphiphilicity, the surfactant molecules arrange at the surface, which reduces the interfacial tension (Figure 3.2).[17]

At a complete surface coverage, micelles are formed and the interfacial tension remains constant when further increasing the surfactant concentration. Micelles are mostly spherical aggregates with a diameter between 5-10 nm. As their size is below the wavelength of the visual light, micellar solutions are translucent. In O/W-emulsions, the polar head group is oriented into the direction of the water, whereas the hydrophobic tail is pointing into the micelle. An inverse orientation occurs in W/O-emulsion respectively. The micelle formation is entropically driven as the self-assembly leads to a disintegration of the hydrate shell of surfactant molecules. The concentration at which micelles are formed is surfactant-specific and is called “critical micellar concentration” (CMC). The CMC can be obtained graphically from the kink when measuring the surface tension against the surfactant concentration. Next to spherical micelles, surfactants can arrange in other geometries with such as laminar or cylindrical shape. The geometry depends on the temperature as well as on the balance between hydrophilic head and hydrophobic tail.[17]

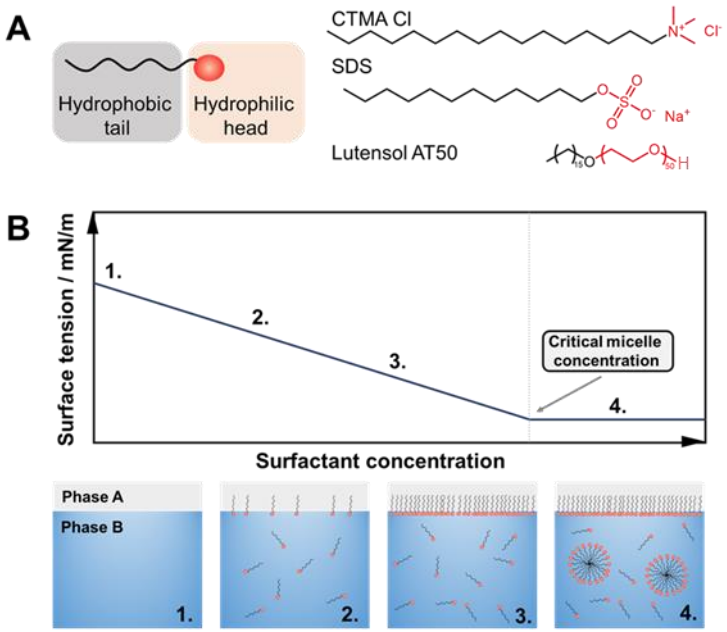

Figure 3.2: (A) Amphiphilic structure of a surfactant leading to its interfacial activity. The ionic surfactants cetyltrimethylammonium chloride (CTMA-Cl), sodium lauryl sulfate (SDS) and the non-ionic amphiphile Lutensol AT50 are given as examples. All were used to stabilize emulsions in this thesis. (B) Mechanism of micelle formation and the respective surface tension.

According to their head group, surfactants are classified in “ionic” and “non-ionic”. Ionic surfactant are either anionic, cationic or are zwitterionic:[17]

Anionic surfactants often show high stability in alkaline media but can lose their interfacial activity under acidic conditions due to the formation of the free acid. Besides the pH, electrolytes can influence the performance of the surfactant, as cations can shield the negatively charged head group. Therefore, e.g. the water hardness is an important parameter. A classic example for an anionic surfactant is sodium lauryl sulfate (SDS), which is used in various applications e.g. in personal care products.[17]

The most often used class of cationic surfactants are quaternary ammonium salts like cetyltrimethylammonium chloride (CTMA-Cl). The compound is applied for example as a cleaning agent, because of its disinfecting properties but also in hair conditioners due to its ability to adsorb on proteins.

Zwitter ions bear positive as well as negative charges and can be divided into two subclasses: Ampholytes have both acidic and basic groups and therefore act as proton acceptors or donators depending on the pH, whereas betaines have positively charged functional groups without a proton (e.g. quaternary ammonium ions) and therefore cannot act as a Brønsted acid. One example of the latter class is phosphatidylcholine, a type of phospholipid in lecithin, which is used in numerous applications in the food or cosmetic industry.[17]

In comparison to ionic surfactants, the CMC of non-ionic surfactants is lower to a power of ten, as there is no electrostatic repulsion, which must be overcome during their assembly. Simple non-ionic surfactants are mostly amphiphilic copolymers composed of an aliphatic tail and a polar head group based on polyethylene glycol (PEG). In this work, we applied mainly Lutensol AT50 as a non-ionic surfactant. The copolymer is composed of a $C_{16\text{-}18}$ alcohol that was etherified with 50 ethylene oxide monomer units.[18] Further important examples of non-ionic surfactants are polyol esters and ethers. Especially in food or personal care products, mono- and diglycerides but also polyglycerol esters like polyglycerin-polyricinoleat (PGPR) are frequently used to stabilize emulsions. Moreover, alkylpolyglycosides are applied as a bio-based surfactant in many formulations of the cosmetic or in the cleaning agent industry.[17]

3.1.2 Stability of emulsions

The preparation of stable emulsions requires the utilization of surfactants, which lower the surface tension and stabilize the dispersed droplets either by electrostatic or by steric repulsion.[11, 17, 19] The system is called colloidally stable if the droplet size distribution is constant

over time and location. Except for microemulsions, emulsions are thermodynamic unstable or metastable and therefore constantly driven to achieve an energetic minimum by minimization of the interface. Mechanisms that increase the droplet size and thereby reduce the surface energy are aggregation, Ostwald-ripening, or coalescence (Figure 3.3). Aggregation is the assembly of droplets due to attractive interactions, whereas coalescence describes the irreversible fusion of two or more colloids to a bigger one. The growth of large droplets by a diffusive molecule stream from smaller droplets is called Ostwald-ripening. Driving force is the difference in the Laplace pressure. Next to the size of the colloids, the spatial distribution of the droplets can change unstable emulsions by sedimentation and creaming. Both effects result from density differences between dispersed and continuous phase. In the case of creaming, the droplets rise to the surface, whereas sedimenting colloids sink inside the emulsion.[11, 13, 20, 21]

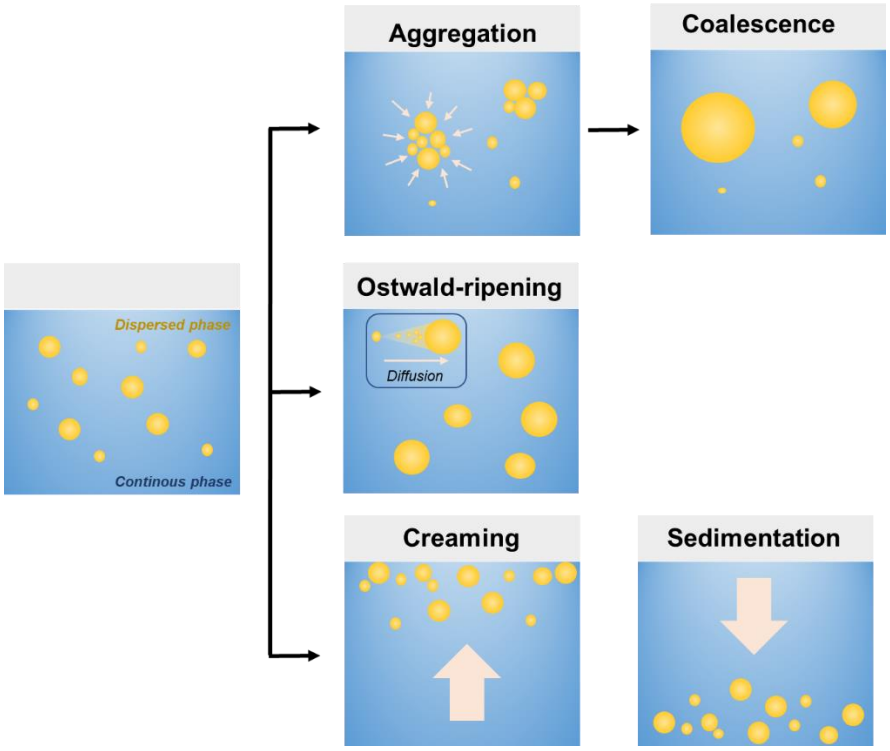

Figure 3.3: Scheme of a stable emulsion (left) and mechanisms in instable emulsions which change the droplet size distribution over time and location (right).

In O/W-emulsions, ionic surfactants can stabilize dispersed droplets or particles by electrostatic repulsion. The hydrophobic tail is oriented to the inner of the droplet whereas the ionic head groups are directed into the water and result in a charged surface. For charge equalization, counter ions assemble around the interface and form an electrostatic double-

layer. To describe the electrostatic potential different models were developed: E.g. the Helmholtz model, the diffusive and the Stern double layer model. The electrostatic potential cannot be determined experimentally though. Therefore, an electrokinetic potential, called ζ-potential, is measured by the mobility of charged colloids in an electric field instead.[17, 19, 22]

The repulsive interactions between two electrostatic double layers hinder the approach of the colloids and stabilize the emulsion. To understand the interplay between two charged colloids Derjaguin, Landau, Vervey, and Overbeek developed the DLVO-theory in the middle of the 20th century. The theory combines the attractive Van-der-Waals interactions with the repulsive electrostatic interactions and the hard-sphere repulsion potential (Born repulsion) to the total interaction energy V. The respective interaction energies depend on the distance d between two particles and the resulting sum function V is shown in Figure 3.4. A positive value for the total interaction energy V means dominating repulsive forces whereas a negative value indicates attractive interaction between the two colloids.[19, 22]

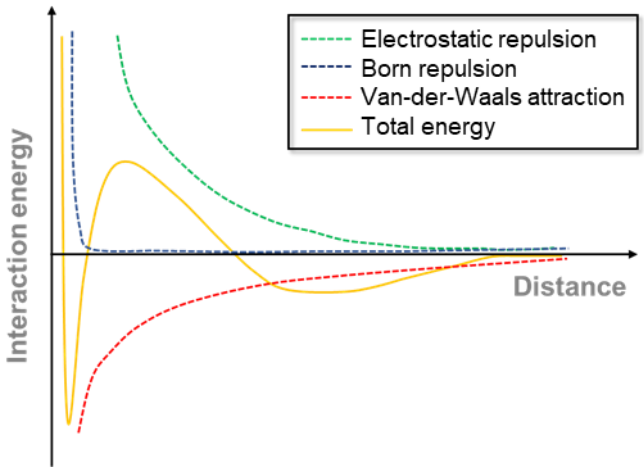

Figure 3.4: Schematic course of the total interaction energy function, which is a sum of respective functions of the electrostatic repulsion and the Van-der-Waals attraction.[22]

At an infinite distance d, there is no particle interaction. While approaching, weak attractive interactions cause a first shallow energy minimum. Particles reaching this minimum agglomerate reversibly in a process referred to flocculation but can be separated by shear forces (e.g. stirring, shaking) or sonication. When further reducing the distance d, the overlapping of the two electrostatic double layers results in a strong repulsion shown by a local maximum. The height of this energetic barrier affects significantly the colloidal stability and is determined by the surfactant and the electrolyte concentration. In case of further approaching due to an insufficient electrostatic repulsion the particles aggregate and form coagulates. Unlike flocculation, coagulation is an irreversible process, since the particles interact strongly

by attractive Van-der-Waals forces as shown by the second energy minimum. At small distances (d<0) Born repulsion hinders the particles from overlapping.[19, 22]

The stabilization with non-ionic surfactants is not based on electrostatic but on steric interactions. For example, when stabilizing an O/W-emulsion with an amphiphilic block-copolymer like Lutensol AT50, the aliphatic tail is oriented to the inner of the oil droplet whereas the polar PEG block is directed to the water forming a protective barrier. For an effective stabilization, the hydrophilic part of the surfactant must be sufficiently soluble in the dispersion agent to guarantee maximum chain expansion and to avoid coil formation. If two sterically stabilized colloids approach, the surfactant layers may overlap, and the degree of freedom of the polymer segments would be reduced. The colloids react with repulsion to counteract the loss of entropy that would increase the energy of the system. Next to the loss of entropy, the stabilization of non-ionic surfactants results from increased osmotic pressure as water is pressed out the overlapping surfactant layers by the denser polymer chains. To equalize the pressure difference, solvent molecules flow in between the colloids and push the particles apart.[22]

3.1.3 Macro-, micro- and miniemulsions

Emulsions can be classified according to the droplet size and preparation method into macro-, micro- and miniemulsions. As this thesis focuses on the miniemulsion approach, macro- and microemulsions are introduced only briefly:[23]

Macroemulsions are prepared by stirring or shaking and have droplets with diameters > 500 nm. As they are thermodynamically unstable, they tend to phase separate and typically, a surfactant concentration at or just above the critical micelle concentration (CMC) is used for stabilization. Macroemulsions are used in versatile applications from cosmetics, over agricultural formulations to pharmaceuticals.[12, 24]

Microemulsions are thermodynamically stable, as the interfacial tension is reduced to almost zero by applying a combination of a co-surfactant and surfactant. Due to the small interfacial tension, microemulsion can form spontaneously without any energy input and contain droplets between 5-50 nm. In contrast to a macroemulsion, the surfactant is used in extremely high concentrations far above the CMC, which allows a diffusive molecule exchange e.g. over micelles between oil droplets. Co-surfactants are often aliphatic alcohols such as *n*-pentanol, which assemble extremely fast at the interface and which stabilize the internal phase of the droplet formation. Due to their comparably smaller molecular weight, they are less tightly bound to the droplet interface and therefore offer only short-term stabilization.[12, 24]

Miniemulsions are composed of finely dispersed droplets in a size range between 50-500 nm, which can be generated by ultasonication or by high shear forces using a homogenizer (Figure 3.5). Compared to the previously described microemulsions, significantly less surfactant is used though. As the surfactant concentration is typically below the CMC after homogenization, the continuous phase contains no micelles and the droplet surface is only partially covered with surfactant molecules. Thus, as steric stabilization requires a high surfactant density on the droplet surface, electrostatically stabilized O/W-emulsions contain smaller droplets in comparison to systems containing non-ionic surfactants.[23, 25, 26]

Next to the surfactant in the continuous phase, O/W-miniemulsions are stabilized by an ultrahydrophob, which is dissolved in the dispersed oil droplet. The ultrahydrophob has an extremely low water solubility and creates an osmotic pressure, which counteracts the Laplace pressure and thereby prevents Oswald-ripening. Therefore, ultrahydrophobes are referred also as osmotic pressure agents. For example, hexadecane or perflourinated species are frequently used ultrahydrophobes. Due to the combination of surfactant and osmotic agent, miniemulsions are kinetically stable but thermodynamically metastable. The colloidal stability of the system is strongly influenced by the ratio between the continuous and dispersed phase, the density of the oil and the oil solubility in the dispersion agent.[23] The miniemulsion concept is not limited to O/W-emulsions but can also be applied for inverse systems. In this work, mostly cyclohexane was used as the continuous phase in combination with water or dimethyl sulfoxide (DMSO) as the dispersed phase. For an inverse miniemulsion, non-ionic surfactants like the block copolymer poly(ethylene-*co*-butylene)-*b*-poly(ethylenoxide) (P(E/B-*b*-EO) give sufficient stabilization. To prevent Ostwald-ripening, instead of an ultrahydrophobe highly lipophobic compounds like sodium chloride or carbohydrates are used.[25] The unique feature of the miniemulsion process is to generate small, homogenous and stable droplets at comparably low surfactant concentration. The combination of surfactant and osmotic pressure agent prevents coalescence and diffusive molecule exchange between the oil droplets so that each droplet acts as an individual entity or “nanoreactor”.[24, 26] This integrity of each droplet distinguishes the miniemulsion significantly from the classic emulsion polymerization. A further advantage is a high versatility of monomers and polymerization techniques. Thus, the miniemulsion is an ideal method for the preparation of nanomaterials with defined size and composition.[24] In this thesis, the miniemulsion approach was used to generate drug-loaded lignin nanocarriers. The biopolymer was crosslinked covalently either in a direct or inverse miniemulsions to yield stable dispersions which might be useful as pesticide formulation. For this reason, the next chapters present the properties of the biopolymer class lignin and discuss the application of nanomaterials in plant protection.

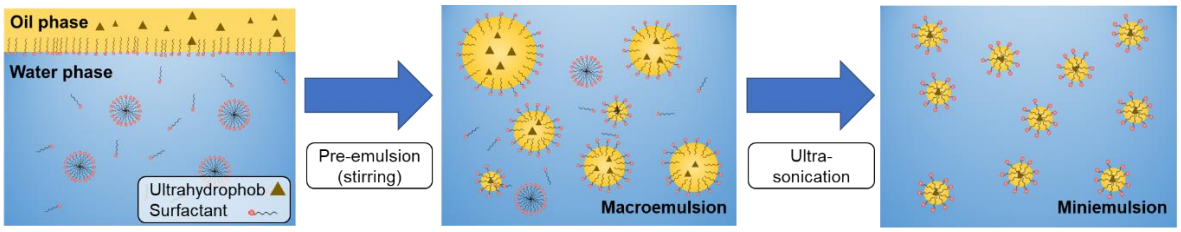

Figure 3.5: Schematic illustration of the miniemulsion preparation. In a first step, the initial two-phase mixture is stirred to get a “pre-emulsion” (macroemulsion). Subsequently, the mixture is treated e.g. by ultrasonication to yield a miniemulsion.

3.2 Lignin - A versatile class of phenolic biopolymers

Lignin forms together with hemicellulose and pectin an interpenetrating matrix that embeds the cellulose nanofibrils in the secondary cell wall of vascular plants. This complex composite material is essential for strength and structure and is referred to as lignocellulose (Figure 3.6).[27, 28] With a dry mass percentage of 15-30%, lignin is a group of phenolic biopolymers that occur in high quantity especially in the vascular tissue of wood and bark. Next to compressive strength, lignin has a protective function and increases the hydrophobicity of the vascular bundles to enable the water transport.[29] As ca. $2 \cdot 10^{10}$ tons of lignin are formed yearly, the macromolecule is next to cellulose and chitin one of the most abundant organic compounds on the planet and constitutes its biopolymer class. Unique is, in particular, the heterogeneous aromatic structure, leading to the characteristic brown color and exceptional chemical properties.[28]

The term “lignin” is derived from the Latin word “lignum”, which means wood. Numerous studies investigated the separation of the lignocellulose components mainly motivated to yield pure cellulose pulp to produce paper or fabrics. Lignin itself was considered as a low-value and undefined by-product.[27] To optimize the pulping process, scientists investigated lignins structure in detail over the last years using various methods: At the beginning of the 20th century, Klason was the first who postulated that lignin is a macromolecular polyether based on coniferyl alcohol. From then on, the structural analyses succeeded stepwise supported by the development of advanced analytical methods such as UV/Vis-, infrared (IR) or nuclear magnetic resonance (NMR) spectroscopy as well as mass spectrometry (MS). In 1977, Adler suggested the most complete structural model of lignin, which is widely accepted today.[30] Nevertheless, a universal structure cannot be postulated, as lignin’s structure strongly depends on the plant origin and the extraction method. Nowadays, especially ^{31}P NMR and two-dimensional NMR spectroscopy like ^{1}H-^{13}C correlated HSQC is used frequently as they enable a fast and relatively detailed structural analysis of lignin-containing biomass.[27, 31]

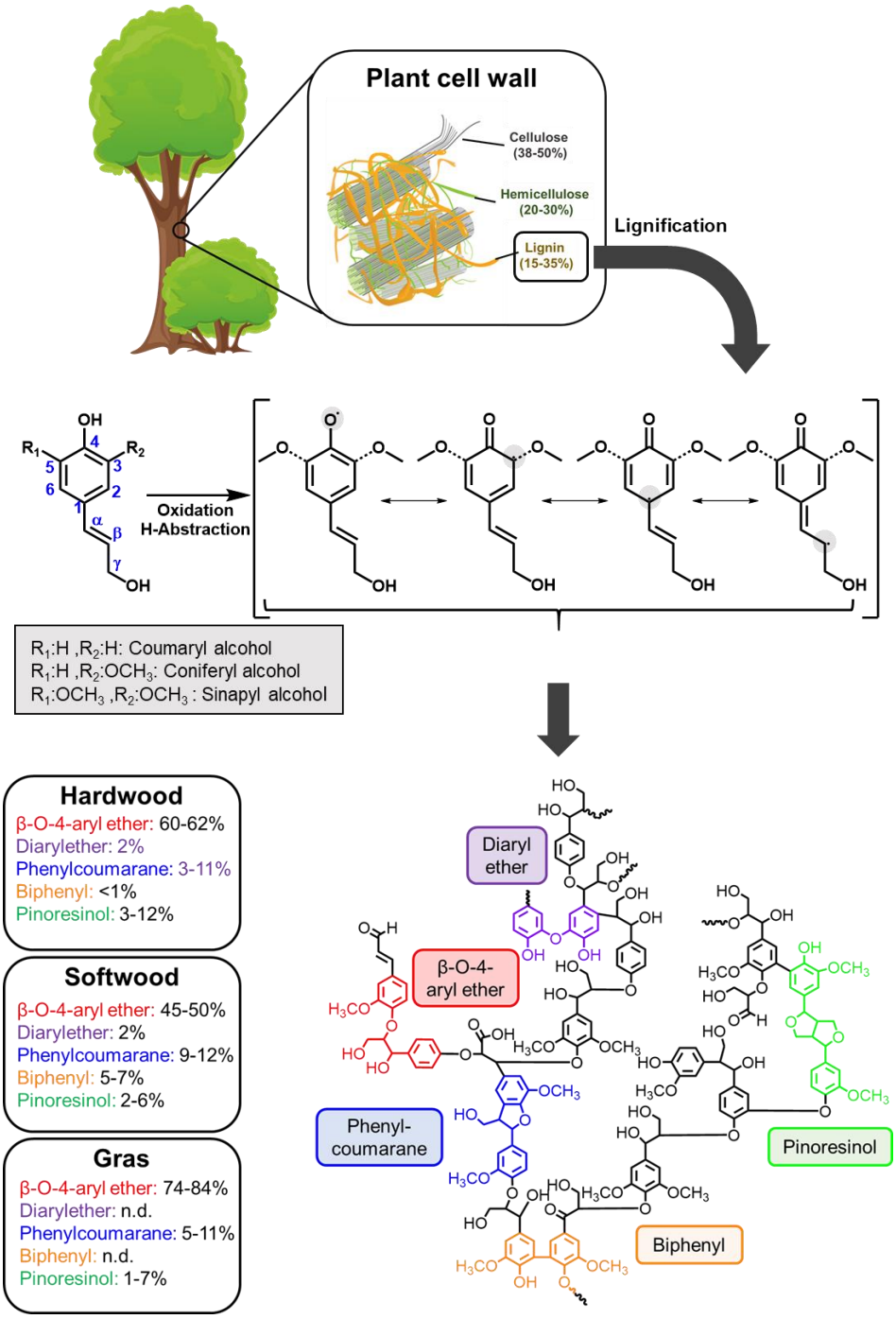

Figure 3.6: Lignin occurs next to cellulose and hemicellulose in the cell wall of vascular plants. During the lignification, the monolignols are crosslinked through a radical process under formation of numerous binding motifs. The lignin structure is plant depended. (The lignocellulose scheme was reprinted from Trends in Biotechnology, Nov, 28(11), Vanholme R, Van Acker R, Boerjan W., Potential of Arabidopsis systems biology to advance the biofuel field, 543-7., Copyright (2010) with permission from Elsevier)

In contrast to other biopolymers like carbohydrates or proteins, lignin is highly aromatic and is composed of numerous monomers (Figure 3.6), which are randomly crosslinked over a variety of binding motifs without stereoregularity.[28] The heteropolymer consists mainly of the three phenyl propanoids coumaryl, coniferyl and sinapyl alcohol, which form the so-called H-, G-, and S-substructures after polymerization. Next to these, studies proved the incorporation

of acylated and acetylated monolignols as well as of *p*-hydroxybenzoate and *p*-coumarate, which further broadens the variety of possible binding options. All building blocks are derivatives of cinnamon acid, which is generated over numerous enzymatic steps from phenylalanine or tyrosin during the phenyl propanoid biosynthesis.[27]

To transport the hydrophobic monolignols after the biosynthesis to the cell wall, most likely, carbohydrates are attached to the phenolic hydroxyl group via β-glycosidic bonds to increase their water solubility.[32] In the cell wall, laccases and peroxidases initiate the lignification by the generation of phenolic radicals by the consumption of oxygen or hydrogen peroxide, respectively. Due to the delocalization of the radicals, lignin polymerizes forming numerous structural motifs. With a percentage of 50-80%, the most common linkage is the ß-O-4 aryl ether. Next to this linkage, phenylcoumaran, resinol or the biphenyl moiety are common substructures (Figure 3.6).[27, 28]

3.2.1 Technical lignin

The monomer ratio, as well as the percentage of each binding motif, is plant-specific. Therefore, lignin's chemical properties depend on the feedstock, which is used for its extraction. Next to pure wood, complex biomass mixtures obtained e.g. as waste from forestry or agriculture are used in biorefineries as lignin resources. One example is "spent mushroom substrate" generated during the mushroom production (cf. Chapter 6). In general, technical lignin is not classified by its plant origin but by its isolation method: several procedures have been developed, which allow the separation from hemicellulose and cellulose but result also in the chemical medication of the obtained lignin. This structural modification determines significantly the material properties, such as solubility or molecular weight. In general, the lignin isolation procedures can be divided into "extracting" and "leaving" methods (Figure 3.7):[33] During the extracting procedures, lignin is solubilized and then separated from the insoluble carbohydrate residue. The by far most important lignin of this category is Kraft lignin, which is obtained in a million-ton scale by treating wood pulp with sodium hydroxide and sodium sulfide during the paper production. Performing the extraction with salts of sulfuric acid instead, water-soluble lignin sulfonates are generated, which can be used for example as surfactants. Additionally, various Organosolv processes have been developed yielding sulfur-free lignin that dissolves in a broad range of organic solvents (further information is given in Chapter 5).[27, 33, 34]

In leaving processes, cellulose and hemicellulose are dissolved either by hydrolysis with acids or by an enzyme pretreatment (e.g. with cellulases), which enables the separation

from the hydrolysis-stable lignin. One example is the so-called Klason lignin, which is obtained after treating wood chips with sulfuric acid.[33]

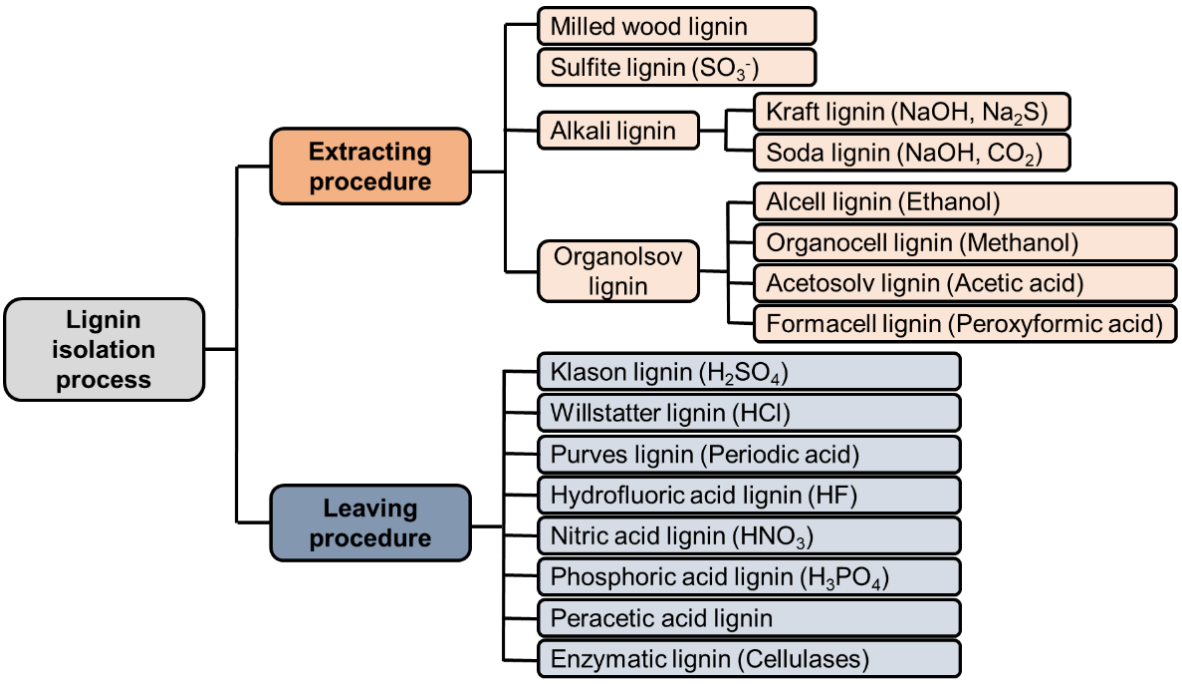

Figure 3.7: Categorization of lignin isolation processes.[33]

3.2.2 Degradability of lignin

Due to its degradability, lignin received increasing attention in academia and industry as a sustainable resource to produce “green” chemicals and materials.[35] In nature, fungi and bacteria degrade lignin by several types of oxidative enzymes leaving a cellulose-enriched, whitish material behind. The degradation of lignocellulosic biomass has been extensively investigated for basidiomycetes, like the white-rot fungi *Phanerochaete chrysosporium*. These fungi produce a mixture of extracellular enzymes including peroxidases (lignin peroxidases (LiP), manganese peroxidases (MnP), versatile peroxidases) and laccases which efficiently break down lignin.[36] LiP and MnP are based on glycoproteins with a central cavity containing a heme group that is stabilized by four nitrogen-containing chelating ligands. Under the consumption of hydrogen peroxide, both enzymes can oxidize phenolic and aliphatic lignin substructures, due to their high redox potential (Figure 3.8). Unlike peroxidases, laccases are copper-based and have a comparably lower redox potential. Therefore, they can degrade phenolic binding motifs by reduction of oxygen to water but require mediators to degrade non-phenolic lignin units (Figure 3.8).[37, 38] These mediators are usually small organic compounds that are continuously oxidized by the laccase and act as electron carriers between the bulky

enzyme and the sterically demanding substrate. In nature, several degradation products such as acetosyringone, syringaldehyde, *p*-coumaric acid, vanillin or acetovanillin can function to mediate the lignin breakdown. However, numerous studies proved that also synthetic compounds like 2,2,6,6-Tetramethylpiperidinyloxyl (TEMPO), 2,2′-azino-di(3-ethylbenzthiazolin-6-sulfonic acid) (ABTS) and 1-hydroxybenzotriazol (HOBt) can be used to promote the degradation of non-phenolic lignin substructures.[38] As laccases can oxidize a broad range of substrates under consumption of exclusively atmospheric oxygen and releasing water as the only by-product, they are rendered as promising candidates for diverse biotechnological applications. For example, laccases are applied as a bleaching agent in pulp delignification and textile dyes or for the detoxification of wastewater.[39]

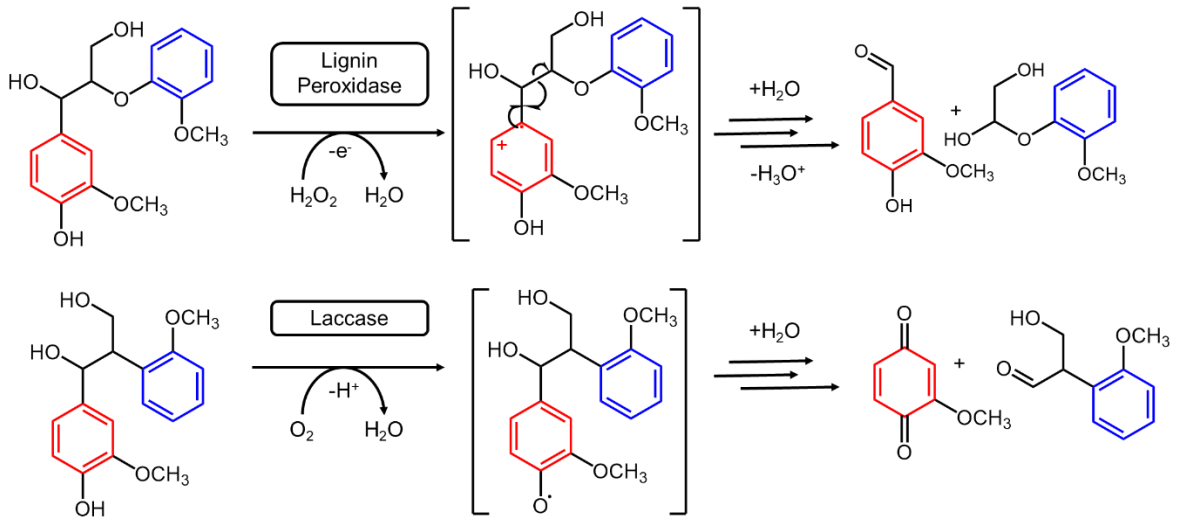

Figure 3.8: Postulated mechanisms for the enzymatic degradation of two lignin binding motifs ß-O-4 aryl ether by lignin peroxidases or laccases.[40-42]

3.2.3 Applications of lignin

Although lignin is a biodegradable, renewable and an abundant feedstock, its exploitation is still relatively limited due to its structural heterogeneity depending strongly on plant and extractions process.[27, 29] Right now, the by far largest lignin amounts are produced as a by-product of the paper production and are used energetically by burning to generate electricity. Only 2% of the potentially available lignin (1,000,000 t/a of lignin sulfonate and 100.000 t/a of Kraft lignin) is commercialized.[43]

Over the last years, numerous strategies to valorize lignin were developed, which can be summarized in three main categories:

A) *Application without further processing*: To date, mainly lignin sulfonates are used without further modification as binders such as in animal feed, coal briquettes or wood-related materials like plywood or particleboards as they are non-hazardous and relatively cheap. Moreover, their amphiphilicity makes them useful surfactants stabilizing dispersions for example in ceramics, in pesticide formulations or concrete and asphalt mixtures.[33, 43]

B) *Integration in polymer matrices*: Several studies report the preparation of lignin-copolymers, in which it is used as a cheap and renewable macro-monomer. Promising is especially the utilization of lignin as a bio-based phenol-replacement in phenol-formaldehyde resins. Copolymers with a lignin percentage of up to 50 wt% were successfully used e.g. as adhesives in plywood.[35] Prior polymerization, the number of lignin's phenolic hydroxyl groups must be increased by phenolization or demethylation though, to introduce more reaction sites towards formaldehyde. A similar approach is reported for the preparation of lignin-based epoxy resins. Herein, lignin is treated with sulfuric acid and phenol to increase the number of phenolate groups and is copolymerized as a crosslinking agent with bisphenol-A and epichlorohydrin subsequently. Likewise, lignin is applied together with cellulose to produce the bioplastic Arboform. The material has wood-like properties and appearance but can be molded like a thermoplastic in the heat and is therefore called "liquid wood".[35, 43] Moreover, numerous lignin-polymer blends were described in the literature in which lignin acts as biodegradable filler or as reinforcement agent and radical scavenger. However, lignin's incompatibility with many polymers even in the presence of compatibilizers often results in phase separation or particle aggregations within the polymer matrix leading to a composite material with weak tensile strength and low elongation at break.[35] To increase the compatibility, various strategies for lignin functionalization were developed. The modifications include the decoration of lignin's hydroxyl groups by etherifications and esterification e.g. by halogenated alkanes, epoxides or anhydrides as well as the introduction of new functional units like amines or nitro groups. Besides, lignin could be grafted with a broad range of polymers like polyacrylamide, polyacrylic acid and polymethylmethacrylate.[35]

C) *Depolymerization for bio-based chemicals and fuel*: Due to the depletion of mineral oil, renewable resources are required to produce fuels and chemicals. Therefore, the fragmentation of lignin by catalytic depolymerization to yield aromatic, low molar mass chemicals, like BTX hydrocarbons, is heavily researched currently.[29] The numerous techniques developed include the depolymerization by oxidation, reduction, base/acid-catalysis as well as solvolytic and thermal approaches. Nevertheless, due to the complexity, heterogeneity, and recalcitrance of lignocellulosic biomass, the exploitation of lignin is still very limited. The only exception right now is the flavoring agent vanillin, which is generated solely

by the Norwegian company Borregaard on a scale of 20.000 t/a by copper-catalyzed oxidation of lignin sulfonates. In total, lignin-based vanillin has 10% of the global vanillin market.[43, 44]

3.2.4 Nano-/microparticles from lignin

Nanomaterials have manifold applications as they offer unique properties, which differ from larger-dimensional materials of the same composition. Beisl *et al*. summarized recently the existing literature dealing with the fabrication of lignin nano- and microparticles.[45] One of the most common preparation methods is the precipitation of lignin from an organic solvent by addition of a nonsolvent like water (or *vice versa*).[45] Alternatively, the precipitation can be induced by decreasing lignin's solubility by solvent exchange via dialysis.[46] The generation of particles by pH-induced precipitation is related to this approach. Here, alkali-soluble lignin is precipitated by shifting the pH into the acidic range.[47] Both techniques yield stable dispersions with either full or core-shell structured nanoparticles with diameters between 50 nm and 3 µm.[45] A different strategy is the production of lignin nanoparticles from aerosols. The process includes an atomizer forming an aerosol out of a lignin precursor solution, which is passed then through a heating tube to evaporate the solvent. Afterwards, dry particles with diameters between the 30 nm and several micrometers can be collected with a carrier gas. The technique can be performed continuously, requires only low-cost equipment and produces no liquid by-products and is therefore considered as a promising method to produce lignin nanoparticles with defined size distribution.[45, 48]

In this thesis, covalently crosslinked lignin nanomaterials were prepared in emulsions. The approach was used for the first time by our group for the crosslinking of lignin sulfonate with toluene diisocyanate (TDI) at the droplet interface of an inverse miniemulsion to yield biodegradable lignin-polyurethane/polyurea nanocontainers, which could be loaded with the hydrophilic model compound sulforhodamine.[9] In a comparable approach, Chen *et al*. generated pH-responsive nanoparticles with a diameter between 100 and 400 nm by interfacial crosslinking of allylated lignin sulfonates via thiol-ene-click reaction.[49] In further studies, we showed that lignin nanocarriers for hydrophobic drugs can be obtained by polyaddition with diamines or by radical polymerization of methacrylated Kraft lignin in direct miniemulsions.[7, 8] Based on these initial results, this thesis further exploited the crosslinked lignin nanocarriers as a versatile platform for sustainable agriculture as outlined in the experimental chapters.

3.3 Nanotechnology for plant protection

While over the last years, nanotechnology made enormous progress in therapeutic applications in medicine, the development of nanomaterials for agriculture such as the delivery

of pesticides or fertilizer is still in its infancy.[50] For protection against plant pathogens, most studies used inorganic materials such as metallic nanoparticles (e.g Cu, Ag, Au particles, ca. 1-50 nm) or metal-based materials (e.g. CdSi/ZnS quantum dots, 1-10 nm; CuO, 20-30 nm; Fe_3O_4, <100 nm; TiO_2, > 5 nm) as nanopesticides.[6, 50, 51] The particles act strongly antimicrobial and can hinder the growth of numerous bacteria or fungi.[52] In comparison to a macroscopic structured reference of the same material, the nanomaterials often showed a stronger effect due to their higher surface-to-volume ratio.[53, 54]

A different concept is the utilization of nanomaterials as a carrier agent for pesticides or fertilizers. In this case, the nanomaterial is inert and acts as a protective container, enabling safe handling or improving dispersability and leaf adsorption.[3] To protect the environment, especially degradable polymers such as polylactic acid (PLA) or the copolymer poly(lactic-*co*-glycolic acid) (PLGA) are used in agricultural formulations.[3] Recently, for example, Tong *et al*. reported that the micellar formulation of amphiphilic mPEG-*b*-PLGA nanoparticles (diameter ca. 100 nm) allowed to disperse the hydrophobic herbicide metolachlor, which improved the root uptake in *oryza sativa* and *digitaria sanguinalis*.[55]

In general biopolymers were used more often to formulate pesticides in comparison to synthetic materials, as many of them combine biocompatibility with a relatively low price and high abundancy.[3] In particular, natural polysaccharides such alginate, starch, cyclodextrins, cellulose or chitosan were reported in several papers as carrier materials.[56] Especially chitosan is an ideal feedstock for agricultural applications, as the biopolymer is produced from the abundant and bio-based resource chitin that occurs naturally in the shell of sea crustaceans by deacetylation.[57] Chitosan nanoparticles have been generated by various techniques e.g. via crosslinking in emulsion, self-assembly, precipitation or by membrane extrusion.[58] For example, Liang *et al.* encapsulated the nematodicide avermectin in chitosan/poly-*γ*-glutamic acid nanocarriers produced by polyelectrolyte self-assembly. The formulation could increase the pesticide efficiency from 70% to almost 100%.[59] Using a similar preparation strategy, chitosan was used in combination with sodium alginate to encapsulate the insecticide acetamiprid.[60] The latter biopolymer is extracted from brown seaweeds and proved already in several tests to be a promising carrier agent for agrochemicals.[56] Useful is especially its ability to form hydrogels with divalent cations like Ca^{2+}, which could be applied to prepare for example alginate microspheres loaded with hormone ecdysone or the herbicide isoproturon.[57, 61, 62] Next to chitosan and alginate, cyclodextrines, cyclic oligosaccherides synthesized enzymatically by bacteria from starch, gained increasing interest as potential drug delivery vehicles over the last years. Cyclodextrines have a hydrophobic cavity and a hydrophilic exterior that allows them to carry water-insoluble compounds like hydrophobic pesticides in host-guest complexes being simultaneously solubilized in aqueous medium.[56, 57, 63] Next to polysaccharides, silica-based

materials are considered as potential candidates to control a range of agricultural pests.[64] Interesting are in particular porous and mesoporous formulations which allowed the controlled release of different agrochemicals like pyoluteorin[65], avermectin[66] or pyraclostrobin[67].

A very promising carrier agent is also lignin, as it is abundant, relatively cheap, bio-based and degrades enzymatically by specific fungi.[28] Additionally, lignin is antimicrobial and has antioxidative properties, which protects the encapsulated cargo against UV-degradation. Most recently, Sipponen and colleagues summarized the existing literature reporting nano- and microscaled lignin carrier systems loaded with several pharmaceuticals, pesticides (insecticide, herbicides, microbicides) and model drugs.[68] The formulations are either prepared by entrapment (e.g. while precipitation), encapsulation or surface adsorption. The generated formulation usually releases the drug subsequently via diffusion, desorption or by degradation of the nanoparticle matrix.[68] Examples are given in the previous chapter 3.2.4.

3.3.1 *In planta* uptake and transport

Nanomaterials can be delivered either by the roots or by the vegetative parts of the plant such as leaves, shoots or trunk. Uptake and transport of metal nanoparticles, used for example as nanofertilizers, after foliar or root application, were described in some previous studies.[69] However, most investigations are only descriptive and the biological mechanisms as well as the interaction between plant and nanomaterial cannot be explained yet. The next paragraph summarizes the natural barriers for a nanocarrier which must be overcome to enter vascular plants (illustrated in Figure 3.9). As most cultivated plants used for food production are angiosperms (flowering plants), the here explained morphological and physiological features focuses on this type:

1. The plant surface as a first barrier

Leaves: All leaves have an epidermis with stomata, mesophyll and vascular tissue. The precise morphology is plant-specific and is adjusted to the environment. The epidermis is the outer layer of the leave that is covered with a protective hydrophobic film referred to as cuticula composed of the waxy heteropolymers cutin and cutan. Cutin is a polyester of omega hydroxy fatty acids and their derivatives whereas cutan is a hydrocarbon without ester linkages. The structure of both is still not fully understood.[70] The cuticula has pores of < 5 nm and is therefore an almost invincible size barrier for most nanoparticles.[69] A higher chance to enter the plant offer the stomate, pores of several micrometers responsible for gas exchange, which are embedded in the epidermis.[50] However, the penetration efficiency might vary strongly with the environmental conditions as the plant can close the stomate depending on moisture,

temperature and light intensity.[70] Moreover, the structure of the mesophyll, the tissue inside the leaf, could influence the transport after penetration of the epidermis. If the mesophyll is dense or loose is plant-specific and must be considered individually for each nano-formulation.[69]

Roots: The roots offer further possibilities for nanoparticle uptake. In contrast to the leaves, the outer root layer, referred as rhizodermis, is usually not protected by a cuticula and therefore might allow comparably easier penetration. The barrier, which is to overcome in this case, is the endodermis, which surrounds the vascular bundles.[69, 70] The endodermis forces a switch of the nanoparticle transport from the extracellular room (apoplast) to the inside of the cells (symplast) by the casparian strip - a hydrophobic layer composed e.g. of lignin. Symplastic transport is performed via plasmodesmata, pores in the cell wall with a diameter of 30-50 nm used for cell-cell material exchange.[69, 70] Hence, again only very small nanoparticles that are smaller than the diameter of the plasmodesmata are able to enter the plant.

2. Transport via phloem and xylem

Plants have a complex conductive system composed of xylem and phloem. The xylem tissue transports water and nutrients from the roots to the leaves driven by a vacuum generated from the transpiration of water via the plant surface. Reversely directed to this transpiration stream is the distribution of carbohydrates via the phloem tissue. Driving force is an osmotic pressure gradient after photosynthesis from the leaves to the residual plant.[70, 71] The fluid flow in the xylem is ca. 0.47 to 4.8 mm/s, whereas the phloem stream is estimated to be 0.07-0.58 mm/s. This means, that even at the lowest stream velocity, a nanoparticle might move up to 6 m within a day inside the vascular tissue. Therefore, both might allow a fast *in planta* uptake of nanomaterials. However, the complex porous structure of xylem and phloem might act as a natural size barrier that can hinder the transport and lead to accumulation inside the plant:[69] In trees, the phloem is the innermost layer of the bark, composed mainly of sieve cells that are connected by porous plates.[70] For these pores, diameters between 200 nm to 1.5 µm (e.g.v*itis vinifera*: 1.4 µm) were measured depending on the plant type.[69] The xylem is best known as “wood”. The tissue is composed of two different hollow cell types, called tracheids and vessel elements, which form a tubular system. Both usually have a diameter of several micrometers and pores in the range of 40 nm – 350 nm at the lateral cell walls referred as pits.[69, 70] These have a diameter of ca. 40 nm such as for *vitis vinifera*. Vessel elements are additionally connected end-to-end by perforations plates. The high porosity combined with the strong transpiration flow might offer ideal transport conditions for various nanomaterials inside the plant.[50, 69] Next to the structure of xylem and phloem, the composition of the biological fluid named “sap” can have an impact on the transport *in planta*. Xylem sap contains several minerals, whereas phloem sap is a mixture of various salts, organic acids and carbohydrates.[69,

[72] The composition of both varies strongly from plant to plant, but even depends on organ (e.g. leaf, trunk, root), age or environmental factors (e.g. soil composition, season) within a plant. The solutes might adsorb at the nanocarrier surface and decrease the colloidal stability, similar to the formation of a “bio-corona” after injection into blood or serum. Aggregation or sedimentation might hinder the transport inside the plant tissue.[73] The interaction between plant-based solutes and polymeric nanocarriers within xylem and phloem has not been investigated yet and was therefore studied in this thesis (Chapter 9).

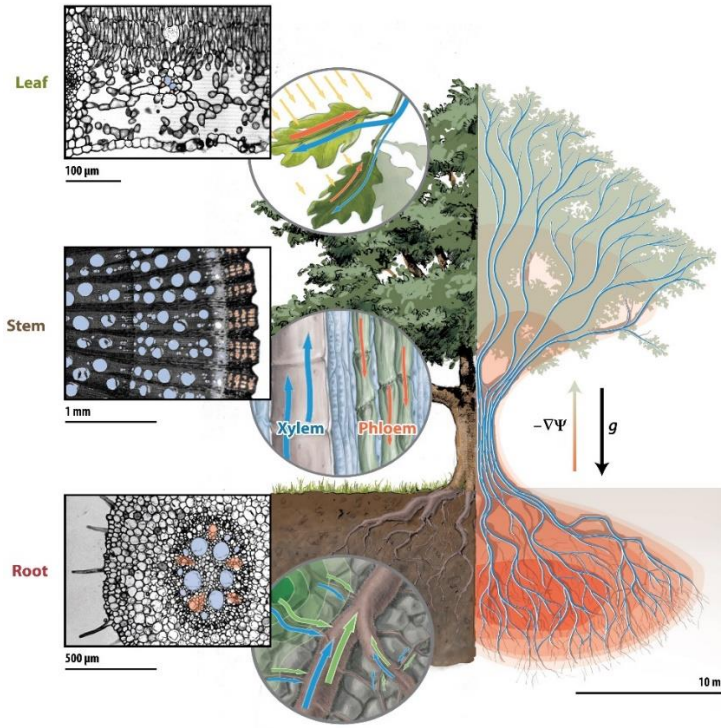

Figure 3.9: Overview of biological size barriers which nanomaterials must overcome to enter a plant and possible transport mechanisms for distribution *in planta*. Optical micrographs show the cross sections of leaf, stem and root tissue. The xylem that is responsible for the water and nutrient transport is highlighted in blue whereas the phloem, which carries a flow of sugars and other metabolizes is shown in orange. (Reprinted from “Annual Review of Fluid Mechanics”, October, 2014(46), A. Stroock, V. Pagay, M. Zwieniecki, N. Holbrook, The physicochemical hydrodynamics of vascular plants, 615-42., Copyright (2014) with permission from Annual Reviews).

4 Targeted Drug Delivery in Plants: Enzyme-Responsive Lignin Nanocarriers for the Curative Treatment of the Worldwide Grapevine Trunk Disease Esca

Jochen Fischer, Sebastian J. Beckers, Doungporn Yiamsawas, Eckhard Thines, Katharina Landfester, and Frederik R. Wurm

Published in “Advanced Science” (WILEY-VCH). Adv. Sci. 2019, 6, 1802315. (Open access)
doi.org/10.1002/advs.201970091

This study was performed under the scientific guidance of PD. Dr. Frederik R. Wurm, Prof. Eckhard Thines and Prof. Katharina Landfester. The nanocarrier preparation, the respective characterisation and the field study was performed by Dr. Doungporn Yiamsawas and Sebastian Beckers. All *in vitro* as well as *in vivo* tests were performed by Dr. Jochen Fischer, who additionally provided the ‘wood extracts’ and evaluated the field trails. For publication, the experimental results were summarized in a manuscript by PD. Dr. Frederik Wurm, Sebastian Beckers, Dr. Jochen Fischer, Prof. Eckhard Thines and Prof. Katharina Landfester. The cover was created by Katharina Maisenbacher.

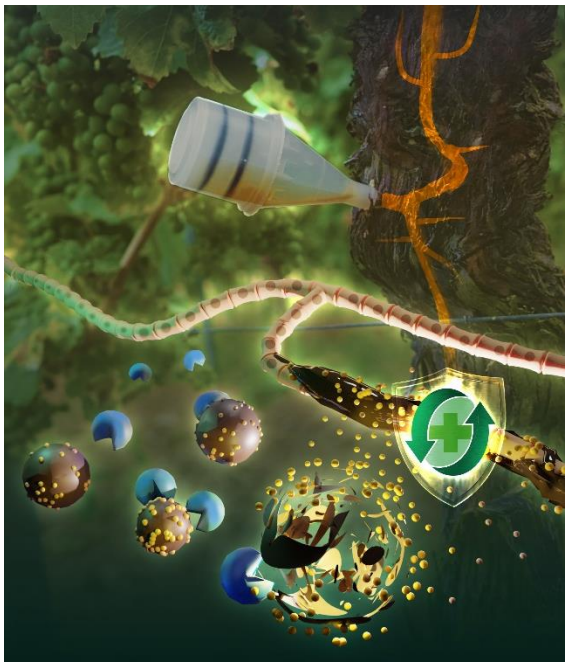

Keywords: *Agriculture, nanocarriers, miniemulsion, plant protection, grapevine trunk diseases*

4.1 Abstract

This chapter presents the first curative nanocarrier (NC)-based treatment of the grapevine trunk disease Esca. Globally more than 2 billion plants are infected causing a loss of $1.5 billion yearly. To date, only repetitive spraying of fungicides is used to reduce chances of infection. This long-term treatment against Esca uses minimal amounts of fungicide encapsulated in bio-based and biodegradable lignin NCs. A single trunk injection of <10 mg fungicide results in curing of an infected plant. Only upon Esca infection, ligninolytic enzymes, secreted by the Esca-associated fungi, degrade the lignin NC to release the fungicide. The specific antifungal activity is confirmed in vitro and in planta (in *Vitis vinifera* L. cv. 'Portugieser'). All treated plants prove to exhibit significantly fewer symptoms several weeks after treatment, and their condition is monitored for 5 years (2014–2018), proving a long-term curative effect of this NC treatment. This study proves the efficacy of this NC-mediated drug delivery for agriculture, using a minimum amount of fungicides. It is believed that this concept can be extended to other plant diseases worldwide to reduce extensive spraying of agrochemicals.

4.2 Introduction

The development of nanomaterials for targeted drug delivery with a release on demand is heavily researched in medicine.[74, 75] Such NCs are designed to respond on external stimuli at sites of infection, which trigger release of loaded therapeutics.[9, 76] As bacteria or fungi secrete certain enzymes (Scheme 4.1A, green pathway), a pathogen-specific mechanism for drug release is available, relying on negative feedback, i.e., destruction of the pathogen, after enzymatic degradation of a nanocarrier (Scheme 4.1A, orange pathway). If the NCs are composed of a nutrient for the pathogen, they will be consumed and degraded by the enzymes, which trigger "unintentionally" a drug release (Scheme 4.1A). This strategy releases a drug only after an infection and may act as a depot or vaccination for future infections. For the first time, this concept was demonstrated for a fungal disease in living plants, which were infected with the worldwide occurring disease "Esca" (Scheme 4.1B). A conventional method to distribute herbicides and pesticides in agriculture is unspecific spraying and of 1–2.5 million metric tons of annually applied active ingredients only 30–40% reach targeted crops.[1, 77] This is because the sprayed agrochemicals are washed off by rainfall or are degraded by light, temperature, or microorganisms.[78] Application of higher drug amounts and more frequent spraying could compensate for these effects, but would also increase costs and environmental contamination. Thus, to minimize the amounts of agrochemicals required, an efficient delivery

method for plants is needed, which can withstand rain and guarantees durable protection after application. Here, we present the first long-term effective, curative NC-mediated treatment against fungal trunk infections of grapevine plants. This disease is called Esca[79] and is based on a series of fungal strains, which infect millions of grapevine plants worldwide every year.[80-82] As no curative treatment is available, the infected grapevines must be replaced, which leads to a financial loss of ca. $1.5 billion per year. Up to now, there has not been an effective curative treatment against Esca, resulting in drastic spreading of this disease around the world. Only preventive spraying of fungicides several times per year (up to 650 mg per year and plant) can reduce the danger of infection, which is detrimental for the environment and uneconomical. Instead of extensive spraying, we provide a fungicide, encapsulated in a protective NC by a single injection into the trunk. Even with a minimum amount of less than 10 mg fungicide per plant, the disease symptoms were reduced significantly. Esca is associated with the occurrence of several fungi, including the tracheomycotic *Phaeomoniella chlamydospora* (Pch) and *Phaeoacremonium minimum* (Pmi).[77, 78, 81] These pathogenic fungi segregate lignin-degrading enzymes (e.g., laccases and peroxidases). Therefore, the substrate lignin was chosen as a carrier material, to develop an enzyme-responsive drug delivery system. Since the disease-associated fungi degrade the loaded lignin NCs, the fungicide is released exclusively in the case of infection, which allows not only a curative treatment but also long-term protection (Scheme 4.1). The lignin NCs were prepared by crosslinking methacrylated Kraft lignin in the presence of a non-systemic drug pyraclostrobin by a combination of miniemulsion polymerization and solvent evaporation.[83] This procedure directly produces an aqueous dispersion of the drug-loaded NCs and can be easily scaled-up to several liters in the lab using standard equipment (Figure 4.2). Furthermore, no leakage of the drug was detected from the NCs during storage. The lignin NCs were studied in vitro and in planta against Esca pathogens: Only in the presence of lignin-degrading fungi, pyraclostrobin was released and became active against the fungal infection. From a vineyard containing approximately 3000 plants, we selected 43 plants with early symptoms of Esca for the treatment. Injections of the NC dispersions into the trunks of these plants were conducted and the plants were monitored over a period of 5 years for effectiveness against Esca. In all treated plants, the Esca symptoms were reduced rapidly, and most treated plants were found with considerably less Esca symptoms than the control plants after 1 year. The majority of the treated plants did not show any signs of Esca during the following 3 years. This is the first demonstration treating Esca-infected grapevine with a minimum amount of 10 mg fungicide and a single dose treatment. We believe that this general strategy of NC-mediated drug delivery enabling a selective release by pathogen-specific enzymes can be further extended to other plant diseases and will facilitate reducing the extensive amounts of agrochemicals distributed by conventional spraying.

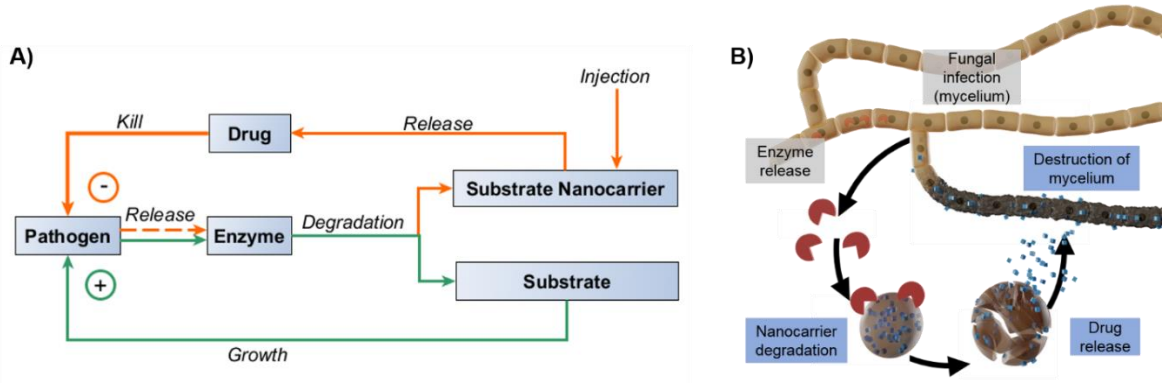

Scheme 4.1: A) Reduction of pathogen due to a nutrient-based drug-delivery system. B) Enzyme-responsive lignin nanocarriers against Esca: they release the antifungal drug load only when the Esca fungi release lignin-degrading enzymes.

4.3 Experimental section

Materials

Kraft lignin (alkaline, 95%), lithium chloride (99%), triethylamine (99%), methacrylic anhydride (94%), sodiumdodecyl sulfate (99%), 2,2′-(ethylenedioxy)bis(ethylamine) (98%), 2-chloro-4,4,5,5-tetramethyl-1,3,2-dioxaphospholane and endo-N-hydroxy-5-norbornene-2,3-dicarboximide (97%) were purchased from Sigma Aldrich. The solvents dimethylformamide and chloroform were of analytical grade and supplied from Fischer Chemicals. Pyraclostrobin (98%) and hexamethylcyclotrisiloxane (98%) were bought from Toronto Research Chemicals and Acros. Lutensol AT50 was provided by the BASF.

Methods

Fourier transform infrared (FTIR) spectroscopy

To confirm the successful methacrylation of lignin, FTIR spectra were measured before and after functionalization using a Nicolet iS10 with Vertical ATR Accessory. Spectra were recorded from dried nanocarrier samples between 600 and 4000 cm^{-1}.

Nuclear magnetic resonance (NMR) spectroscopy

^{1}H and ^{31}P NMR (nuclear magnetic resonance) spectroscopy were performed on a Bruker AVANCE at 500 MHz using hexamethylcyclo trisiloxane as an internal standard. The samples for the ^{31}P-NMR spectra were prepared following the method of Balakshin *et al*. Herein, lignin's hydroxyl groups are first fully converted with 2-chloro-4,4,5,5-tetramethyl-1,3,2-

dioxaphospholane and quantified afterward using the phosphorylated endo-N-hydroxy-5-norbornene-2,3-dicarboximide as an internal standard (SI: Figure 4.4 and Figure 4.5).[84] Lignin's hydroxyl groups are calculated as follows:

Equation 4.1

$$c(OH-Lignin) = \frac{n(Std.) \cdot Integral(150-137\ ppm)}{m(Lignin)} \left[\frac{mmol}{g}\right]$$

Solid State ^{13}C CP/MAS NMR spectra were obtained on a Bruker Avance II operating at 300 MHz proton Larmor frequency equipped with a 4 mm MAS double resonance probe. All experiments were carried out at room temperature with MAS at 10 kHz. Peaks were referenced to alanine (177.9 ppm). A Contact times 3 ms were used.

Dynamic Light Scattering (DLS)

After the nanocarrier preparation the hydrodynamic diameters of the particles were measured by a NICOMP 380 at a fixed angle of 90° and a laser diode running at 635 nm.

To investigate the colloidal stability of the particles inside a plant, 250 µL of a SDS stabilized lignin nanocarrier dispersion (1 wt%) was added to 750 µL "wood extract" and the mixture was kept for 48 h at room temperature. Before the light scattering experiments, 20 µL of the mixture was added to 1 ml of water and filtered through a 5 µm syringe filter. DLS measurements were performed on a commercially available instrument from ALV GmbH, Germany consisting of an electronically controlled goniometer and an ALV-5000 multiple tau full-digital correlator. A He Ne laser with a wavelength of 632.8 nm and output power of 25 mW (JDS Uniphase, USA, Type 1145P) was utilized as the light source. The evaluation of the data was performed following the procedure of Rausch.[85]

Transmission electron microscopy (TEM)

The morphology of the particles was observed by transmission electron microscopy (TEM) using a Joel 1400 at an accelerating voltage of 120 kV. Samples were prepared by casting a drop of diluted dispersion on a carbon-coated copper grid (300 square meshes) and then dried at room temperature.

High pressure liquid chromatography (HPLC)

To determine the encapsulation efficiency, the amount of pyraclostrobin loaded into the lignin nanocarriers was measured by HPLC. Two methods were applied:

(1) *Indirect method*: The sample was centrifuged at 10000 rpm for 60 min and the supernatant containing the non-encapsulated fungicide was freeze-dried. Pyraclostrobin left was then dissolved in THF and quantified by HPLC.

(2) *Direct method*: After isolation of the lignin-nanocarriers by centrifugation at 10000 rpm, the pellet obtained was freeze-dried and suspended in THF To extract the previously loaded drug.

All solutions were passed through a 0.2 µm filter and analyzed by HPLC (Agilent Elicpse Plus RP18) using THF: water/ 0.1 wt% as mobile phase and TFA-gradient, injection volume was 10 µL and the column temperature maintained at 20 ºC. The analysis was performed at a flow rate of 0.2 mL min^{-1} with the UV detector at 280 nm. The encapsulation efficiency (EE) and the weight percentage of pyraclostrobin nanocarriers were determined according to the following equation:

Equation 4.2

$$EE = \frac{\mathrm{m(pyraclostrobin\ in\ nanocarrier)}}{\mathrm{m(pyraclostrobin\ initial)}} \cdot 100\%$$

In vitro phytotoxicity test with *Vitis vinifera* callus culture

The callus culture (*Vitis vinifera* L. PC-1137, DSMZ) was incubated in 50 mL B5VIT medium for 6 days and then centrifuged (5 min, 1500 rpm, 22°C) and dissolved in 45 mL of fresh B5VIT medium. 200 µL of the cell suspension was incubated (40 rpm, 27°C) in a 96-well plate supplemented with 1 µg of pyraclostrobin-loaded nanocarriers. 20 µL of the culture were stained with 2 µL fluorescein-diacetate solution (1 mg / 10 mL) after 24 hours to determine the number of viable cells (Widholm, 1972).

In vitro and *in vivo* antifungal test - Germination assays

Conidia from 18-day-old agar plate cultures were harvested. After centrifugation at 4000 rpm for 10 minutes, the conidia were re-suspended in HMG-medium (10 g·L^{-1} malt extract, 10 g L^{-1} glucose, 4 g L^{-1} yeast extract, pH 5.5) to a concentration of 1 x 10^5 per mL. The test was carried out in 96-well microliter plates (Greiner Bio-One GmbH, Frickenhausen) with conidia in 200 µL of YMG-medium and an incubation time of 72 hours at 27°C.[86] The optical density was measured at a wavelength of 600 nm (Benchmark Plus Microplate reader, BioRad, Munich). Tests were conducted in triplicates. The concentration of the used fungicide was 5 µg per 200 µL medium in a well.

Evaluation of the field trials

All plants used for the injection tests (as well as the control group) were tested for the presence of Esca-associated fungi. Therefore, wood samples of shoots were harvested and analyzed on endophytic fungi afterward using the method of an endophyte isolation protocol. The isolation of fungi was performed from surface-sterilized grapevine plant material (1 min 70% ethanol, 3 min 5% sodium hypochlorite, 30 s 70% ethanol) onto 2% YMG agar augmented

with 200 mg L^{-1} each of penicillin G and streptomycin sulfate (both from, Carl Roth GmbH & Co. KG, Germany). For maintenance and submerged cultivation, YMG medium was used. To solidify media, 2% agar was added. The morphological features of the fungal colonies were determined on YMG agar. For microscopy, squares of 0.2% malt extract agar were mounted directly in water. For molecular identification, the ITS sequences were obtained and analyzed using the method of Köpcke et al.

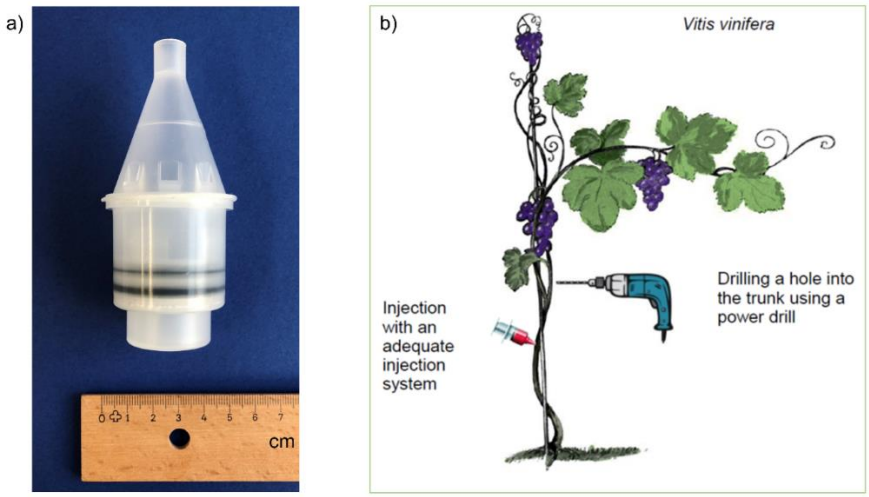

Figure 4.1: A) Injection device used for the *in planta* studies. B) Lignin-Nanocarrier injections procedure scheme; 1. drilling of the application inlet, 2. injection of the nanocarrier suspension.

The side of the trunk that was selected for the injection was sprayed with 5% sodium hypochlorite to sterilize the wooden surface of the plant. Afterwards, an 8mm deep and 6mm wide hole was drilled into the grapevine trunk. The chosen plants always had a trunk diameter greater than 20 mm. The drill head was always sterilized in 70% ethanol for 1 minute before the next plant was treated. After the drilling, the injection system (supplied from Tree Tech Microinjection Systems (FL, US), Figure 4.1A) was filled with the lignin particle suspension and inserted to the grapevine trunk hole. The scroll spring pressure system was activated afterward and the solution was injected into the trunk in less than 24 h. After one day the injection systems were removed and the wound was sealed with grafting wax. The injection application is presented in Figure 4.1.

The plants were monitored for five months after the injection. The monitoring ended when the autumn leaf coloration started. The plants were controlled on a six weeks' basis for increasing or decreasing foliar Esca symptoms in comparison to their appearance to the previous control and the untreated plants. The discolorations were documented using a digital camera. Furthermore, samples of grapes (1 kg, each) from the treated plants were harvested

in October and analyzed. The samples were analyzed by Eurofins (Hamburg, Germany) for residues of pyraclostrobin by mass spectrometry. No pyraclostrobin was detected.

Pesticide screening

Ca. 3 month after injection 400 g of grapevines were collected and analyzed on their pesticide pollution by LC-MS/MS following the method DIN EN 15662:2009-02, mod., P-14.141, LC-MS/MS. Eurofins / Dr. Specht Laboratorien GmbH (Hamburg; Germany) performed the screening. A pyraclostrobin content of < 0.01 mg kg^{-1} was detected.

Preparation of "wood extract"

20 g of lyophilized wood chips (length: 1-3 cm) of *Vitis vinifera* (18 years, from Rheinhessen) was blended for 1 min with 100 ml of water. Afterwards, the mixture was filtered through a paper filter to separate the solid. Prior to use, the extract was filter through a 5 µm syringe filter additionally.

The wood extract is a mixture of xylem and phloem sap and has a pH of 6.6. According to literature, it contains a variety of sugars (mostly sucrose 100-300 g L^{-1}), amino acids (mostly glutamine 5-40 g L^{-1}), organic acids (mostly malate g L^{-1}) and inorganic ions.[72]

Synthesis

Methacrylated lignin

2 g of lignin (12.26 mmol OH groups) was added to 60 ml LiCl/dimethyl formamide (DMF) and heated under an argon atmosphere to 90°C until completely dissolved. After cooling to 50°C, 1 ml of triethylamine (10 mmol) was added and the mixture was stirred for further 15 min. 3 ml of methacrylic anhydride (20 mmol) was then injected over 30 min and the reaction was allowed to proceed at 50°C overnight. The mixture was precipitated into a large excess of isopropyl alcohol and isolated by centrifugation. When precipitated further three times, the product was dried at room temperature under vacuum. Typically yields of 60% were obtained. By ^{1}H and ^{31}P-NMR spectroscopy, a hydroxyl group conversion of 90% (5.5 mmol g^{-1} methacrylic groups) was determined.

Preparation of crosslinked lignin nanocarriers

Crosslinked-lignin nanocarriers were prepared by a combination of miniemulsion polymerization and solvent evaporation. Typically, 500 mg (2.75 mmol methacrylic groups) of methacrylated-lignin and 100 mg (for a pyraclostrobin: lignin ratio of 20%) pyraclostrobin were dissolved in 5 g of chloroform ($CHCl_3$). To form a pre-emulsion, the mixture was given to 45 g of a surfactant solution (for concentrations see Table 4.1) and stirred at 1000 rpm for 1 h. The

emulsion was sonicated in the next step for 3 min (1/2 inch tip, 70% amplitude, 20 s ultrasound followed by 10 s pause) under ice cooling to prevent any solvent evaporation. Afterwards, a solution of 250 mg 2,2´(ethylenedioxy)bis(ethylamine) in 5 mL water was added dropwise to the emulsion. The reaction was performed at 50°C for 15 h. Finally, the solvent was evaporated by stirring the opened reaction vessel overnight at room temperature. The volume of the dispersion was adjusted to 50 mL by addition of water (this corresponds to a solid content of 19 mg mL^{-1} and a pyraclostrobin concentration of 2 mg mL^{-1}). The dispersion can be diluted to the desired concentration and is stable against coalescence or aggregation upon the addition of water. The nanocarriers obtained were characterized by dynamic light scattering (DLS) and transmission electron microscopy (TEM).

Table 4.1: Characterization data of lignin nanocarriers.

No.	surfactant type/	Surfactant [1]/ mg/mL	Diameter [2]/ nm	PDI	pyraclostrobin: lignin mass ratio /%	encapsulation efficiency /%
1	SDS	1.0	260	0.3	-	-
2	SDS	1.0	310	0.2	5	94
3	SDS	1.0	330	0.3	10	94
4	SDS	1.0	310	0.4	20	98
5	SDS	0.5	510	0.4	5	99
6	SDS	2.0	220	0.3	5	64
7	SDS	2.0	213	0.4	20	97
8	Lutensol AT50	1.0	640	0.3	5	100

[1] surfactant concentration for nanocarrier synthesis.
[2] determined by DLS

4.4 Results and Discussion

Synthesis of lignin NC's

To allow the encapsulation of the hydrophobic fungicide pyraclostrobin, we modified the hydroxyl groups of the hydrophilic Kraft lignin with methacrylic groups by the reaction with methacrylic anhydride (Figure 4.2A). Both NMR and IR spectroscopy proved the successful modification of lignin with methacrylic groups (Figure 4.6: IR: ester bond vibrations at 1736 cm^{-1} (-C=O); reduction of the hydroxyl vibration (-OH) at 3000–3800 cm^{-1} after the reaction, indicating a high degree of functionalization). ^{1}H NMR spectroscopy proved the attachment of the methacrylic group by the distinctive resonances of the vinyl group at 5.88

and 6.22 ppm. The diffusion-ordered NMR spectroscopic ^{1}H NMR analysis confirmed a covalent coupling of the vinyl groups to the polymeric lignin (Figure 4.3), as the two protons of the vinyl group were detected at the same diffusion coefficient as the lignin backbone at approximately 1.7×10^{10} m^2 s^{-1}. The number of methacrylates was determined by the method of Balakshin and Capanema using 2-chloro-4,4,5,5-tetramethyl-1,3,2dioxaphospholane as a phosphorylation agent and found to be 5.5 mmol g^{-1} (Figure 4.4 and Figure 4.5).[84] Lignin NCs were prepared by crosslinking the methacrylated lignin in miniemulsion droplets: methacrylated lignin was dissolved together with the fungicide pyraclostrobin in chloroform to generate the dispersed phase. The solution was then mixed with the aqueous phase containing either sodium dodecyl sulfate ("SDS," an anionic surfactant) or Lutensol AT50 ("Lut," a nonionic poly(ethylene glycol)-based surfactant) as a stabilizer. A stable miniemulsion with homogenously distributed droplets was prepared by ultrasonication of the hydrophobic and the hydrophilic solutions. By using a microfluidizer instead of a sonication tip, the process was scaled easily to the liter-level (Figure 4.2B). Afterward, 2,2´(ethylenedioxy)bis(ethylamine), which is soluble both in the aqueous and in the organic phase, was added to crosslink the methacrylated lignin via an aza-Michael addition at 50°C over a period of 15 h. Finally, chloroform was evaporated at room temperature to yield a stable lignin NC dispersion.

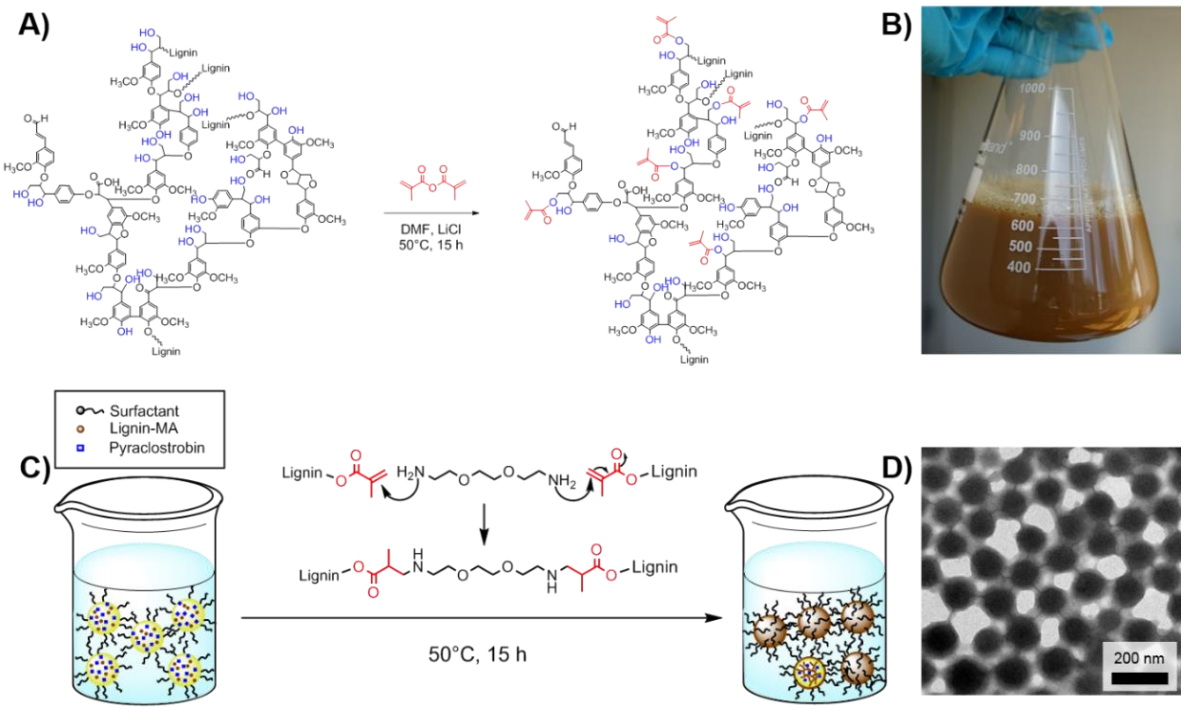

Figure 4.2: Synthesis of methacrylated-lignin and formation of lignin nanocarriers by crosslinking in miniemulsion. A) Methacrylation of lignin with methacrylic anhydride (note: representative structure of lignin may vary depending on the biological source). B) Photo of ca. 600 mL of lignin nanocarrier dispersion (1 wt%). C) Crosslinking mechanism of lignin nanocarriers in miniemulsion. D) Transmission electron microscopy (TEM) image of lignin nanocarriers.

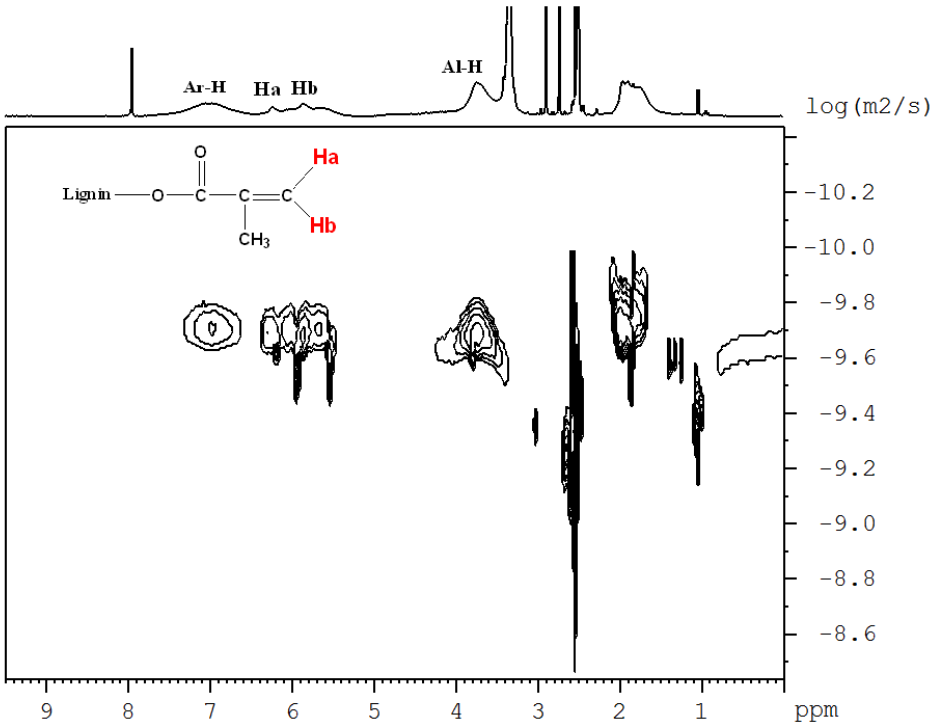

Figure 4.3: ^{1}H DOSY-NMR (700 MHz, 298 K, $CDCl_3$) spectrum of methacrylated Kraft lignin.

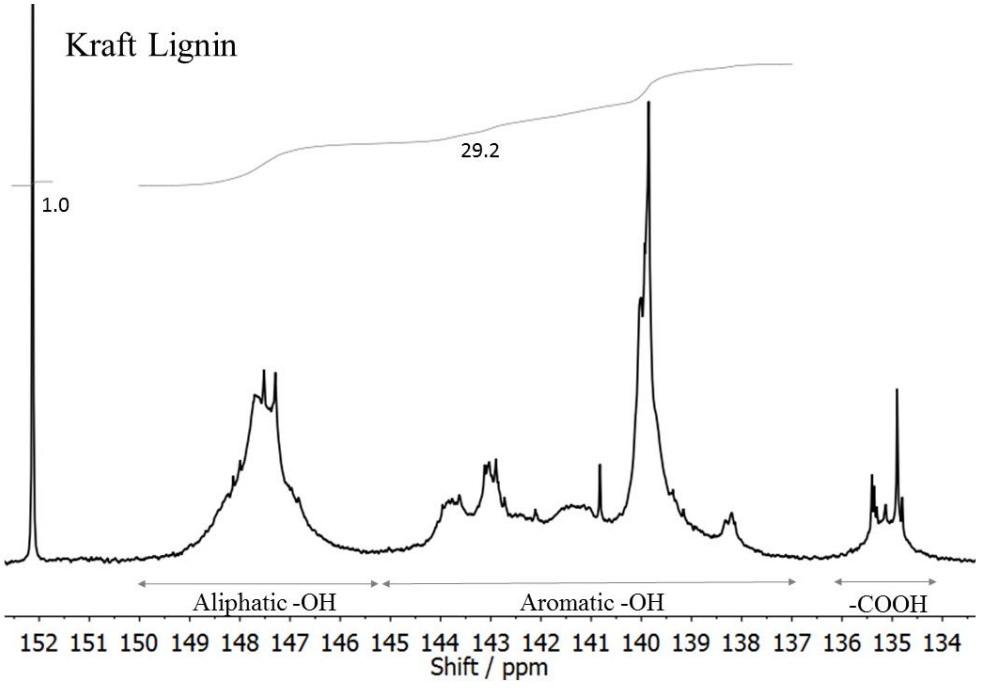

Figure 4.4: ^{31}P-NMR of Kraft lignin after reaction with 2-Chloro-4,4,5,5-tetramethyl-1,3,2-dioxaphospholane

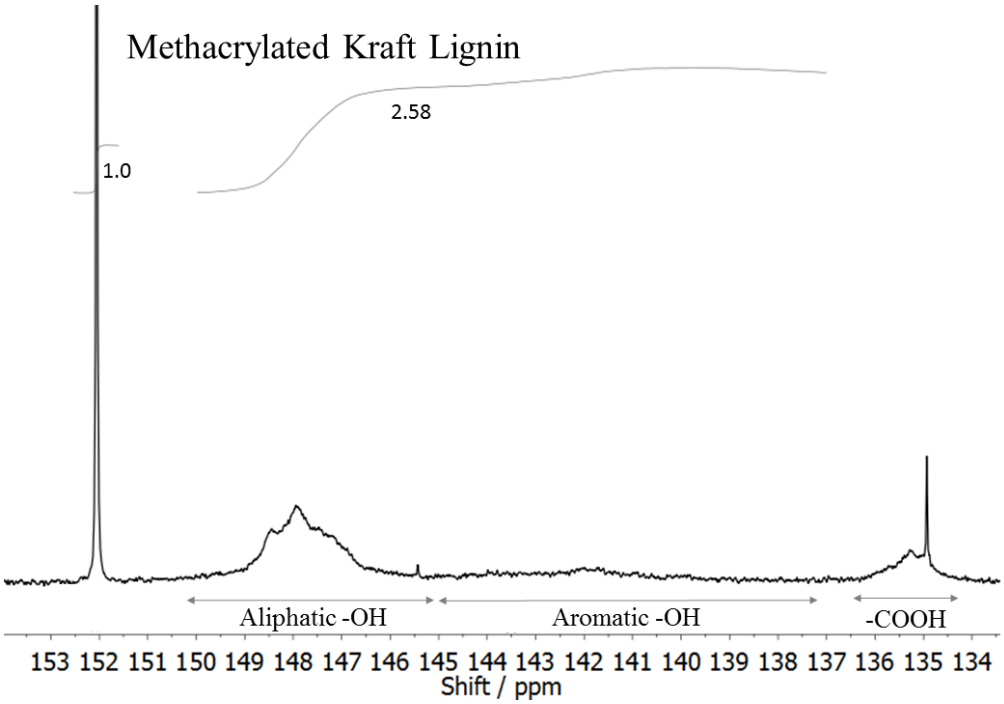

Figure 4.5: ^{31}P-NMR of methacrylated Kraft lignin after reaction with 2-Chloro-4,4,5,5-tetramethyl-1,3,2-dioxaphospholane.

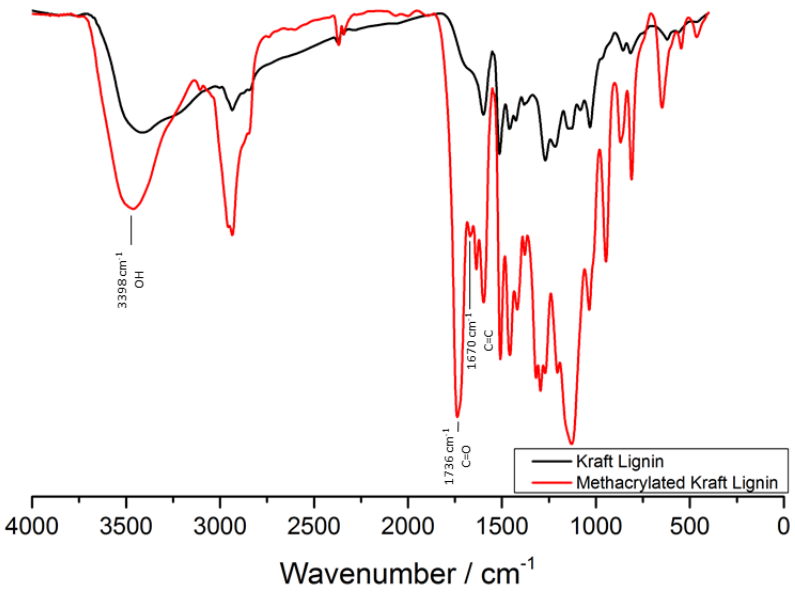

Figure 4.6: FTIR spectra of Kraft lignin and methacrylated Kraft lignin.

Solid-state ^{13}C NMR spectroscopy of the freeze-dried product proved the covalent crosslinking of the NCs (Figure 4.7). Depending on the preparation conditions, NCs with diameters between 200 and 700 nm (determined by dynamic light scattering, DLS) were obtained. The sizes of

the NCs were varied by adjusting the concentration of lignin-MA in the droplets and the amount and type of surfactant (Table 4.1). The addition of pyraclostrobin to the miniemulsion did not result in any significant change of the NC size, compared to “empty” lignin NCs. Transmission electron images show the spherical morphology of all fungicide-loaded lignin NCs (Figure 4.2D). The diameters of the NCs were monitored over a period of several months at room temperature but did not significantly change, proving high colloidal stability without aggregation or degradation during storage. Furthermore, the encapsulation efficiency for pyraclostrobin was determined by high-performance liquid chromatography (HPLC) and found to be typically above 90%. Even at 20 wt% of fungicide loading, an encapsulation efficiency of more than 97% was obtained (Table 4.1). Besides, no pyraclostrobin was released from the lignin NC during storage over a period of at least 1 month proving that no cargo is lost by leaking.

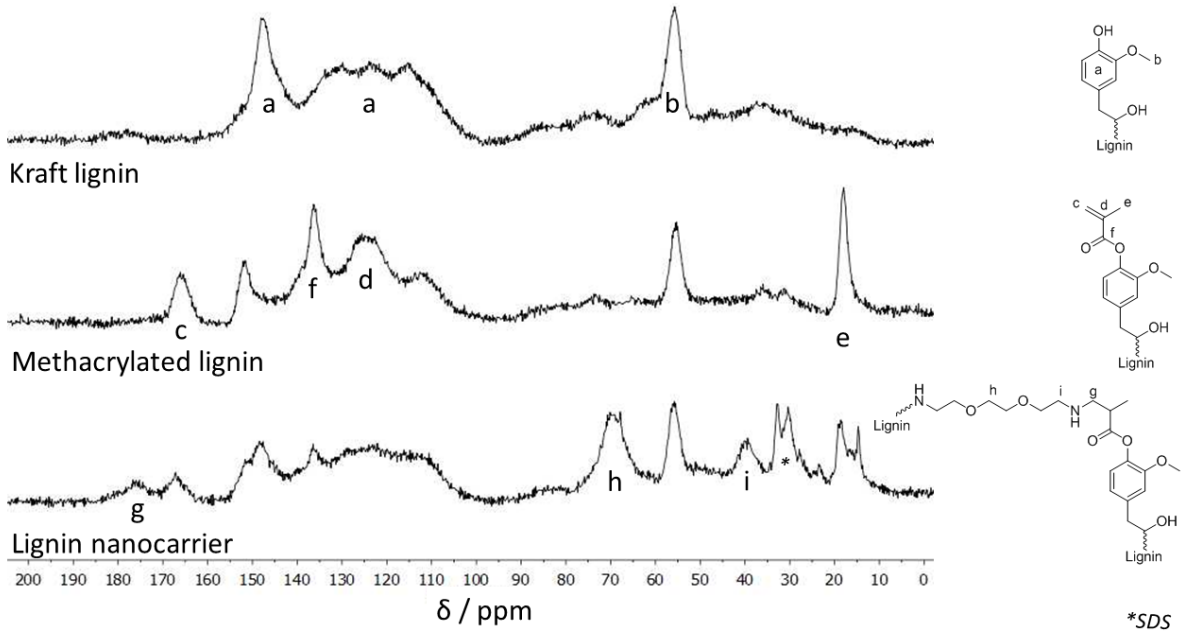

Figure 4.7: Solid State ^{13}C NMR spectra of Kraft lignin (top), methacrylated lignin (middle), and lignin nanocarriers (after drying of the dispersion, bottom) with peak assignments.

***In vitro* and *in vivo* antifungal activity**

The drug release of lignin NCs with a pyraclostrobin loading of 20 wt% was quantified in vitro by HPLC-MS (mass spectrometry). After mixing an NC dispersion with the filtrate of a 72 h well-grown culture from the Esca-associated fungus Pch, more than a third of the encapsulated fungicide was released to the medium, proving that the segregated lignolytic enzymes can induce the degradation of the NC matrix (Figure 4.8B). A complete drug release could not be measured as the released drug effectively destroyed the fungi during the

experiment. In previous studies, we already used isolated enzymes to degrade lignin NCs *in vitro*, but no living fungi were involved so far.[8, 9] Furthermore, those results indicate that a drug release in planta is not affected by xylem sap, since a similar pH level was used for the test compared to plant sap.[87] In addition, aggregation tests in grapevine canes were conducted and no influencing effects to lignin NCs activity were observed. In further tests, the drug release was analyzed by determining the growth-inhibition of spores and mycelium belonging to the Esca-associated fungi Pch and Pmi in a malt yeast medium supplemented with lignin NCs.

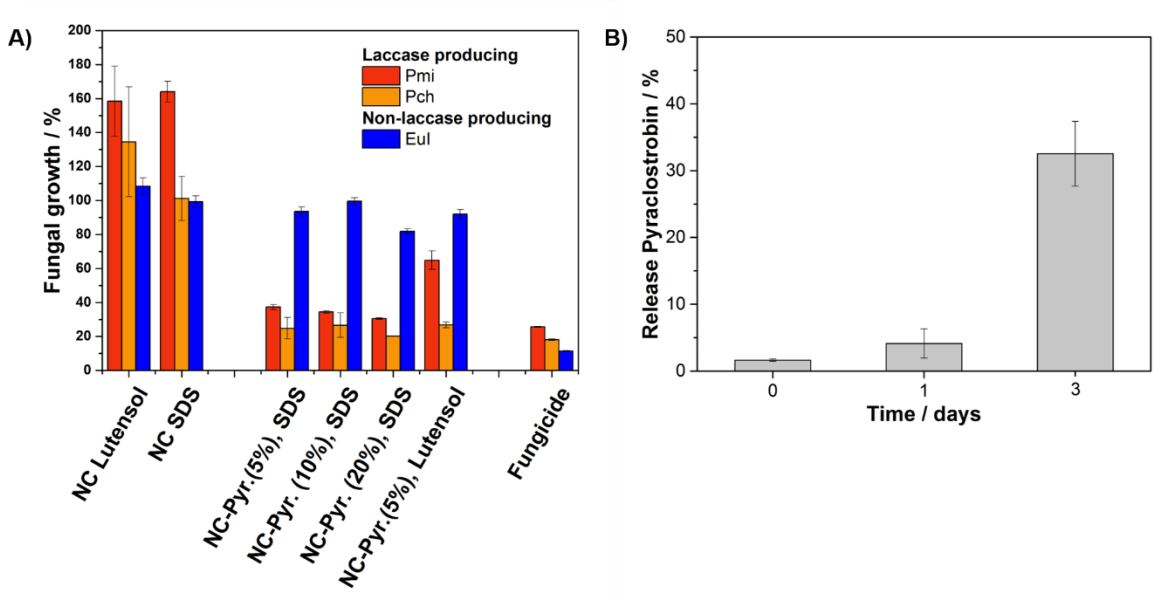

Figure 4.8: *In vitro* investigations of lignin nanocarriers (NC). *Phaeomoniella chlamydospora* (Pch) and *Phaeoacremonium minimum* (Pmi) were used as ligninolytic enzyme-segregating fungi, whereas *Eutypa lata* (Eul) was applied as control fungus without laccase segregation. A) Optical density (at 600 nm) of fungal cultures in 96-well microtiter plates after 48 h for samples empty and pyraclostrobin-loaded lignin nanocarriers (see Table 4.1 for details). B) HPLC-MS analysis of nanocarrier supernatant after the incubation with culture filtrate of Pch after 24 and 72 h. Release compared to a pyraclostrobin standard curve and the amount of applied fungicide.

To prove the selective enzymatic release of pyraclostrobin, *Eutypa lata* (Eul), which does not produce lignin-degrading enzymes, was used as a control fungus.[88] Eul grew unaffected in the presence of the drug-loaded NCs, proving no release of the fungicide and thus the density of the NCs without the presence of lignin-degrading enzymes (Figure 4.8A, blue bars). Pch and Pmi, however, which produce lignin-degrading enzymes, were able to release the drug and their growth was suppressed completely. An additional proof that the lignin NCs act as nutrient for these fungi is obvious, when “empty” NCs were incubated with Pch and Pmi: the fungal growth was even higher after the addition of the NCs without

encapsulated fungicide (Figure 4.8A, “NC SDS” and “NC Lutensol”) than in the negative control (medium only). Both SDS and Lutensol did not influence the mycelium growth and the lignin carrier material itself may have acted as a nutrition source. We could, therefore, prove that the NCs alone or the surfactants did not inhibit fungal growth. In contrast, all fungicide-loaded NCs resulted in the suppression of growth of Pch and Pmi. NCs with different drug loading concentrations (5, 10, and 20 wt% pyraclostrobin compared to lignin), surfactant, or diameters exhibited similar activities against the fungi (Figure 4.8A). Importantly, the results prove that the lignin NCs (NC-Pyr. (20%), Sample 4, Table 4.1) stabilized with SDS exhibit almost the same germination inhibiting rate as the positive control. Furthermore, we observed that lignin-NC dispersions stored at 4°C for over 2 years remained the same antifungal activity, proving their long shelf-life. Whereas the NCs should kill the Esca fungi, they should not harm plant cells in general. To elucidate the phytotoxicity of the lignin NCs on plant cells, the dispersions were tested on *Vitis callus* cultures (DSMZ- PC-1137). No effect on the viability of the callus cells in the presence of the lignin NCs was observed (Figure 4.9). In contrast, a positive control (the herbicide glufosinate-ammonium) causes the cell death of the *Vitis callus* cells. These experiments prove that the lignin NCs (loaded with the fungicide pyraclostrobin and “empty”) are non-phytotoxic to plant cells, making them attractive candidates to treat various plant diseases.

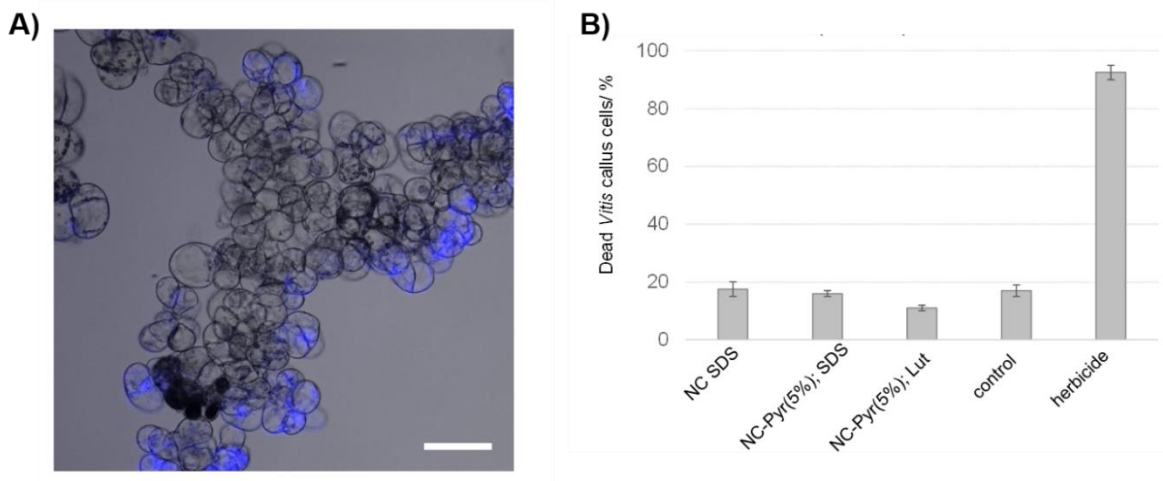

Figure 4.9: A) Fluorescent microscope image (Zeiss Axio Imager) scale bar = 100 µm; fluorescein diacetate (FDA) staining and artificial coloration (fluorescence filter 38; BP 525/50). B) Number of dead *Vitis vinifera* callus culture cells after 24 h (Samples: NC Lut / SDS: lignin nanocarriers without fungicide; 2. NC-Pyr (x%): lignin nanocarriers loaded with different amounts of pyraclostrobin; SDS or Lut indicates the surfactant used for stabilization of the nanocarrier dispersion; controls: without the addition of nanocarriers or fungicide; herbicide: glufosinate-ammonium (0.5 mg mL^{-1}), fungicide: pyraclostrobin (0.5 mg mL^{-1}).

***In Planta* Studies**

Up to now, there are only two injection-based drug delivery systems for plant protection: i) injection of soluble systemic insecticides in loblolly pine trees against southern pine bark beetles.[89] ii) Injection of fungicides in trees against apple scab (*Venturia inaequalis*) and powdery mildew (*Phyllactinia sp.*) was able to reduce disease severity.[90] Such strategies, however, rely on a systemic treatment of a plant with the drug. To date, no nano- or microcarriers were able to protect plants from diseases and release the cargo only in case of infection. Thus, the colloidal properties of the NCs inside of the plant are unknown. Do they aggregate, when in contact with the fluid in phloem or xylem? Or do they retain their colloidal stability and can be transported inside of the plant? To study the colloidal stability, which is required for a potential transport of the NCs inside of living plants, we used DLS in "wood extract" (see experimental section for details). This complex mixture simulates the conditions inside of a plant. DLS was used to assess the colloidal properties, following a method established by Rausch *et al.* for the determination of NC aggregation in human blood plasma.[85] After the addition of the NC dispersion to the "wood extract," no macroscopic phase separation occurred and DLS proved only a few smaller aggregates <1 µm, indicating a potential transport inside of the plant tissue. This was further supported by an *in planta* experiment, in which we passed an NC dispersion through a shoot of a young grapevine plant (Figure 4.10A). A vacuum of 75 mbar was applied, simulating the natural transpiration pull.[72] Also in this experiment, the size distribution determined by DLS remained almost unchanged after the transport through the vascular plant tissue (Figure 4.10A,B). These experiments indicate the colloidal stability and therefore the ability for transport inside of the plant. In on-going research, the NC transport inside of living plants is studied and will be reported in near future.

After the verification that the lignin NCs can distribute within the plant through the vascular tissue as well as their antifungal activity and non-phytotoxicity *in vitro*, the aqueous dispersions were injected *in planta* into *Vitis vinifera* L. cv. 'Portugieser' plants in a vineyard in Forst an der Weinstraße, Germany. An early symptom of Esca is necrotic yellow-brownish tissues around the leaf veins described as "tiger stripes" (see images in Figure 4.10D).[91] Often accompanied by wilting grapes, showing brown spots on the surface and becoming inedible.[92, 93] Cross-sections of infected trunks show necrotic tissue with brown to black spots and dry wood.[94] We categorized the progress of Esca symptoms in six categories (Figure 4.10D). The plants were cultivated with two branches, which allowed a ranking system based on the number of affected twigs of each plant. All selected grapevine plants showed symptoms of an early stage of an Esca infection (≈1–2 on the severity level).

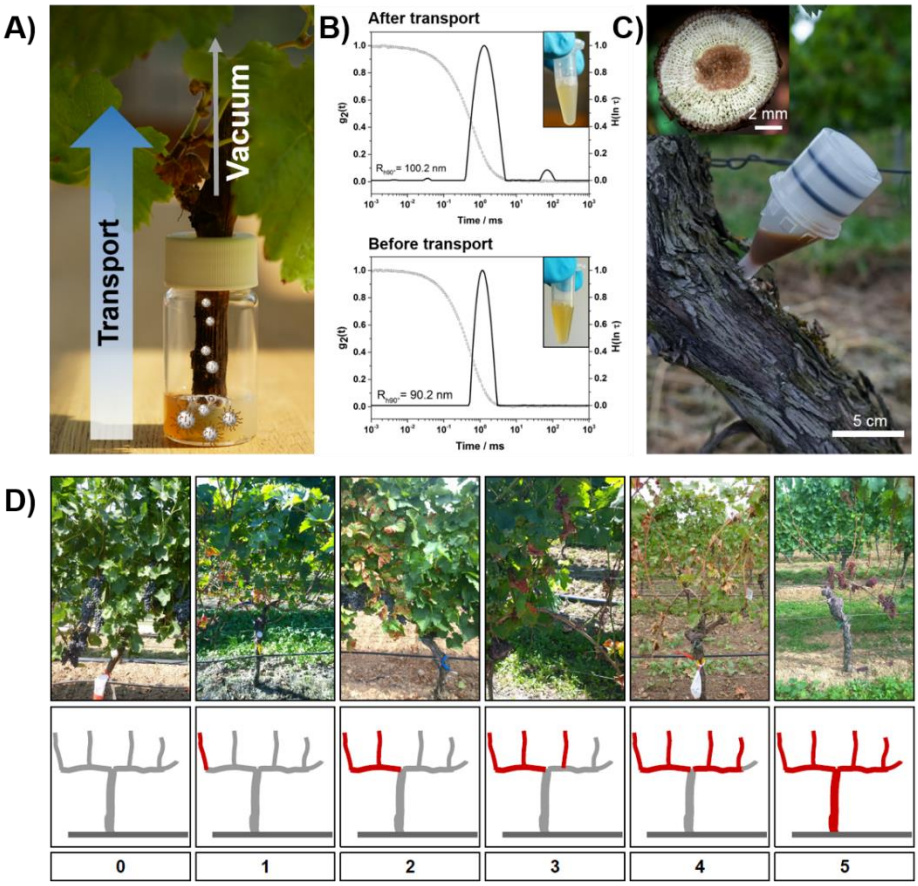

Figure 4.10: A) Shoot of a young grapevine plant through which a nanocarrier dispersion was sucked by vacuum simulating the natural transpiration pull. B) Photos and respective particle size distributions of the lignin nanocarrier dispersion before and after transport through a grapevine shoot. C) Injector filled with 5 ml of 1 wt.% lignin nanocarrier dispersion and cross-section of a grapevine plant, showing the size of the vascular bundles. D) Categorization of Esca symptoms determined in field trials, graduated in six severity degrees (grey: normal growth, red: Esca symptoms observable).

Into the plant's trunk, a hole was drilled (6 mm diameter, 8 mm depth) and the aqueous NC dispersion was injected (≈1 wt% solid content) via a microinjection system (from TreeTec, Morriston, Florida) over a period of several hours (Figure 4.10C). Afterward, the wound was sealed with a pruning wound seal product (Figure 4.13). In total, 70 plants were treated with different NC dispersions. In addition, all 2958 plants of the vineyard were monitored over a period of 5 years (2014–2018). Forty-three plants were treated with the pyraclostrobin-loaded lignin NCs, 19 plants were treated with "empty" lignin NCs, 8 plants were treated by the injection of an F500 formulation (commercialized product of BASF, Germany), and the remaining 2877 plants were not treated. The Esca symptoms on all plants untreated or treated with "empty" lignin NCs (see Figure 4.11 "empty NC," gray) increased significantly during the next months and more particularly the following years. After 12 months, these plants either did not survive or showed more severe Esca symptoms. In contrast, the fungicide-treated plants (0.7 mg mL^{-1} encapsulated pyraclostrobin) showed a significant improvement in their

conditions after 3 months and up to 4 years. In the first year, the overall Esca severity was reduced <1 (Figure 4.11, field study 2014) and plants treated with loaded lignin NCs showed 62% (Autumn 2014) and 58% (after 2 years, 2016) fewer symptoms than the control plants (Figure 4.12 shows representative photographs of a treated and a nontreated plant from 2014 to 2018). Furthermore, monitoring of the treated plants in the following 2 to 4 years, respectively, proved a further improvement as less or even no leaf symptoms (in 2018) were detectable. Two additional field trials were started in 2015 and 2016: in 2015, we compared the NC treatment with a trunk injection of the commercial formulation (F500, 6 mg mL^{-1} pyraclostrobin). Treatment with F500 resulted in an initial improvement (2016) of the symptoms (Figure 4.11, field study initiated in 2015), but in the following years (2017 and 2018) the symptom level increased again, although an almost nine higher amount of the fungicide was injected in the commercial suspension. In contrast, the symptoms of the NC-treated plants further decreased over the following years, even without additional injections. An additional field study was started in 2016, and again after 2 years, no leaf symptoms were visible in 2018, while the nontreated plants still showed Esca symptoms. These results clearly prove the release of the fungicide and the long-term curative effect of the treatment (note: the plants are still under observation for the next years). To our knowledge, the herein reported lignin NCs is the first report of an injection system based on long-term active and stimuli-responsive NCs for drug delivery inside of living plants. In addition, these results prove that lignin NCs, loaded with a hydrophobic fungicide and injected into the trunk of wine plants, act as a curative treatment for Esca-infected grapevine plants. Together with the in vitro studies, we also suppose no release of the fungicide in a noninfected plant, as only the laccase segregated from the fungi, would open the NCs.

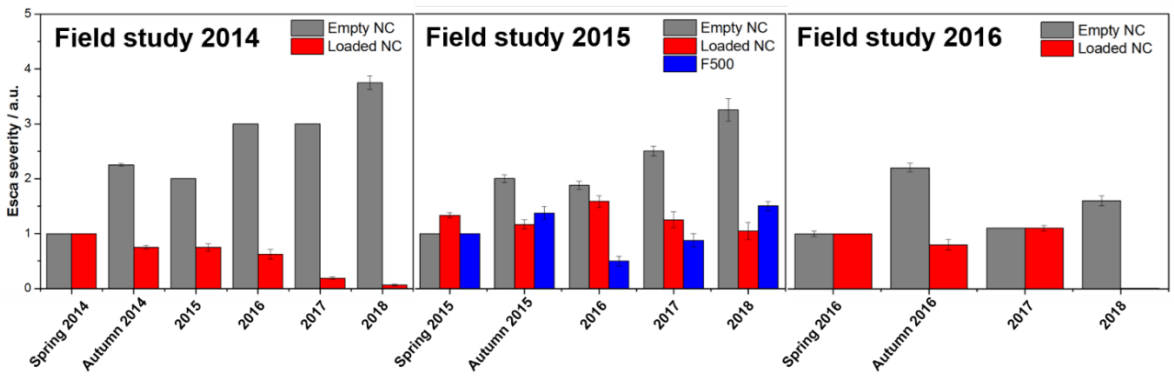

Figure 4.11: *In planta* application of lignin nanocarriers. Bar diagram showing severity of wine plants in the years 2015 until 2018: comparison between treatments with empty lignin nanocarriers (i.e. without loaded fungicide); lignin nanocarriers (loaded with pyraclostrobin (0.7 mg mL^{-1})); F500 (i.e. the injection of the F500 formulation (BASF) with pyraclostrobin (6 mg mL^{-1}).

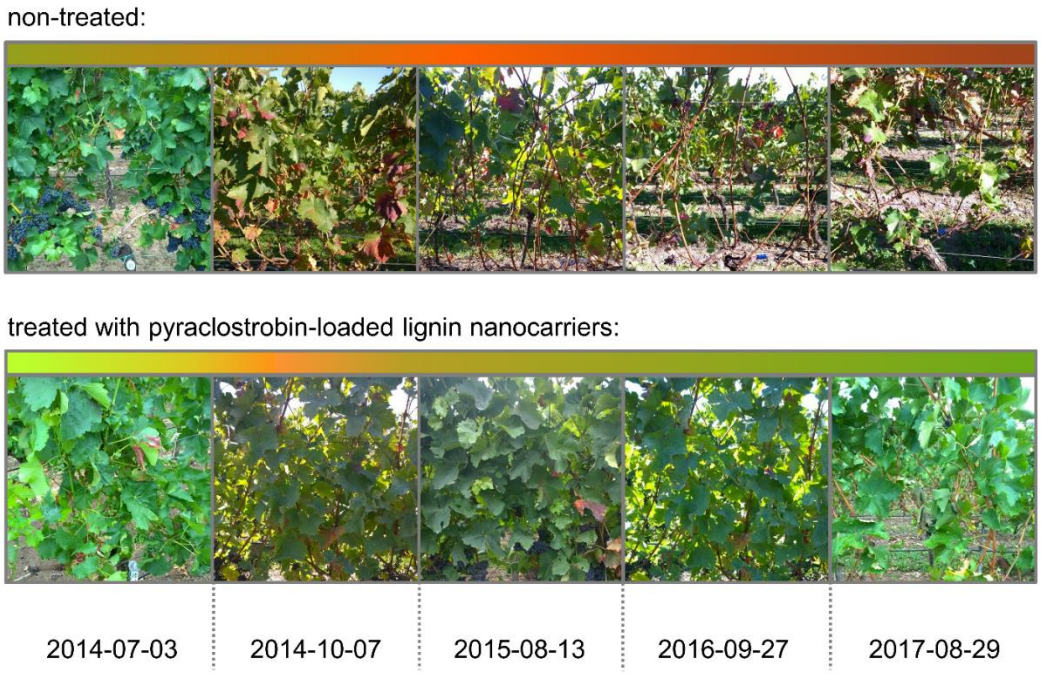

Figure 4.12: Photographs of a treated wine plant (with pyraclostrobin-loaded nanocarriers, top) and a non-treated plant (bottom) over a period of 4 years (dates are noted below the photos).

Figure 4.13: Photographs of the treatment with the nanocarrier dispersion of an Esca-infected wine plant

The lignin NCs are an effective cure to treat already Esca-infected grapevine plants. All plant protection product treatments that are currently available in the market, only aim a preventive fungal infection, but are not custom made for GTD (grapevine trunk disease) pathogens or other trunk diseases, e.g., in plums, peaches, or almonds and are futile after the

infection and colonization in the plant occurred. Since GTD pathogens grow mostly in the xylem vessels, we assume that the introduced injection method is capable to reach the fungal mycelium inside the plant.[95] Another important advantage of the proposed method is the significant reduction of the amount of fungicide applied per plant. This drastically reduces the release of fungicide to the ecosystem. The amount recommended for one foliar application in conventional viticultural farming of a strobilurine derivative in a German vineyard is at least 70 mg (after blossom) but up to 640 mg (at full foliation) per year and plant depending on the month of spraying.[96] In contrast, by a single injection of the enzyme-responsive lignin NCs into the trunk, we are able to reduce the amount of fungicide to less than 3% compared to preventive spraying without the need for treatment in the following years (Figure 4.14). Furthermore, handling of the aqueous NC dispersion is safe and easy and prevents unwanted release of the fungicide into the environment as the fungicide is embedded into the plant and not sprayed unselectively, without the undesired release of the drug.

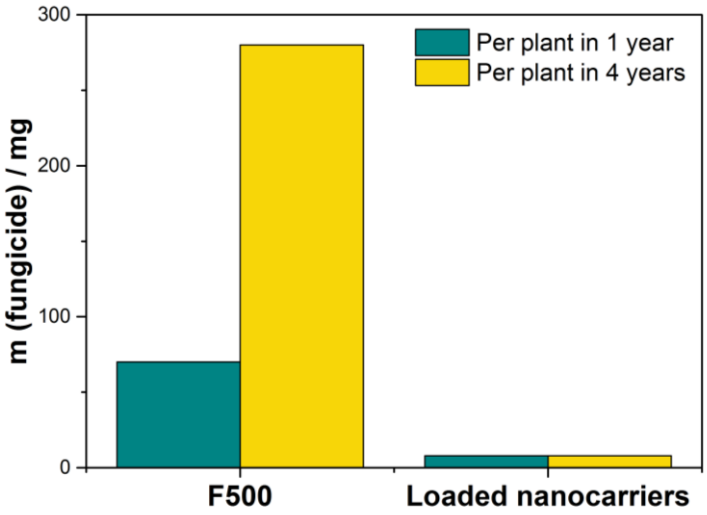

Figure 4.14: Comparison of fungicide amount used via the injection of the lignin nanocarriers compared to preventive spraying according to: http://www.dlr.rlp.de/Internet/global/themen.nsf/Web_P_WB_Rebschutz_XP/0213F4E9F3596261C12580AC0056E34A/$FILE/Rebschutz%202017_03.pdf.

Another important finding was that after the treatment with the lignin NCs no pyraclostrobin was found in the harvested grapes (≈0.5 kg were analyzed, compare Supporting Information). In contrast to the injected NCs, it was reported that sprayed fungicides remain in/on the grapes after harvesting: e.g., Angioni et al. proved the presence of boscalid in grapes and wine.[97] While the maximum residue limit by the EU commission was not reached, still the amount of up to 4.23 mg kg^{-1} boscalid was detected in the samples. Also, other fungicides such as iprovalicarb and indoxacarb were detected in the same samples. In another test series

1.01 mg kg^{-1} of iprodione; 0.78 mg kg^{-1} of procymidone; and 0.37 mg kg^{-1} of vinclozolin were detected in grapes.[98] These results further underline that fungicides applied by conventional spraying are always traceable in grapes, whereas drug delivery via the lignin NCs enables a trace-free harvest already in the first year after the application.

4.5 Conclusion

In conclusion, this work presents a general approach for NC-mediated drug delivery in living plants. Although using minimal amounts of fungicide compared to a preventive spraying strategy, this concept successfully acted as the first curative treatment for a GTD “Esca.” With lignin as the matrix of the NCs, the Esca-associated fungi degraded the trunk of the grapevine plant and the NC sufficiently, which results in an enzyme-responsive drug release. These NCs, loaded with pyraclostrobin, were prepared via a miniemulsion polymerization, providing an aqueous NC dispersion with adjustable drug loading and high encapsulation efficiency. The enzyme-triggered fungicide release was demonstrated by in vitro experiments. Thereafter, we injected this aqueous dispersion into the trunks of infected and symptomatic grapevine plants using a ready-made injection system. The NCs were non-phytotoxic and do not release the drug unless an Esca-associated pathogen (Pmi and Pch) secretes lignin-degrading enzymes. Furthermore, a single trunk injection resulted in a significant reduction of Esca symptoms monitored in plants over a period of 5 years. This concept provides as curative treatment against Esca but might be extended as a preventive treatment as no drug is released without an Esca infection. Hence, by transferring the controlled drug delivery approach from medicine to agriculture, we envision establishing an inexpensive and targeted technique for advanced plant protection. This general strategy will be extended for various plant diseases such as plum and peach infections and will contribute to decreasing untoward environmental effects from pollution of agrochemicals.

5 Drug-loaded Lignin Nanocarriers from Methacrylated Lignin: Upscaling and Reaction Variations

Sebastian J. Beckers, Frederik R. Wurm

Parts of the data (method B) will be submitted under the title “Pesticide-loaded Nanocarriers from Lignin Sulfonates – A Promising Tool for Sustainable Plant Protection” in the “European Polymer Journal” (Elsevier).

This study was performed under the scientific guidance of PD. Dr. Frederik Wurm. The experiments and analytics were performed by Sebastian Beckers.

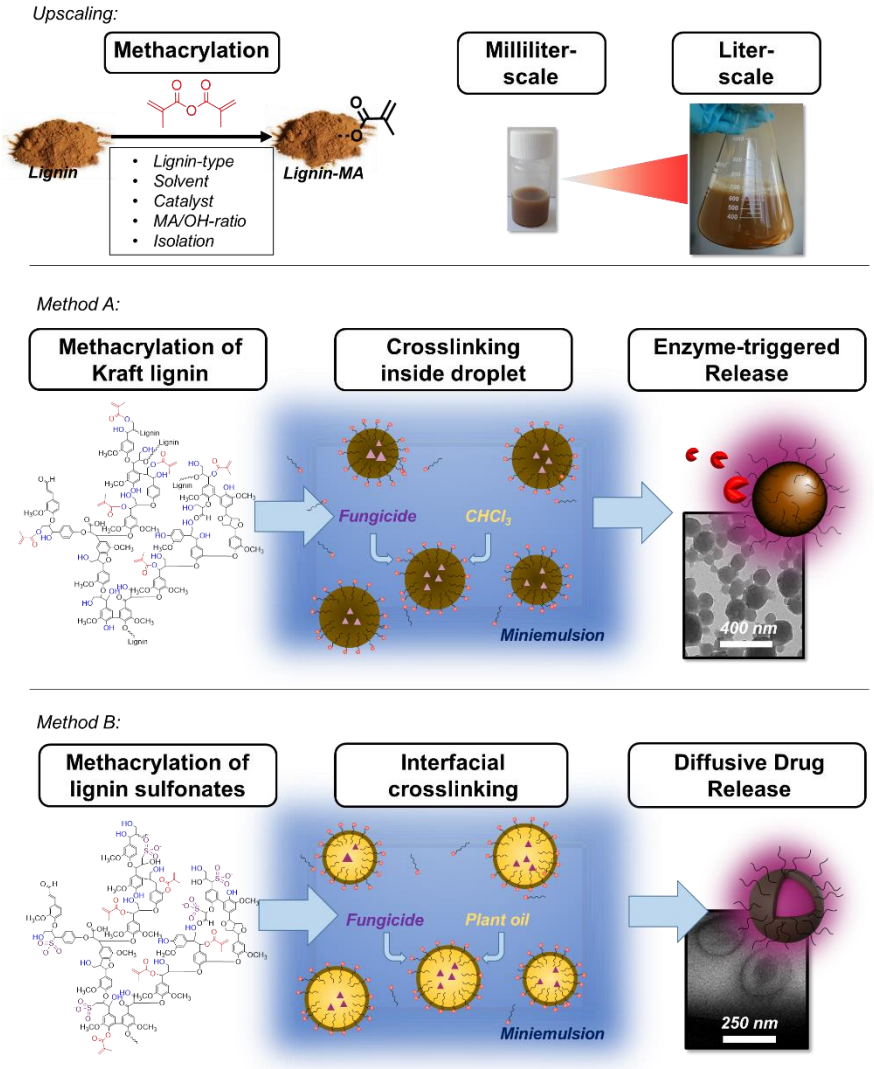

Keywords: *Methacrylation, Nanocarriers, lignin, miniemulsion, drug delivery, agriculture*

5.1 Abstract

This chapter describes the suitability of various technical lignins and the screening of numerous reaction conditions of methacrylation and nanocarrier production. The characterization of Kraft lignin, Organosolv lignin and different lignin sulfonates as well as the esterification with methacrylic anhydride is presented under various reaction conditions. Depending on the solubility of the modified lignin derivatives, we applied them in two different formulation strategies based on an O/W-miniemulsion: A: Hydrophobic methacrylated Kraft lignin was crosslinked inside a dispersed chloroform droplet by different amine or thiol crosslinking agents. The nanocarrier dispersion are tight and long-term stable and release the encapsulated drug only in the presence of lignin-degrading enzymes produced by specific microorganisms like fungi or bacteria. B: Water-soluble and amphiphilic methacrylated lignin sulfonate was crosslinked at a droplet interface forming nanoparticles with a core-shell structure, which allow a controlled release of loaded cargo by diffusion. The release kinetics could be adjusted by the crosslinking density. Both strategies prove the potential of lignin as a feedstock for drug delivery systems for advanced plant protection.

5.2 Introduction

Lignin is the second most abundant biopolymer on earth, which can be extracted from the cell wall of terrestrial plants.[27] Although, the biopolymer is available in a million ton scale, only 2% of the worldwide lignin production is further processed to value added products.[10, 33] Lignin is composed of the three phenolic building blocks 4-hydroxyphenyl-, guaiacyl-, and syringyl alcohol, which are crosslinked in different ratios by a variety of ether-based binding motifs.[10] Especially, the structural complexity of the hyperbranched polyether polyol, which depends on the plant source and extraction method, have hindered the utilization in industrial production processes until now.[27, 34] Nevertheless, recently the plant-based biopolymer received increasing attention as a sustainable carrier material for agricultural formulations, due to its biocompatibility, biodegradability, and its UV-absorbance.[68]

Pesticide formulations usually contain beside active ingredients a variety of adjuvants like surfactants, carrier materials, or thickeners guaranteeing optimal shelf life and performance when distributed on the field. As carrier agent usually inorganic materials like silica, clay minerals and hydroxyapatite, or organic compounds such as chitosan, alginate and cyclodextrins are used.[3] These materials protect the drug against degradation, improve leaf adsorption and allow a safe handling of toxic pesticides. During the last ten years, some studies

reported the preparation of lignin-based nano-/micro-materials which were used as carrier agent for a variety of agrochemicals like insecticides (e.g. avermectin[10]) or herbicides (e.g. atrazine[99]).[68]

Most lignin carrier systems are based on the entrapment of an active ingredient during a controlled lignin precipitation which is induced either by addition of a precipitation agent or by solvent evaporation.[45, 68] A strategy that is more advanced and allows tailoring of the product properties is the encapsulation of pesticides by crosslinking in miniemulsion. In a miniemulsion, nanodroplets are dispersed in a continuous phase and form nanoscopic, individual batch reactors that allow a broad range of reactions to prepare nanomaterials.[26] For example, unmodified lignin sulfonate was crosslinked at the droplet interface of a water-in-oil miniemulsion with toluene diisocyanate to yield loaded lignin-polyurethane nanocarriers with a core-shell structure.[9, 100] In other studies, reactive functional groups were attached to lignin first which enabled a covalent crosslinking subsequently: Chen *et al.* etherified lignin sulfonate with allyl bromide and converted it at the interface by a radically induced thiol-ene reaction in an oil-in-water -miniemulsion.[49] However, although high amounts of radical starter were used to overcome lignin's radical scavenger properties, the nanomaterials released more than 50% of the encapsulated cargo after 24 h indicating a relatively low crosslinking efficiency. Dense nanocarriers were prepared from Kraft lignin, which was esterified with methacrylic anhydride.[7, 101] The methacrylate groups were crosslinked via an aza-Michael addition in fungicide-containing chloroform droplets of an O/W-miniemulsion to produce loaded lignin nanocarriers.[101] What is still unknown is if the approach can be transferred to other lignin feedstock like Organosolv or lignin sulfonates. [34, 102] Particularly, the methacrylation of lignin sulfonate is of great interest, as the functionalized product might allow a more efficient interfacial crosslinking in comparison to the established radical-based crosslinking strategy due to the presence of interfacially active sulfonate groups.

In this chapter, we investigated the functionalization of Kraft and of Organosolv lignin as well as of several lignin sulfonates with methacrylic anhydride. As the functionalized lignin derivatives might be used as a carrier material for sustainable agricultural formulations, the process conditions were further adjusted to be scalable. Two miniemulsion-based strategies were used to prepare loaded nanocarriers: A: The chloroform-soluble methacrylated Kraft lignin was crosslinked in a dispersed chloroform droplet with various crosslinking agents. B: Methacrylated lignin sulfonate was dissolved in the continuous phase (water) and crosslinked at the droplet interface. Both strategies successfully produced lignin nanoparticle dispersions, which were *in situ* loaded with fungicides and which might be used as controlled release systems of agrochemicals for sustainable crop protection.

5.3 Experimental section

Materials

Lithium chloride, triethylamine, methacrylic anhydride, sodiumdodecyl sulfate (SDS), 2-chloro-4,4,5,5-tetramethyl-1,3,2-dioxaphospholane, prothioconazol, endo-*N*-hydroxy-5-norbornene-2,3-dicarboximide, potassium carbonate, chrome(III)acetylacetonate, ninhydrin, 2,2'-(ethylenedioxy)bis(ethylamine) (EDBEA), ethan-1,2-diamine (EDA), ethylenetriamine (DETA), tris(2-aminoethyl)amine (TREN) and 2,2'-ethylenedioxy)bis(ethylthiol), KL (Kraft lignin, alkaline product number: 370959), LSCa (lignin sulfonic acid calcium salt, product number: 47054), LSCH (sugared lignin sulfonic acid sodium salt, product number: 47011) and LSNa2 (lignin sulfonic acid sodium salt, product number: 471038) were obtained from Sigma Aldrich. LSNa1 (lignin sulfonic acid sodium salt, product number: 8999-1) was bought from Carl Roth and LSNa3 (lignin sulfonic acid sodium salt, product number: L0098) was a product of TCI Chemicals. OL (Organosolv lignin, product number: CP8068-03-9) was obtained from Chemical Point. Pyraclostrobin was purchased from Toronto Research Chemicals. Rapeseed oil produced from Rapso was used.

Methods

Nuclear magnetic resonance (NMR) spectroscopy

^{1}H, ^{1}H-^{13}C-HSQC and ^{31}P nuclear magnetic resonance (NMR) spectroscopy was performed at a Bruker AVANCE (USA) spectrometer at 300 MHz. For ^{1}H NMR spectroscopy, 5 mg of the sample was dissolved in 600 µL DMSO-d_6. A ten times higher concentration was used for the identification of lignin binding motifs by ^{1}H,^{13}C-heteronuclear single quantum coherence (HSQC) 2D-NMR spectroscopy. For interpretation, the NMR signals were compared with chemical shifts of lignin model compounds documented in the literature.[31] Lignins hydroxyl groups were quantified by ^{31}P NMR after derivatization with 2-chloro-4,4,5,5-tetramethyl-1,3,2-dioxaphospholane in a $CDCl_3$-pyridine-d_5 (4/6 v/v ratio) mixture in the presence of the internal standard endo-*N*-hydroxy-5-norbornene-2,3-dicarboximide and the relaxation agent Cr(III)acetylacetonate using the method of Balakshin *et al.*.[84]

Fourier transform infrared (FTIR) spectroscopy

Lignin, lignin-MA and crosslinked nanocarriers were analyzed by Fourier transform infrared (FTIR) spectroscopy using a Nicolet iS10 spectrometer with Vertical ATR Accessory. Spectra were recorded between 600 and 4000 cm^{-1}.

For analysis of nanocarriers produced from methacrylated Kraft lignin (strategy A), a dispersion was centrifuged at 14k rpm for 30 min first and the pellet was washed twice with MilliQ water subsequently. The samples were dried in a vacuum oven at 40°C overnight before being analyzed by FTIR spectroscopy.

Nanocarrier dispersions (2 mL) generated from methacrylated lignin sulfonate (strategy B) were washed twice with water (10 mL) to remove non-crosslinked lignin and SDS. Afterwards, the dispersion was washed with cyclohexane (10 mL) To remove excess EDBET by vigorous shaking of the mixture and subsequent centrifugation to fasten the phase separation. Finally, the purified dispersion was freeze-dried.

Size exclusion chromatography (SEC)

The molecular weight of Kraft and Organosolv lignin was determined using dimethylformamide (containing 0.25 g/L of lithium bromide) as an eluent. The measurement was performed at an Agilent 1100 Series (Agilent Technologies 1260 Infinity) as an integrated instrument, including three PSS GRAM columns (1000 / 1000 / 30A) at 60°C and a UV detector (270 nm) at a flow rate of 1 mL/min.

As the most lignin sulfonates were not soluble in DMF, a mixture of a sodium hydroxide solution (0.1 M) and 20% acetonitrile was used as eluent for them instead. The measurement was performed at an Agilent 1100 Series (Agilent Technologies 1260 Infinity) system using two PSS MCX columns (1k, 100k) and a UV detector (270 nm) at a flow rate of 1 mL/min.

Inductively coupled plasma emission spectroscopy (ICP-OES)

The sulfur content of aqueous 0.1 N NaOH solutions containing 1 mg/mL lignin was determined by spectral lines at 180 nm and 182 nm using an Activa M spectrometer from Horiba.

Dynamic light scattering (DLS)

The hydrodynamic diameter of the colloids was measured by DLS with a Zetasizer Nano S90 submicron particle sizer (Malvern Panalytical, UK) at a fixed angle of 90° and a laser diode running at 633 nm.

Transmission electron microscopy (TEM)

The morphology of the nanocarriers prepared according to strategy A was investigated with a JEOL 1400 transmission electron microscope with a LaB6 cathode (JEOL GmbH, Eching, Germany) at an acceleration voltage of 120 kV. Samples were prepared by casting a drop of diluted and purified dispersion on a carbon-coated copper grid (300 mesh, Science Services, Munich, Germany) and then dried at room temperature.

To analyze the morphology of the nanocarriers prepared following strategy B, a TEM specimen was stained with uranyl acetate and a drop of sample solution was placed onto a carbon coated copper grid. A Tecnai F20 device from FEI was used at an acceleration voltage of 200 kV.

High pressure liquid chromatography (HPLC)

Before measurement all samples were passed through a 0.2 µm filter and analyzed by Agilent Eclipse Plus RP18 HPLC system using THF: water/ 0.1 wt% as mobile phase and a TFA-gradient. The injection volume was 10 µL and the column temperature maintained at 20 ºC. The analysis was performed at a flow rate of 0.2 mL/min with the UV detector at 280 nm for Pyraclostrobin, and 260 nm for Prothioconazol. The non-encapsulated fungicide in the supernatant was calculated according the following equation:

Equation 5.1

$$EE\% = \frac{\mathrm{c(cargo\ initial)} - \mathrm{c(cargo\ in\ supernatant)}}{\mathrm{c(cargo\ initial)}} \cdot 100\%$$

Fluorescence spectroscopy

The encapsulation of Bodipy 326/515 was detected by its fluorescence (ex.: 326 nm; em.: 515 nm) using a TECAN infinite M1000 Microplate reader.

Tensiometry (spinning drop method)

The interfacial tension between cyclohexane and water was measured with a spinning drop tensiometer (SVT 20N from DataPhysics). A glass capillary was filled with cyclohexane and a small droplet of MilliQ water (as a reference) or an aqueous solution containing 5 mg/mL of methacrylated lignin sulfonate. Then the capillary was placed horizontally and equilibrated at 20°C for 10 min under rotation at 8000 rpm until a cylindrical droplet at the axis of rotation was obtained. The interfacial tension based on the theory of Cayias, Schechter, and Wade was used for data analysis.

Sol-gel-test

To determine the percentage of crosslinked lignin-MA, 1 mL of nanocarrier suspension was centrifuged at 14k rpm for 30 min first. After removal of the clear supernatant, the pellet was dried at 40°C in a vacuum oven, and 0.5 mL chloroform was added to dissolve insufficiently crosslinked methacrylated lignin. The mixture was centrifuged again and the mass of the chloroform-insoluble solid was quantified gravimetrically after drying.

Ninhydrin assay

To quantify the conversion of the amine crosslinkers after 24 h, 0.5 mL of a 10 mg/mL dispersion was centrifuged at 14k rpm for 30 min to separate the nanocarriers. Afterwards, 50 µL of the clear supernatant was added to 450 µL of a 6 mg/mL ninhydrin-ethanol solution and the reaction was allowed to proceed for 1 h at 25°C. Finally, Ruhemans purple, correlating with the number of primary amines, was quantified at 570 nm using a TECAN infinite M1000 Microplate reader.

Determination of encapsulation efficiency and drug release

To determine the encapsulation efficiency two approaches were used:

(A) 0.5 mL of a 10 mg/mL nanocarrier suspension was centrifuged at 14k rpm for 30 min and the non-encapsulated amount cargo was quantified from the supernatant.

(B) 0.25 mL cyclohexane was added to 0.25 mL of a loaded nanocarrier suspension. The two-phase mixture was shaken for 30 seconds to transfer free cargo, which could not be encapsulated, to the cyclohexane phase. To fasten the phase separation the mixture was centrifuged (14k rpm, 30 min) subsequently.

To record the release kinetics, the encapsulation efficiency was measured after two, four and seven days using method B. Bodipy 326/515 transferred to the cyclohexane phase was quantified photometrically by its fluorescence whereas Prothioconazol and Pyraclostrobin were quantified by HPLC.

Synthesis

Synthesis of methacrylated lignin

Kraft lignin, Organosolv lignin and different lignin sulfonates were synthesized using a slightly modified protocol of Yiamsawas *et al.*[7]: 1 g of lignin (for number of hydroxyl groups see Table 5.2) was added to 15 mL dimethyl formamide (DMF) and 1.27 LiCl. Kraft lignin (KL, Sigma Aldrich, product number: 370959), Organosolv lignin (OL, Chemical Point, product number: CP8068-03-9) and sugared sodium lignin sulfonate (LSCH, Sigma Aldrich, product number: 47011) dissolved completely at 65°C after 30 min, whereas the lignin sulfonates LSNa1-3 (LSNa1: Carl Roth, product number: 8999-1; LSNa2: Sigma Aldrich, product number: 471038; LSNa3: TCI Chemicals, product number: L0098) and LSCa (Sigma Aldrich, product number: 47054) remained a suspension. Subsequently, 0.45 mL triethylamine and 1.7 eq. methacrylic anhydride (relative to lignin's hydroxyl groups) were added dropwise and the reaction was allowed to proceed at 65°C overnight under stirring. The mixture was precipitated into 300 mL isopropanol and isolated by centrifugation (10k rpm, 30 min). The solid was

washed further two times. Finally, the product was dried at 40°C under vacuum. Yields and hydroxyl group conversion (determined by ^{31}P NMR[84]) are summarized in Table 5.1. To increase the yield of methacrylated lignin sulfonates, instead of isopropanol, diethyl ether can be used for precipitation. Typically yields of more than 95% were achieved.

The process described above was optimized regarding safety issues and production costs To allow a further upscaling of the reaction: 1 g Kraft lignin (6.64 mmol hydroxyl groups) and 0.05 mg (0.36 mmol) K_2CO_3 was added to 15 mL DMSO. The mixture was heated to 65°C under stirring until the Kraft lignin was completely dissolved. Afterwards 1.55 mL (10.39 mmol) methacrylic anhydride was added dropwise and the reaction was allowed to react at 65°C overnight. Methacrylated Kraft lignin was precipitated in 300 mL of a 0.1 M HCl solution and isolated by centrifugation subsequently. The solid was washed further two times until it was finally dried at 40°C in the vacuum oven. Typically, a yield of 70% and a conversion of hydroxyl groups of > 90% was achieved.

Table 5.1: Varied process parameters to synthesize methacrylated lignin by esterification of lignin with methacrylic anhydride. The conversion of hydroxyl groups was determined with ^{31}P NMR after phosphorylation. To allow a comparison, all reaction products were isolated by precipitation in isopropanol.

No.	Lignin	Solvent	Eq. (Anhydride)	Base	X% arom OH	X% aliph OH	X% total OH	n(MA) / mmol g^{-1}	Yield%
1	KL	DMF	1.70	TEA	100	73	90	6.0	52
2	OL	DMF	1.70	TEA	100	84	94	4.2	70
3	LSCH	DMF	1.70	TEA	90	89	90	18.1	11
4	LSCa	DMF	1.70	TEA	95	93	95	12.0	35
5	LSNa1	DMF	1.70	TEA	100	95	96	12.7	33
6	LSNa2	DMF	1.70	TEA	73	72	73	5.8	33
7	LSNa3	DMF	1.70	TEA	90	87	90	17.9	22
8	KL	DMF	1.00	TEA	100	48	81	5.4	39
9	KL	DMF	0.75	TEA	92	35	72	4.8	51
10	KL	DMF	0.50	TEA	81	34	64	4.3	62
11	KL	DMF	0.35	TEA	61	25	48	3.2	69
12	KL	DMF	0.25	TEA	56	26	45	3.0	72
13	KL	DMF	0.17	TEA	47	24	39	2.6	79
14	KL	DMF	0.10	TEA	41	23	34	2.3	84
15	KL	DMSO	1.70	TEA	94	85	91	6.0	44
16	KL	Acetone	1.70	TEA	100	80	89	6.2	55
17	KL	$CHCl_3$	1.70	TEA	100	80	89	6.2	26
18	KL	Pyridine	1.70	-	100	96	99	6.6	42
19	KL	DMF	1.70	K_2CO_3	99	68	88	5.8	47

Preparation of lignin nanocarriers from methacrylated Kraft lignin (Strategy A)

Analog to the method described in chapter 4, crosslinked lignin nanocarriers were prepared by a combination of O/W-miniemulsion polymerization and solvent evaporation. Typically, 50 mg of methacrylated lignin (0.30 mmol methacrylic groups) and 10 mg pyraclostrobin were dissolved in 0.5 g of chloroform. The solution was then mixed vigorously for 1 min at 20k rpm with 4.5 g of 2 mg/mL SDS solution at 0°C using an IKA Ultraturrax disperser to form a pre-emulsion. The emulsion was sonicated in the next step for 3 min (1/4 inch tip, 70% amplitude, 20 s ultrasound followed by 10 s pause) under ice-cooling to prevent any solvent evaporation. Afterward, 0.5 mL of crosslinker solution was added dropwise containing 1.1 equivalents of amine or thiol groups relative to lignin's methacrylate groups. 2,2'-(Ethylenedioxy)bis(ethylamine) (EDBEA), ethan-1,2-diamine (EDA), ethylenetriamine (DETA), tris(2-aminoethyl)amine (TREN) or 2,2'-ethylenedioxy)bis(ethylthiol) were tested as crosslinking agents. The reaction was allowed to proceed at 50°C for 15 h under stirring (250 rpm). In a last step, chloroform was evaporated by stirring the opened reaction vessel overnight at room temperature. Finally, the volume was adjusted to 10 mL by addition of water to yield a ca. 10 mg/mL nanocarrier dispersion. The nanocarriers were characterized by dynamic light scattering (DLS) and transmission electron microscopy (TEM).

Preparation of lignin nanocarriers from methacrylated lignin sulfonate (Strategy B)

Crosslinked lignin nanocarriers were prepared by interfacial crosslinking of an O/W-miniemulsion. Typically, 50 mg of methacrylated lignin sulfonate (LSNa1-MA; 0.64 mmol methacrylated groups) and 44 µL (0.32 mmol) triethylamine were dissolved in 5 mL MilliQ water. Afterwards, a solution of 122 µL cyclohexane or rapeseed oil, 56 µL (0.69 mmol) 2,2'-ethylenedioxy)bis(ethylthiol) (EDBET) and a hydrophobic cargo like prothioconazol (2.5 mg) or Bodipy 326/515 (0.0122 mg; using a stock solution) was added. Immediately, the two-phase mixture was sonicated for 3 min (1/2 inch tip, 70% amplitude, 20 s ultrasound followed by 10 s pause) under ice-cooling to prevent premature crosslinking. Subsequently, the reaction was allowed to proceed for 24 h at 50°C under stirring to yield a colloidally stable, brownish dispersion. The nanocarriers obtained were characterized by dynamic light scattering (DLS) and scanning electron microscopy (SEM).

For purification, the dispersion was centrifuged at 4000 rpm for 30 min. The obtained yellowish pellet was washed with water twice to remove non-crosslinked methacrylated lignin sulfonate and free drug. A slightly yellowish dispersion was obtained.

5.4 Results and Discussion

Characterization of different lignin feedstock

The implementation of lignin in industrial production processes is hindered especially by its structural diversity. Functionalities, binding motifs, and molecular weight can strongly vary between softwood, hardwood, or grass lignin and are even more diverse using complex feedstock mixtures like agricultural waste.[10, 27, 34] Next to the lignin source, the chemical properties of the polymer strongly depend on the method applied for lignin isolation (Table 5.2). To find the optimal starting material to produce lignin nanocarriers, Kraft lignin (KL, Sigma Aldrich, product number: 370959), Organosolv lignin (OL, Chemical Point, product number: CP8068-03-9) and different lignin sulfonates (Sodium salts: LSNa1: Carl Roth, product number: 8999-1; LSNa2: Sigma Aldrich, product number: 471038; LSNa3: TCI Chemicals, product number: L0098; calcium salt: LSCa, Sigma Aldrich, product number: 47054; "sugared" sodium salt: LSCH, Sigma Aldrich, product number: 47011) were characterized regarding to their chemical structure and properties, before they were investigated for nanocarrier production.

Kraft lignin: Kraft lignin is generated as a side product in the paper industry. During the Kraft or sulfate process, hemicellulose and lignin are solubilized in a solution of sodium hydroxide (NaOH) and sodium sulfite (Na_2S) as "black liquor" and are separated from the insoluble cellulose fibers.[34] By dissolution of carbon dioxide or hydrochloric acid, the process could potentially yield 55-90 million tons of lignin by precipitation yearly. However, as 98% of the produced Kraft lignin is burned for energy generation, Kraft lignin is an expensive raw material for the chemical industry due to a relatively low availability on the market.[33, 34, 102]

The here investigated Kraft lignin (KL, Sigma Aldrich, product number: 370959) was soluble only in highly polar solvents like DMF, DMSO, pyridine or alkaline water (pH > 8). After derivatization with 2-chloro-4,4,5,5-tetramethyl-1,3,2-dioxaphospholane using the method of Balakshin *et al*., ^{31}P NMR revealed 0.45 mmol/g carboxyl and 6.64 mmol/g hydroxyl groups (61% phenolic and 33% aliphatic, Table 5.2, Figure 5.1). Furthermore, guaiacyl was found as the dominating phenylpropanoid by HSQC 2D-NMR spectroscopy (Figure 5.6).[31] Next to the main binding motif β-O-4-aryl ether, in particular phenylcoumaran but also resinol was identified. These findings are typical for softwood, which is mostly used as cellulose feedstock in the paper industry.[33] Furthermore, ICP-OES showed that KL contains 0.52 mmol/g sulfur, which results from the nucleophilic addition of HS^--ions during the Kraft pulping introducing thiol moieties to the lignin backbone (Table 5.2).[27]

Lignin sulfonates: With an annual availability of 7 million tons on the market, lignin sulfonates are more available and therefore less expensive than Kraft lignin.[34, 102] The

biopolymer is produced via the so-called sulfite process, in which wood pulp is treated with aqueous solutions of sulfite (SO_3^{2-}) or bisulfite (HSO_3^-) with various counter ions like sodium (LSNa1: Carl Roth, product number: 8999-1; LSNa2: Sigma Aldrich, product number: 471038; LSNa3: TCI Chemicals, product number: L0098, LSCH: Sigma Aldrich, product number: 47011) or calcium (LSCa: Sigma Aldrich, product number: 47054). During the treatment, lignin is solubilized by sulfonylation, enabling an easy separation from the water-insoluble cellulose. With the negatively charged sulfonate groups, lignin sulfonates are approved as emulsifiers e.g. in agrochemical, dye, pigment or animal feed formulations in Europe.[34]

For all investigated lignin sulfonates the number of sulfonic acid groups was estimated by their sulfur content quantified by ICP-OES to be 1.6 – 2.0 mmol/g (Table 5.2). Typically, lignin sulfonates exhibit high water-solubility in acidic as well as in alkaline media but were insoluble in most organic solvents. The only exception was the sugared lignin sodium sulfonate (LSCH), which was also soluble in polar solvents like DMSO and DMF. As all tested lignin sulfonates showed a relatively high percentages of aliphatic hydroxyl groups (e.g. up to 16.66 mmol/g for LSCH), most likely the materials contained more hemicellulose residues in comparison to KL and OL (Table 5.2). The significant difference between LSNa1, 2, and 3 regarding their total hydroxyl number but also in the varying ratio between phenolic and aliphatic OH-moieties, underlines the structural diversity of the material even when isolated under comparable extraction conditions.

Organosolv lignin: Organosolv lignin is generated by extraction of biomass with organic solvents like ethanol, methanol, acetone, or acetic acid. As the isolation is comparably mild, OL is less structurally altered during the extraction and is therefore more alike to native lignin. As the process includes high solvent recovery cost though, no pilot plant was operated longer than 5 years so that the technology has not been established in industrial-scale production processes yet.[27] Therefore, Organosolv lignin is more expensive than most Kraft lignins or lignin sulfonates.

The herein used Organosolv lignin (OL, Chemical Point, product number: CP8068-03-9) exhibited with 4.48 mmol/g the lowest number of hydroxyl groups but with 2.03 mmol/g the highest amount of carboxyl groups. These findings correlated with the less intense $\nu(OH_{arom.})$-band at 3214 cm^{-1} and a strong $\nu(C{=}O, _{carboxyl})$-band at 1700 cm^{-1} in the FTIR spectra (Figure 5.3). According to HSQC NMR spectroscopy, OL was mainly composed of guaiacyl- and syringyl units. The β-arylether linkage was identified as the main binding motif, which is typical for lignin obtained by extraction of hardwood (Figure 5.6).

Table 5.2: Structural properties of Kraft lignin, Organosolv lignin and several lignin sulfonates. The hydroxyl and carboxyl groups were determined with ^{31}P NMR after phosphorylation.[84] ICP-OES was used to quantify the sulfur content.

	Kraft lignin	Organsolv lignin	Lignin sulfonates (LS)				
Structure							
Code	**KL**	**OL**	**LSCa**	**LSCH**	**LSNa1**	**LSNa2**	**LSNa3**
Supplier	Sigma Aldrich (370959)	Chemical Point (CP8068-03-9)	Sigma Aldrich (47054)	Sigma Aldrich (47011)	Carl Roth (8999-1)	Sigma Aldrich (471038)	TCI (L0098)
c(OH) total mmol/g	6.6	4.5	12.6	20.2	13.2	8.1	19.9
c(OH) arom mmol/g	4.3	2.8	4.9	3.6	1.7	2.3	4.5
c(OH) aliph mmol/g	2.4	1.6	7.8	16.7	11.5	5.9	15.4
c(COOH) mmol/g	0.5	2.0	0	0	0	0	0
Sulfur mmol/g	0.5	0	2.7	1.6	1.6	2.0	1.9
Solubility	DMF, Pyridine, DMSO, Alkali	Versatile org. solvents	Water (pH 0-14)	Water (pH 0-14) DMF, DMSO	Water (pH 0-14)		

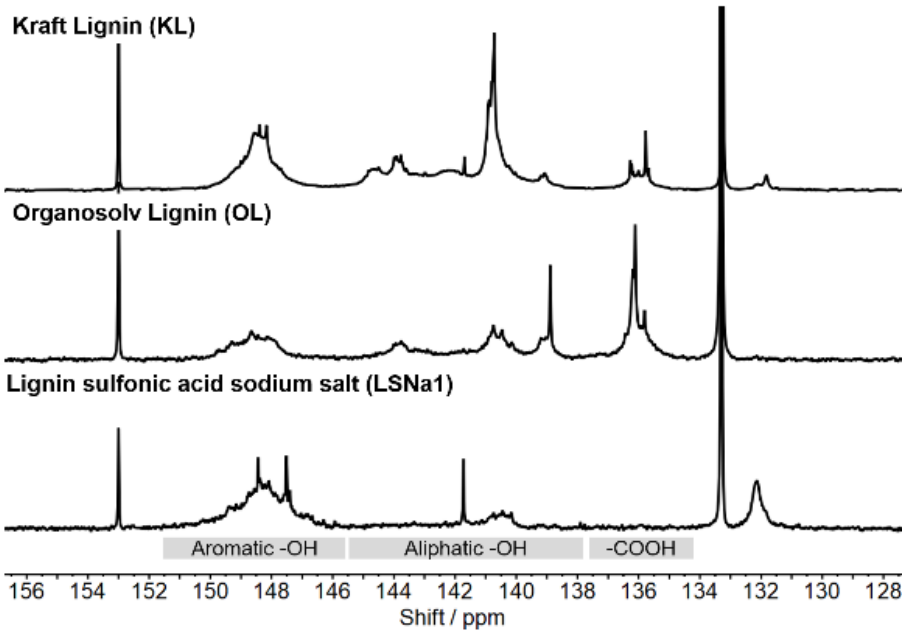

Figure 5.1: ^{31}P NMR spectra (300 MHz, 298 K, $CDCl_3$/pyridine-d_5) of different lignin batches after derivatization with 2-chloro-4,4,5,5-tetramethyl-1,3,2-dioxaphospholane (153 ppm) in the presence of a standard (133 ppm) using the method of Balakshin *et al.*. By integration, the amount of aromatic and aliphatic hydroxyl groups as well as carboxylic acids were quantified.[84] The following lignins were investigated: KL (Kraft lignin, Sigma Aldrich, product number: 370959), LSNa1 (lignin sulfonic acid sodium salt, Carl Roth, product number: 8999-1), OL (Organosolv lignin, Chemical Point, product number: CP8068-03-9).

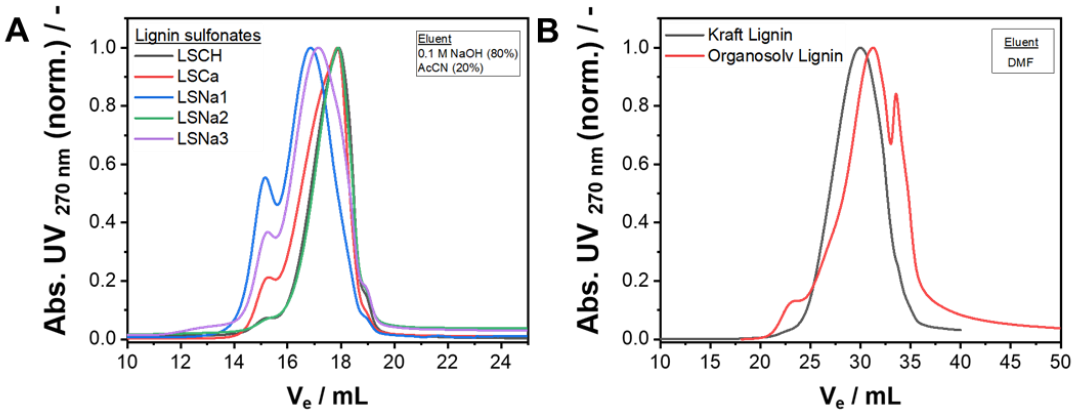

Figure 5.2: (A) SEC elugrams of different lignin sulfonates using a mixture of 0.1 M NaOH and acetonitrile as an eluent. The lignin sulfonates are abbreviated as follows: LSCH (Sugared lignin sulfonic acid sodium salt, Sigma Aldrich, product number: 47011), LSCa (Sulfonic acid calcium salt, Sigma Aldrich, product number: 47054), LSNa1-3 (Sulfonic acid sodium salts,1: Carl Roth, product number: 8999-1; 2: Sigma Aldrich, product number: 471038; 3: TCI Chemicals, product number: L0098). (B) SEC elugrams of KL (Kraft Lignin, Sigma Aldrich, product number: 370959) and OL (Organosolv lignin, Chemical Point, product number: CP8068-03-9) using DMF as an eluent.

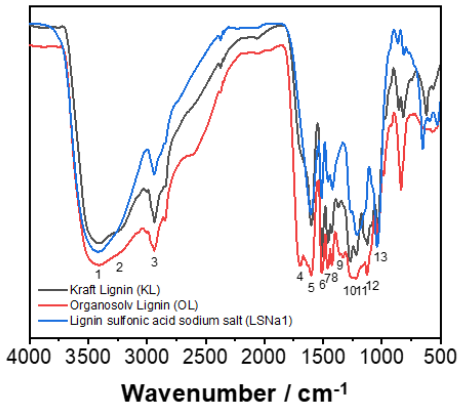

No.	Wavenumber / cm^{-1}	Band origin
1	3414	O-H stretch; Aliphatic
2	3214	O-H stretch; Aromatic
3	2935	CH- stretch; Methyl
4	1700	C=O stretch, Carboxylic
5	1608	Aromatic skeletal stretch
6	1514	Aromatic skeletal vibration
7	1460	CH deformation; asymmetric in CH_3 und CH_2
8	1424	Aromatic skeletal vibrations & C-H in plane deformation
9	1368	Aliphatic C-H stretch, Phenolic OH
10	1270	C=O stretch
11	1222	C-C, C-O, C=O stretch
12	1122	Aromatic CH in plane deformations; secondary alcohols, C=O stretch
13	1044	Aromatic CH in plane deformation

Figure 5.3: Structural analysis of KL (Kraft lignin, Sigma Aldrich, product number: 370959), LSNa1 (lignin sulfonic acid sodium salt, Carl Roth, product number: 8999-1) and OL (Organosolv lignin, Chemical Point, product number: CP8068-03-9) by FTIR spectroscopy including a list with interpretations of the respective bands.[105]

Methacrylation of different lignin types

To prepare drug-loaded lignin nanocarriers, we functionalized Kraft, Organosolv lignin, and different lignin sulfonates with reactive methacrylate groups by esterification with methacrylic anhydride (Figure 5.4). Yiamsawas *et al.* reported the methacrylation of Kraft lignin using an excess of methacrylic anhydride (1.7 eq. with respect to lignin's OH-groups), triethylamine (TEA) as a catalyst, and DMF as a reaction solvent (conditions summarized in Table 5.3 at the end of the chapter).[7] To find the optimal lignin feedstock to produce lignin nanocarriers, these reaction conditions were adapted for the modification of Organosolv lignin and lignin sulfonates.

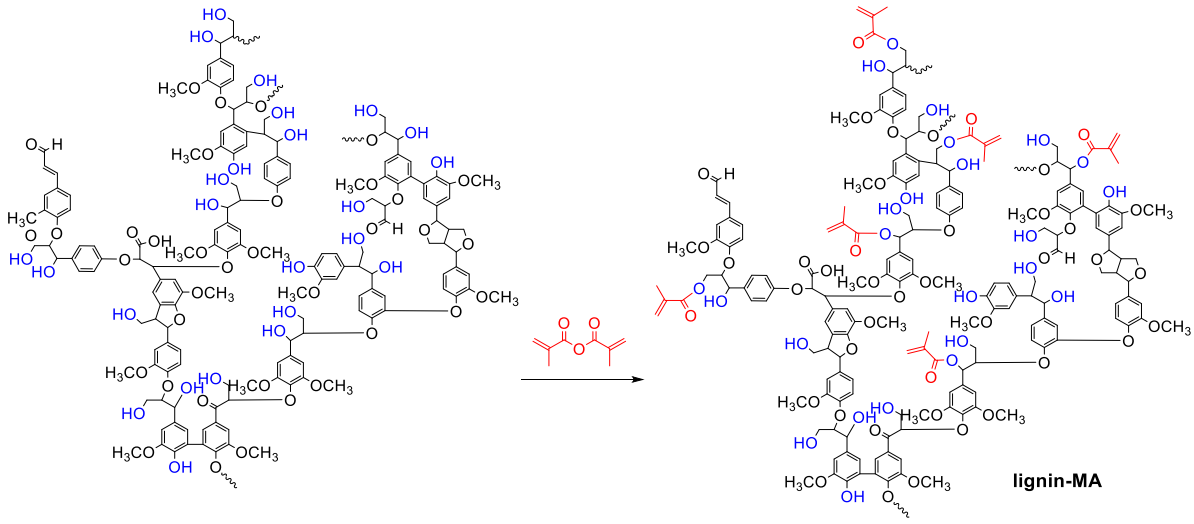

Figure 5.4: Functionalization of lignin with methacrylic anhydride. The shown chemical structure represents typical lignin binding motifs.

In the case of KL (Kraft lignin, Sigma Aldrich, product number: 370959), OL (Organosolv lignin, Chemical Point, product number: CP8068-03-9) and LSCH (sugared sodium salt lignin sulfonate, Sigma Aldrich, product number: 47011) the reaction was performed in solution, whereas the lignin sulfonates LSCa (calcium salt lignin sulfonate, Sigma Aldrich, product number: 47054) and LSNa1-3 (sodium salt lignin sulfonates, LSNa1: Carl Roth, product number: 8999-1; LSNa2: Sigma Aldrich, product number: 471038; LSNa3: TCI Chemicals, product number: L0098) had to be functionalized in suspension, due to their insolubility in organic solvents. After the reaction, ^{1}H-^{13}C-HSQC 2D-spectroscopy indicated a successful methacrylation of all lignin types by two signals at 6.5-5.5 ppm (^{1}H) and 130-125 ppm (^{13}C) belonging to the C=C double bond of the methacrylate group. Correlating with this, signals of several binding motifs such as of β-O-4-aryl ether and phenylcoumaran shifted in comparison to spectra of unmodified lignin, whereas groups like the methoxy or the pinoresinol moiety that cannot be etherified remained unchanged (Figure 5.6). The degree of functionalization was determined by ^{31}P NMR after phosphorylation of the reaction product using the method of Balakshin *et al.* (Figure 5.5).[84] In line with Yiamsawas et al, 90% fewer hydroxyl groups were observed after esterification of KL with methacrylic anhydride in comparison to pristine lignin, proving the attachment of 6.0 mmol methacrylate groups per gram product. The phenolic hydroxyl groups were converted completely, whereas 27% of the aliphatic groups remained not functionalized. Very similar observations were made, replacing KL with Organosolv lignin or lignin sulfonates. Almost all synthesized products showed a degree of functionalization of more than 90%. However, in contrast to KL, only less than 10% aliphatic hydroxyl groups did not react during the methacrylation using OL, LSCa, LSNa1 or 2 indicating a slightly higher reactivity. As lignin sulfonates bear twice to three times more hydroxyl groups per gram in comparison to KL or OL, a significantly higher number of methacrylate groups (12 - 18 mmol/g) was attached absolutely. The only exception was LSNa2 with a total degree of functionalization of only 73%, which resulted in 5.8 mmol/g attached methacrylate groups. Although their lower nucleophilicity, a higher conversion of phenolic than aliphatic hydroxyl groups was observed independent on the lignin type. One explanation might be an easier steric accessibility.

To confirm the chemical modification of lignin, the products were characterized by SEC and FTIR spectroscopy. For all modified lignin derivatives, the molar mass distribution in SEC shifted to lower elution times (i.e. higher molecular weights) relative to the pristine lignin (Figure 5.7). FTIR spectroscopy showed a decreased $\nu(OH_{arom.})$-band at 3214 cm^{-1} and additional bands at 1736 cm^{-1} and 1668 cm^{-1}, belonging to the C=C and C=O stretching band of the attached methacrylic groups respectively (Figure 5.17). Likewise, we found that methacrylated Kraft and Organosolv lignin was well-soluble in chloroform and dichloromethane, while the pristine KL and OL was insoluble in both solvents.

Hence, the functionalization increased the hydrophobicity of the material, indicating a reduction of hydroxyl groups, and thus also of hydrogen bonds. Indeed, also the lignin sulfonates exhibited a lower solubility in water after methacrylation but the modification was not enough, to guarantee the solubility in organic solvents.

For isolation, all modified lignin derivatives were precipitated from the reaction mixture into isopropanol following the protocol of Yiamsawas *et al.*.[7] In line with the literature, methacrylated Kraft lignin (KL-MA) was obtained with yields of ca. 52%. In contrast to this, yields of 70% or 10-30% were measured using Organosolv lignin or lignin sulfonates as a starting material respectively (Table 5.1, No. 1-7). To increase the yield of the methacrylated lignin sulfonates diethyl ether can be used instead of isopropanol. All sulfonates precipitated almost completely (> 96%) from the reaction mixture.

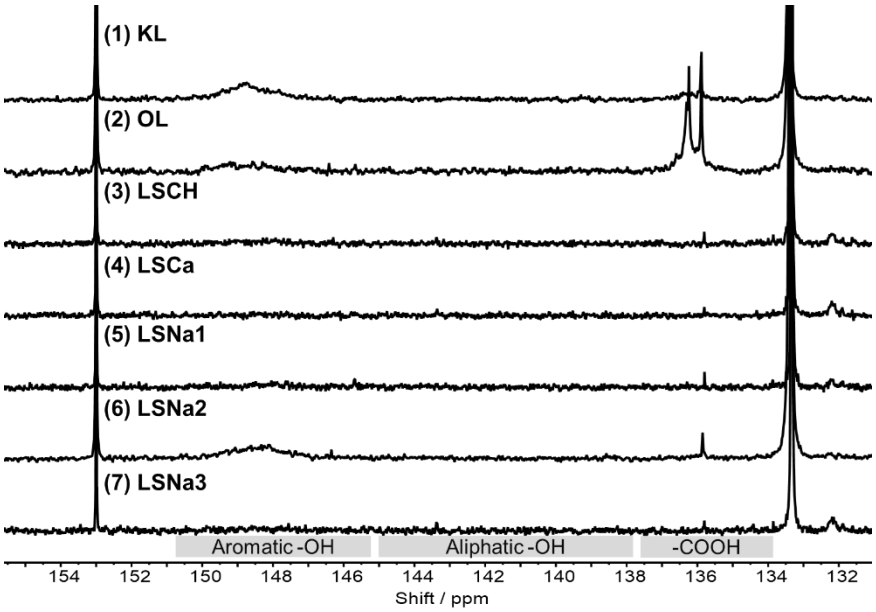

Figure 5.5: ^{31}P NMR spectra (300 MHz, 298 K, $CDCl_3$/pyridine-d_5) of methacrylated lignins after phosphorylation according the method of Balakshin *et al*.[84] Different lignin types were used as starting material: Kraft lignin (KL, Sigma Aldrich, product number: 370959), Organosolv lignin (OL, Chemical Point, product number: CP8068-03-9) and different lignin sulfonates (LSCH: Sigma Aldrich, product number: 47011; LSCa: Sigma Aldrich, product number: 47054, LSNa1: Carl Roth, product number: 8999-1; LSNa2: Sigma Aldrich, product number: 471038; LSNa3: TCI Chemicals, product number: L0098). The numbers refer to the entries in Table 5.1.

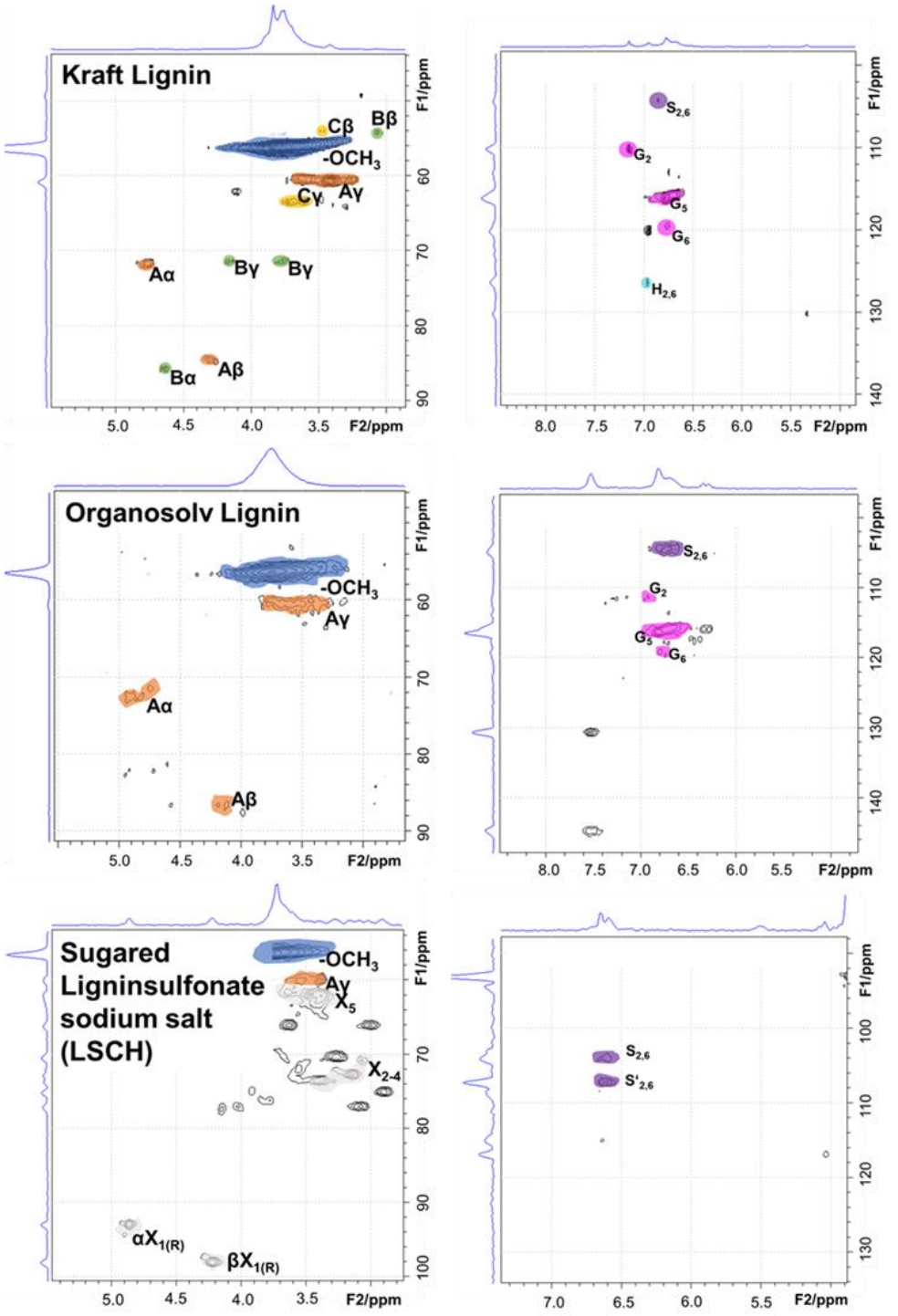
Kraft Lignin
Cβ
Bβ
-OCH3
Cγ
Aγ
Aα
Bγ
Bγ
Bα
Aβ
S2,6
G2
G5
G6
H2,6
Organosolv Lignin
-OCH3
Aγ
Aα
Aβ
S2,6
G2
G5
G6
Sugared Ligninsulfonate sodium salt (LSCH)
-OCH3
Aγ
X5
X2-4
αX1(R)
βX1(R)
S2,6
S'2,6
F1/ppm
F2/ppm

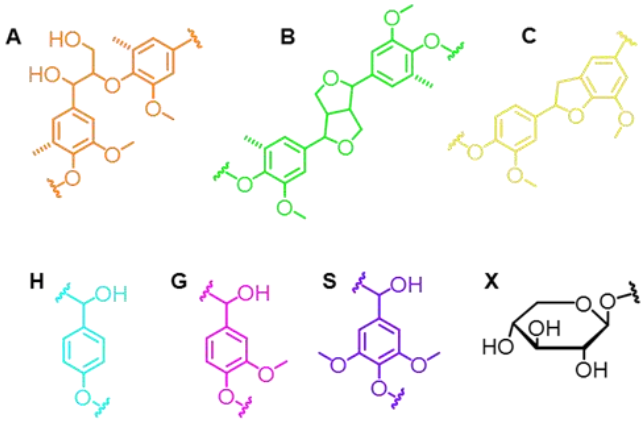
A
B
C
H
G
S
X
HO
OH
OH
OH

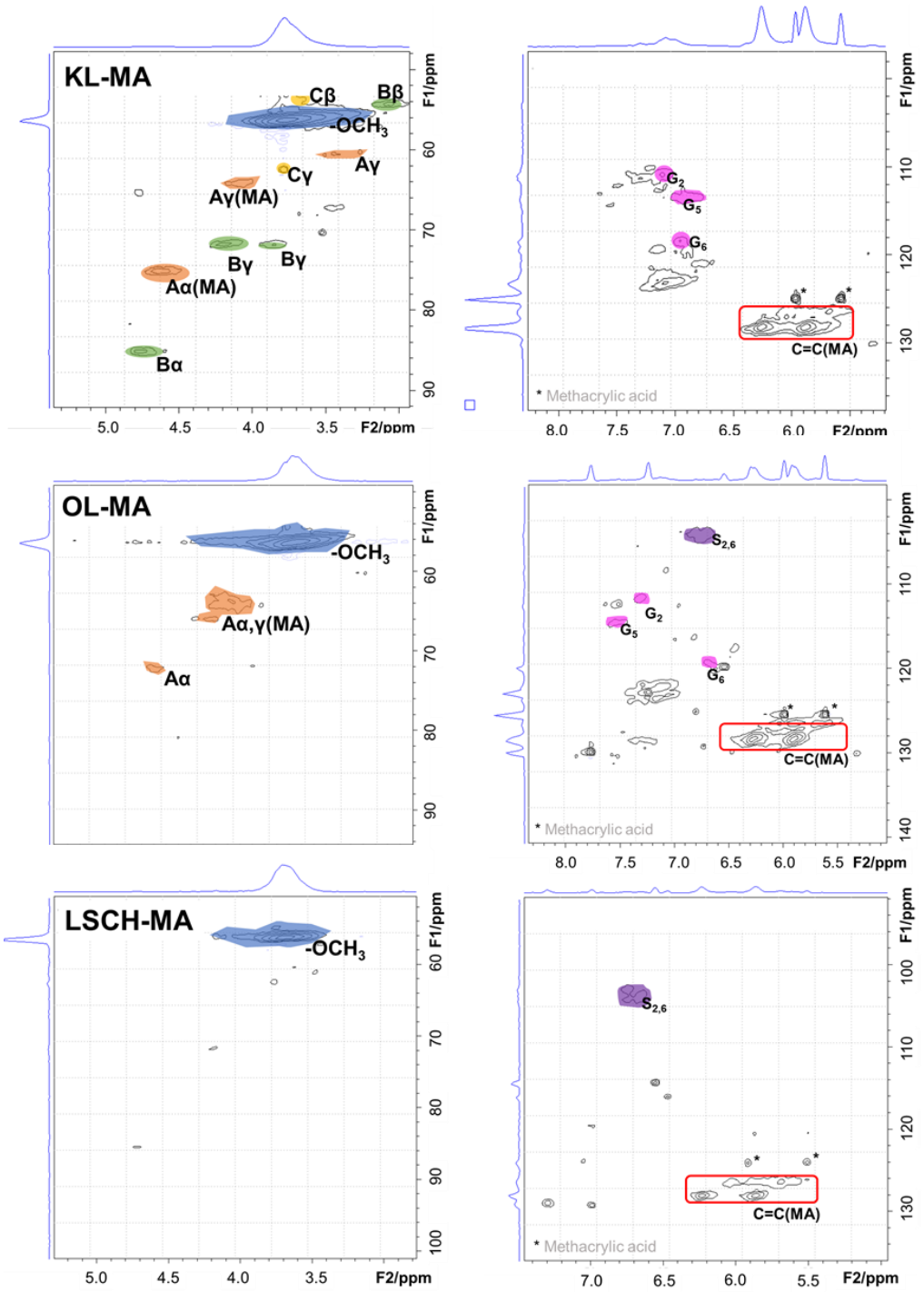

Figure 5.6: HSQC 2D-NMR (300 MHz, 298 K, DMSO-d_6) spectra of KL (Kraft lignin, Sigma Aldrich, product number: 370959), OL (Organosolv lignin, Chemical point, product number: CP8068-03-9) and LSCH (sugared lignin sulfonic acid sodium salt, Sigma Aldrich, product number: 47011) before and after methacrylation The identified binding motifs (A-C) and three phenolic building blocks based on 4-hydroxyphenyl-, guaiacyl- and syringyl alcohol are shown below.

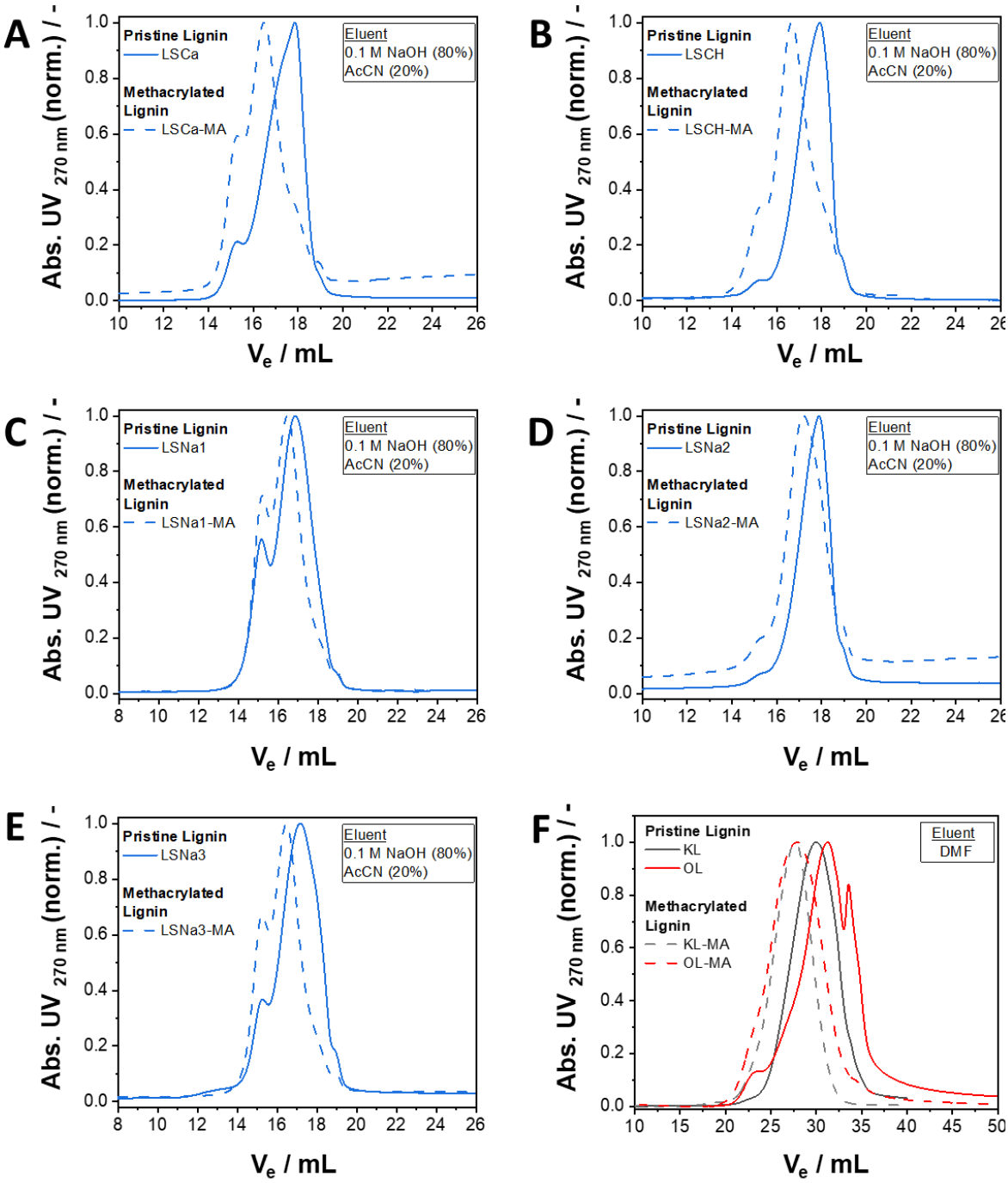

Figure 5.7: SEC elugrams before and after methacrylation using different lignin types as a starting material: Kraft lignin (KL, Sigma Aldrich, product number: 370959), Organosolv lignin (OL, Chemical Point, product number: CP8068-03-9) and different lignin sulfonates (LSCH: Sigma Aldrich, product number: 47011; LSCa: Sigma Aldrich, product number: 47054, LSNa1: Carl Roth, product number: 8999-1; LSNa2: Sigma Aldrich, product number: 471038; LSNa3: TCI Chemicals, product number: L0098).

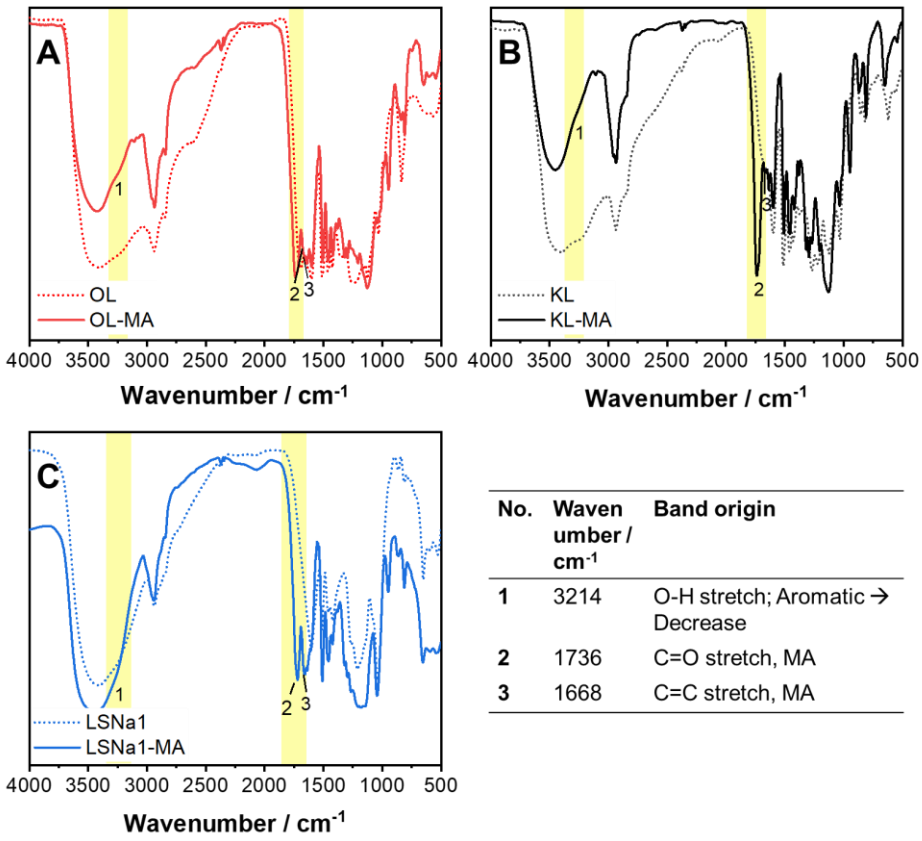

No.	Waven umber / cm^{-1}	Band origin
1	3214	O-H stretch; Aromatic → Decrease
2	1736	C=O stretch, MA
3	1668	C=C stretch, MA

Figure 5.8: FTIR spectra before and after methacrylation of Organosolv lignin (OL), Kraft lignin (KL) and lignin sulfonate (LSNa1). List of additional signals found after functionalization belonging to the attached methacrylate group.

Taken together, these experiments underline that different lignin derivatives (Kraft lignin, Organosolv lignin, and lignin sulfonates) can be methacrylated effectively under various reaction conditions. However, despite of their similar origin, we obtained products strongly differing in their chemical properties. For example, the chloroform / DCM solubility of methacrylated Kraft and Organosolv lignin allows the application as a carrier material for nano-formulations generated by a direct O/W-dispersion analogue to the protocol of Yiamsawas *et al*. However, if methacrylated lignin sulfonates shall be used for nanocarriers production, a different approach is needed (e.g. the polymer must be dissolved either in the continuous phase of an O/W-emulsion or an inverse W/O-approach has to be used).

Optimization of methacrylation conditions

To use methacrylated lignin as carrier material for the formulation of agrochemicals, the functionalization needs to be scalable. This means a safe, sustainable and inexpensive reaction protocol needs to be defined for production on an industrial scale. To simplify the

registration as a formulation in Europe, the process should only rely on raw materials, which had been approved by the “Bundesamt für Verbraucherschutz und Lebensmittelsicherheit” (BVL) as adjuvants previously.

In the original literature procedure established by Yiamsawas *et al.*, DMF was used as a solvent for Kraft lignin (33 mg/mL) to produce methacrylated lignin.[7] However as, DMF is a toxic solvent and hard to remove from the product, due to its high boiling point of 153°C, finding alternative solvents is an essential step to a scalable process with reduced costs but retained effectivity. In addition, alternatives for the alkaline catalyst TEA need to be identified and the amounts of the reactive methacrylic anhydride should be minimized to further increase the process safety and effectivity. Also for the purification, a substitute to the flammable isopropanol would be desirable. For this purpose, we investigated the effects of varying the reaction solvent, the lignin-anhydride ratio, the catalyst, and the precipitation agent on the degree of functionalization and the product yield. The study was performed exemplarily for the methacrylation of Kraft lignin:

(A) Solvent: Pyridine and dimethyl sulfoxide (DMSO) were investigated as alternatives for DMF because KL is well soluble in both solvents. In the original literature process, DMF together with lithium chloride was used, but due to the high solubility of Kraft lignin in pyridine or DMSO, the additive was not necessary. As DMSO is a registered adjuvant for agricultural formulations, a quantitative removal is not essential.[103] However, due to its high boiling point (bp.: 189°C), distillation is still challenging. Furthermore, DMSO is less harmful than DMF, which increases the safety of the process. Analog to the methacrylation in DMF, 91% of lignin’s hydroxyl groups were functionalized, when DMSO was used as a reaction solvent. An even higher degree of functionalization of 99% was reached performing the lignin modification in pyridine (Table 5.1, No. 15, 18; Figure 5.9) without the additional use of triethylamine or lithium chloride. However, pyridine is relatively toxic.[104] Next to DMSO and pyridine, acetone and chloroform were tested as reaction solvents. Both have low boiling points (acetone: 56°C, chloroform: 61°C) which could enable easy recycling after the modification. Acetone is relatively cheap, marginally toxic but dissolves KL only weakly. Therefore, the reaction was performed in a supersaturated acetone solution. Nevertheless, the reaction resulted in a degree of functionalization of almost 90%. In contrast to acetone, chloroform does not dissolve lignin at all and is more harmful. However, as chloroform is immiscible with water, insufficiently functionalized lignin, lithium chloride, methacrylic acid and triethylamine might be removed easily by extraction with alkaline water leaving only the pure product in the organic phase. Although 89% of lignin’s hydroxyl groups were functionalized, the solvent is considered not suitable, as the interfacial active methacrylated KL hindered an efficient phase separation during the product extraction (Table 5.1, No. 16, 17).

In summary, especially DMSO and acetone were found as good alternatives to DMF as they combine low toxicity with a high degree of functionalization. Acetone additionally offers the possibility for recycling but required increased safety standards due to its low boiling and flash point (-20°C) at the same time.

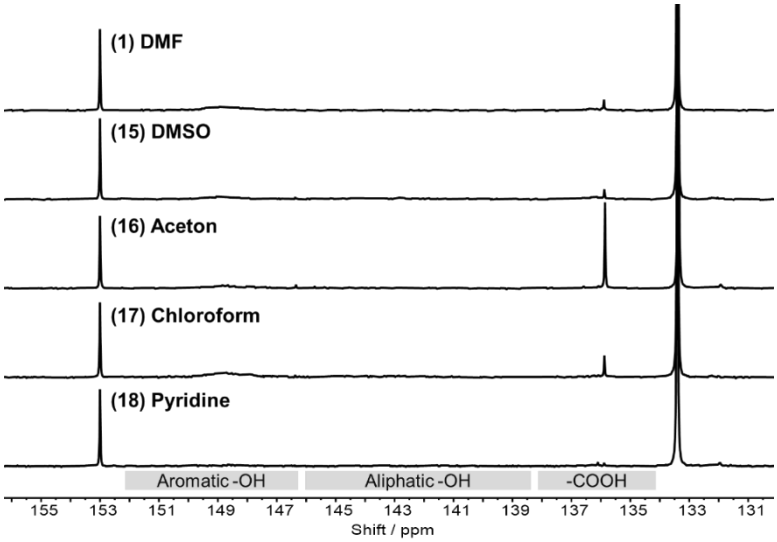

Figure 5.9: ^{31}P NMR spectra (300 MHz, 298 K, $CDCl_3$/pyridine-d_5) of methacrylated lignin after phosphorylation according the method of Balakshin *et al*.[84] The methacrylation was performed in various solvents. As a starting material Kraft lignin (KL, Sigma Aldrich, product number: 370959) was used. The numbers refer to the entries in Table 5.1

(B) Minimization of methacrylic anhydride: To minimize the amount of toxic methacrylic anhydride, we reduced stepwise the ratio between methacrylic anhydride and the hydroxyl groups of KL from 0.1 to 1.7. SEC showed a continuous shift from lower to higher molecular weights with an increasing amount of reagent, indicating the stepwise rising number of methacrylate functional groups attached to lignin's hydroxyl groups (Figure 5.10 and 5.11B). With the increasing degree of functionalization, the material became continuously more hydrophobic and less water-soluble. Only above a degree of functionalization of ca. 80% and a full phenolate conversion a material was obtained, which can be dissolved properly in water-immiscible solvents like chloroform or DCM (Figure 5.11). As the product solubility in these solvents is essential for a later nanocarrier production in an O/W-miniemulsion according to the protocol of Yiamsawas *et al.*, a lignin and methacrylic anhydride ratio of at least in 1 to 1 is considered to be optimal.

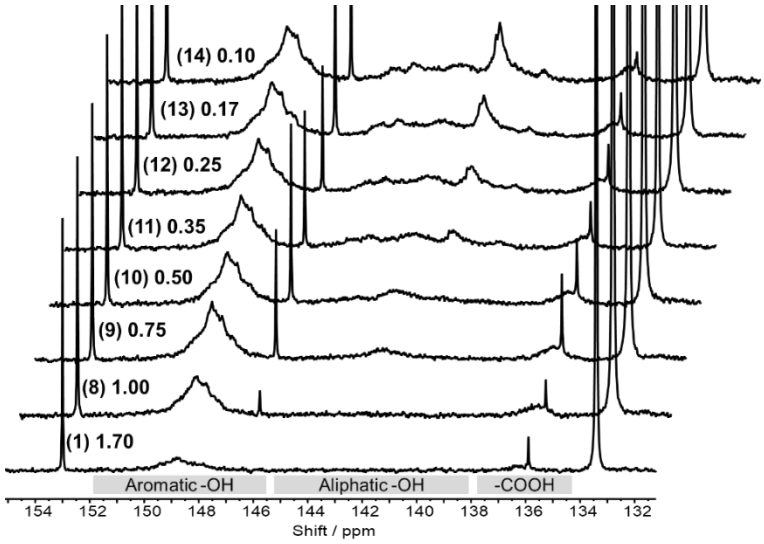

Figure 5.10: ^{31}P NMR spectra (300 MHz, 298 K, $CDCl_3$/pyridine-d_5) of methacrylated lignins after phosphorylation according the method of Balakshin *et al*.[84] The methacrylation was performed using methacrylic anhydride and lignin's hydroxyl groups in various ratios. As a starting material Kraft lignin (KL, Sigma Aldrich, product number: 370959) was used. The numbers refer to the entries in Table 5.1).

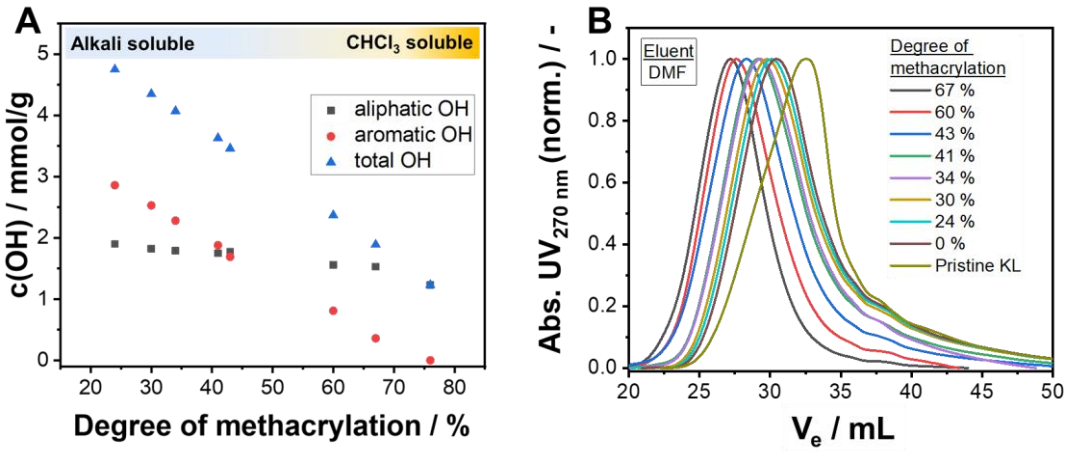

Figure 5.11: A) Number of remaining hydroxyl groups in modified lignin (determined after derivatization by ^{31}P NMR spectroscopy and B) molecular weight distributions measured by SEC after esterification of Kraft lignin with methacrylic anhydride. The degree of functionalization was set by adjusting the ratio between methacrylic anhydride and lignins hydroxyl groups. The products were isolated by precipitation in isopropanol.

(C) Catalyst: To further increase the process safety, the toxic catalyst TEA was replaced against the less harmful and cheaper base potassium carbonate. In contrast to TEA, the latter compound is not soluble in DMF and was therefore suspended in the reaction mixture. Nevertheless, almost analog degrees of modification were achieved: we reached a conversion of 99% phenolates and 68% aliphatic hydroxyl groups yielding an 88% total degree

of functionalization (Figure 5.12). Hence, the compound is a suitable alternative making the process safer and less expensive.

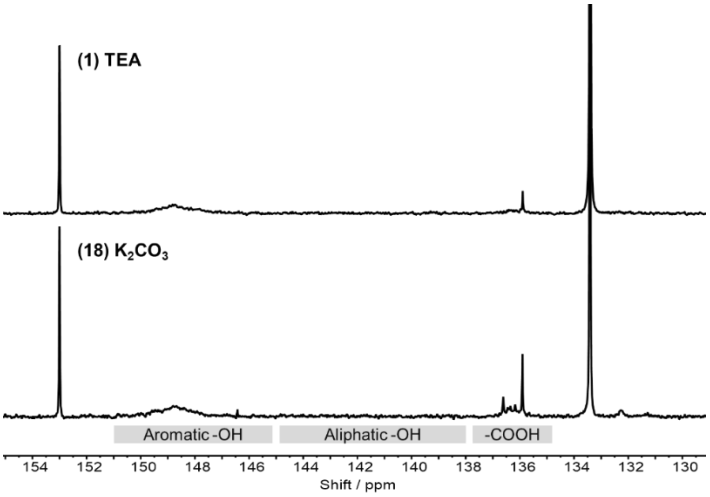

Figure 5.12: ^{31}P NMR spectra (300 MHz, 298 K, $CDCl_3$/pyridine-d_5) of methacrylated lignins after phosphorylation according the method of Balakshin *et al*.[84] The methacrylation using either trimethylamine or K_2CO_3 as a catalyst. As a starting material Kraft lignin (KL, Sigma Aldrich, product number: 370959) was used. The numbers refer to the entries in Table 5.1)

(D) Product isolation and purification: Methacrylated Kraft lignin can be isolated from DMF or DMSO by precipitation and subsequent centrifugation to separate the solid. A yield of typically 50% was achieved using isopropanol as precipitation agent. To optimize the purification process, we replaced isopropanol against ethanol, MilliQ water, a 0.1 M NaOH(aq.) or a 0.1 M HCl(aq.) solution (Figure 5.13B). When adding the reaction mixture after methacrylation into the alcohols, aggregates are formed immediately which sediment quickly. In ethanol, faster sedimentation was observed compared to isopropanol. After centrifugation, a brownish supernatant was obtained, indicating the presence of low molecular weight lignin oligomers (Figure 5.13A), which reduced the product yield and altered the molar mass of the product. In contrast, an almost colorless supernatant was obtained using aqueous precipitation agents, indicating a complete precipitation of lignin and small oligomers and resulting in a product with a lower overall molar mass. However, ca. 30-50% of the product was lost as the solid forms a fragile filter cake after centrifugation which could hardly be separated from the aqueous supernatant (Figure 5.13B). Significant amounts of product were lost when using MilliQ water as a precipitation agent. With ca. 75%, the highest yield was obtained using a 0.1 M HCl(aq.) solution as a precipitation agent. A similar yield resulted from precipitation in a 0.1 M NaOH(aq.) solution.

As pristine Kraft lignin is well soluble in aqueous, alkaline conditions, the insolubility of the products proves again the successful lignin modification. Attempts to separate the product

by filtration were not successful, as the methacrylated lignin blocked the pores of filter papers or glass frits. However, as centrifugation is limited to small production volumes, a filter system shall be designed in future experiments able to separate the precipitate completely from the supernatant to improve the product yield. An easy but time-consuming alternative would be to wait for sedimentation and to remove the supernatant from the product.

In summary, aqueous precipitation agents are considered more suitable for an upscaled lignin methacrylation in comparison to ethanol or isopropanol, because they are inexpensive, non-flammable, and precipitate the product almost quantitatively. The disadvantage of the aqueous precipitation agents is the generation of costs due to wastewater recycling or disposal. In comparison, recycling of ethanol or isopropanol might be realized by distillation. Product yield, costs for the precipitation agent and wastewater recycling/disposal must be compared precisely to design a maximally cost-efficient production process.

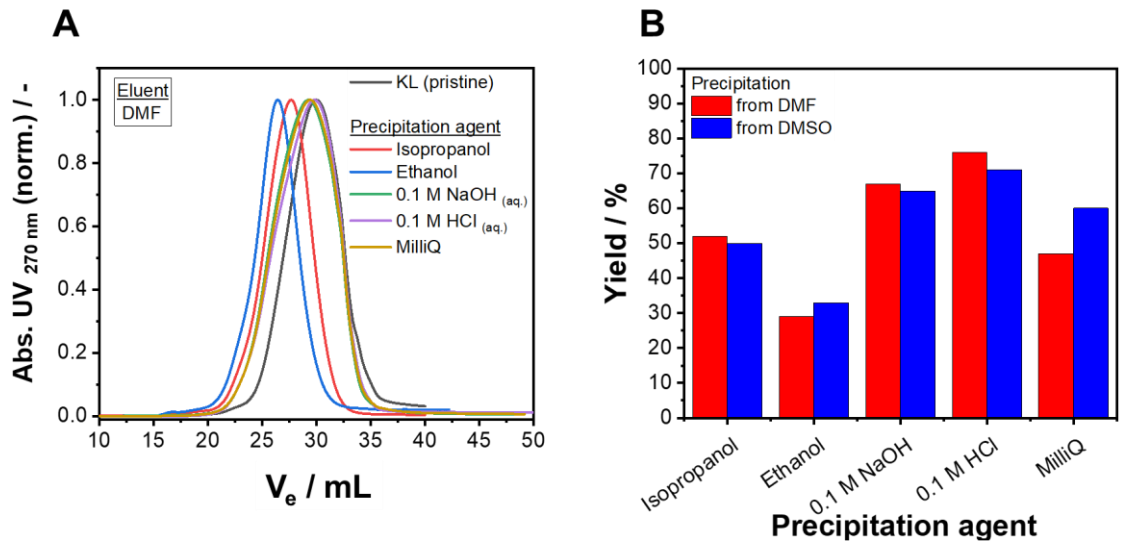

Figure 5.13: A) Size distribution of methacrylated Kraft lignin depending on the precipitation agent used for product isolation. B) Yields of methacrylated Kraft lignin obtained after precipitation in various precipitation agents from reaction mixtures using DMF (red) or DMSO (blue) as a solvent.

Table 5.3: Comparison of process parameters chosen from Yiamsawas *et al.* for the methacrylation of Kraft lignin with methacrylic acid anhydride and the reaction conditions chosen after process optimization.

Process parameters	Literature process according to Yiamsawas *et al.*[9]	Optimized process developed in this thesis
Solvent	**DMF** ▪ H: 226-312-332-319-360D P: 201-210-302+352-304+340-305+351+338-308+313 ▪ Recycling is energy-intensive (bp. 152°C) ▪ Intense smell	**DMSO** ▪ No risks ▪ Listed by the BVL as adjuvant[103] ▪ Recycling is energy-intensive (bp. 189°C); Thermal degradation possible
Lignin solubility	**Sufficient** ▪ Increased by LiCl (not necessary)	**Sufficient** ▪ No LiCl used
Methacrylic acid anhydrate	**Excess** ▪ 1.7 Eq. relative to Lignin-OH	**Equimolar** ▪ 1.0 Eq. relative to Lignin-OH
Catalyst	**Triethylamine** ▪ Soluble in many organic solvents ▪ H225, H302, H312, H314, H332 P210, P280, P305+351+338, P310 ▪ Intense smell	**Potassium carbonate** ▪ Solid; Reaction performed in suspension ▪ H: 315-319-335; P: 302+352-305+351+338 ▪ Cheap
Purification by precipitation in	**Isopropanol** ▪ H: 225-319-336 ▪ P: 210-233-240-305+351+338-403+235recycling by distillation (bp. 82°C) ▪ Yield: 50%	**0.1 M HCl (aq.)** ▪ H: 290-314-335 ▪ P: 260-280-303+361+353-304+340+310-305+351+338 ▪ Recycling is energy-intensive (bp. 100°C) ▪ Yield: 70%

Nanocarrier preparation using Kraft Lignin or Lignin Sulfonate

Strategy A - Preparation of lignin nanocarriers from methacrylated Kraft lignin

For successful use of the lignin nanocarriers as a plant protection formulation, long-term colloidal stability combined with maximal leaking tightness is desired to guarantee optimal performance even after several years of storage. In chapter 4, we proved the successful preparation of pyraclostrobin loaded lignin nanocarriers by crosslinking of methacrylated Kraft lignin in an O/W-miniemulsion. During the reaction, the double bonds of the methacrylate groups were converted with 2,2'-(ethylenedioxy)bis(ethylamine) (EDBEA) via an aza-Michael-addition to form a dense lignin matrix which encapsulated over 90% of the hydrophobic

fungicide pyraclostrobin.[101] Such nanocarriers were successfully tested in field tests. Herein, we investigated the effect on the particle size distribution, the morphology, and the encapsulation efficiency of alternative crosslinking agents like the diamine ethan-1,2-diamine (EDA) or ethylenetriamine (DETA) (Figure 5.14A-F). Both crosslinkers are listed as adjuvants in the list of the BVL and would be desired compounds for a potential scale-up or commercialization of the formulation.[103] Furthermore, we studied if EDBEA can be replaced by the reductive cleavable diamine cystamine (used as a free base), the triamine tris(2-aminoethyl)amine (TREN) or the dithiol 2,2'-ethylenedioxy)bis(ethylthiol) (EDBET). The procedure was conducted in analogy to the process presented in Chapter 4 but exchanging the crosslinkers. After the reaction and solvent evaporation, in all cases stable brownish dispersions were obtained without any visible aggregates. EDBEA, DETA, and EDA crosslinked dispersions are colloidally stable for several month forming only minimal sediment, whereas nanocarriers crosslinked with TREN, EDBET, and cystamine precipitated within ca. 24 h but could be redispersed easily by gentle shaking of the mixture. Next to optimal performance of the nanocarriers *in planta*, long-term stability during storage must be guaranteed, though. Plant protection formulations can be stored either in liquid form (in solution, suspension, emulsion) or as a solid (e.g. as powder, granulate), which can be redispersed before application. To test if a homogeneous formulation can be obtained from dried nanocarriers, dispersions of EDBEA crosslinked nanocarriers were dried either by lyophilization or in the vacuum oven (40°C) and an aqueous 2 mg/mL SDS solution was added to the powders afterwards (Figure 5.15). However, as suspension contained macroscopic aggregates, which sedimented quickly also after intensive shaking and sonication, we are convinced that the nanocarriers should be stored not as a dried powder but as a dispersion.

A 1 wt% dispersion could be stored (at room temperature, no shaking, protected from light) for ca. 3 years without significant change of its size distribution according to DLS measurements (Figure 5.14H). Moreover, no loss of pyraclostrobin was detected by HPLC, suggesting that the nanocarriers are still applicable (Figure 5.14G). To reduce the storage volume, the solid content of the suspensions was increased by centrifugation (4000 rpm, 30 min). Even at 20 wt% the dispersion remained macroscopically stable without forming any aggregates according to DLS (Figure 5.14I) but the particles sedimented slightly faster.

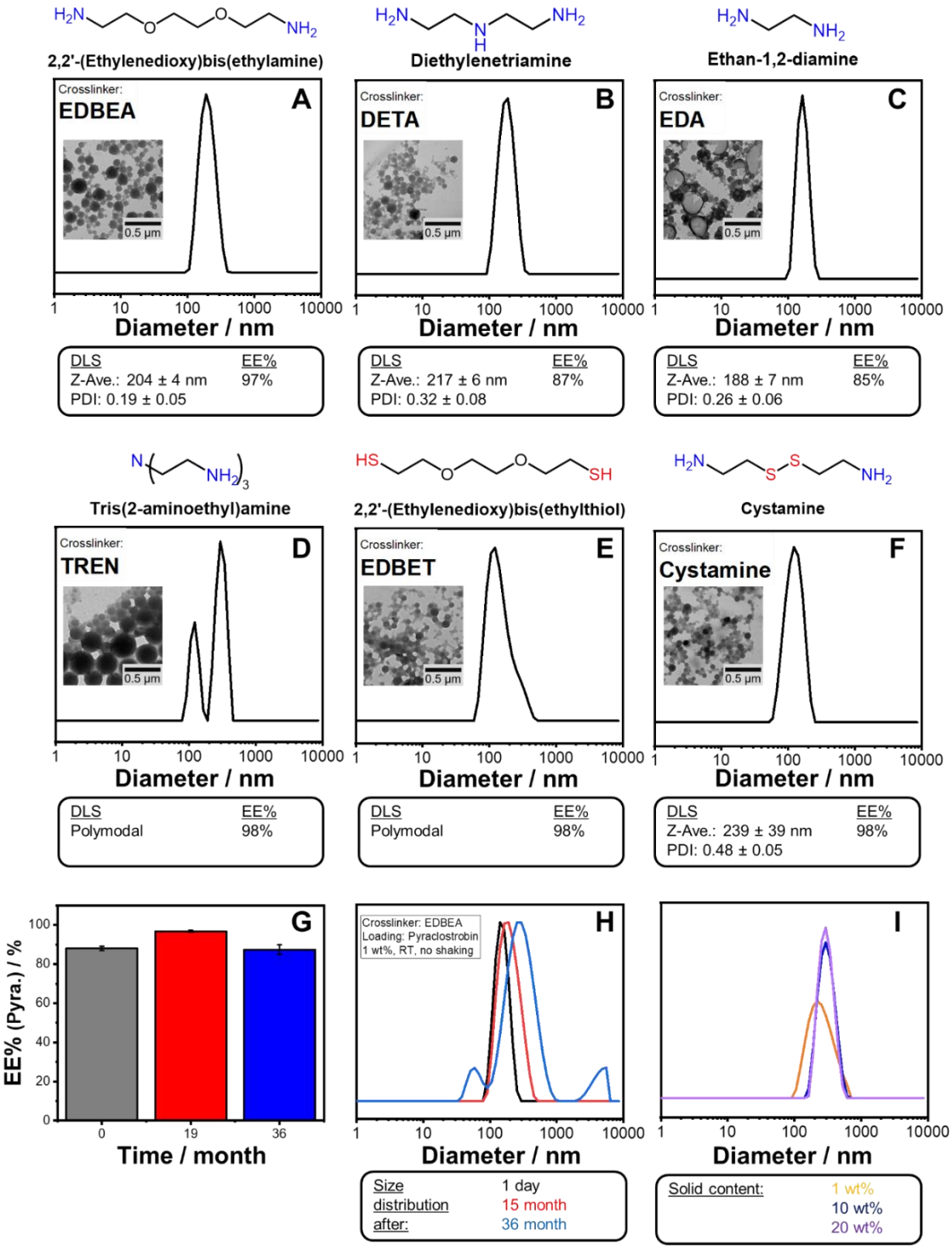

Figure 5.14: A) - F) Characterization of pyraclostrobin-loaded nanocarriers prepared from methacrylated lignin using versatile crosslinking agents: The particle size distribution was determined by DLS. TEM showed the morphology of the nanocarriers and the encapsulation efficiency (EE%) was determined by quantification of "free" pyraclostrobin in the continuous phase by HPLC ("method A", see experimental section). Encapsulation efficiency G) and particle size distribution H) of loaded nanocarriers directly after the crosslinking, after 15 and after 36 month. I) Size distribution of lignin nanocarriers with various solid contents. The solid content was increased by centrifugation and subsequent removal of excess supernatant.

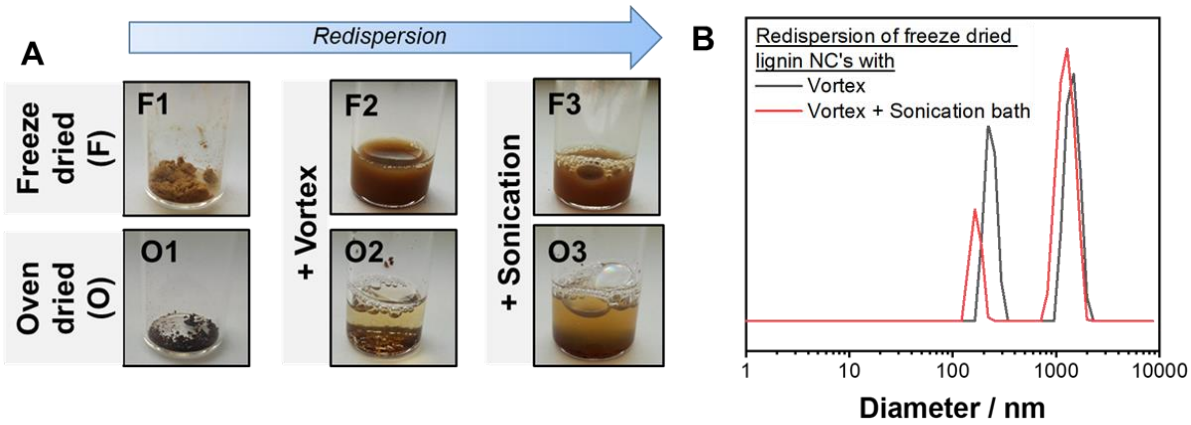

Figure 5.15: A) Attempt to redisperse freeze dried (F1-3) and oven dried (40°C, vacuum oven, O1-3) nanocarriers in 1 mg/ mL SDS solution. B) Polymodal particle size distribution of nanocarrier suspensions obtained after redispersion of lyophilized nanocarriers.

According to dynamic light scattering experiments (DLS), nanocarriers with a monomodal size distribution and an average diameter of 200-250 nm were obtained when using the crosslinkers EDBEA, DETA, EDA, or cystamine (Figure 5.14A-F). A polymodal size distribution (between 50-1000 nm) was detected in the cases of EDBET and TREN but without any macroscopic aggregates. Transmission electron microscopy (TEM) further proved the formation of spherical nanocarriers in the nanometer range with a relatively broad size distribution. Interestingly, a mixture of capsules and particles was formed using the diamine EDA, indicating that lignin-MA was partially precipitated at the droplet interface (Figure 5.14C). However, these results prove that all investigated crosslinkers were able to generate lignin nanocarrier dispersions. To determine the efficiency of the aza-Michael reaction, the amount of residual amine crosslinker in the continuous phase of the dispersion was quantified photometricaly via the Ninhydrin assay. During the assay, Ninhydrin reacts with primary amines to Ruhemans purple, which has an absorbance maximum at 570 nm and with secondary amines to a red-orange dye absorbing light at 440 nm. An almost complete conversion was determined for EDA and DETA, whereas only 80% of TREN and 50% of EDBEA were consumed respectively (Figure 5.16). The incomplete conversion of EDBEA most likely resulted from a comparably lower electron density of the $-NH_2$ moieties, due to its electron withdrawing oxygen atoms in the carbon chain. As cystamine and EDBET have only a low water solubility and therefore phase separate from the aqueous supernatant, these suspensions were excluded from this study.

After the crosslinking reaction, the final nanocarriers were dried and investigated by FTIR spectroscopy. The spectrum of methacrylated lignin showed bands at 1621 cm^{-1} and at 950 cm^{-1} belonging to the vinyl stretching and the vinyl bending motion of the methacrylate

group respectively. After the crosslinking, we observed a decreased intensity of the vinyl bands confirming the Michael addition between crosslinker and methacrylated lignin (Figure 5.17)

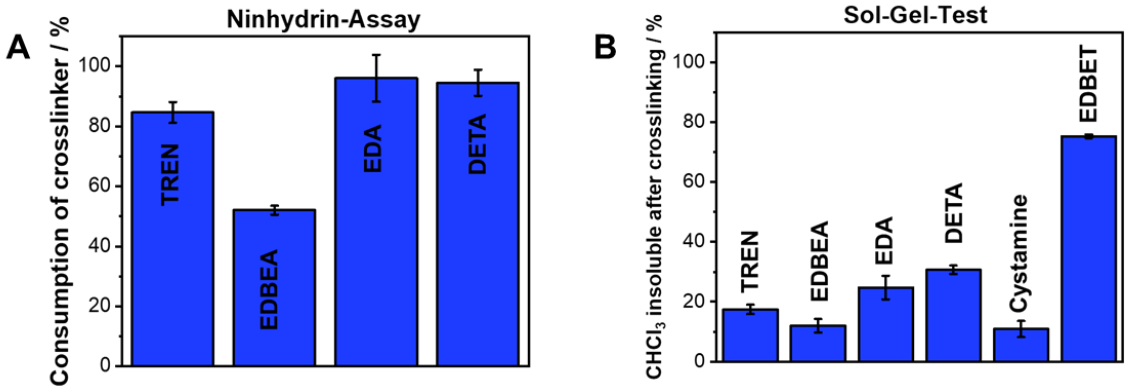

Figure 5.16: A) Quantification of residual amines after crosslinking methacrylated Kraft lignin in a miniemulsion with different diamines. The diamines were quantified photometrically in the continuous phase after conversion with Ninhydrin to Ruhemans purple. B) Quantification of the $CHCl_3$ soluble solid generated after conversion of methacrylated Kraft lignin with different crosslinkers in a miniemulsion. The amount correlated with the conversion of methacrylated groups and with the nanocarrier density.

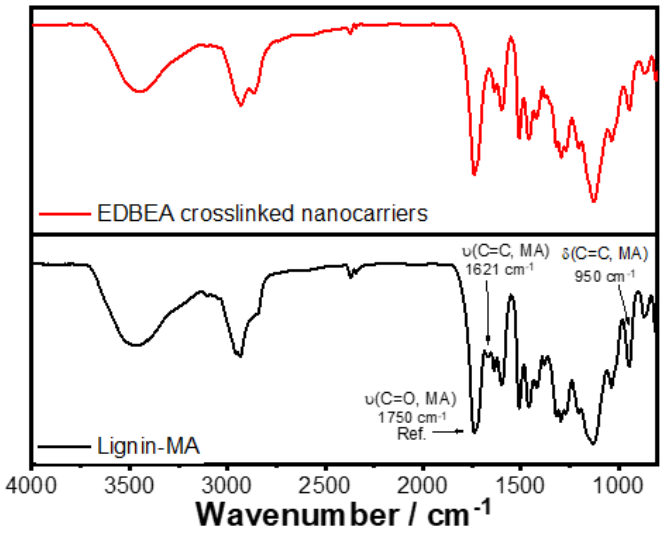

Figure 5.17: Comparison of a FTIR spectra of methacrylated Kraft before (black) and after crosslinking (red). As a crosslinker the diamine EDBEA was used.

To compare the efficiency of each crosslinker, we quantified gravimetrically the amount of chloroform-insoluble product (see “sol-gel-test” in the Experimental Section). Insufficiently converted lignin-MA dissolved in chloroform, while an insoluble material is obtained after

successful crosslinking. A smaller amount of chloroform-insoluble solid was formed when EDBEA was used as a crosslinker in comparison to a reaction performed with DETA and EDA (Figure 5.16). This suggests a more efficient crosslinking for the latter two compounds. The dithiol EDBET clearly showed the highest crosslinking efficiency, as ca. 80% of the methacrylated lignin reacted to insoluble nanocarriers. The apparently higher reactivity resulted from a higher nucleophilicity of the thiol groups relative to the amines. Additionally, EDBET is not water-soluble but dissolves well in chloroform. Hence, the crosslinker is concentrated primarily in the droplets, whereas the water and chloroform soluble amines occur more diluted in the dispersed and in the continuous phase.

To determine if the crosslinker affects the encapsulation efficiency, we measured the fungicide loading. The amount of non-encapsulated pyraclostrobin was quantified after the removal of the nanocarriers in the supernatant by HPLC using method A (see experimental section). In chapter 4, we demonstrated the successful loading of pyraclostrobin by using EDBEA as a crosslinker (encapsulation of up to 97% fungicide). When EDA, DETA, cystamine, EDBET or TREN were used to crosslink lignin-MA, encapsulation efficiencies of > 85% pyraclostrobin were achieved and the loading did not influence the size distribution according to DLS, which proves the robustness of the dispersions and the versatility of suitable crosslinkers (Figure 5.14).

<u>Strategy B:</u> Preparation of lignin nanocarriers from methacrylated lignin sulfonates

Due to their amphiphilic molecular structure, lignin sulfonates are used in a million-ton-scale as inexpensive, nontoxic, and bio-based emulsifiers in agrochemical, dye, pigment, and animal feed formulations.[34] Recently, Chen *et al.* demonstrated that the surface activity of lignin sulfonate could be used to generate loaded lignin sulfonate nanocarriers by interfacial crosslinking in a direct miniemulsion.[49] Despite a covalent crosslinking, the prepared capsules lost 50% of the encapsulated cargo after a day. Hence, a more efficient crosslinking strategy must be developed, which prevents uncontrolled leaking. As proven with the above experiments on Kraft Lignin, tight nanocarriers can be obtained via Michael-addition in a miniemulsion. However, during preparation organic solvents, such as chloroform or DCM are needed as a dispersed phase, as these are the only common water-immiscible solvents, which dissolved methacrylated Kraft lignin in appropriate amounts. A “greener” process to generate biodegradable lignin nanocarriers with loaded actives is needed. In this chapter a safe and sustainable strategy based on the interfacial crosslinking of methacrylated lignin sulfonates to generate loaded lignin nanocarriers without using halogenated solvents. The formulation allows a slow and controlled drug release over weeks.

As a starting material we used different methacrylated lignin sulfonates (LSCH-MA, LSCa-MA, LSNa1-3-MA), which were characterized in detail previously (Table 5.2). An efficient crosslinking at the droplet interface of a miniemulsion requires interfacially active monomers. To find the most appropriate starting material, we therefore measured the decrease of the interfacial tension between an aqueous lignin sulfonate solution and cyclohexane by spinning drop tensiometry. At a concentration of 5 mg/mL, the methacrylated lignin sulfonates were able to decrease the interfacial tension from 44.0 mN/m to typically 12 mN/m. Hence, the functionalized lignins showed an interfacial activity that is comparable to the common polymeric surfactant Lutensol AT50 (12 mN/m at c = 5 mg/mL). LSNa1-MA decreased the interfacial tension to 6.6 mN/m which is similar to the value determined e.g. for the anionic surfactant sodium dodecyl sulfate (SDS, 5 mN/m at c = 5 mg/mL). For the nanocarrier preparation, therefore LSNA1-MA was used. The comparison of molecular weight and functional groups of each methacrylated lignin sulfonate gave no clear explanation for the exceptional position of LSNA1-MA. Noticeable, however, is that that latter compound is only one without phenolate groups (Table 5.4).

Table 5.4: Functional groups found in different methacrylated lignin sulfonates. The amount of hydroxyl groups and the number of methacrylate groups was calculated from ^{31}P NMR using the method of Balakshin *et al.*.[84] The sulfur content was determined by ICP-OES and can be used to estimate the number of sulfonate groups. The weight averaged molecular weight (M_w) was measured by aqueous SEC vs. polystyrene sodium sulfonate as a reference. The ability to decrease the interfacial tension was measured by spinning drop tensiometry between cyclohexane and a 5 mg/mL aqueous lignin-MA solution. The interfacial tension between water and cyclohexane is 44.0 Nm/m without using a surfactant.

No.	Lignin-MA	arom OH / mmol g^{-1}	aliph OH / mmol g^{-1}	n(MA) / mmol g^{-1}	Sulfur / mmol g^{-1}	M_w / g mol^{-1}	Interfacial tension / Nm m^{-1}
1	LSCH	0.36	1.83	18.1	1.64	$3.0 \cdot 10^4$	12.5 ± 0.3
2	LSCa	0.25	0.54	12.0	2.70	$5.5 \cdot 10^3$	12.2 ± 0.3
3	LSNa1	0.00	0.57	12.7	1.63	$1.2 \cdot 10^4$	6.6 ± 0.4
4	LSNa2	0.61	1.65	5.8	1.95	$5.1 \cdot 10^3$	14.5 ± 0.3
5	LSNa3	0.45	2.00	17.9	1.93	$1.5 \cdot 10^4$	12.8 ± 0.6

Lignin nanocarriers were prepared by crosslinking methacrylated lignin sulfonate at the droplet interface of a direct miniemulsion (Figure 5.18): The water insoluble dithiol crosslinker 2,2'-ethylenedioxy)bis(ethylthiol) (EDBET) was dissolved together with an hydrophobic cargo in cyclohexane. Afterwards the mixture was added to an aqueous solution containing methacrylated lignin sulfonate, the alkaline catalyst triethylamine (TEA), and an additional surfactant; either the anionic SDS or the nonionic Lutensol AT50. To generate a stable miniemulsion, the two-phase mixture was ultrasonicated under ice-cooling; a brownish

emulsion was obtained. The polyaddition at the interface of the dispersed oil droplets was initiated by increasing the temperature to 50°C under vigorous stirring. The reaction was allowed to proceed for ca. 15 h yielding a stable dispersion, with a solid content of ca. 10 mg/mL. The product was stored in a closed vial to prevent the evaporation of cyclohexane. No aggregates were formed for several weeks.

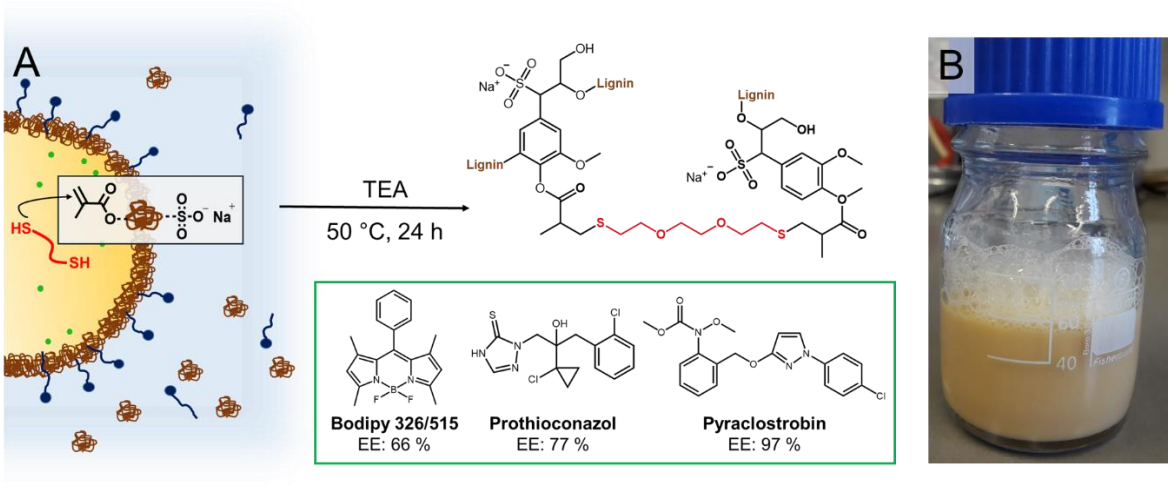

Figure 5.18: A) Formation of lignin nanocarriers from methacrylated lignin sulfonate by interfacial crosslinking in miniemulsion. The encapsulated model drug Bodipy and the fungicides prothioconazol and pyraclostrobin and the respective encapsulation efficiencies (EE measured by extraction; indirect method) are shown. B) Photograph of ca. 50 mL of a dispersion containing crosslinked lignin sulfonate nanocarriers loaded with prothioconazol.

The formation of a water- and oil-insoluble product indicated the chemical crosslinking of the methacrylated lignin sulfonate during the reaction. For further confirmation, we washed the nanocarrier dispersion with cyclohexane to remove unconverted EDBET and analyzed the purified reaction product by FTIR spectroscopy after lyophilization. The spectrum of the brownish solid confirmed a covalent crosslinking by a decreased intensity of the stretching (1668 cm^{-1}) and bending (950 cm^{-1}) band belonging to the C=C double bond (taking the signal of the carbonyl stretching motion at 1723 cm^{-1} as a reference). Additionally, we found an intense C-O stretching signal of EDBET's glycol moiety at 1100 cm^{-1} suggesting a successful nucleophilic attack of the thiol on the methacrylate double bonds by thiol-Michael addition (Figure 5.19B).

To develop a maximum stable formulation, we investigated the effect of surfactant, cargo, oil phase and amount of crosslinking agent on the nanocarrier formation. Under most reaction conditions, carriers with diameters between 200 and 300 nm and narrow size distribution were obtained (PDI< 0.32, Figure 5.19A, Table 5.5). Transmission electron microscopy (TEM) showed spherical nanoparticles with a core-shell structure proving that the reaction between methacrylate and thiol groups was performed at the droplet interface (Figure

5.21A). No significant difference regarding to particles size distribution was observed by DLS when stabilizing the emulsion with the anionic surfactant SDS or with the nonionic poly(ethylene glycol)-based surfactant Lutensol AT50. The stabilization only with the amphiphilic methacrylated lignin and without an additional surfactant led to a polymodal particle size distribution according to DLS (Table 5.5, Figure 5.20A). Nevertheless, the suspension was macroscopically stable, and no phase separation was observed even after weeks of storage.

Table 5.5: Reaction conditions for the formation of lignin nanocarriers from methacrylated lignin sulfonate. The particle size distribution (PDI and Z-Average) was determined by DLS. The encapsulation efficiency (EE%) was measured after extraction (indirect method) photometrically for Bodipy and by HPLC for prothioconazol and pyraclostrobin.

No.	Surfactant	c(TEA) / mmol/mL	c(CL) / mmol/mL	Oil phase	Cargo	Diameter / nm (PDI)	EE %
1	-	-	0.060	Cyclohexane	-	Polymodal	
2	SDS	-	0.060	Cyclohexane	-	270 (0.22)	
3	Lutensol AT50	-	0.060	Cyclohexane	-	240 (0.26)	
4	SDS	0.066	0.132	Cyclohexane	Bodipy	250 (0.02)	66
5	SDS	0.054	0.108	Cyclohexane	Bodipy	240 (0.09)	67
6	SDS	0.042	0.084	Cyclohexane	Bodipy	240 (0.04)	66
7	SDS	0.030	0.060	Cyclohexane	Bodipy	250 (0.07)	66
8	SDS	0.066	0.132	Rapeseed oil	-	200 (0.23)	
9	SDS	0.066	0.132	Rapeseed oil	Pyraclostrobin	Polymodal	97
10	SDS	0.066	0.132	Rapeseed oil	Prothioconazol	207 (0.32)	77

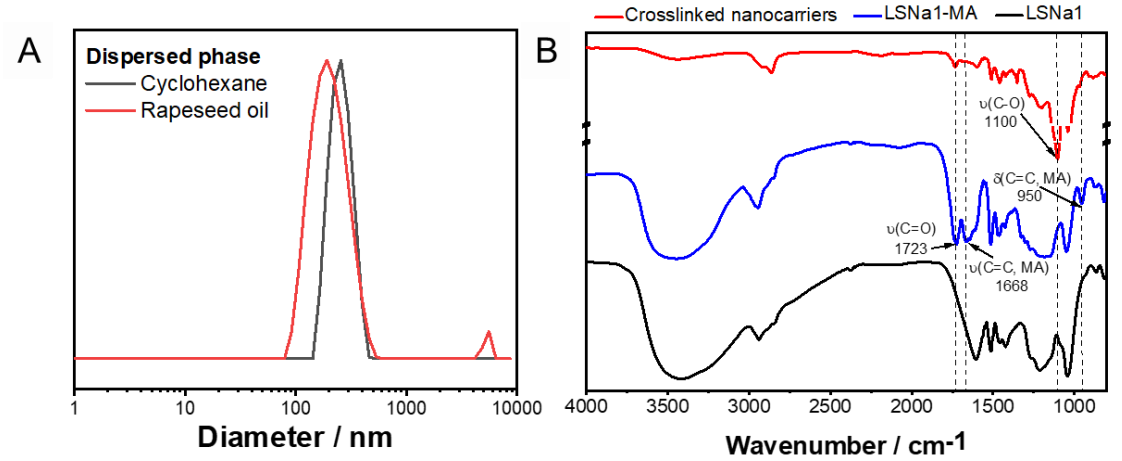

Figure 5.19: A) Particle sized distribution of lignin nanocarriers using either cyclohexane or rapeseed oil as dispersed phase. B) FTIR spectrum of nanocarriers prepared by interfacial crosslinking of methacrylated lignin sulfonate using cyclohexane as dispersed phase (Reaction conditions No. 4, see Table 5.5).

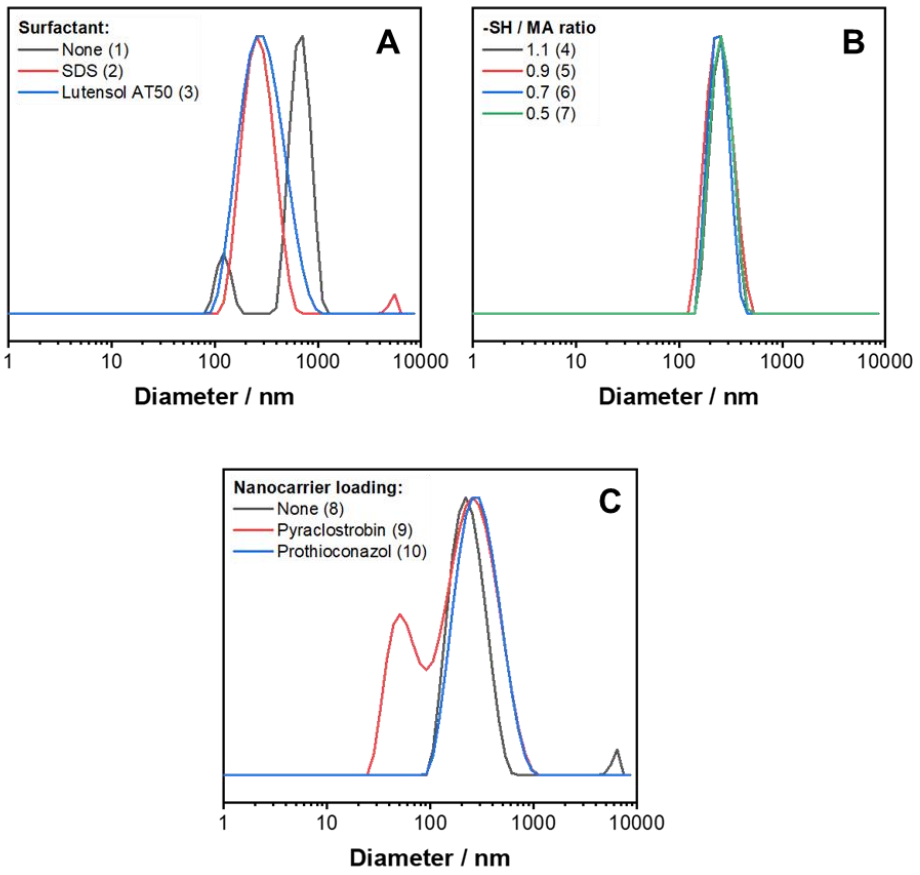

Figure 5.20: Particle size distributions according to DLS. The nanocarriers dispersions were prepared by interfacial crosslinking of methacrylated lignin sulfonate in a miniemulsion. The effect of surfactant A), ratio between thiol-crosslinker and methacrylate moieties B) and loading C) was investigated.

To apply the nanocarriers for drug delivery, the formulation must allow encapsulation and controlled release of the active ingredients. We first encapsulated the hydrophobic dye Bodipy 326/515 as a model drug and investigated the release kinetics. To adjust the speed of diffusion from the nanocarriers to the aqueous phase, we generated nanocarriers with varying crosslinking density by a stepwise reduction of EDBET from 1.1 to 0.5 equivalents relative to the number of methacrylate groups. The encapsulation of Bodipy 326/515 (24 µg/mL), did not change the average size distribution compared to “empty” lignin NCs but decreased the PDI (Table 5.5, No. 4-7). To determine the encapsulation efficiency of the hydrophobic cargo, two different approaches were used: A) Nanocarriers were centrifuged and the supernatant was analyzed for Bodipy 326/515 (either dissolved or solubilized in micelles). B) Cyclohexane was used to extract the dye from the dispersion; this approach also detects surface-adsorbed or precipitated Bodipy 326/515. However, also parts of the encapsulated dye might be extracted so that the actual encapsulation efficiency might be underestimated in this case.

Using method A, and encapsulation of more than > 90% was determined, independent from the amount of crosslinker. As the used Bodipy is water-insoluble, the residual 10% are adsorbed most likely on the nanocarrier surface or are dispersed in micelles in the continuous phase. As expected, a lower value of ca. 70% was determined for all nanocarriers when measuring the encapsulation efficiency after extraction (method B). Noticeably, the amount of crosslinker did not influence the amount of encapsulated cargo but had effect on the release kinetics due to different diffusivities through the crosslinked membrane (Figure 5.21B). The drug release was measured after two, four and seven days by washing the dispersion with cyclohexane and subsequent quantification of Bodipy 326/515 transferred to the cyclohexane phase (analog to method B). Using thiol and methacrylate groups in a ratio of 0.5, the encapsulated Bodipy 326/515 could be transferred completely to the cyclohexane phase after 5 days. Increasing the ratio stepwise to 1.1 equivalents, the release rate was reduced systematically, which suggests the formulation of nanocarriers with a higher degree of crosslinking. Hence, the formulation provides a time-controlled drug release via diffusion. To prevent premature drug release for example during storage, the nanocarriers were centrifuged (4000 rpm, 30 min) and the aqueous supernatant was removed. The wet pellet allows storage without drug loss and can be redispersed easily in a 1 mg/mL SDS solution by vigorous shaking to yield a stable dispersion (ca. 10 mg in 1 mL solution). According to DLS, the centrifugation did not change the particle size distribution (Figure 5.22).

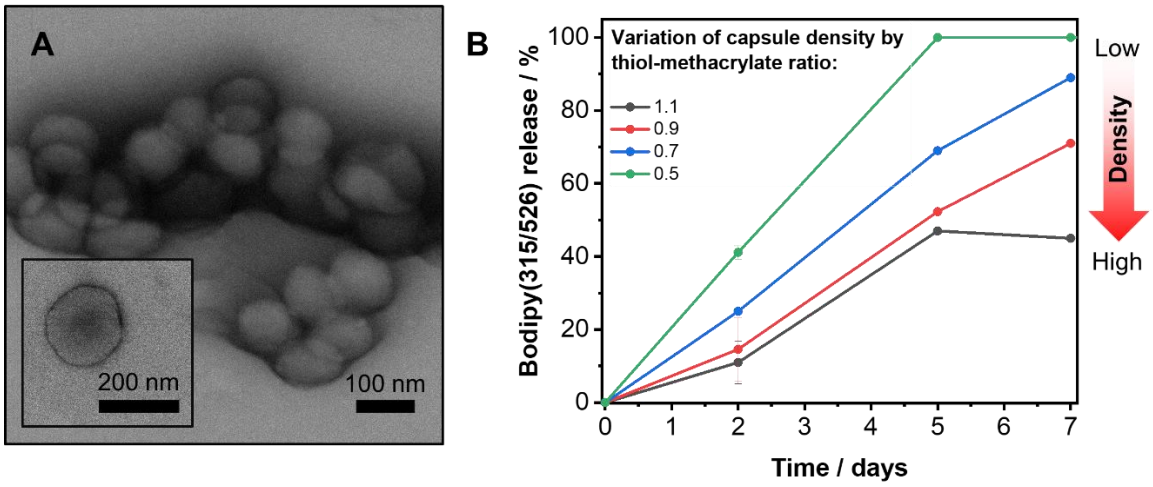

Figure 5.21: A) TEM micrograph of crosslinked nanocarriers (Table 5.5, No.4,). The particles have a platelet-like shape indicating a core-shell structure. C) Release profile of Bodipy 326/515 from loaded lignin nanocarriers by diffusion determined by extraction of “free” dye with cyclohexane. The release kinetics depend on the particles crosslinking density, which can be controlled by adjusting the ratio between thiol crosslinker and methacrylated lignin sulfonate during the particle preparation.

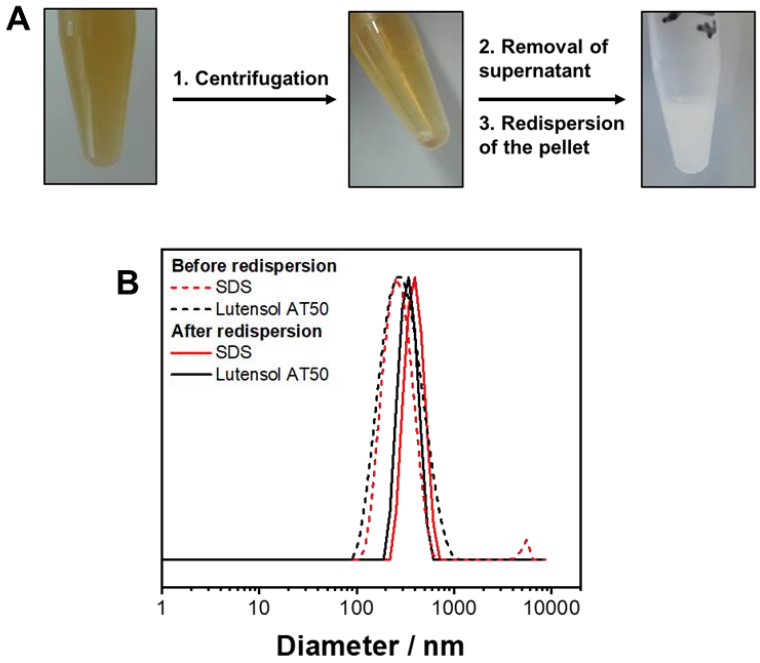

Figure 5.22: A) Nanocarriers were stored as wet pellet to prevent premature release of loaded Bodipy 326/515. B) The particle size distributions before and after redispersion were measured by DLS

As the nanocarrier dspersion are composed on a plant-based, abundant and cheap raw material, the approach might be of interest as formulation for agrochemicals. We therefore replaced cyclohexane with rapeseed oil as sustainable solvent for hydrophobic fungicides. The plant oil is non-toxic and does not need to be removed prior application. The oil contains unsaturated fatty acids offering additional points for crosslinking. However, due to the relatively low electrophilicity of the double bonds and lignins radical scavenger properties no reaction via Micheal- or thiol-ene-addition is likely.

Using the plant oil as a hydrophobic phase, colloidally stable dispersions were obtained, which did not phase separate even after several weeks of storage. As the formed nanocarriers had an average diameter of 200 nm and a PDI of 0.23, rapeseed oil was considered as a suitable alternative to cyclohexane (Figure 5.20). Likewise, the oil was found as a good solvent for the broad-spectrum fungicides prothioconazol (ca. 30 mg/mL at 25°C) and pyraclostrobin (ca. 50 mg/mL at 25°C). When adding EDBET to the mixture, the solubility of prothioconazol further increased (to ca. 70 mg/mL at 25°C), while the solubility of pyraclostrobin remained unchanged. At a loading of 0.5 mg/mL (regarding to the total volume of the dispersion), stable dispersions were obtained in both cases. Prothioconazol-loaded nanocarriers had an average diameter of 207 nm and a monomodal size distribution whereas

a polymodal size distribution was monitored for nanocarriers loaded with pyraclostrobin (Figure 5.20). These differences might be explained by the lower solubility of pyracostrobin in the dispersed phase or some aggregation. The encapsulation efficiencies were determined by extraction of the free fungicide with cyclohexane (see method B above) and quantified their amounts by HPLC. For both fungicides high encapsulation efficiencies with 97% for pyraclostrobin and 77% for prothioconazol were detected, proving that the herein developed nanoformulation as a promising tool for drug delivery in sustainable plant protection.

5.5 Conclusion

Different lignin derivatives (Kraft, Organosolv, sulfonates) were efficiently modified to reactive lignins by methacrylation and crosslinked by different strategies in miniemulsion. Despite the biopolymers differ regarding their chemical structure and their functional groups, > 90% hydroxyl groups were methacrylated typically. The product can be generated without using toxic solvents or catalysts, which would allow a safe and cost-efficient production on industrial scale. Depending on their hydrophobicity, the lignin monomer can be dissolved either in the continuous or in the dispersed phase of O/W-miniemulsion to form loaded lignin nanocarriers:

A: The hydrophobic methacrylated Kraft lignin was crosslinked in dispersed chloroform droplets with various diamine and dithiol crosslinkers, yielding densely crosslinked and long-term colloidally stable dispersions with particles of ca. 200 nm diameter.

B: The amphiphilic and water-soluble methacrylated lignin sulfonate was crosslinked at the droplet interface generating nanocarriers in the nanometer range which can be loaded with fungicides. As the carrier preparation needs no toxic solvents, the approach is rendered of high interest to yield sustainable nanoformulations for controlled drug delivery in agriculture.

6 From Compost to Colloids - Valorization of Spent Mushroom Substrate

Sebastian J. Beckers, Irantzu Alegria Dallo, Inés del Campo, Christine Rosenauer, Katja Klein, and Frederik R. Wurm

This study was performed under the scientific guidance of PD. Dr. Frederik Wurm and Dr. Inés del Campo. The thermochemical pretreatment and the Organosolv extraction of SMS was performed by Dr. Irantzu Alegria Dallo. Filter cakes and liquid extracts were characterized by Sebastian Beckers together with Dr. Irantzu Alegria Dallo. The SEC measurements were performed by Christine Rosenauer. Katja Klein prepared the biosurfactant stabilized polystyrene nanoparticles. The preparation of “lignin”-nanocarriers and the respective enzymatic degradation was performed by Sebastian Beckers. For publication, the data was collected and summarized by Sebastian Beckers. The manuscript was reviewed by PD. Dr. Frederik Wurm, Dr. Irantzu Alegria Dallo and Dr. Inés del Campo. The cover picture was designed by Stefan Schuhmacher.

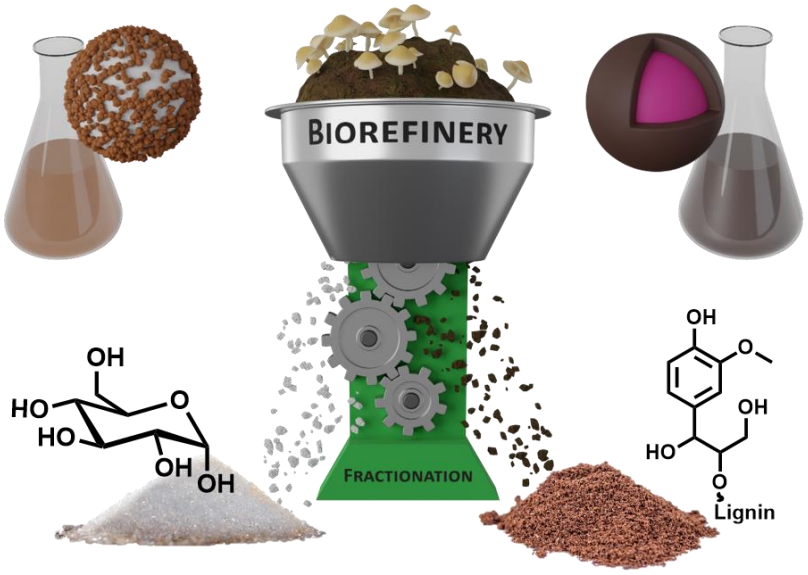

Keywords: *Lignin, carbohydrates, biorefinery, nanocarrier, surfactant*

6.1 Abstract

Yearly, million tons of lignin are extracted from wood by Kraft and sulfite pulping. The technical lignins obtained are referred as Kraft lignin and lignin sulfonates and were used after methacrylation in chapter 4 and 5 to produce nanocarriers for hydrophobic drugs. This chapter explains how also a biomass waste called spent mushroom substrate (SMS) - a mixture of composted soil and fungal mycelium left after the mushroom harvest - can be used as valuable source to produce lignin and carbohydrates. Up to date, SMS is unutilized and causes immense disposal costs. To valorize SMS, it is essential to fractionate the complex mixture into its valuable components, which is a challenge for current bio-refineries and has only been partly achieved. We have developed a novel bio-refinery strategy To separate carbohydrates and soluble lignin from SMS. Therefore, SMS was subjected to two different extraction methods To break the insoluble biopolymer residues: A: A thermochemical treatment (water/basic or acidic catalyst) yielding in a carbohydrate-enriched liquid fraction. B: An Organosolv extraction (with ethanol/water) solubilizing mainly lignin. The carbohydrate fraction possesses surface-active properties and was investigated as a potential bio-based surfactant. The soluble lignin fraction was used for the formation of nanocarriers via an inverse miniemulsion polymerization allowed the encapsulation of the hydrophilic model drug sulforhodamin. The lignin-based nanocarriers were biodegradable by laccases, which renders them of high interest for drug delivery systems for advanced plant protection. This novel bio-refinery is a powerful strategy for the upcycling of SMS into various high-value products.

6.2 Introduction

The fresh mushroom production in Europe amounted to one million tonnes in 2013 with a value of 1.8 billion euro.[106-108] For every ton of mushrooms, approximately three times the amount of spent mushroom substrate (SMS) is generated, which to date has no commercial use.[109] This means such as for Ireland in an annual SMS production of 254,000 t or a production volume of 800,000 t SMS for the Netherlands.[110]

The SMS remains from the mushroom cultivating process and is a complex mixture of composted organics and fungal mycelium left after the mushroom harvest.[110] The substrate is based on various agricultural waste materials, such as sawdust, sugarcane bagasse, oil palm empty fruit bunch, wheat straw-bedded horse manure, hay, poultry manure, ground corncobs, cottonseed meal, cocoa shells, and gypsum.[111] A typical mushroom cultivation cycle lasts for one month; farmers usually store the SMS temporarily before it is landfilled, spread on land,

sold as a soil amendment or conditioner product.[110] Due to the vast amounts of SMS generated during the harvest, farmers are confronted with significant logistical problems.[109] Additionally, current costs for SMS disposal amount from 10 to 50 €/t in Europe, leading to an immense financial burden of up to 150,000,000 €/ year for the mushroom industry.

Valorization of the unutilized SMS feedstock is demanding, as the substrate composition varies locally, seasonally and over the period of the harvest. Nevertheless, few studies had succeeded in using SMS directly or as feedstock for valuable bio-based materials.[112] For example, extra-cellular fungal enzymes like laccases and peroxidases were extracted from SMS after the mushroom harvest.[113] Especially due to its lignases, which enzymatically catalyze the metabolism of lignin and lignin-related compounds, SMS is a potential candidate for bioremediation (e.g. for polycyclic aromatic carbons or agrochemicals like pentachlorophenol, carbendazim, or mancozeb).[110, 114] Besides the enzymes contained in SMS, various natural ingredients such as lignin, proteins, or diverse carbohydrates have been detected in the used compost.[110] To date, only crude carbohydrate fractions containing up to 25% of SMS's sugars were separated by hot water alkali extractions.[27, 115] Carbohydrates from SMS were also used for biofuel production,[116] after extractint the majority of the lignin from the crude SMS by an Organosolv protocol.[117] An efficient fractionation of the complex mixture is still missing. Particularly, as SMS is not competing with food production, the exploitation of its components as a resource is of great interest.

If an efficient fractionation is established, the SMS-derived chemicals might be useful as biodegradable building blocks for nanomaterials. Especially, the development of bio-based nanocarriers as interesting nanomaterials for biomedicine or agriculture is a focus of recent studies.[118] As SMS is composed of carbohydrates and lignin, the development of bio-based surfactants or degradable nanocarriers might be attractive. We have recently used carbohydrates[118] or lignin[7, 9] to prepare biodegradable nanocarriers. The use of SMS derived materials for nanocarrier production would be an attractive pathway of an "upcycling" of a waste product.

Herein, we present an innovative biorefinery concept for fractionation of SMS (and SMS supplemented with wheat straw) into carbohydrate- or lignin-enriched extracts. The soluble carbohydrates or lignin act as starting materials for valuable bio-based products; here we used them as bio-based surfactants or building block for biodegradable nanocarriers. The SMS was either thermochemically pretreated (at elevated temperatures in water containing an acidic or basic catalyst) To solubilize carbohydrates or extracted with ethanol-water mixtures ("Organosolv" treatment) to obtain soluble lignin fractions. The carbohydrate fraction was used as a bio-based surfactant, whereas the lignin-enriched SMS extracts could be applied to prepare biodegradable lignin nanocarriers by a miniemulsion polymerization. With this

concept, a step towards “upcycling” of SMS into bio-based and biodegradable materials is made, which might be used in agricultural applications.

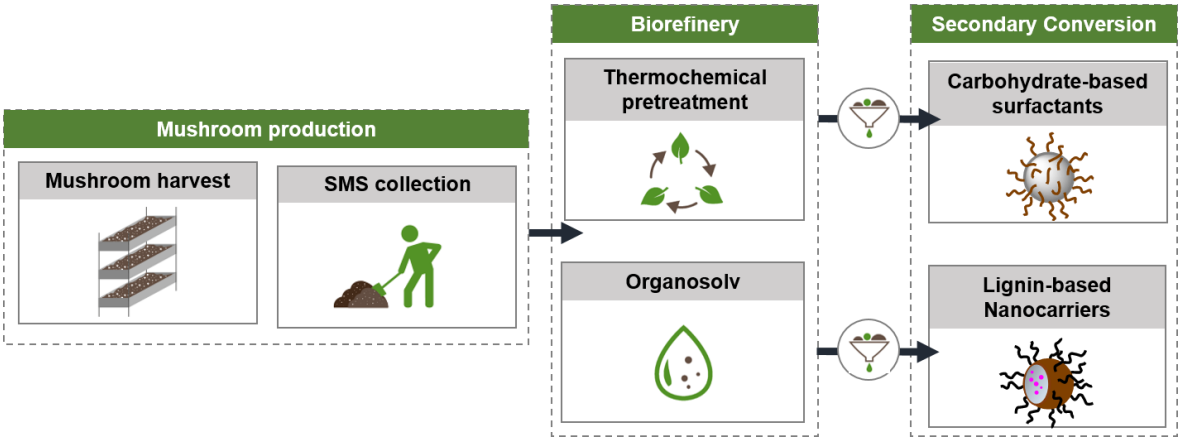

Scheme 6.1: Valorization of the spent mushroom substrate to eco-friendly surfactants and biodegradable nanocarriers.

6.3 Experimental Section

Materials

2,4-Toluene diisocyanate (TDI), sodium dodecyl sulfate (SDS), sulforhodamine-B (SR-B), hexadecane, styrene, 2,2'-azobis(2-methylbutyronitrile), 2-chloro-4,4,5,5-tetramethyl-1,3,2-dioxaphospholane, N-hydroxy-5-norbornene-2,3-dicarboxylic acid imide and solvents were purchased from Sigma Aldrich. Polyglycerol polyricinoleate (PGPR) was obtained from Danisco. The Laccase cocktail MetZyme® PURECO™ 020 (L371) was kindly provided by MetGen (Finland). All chemicals were used without further purification.

Spent mushroom compost was generated at Tyholland Farm (Monaghan, Ireland) and kindly supplied by Monaghan Mushrooms. Wheat straw was harvested in Spain and supplied by local farmers. The SMS was grounded with a mesh of 6 mm and stored at 4 ºC. The wheat straw was milled to a mesh of 4 mm and stored at room temperature. After drying, the moisture content was adjusted to 50% and the SMS was thermochemically pretreated in combination with wheat straw or extracted without additives with ethanol-water mixtures (Scheme 6.1).

Methods

Moisture content

Moisture content in SMS was calculated by drying the samples at 105 ºC up to constant weight following.

Ash content

Ash content was determined after air combustion for 2 h at 550±10 ºC in a muffle oven.

Dynamic Light Scattering (DLS)

The hydrodynamic diameters of the particles were measured by DLS with NICOMP 380 submicron particle sizer (Nicomp Particle Sizing systems, USA) at a fixed angle of 90° and a laser diode running at 635 nm. The sample was diluted to a concentration of 0.01 wt% with water or cyclohexane before measurement.

Tensiometry

(A) Ringtensiometry: The surface tension at the water-air interface was determined with the ring tensiometer DCAT 21 from DataPhysics. An aqueous surfactant solution of 0.15 g/mL was added dropwise into the water. After each addition, the mixture was stirred for 2 min and afterward the surface tension was measured.

(B) Spinning drop method: Between chloroform and water were determined with a spinning drop tensiometer (SVT 20N from DataPhysics). A glass capillary was filled with chloroform and a small droplet of MilliQ water (as a reference) or aqueous extract mixture (10 mg/ mL). Then the capillary was placed horizontally and equilibrated at 20°C for 10 min under rotation at 8000 rpm until a cylindrical droplet at the axis of rotation was obtained. The interfacial tension based on the theory of Cayias, Schechter, and Wade was used for data analysis.

High pressure liquid chromatography (HPLC)

The extracts were analyzed by HPLCperformed at an Agilent Technologies system (model 1200). The content of monosaccharides (D-glucose, D-xylose, L-arabinose) was quantified at an ICSep ION 300 column (7.8 x 300 mm, Transgenomics, Glasgow, United Kingdom) at 72 ºC with a refractive index detection. As an eluent, an aqueous 8.5 mM H_2SO_4 solution was used.

Carbohydrate degradation compounds such as furans (furfural and 5-hydroxymethylfurfural) and phenolic compounds (benzaldehyde, ferulic acid, vanillin-syringaldehyde, vanillin/syringic, coumaric, benzoic, 4-hydroxybenzoic, phenol, syiringol,

guayacol) were measured using a Zorbax column (250 x 4,6 mm, Agilent Technologies) at 50 ºC with a diode array detector. The mobile phase consisted of water and acetonitrile in a ratio of 8:2.

Quantification of carbohydrates in the filter cake

Quantification was performed according to the NREL procedure nº 42618.

Quantification of lignin in the filter cake

Quantification was performed according to the NREL procedure nº 42627.

Size exclusion chromatography (SEC)

SEC analyses of the extracts obtained from the thermochemical pretreatments were performed using an Agilent Technologies 1260 instrument consisting of a pump, autosampler, and column oven. A column set consisting of 2 columns: MCX10^3 Å, and MCX10^5 Å (PSS Standards Service GmbH, Mainz, Germany), both of 300 x 8 mm and 10µm average particle size were used at a flow rate of 1.0 mL/min and a column temperature of 30°C. As eluent 80% 0.1M NaOH and 20% acetonitrile was used. The injection volume was 10 µL. Detection was accomplished with an RI detector (RI-101, ERC) and a UV detector (UV/VIS-2487, Waters) at 270 nm. Data acquisition and evaluation were performed using PSS WINGPC UniChrom (PSS Polymer Standards Service GmbH, Mainz, Germany). Calibration was carried out by using poly(styrene sulfonate) sodium salt provided by PSS Polymer Standards Service GmbH (Mainz, Germany). High-performance size exclusion chromatography (HPSEC) was used for analyses of the Organosolv extracts. As eluent, a solution of 0.1% lithium bromide in *N,N'*-dimethylformamide was used under isocratic conditions. The column was a Polargel-M and detection was accomplished with an RI detector. Polystyrene was used as a reference material.

Nuclear magnetic resonance (NMR) spectroscopy

^{1}H and ^{31}P Nuclear Magnetic Resonance (NMR) spectroscopy was performed at a Bruker AVANCE (USA) system at 300 MHz. For ^{1}H NMR spectroscopy, 5 mg of the sample were dissolved in 600 µL of DMSO-d_6. To determine the number of OH-groups in the sample, ^{31}P NMR spectroscopy was used after derivatization according to the literature for other lignin derivatives[84]: 20 mg of dried sample was dissolved in 550 µL of a $CDCl_3$-pyridine-d_5 (4/6 v/v ratio) mixture and was then treated with 100 µL of 2-chloro-4,4,5,5-tetramethyl-1,3,2-dioxaphospholane in the presence of the internal standard endo-*N*-hydroxy-5-norbornene-2,3-dicarboximide and the relaxation agent Cr(III)acetylacetonate in an NMR tube and ^{31}P NMR spectra were recorded.

Thermochemical pre-treatment of SMS/WS

The thermochemical pre-treatment assays were carried out in a steam pressurized plug-flow horizontal reactor (Advancebio Systems LLC, USA) that allows a high solid load (50% w/w) and operation up to 192 ºC. To avoid clogging, SMS was mixed with wheat straw in a wet weight ratio of 4 to 6 (2 to 8 in dry basis). The operating temperature was adjusted to 160°C, 175°C, or 192 ºC and pressures of 6.5, 8.5, and 15.5 bar, respectively using a residence time of 10 min. The catalyst (NaOH, Na_2CO_3 or H_2SO_4) was added in a relation of 4% by dry weight to the total solid content. For homogenization, the mixture was blended manually first and left overnight at room temperature before feeding the reactor afterward. Finally, the pre-treated samples were filtered with a filter press and subsequent filter cake, as well as extract, were analyzed separately. In total, from 1 kg of SMS and 1.65 kg of wheat straw, 1.4 kg of extract with a solid content of 50-60 mg/mL was generated. In average, a carbohydrate yield of 20% relative to the number of carbohydrates contained in the initial SMS: wheat straw mixture (ratio 6:4) was reached (Figure 6.8B).

Organosolv treatment of SMS

As starting material pristine SMS was used. The Organosolv treatment was performed in a stirred batch reactor (working volume 70 mL) at 250°C for 60 min using either 10 wt% substrate-solvent mixture. Water and ethanol were applied in a ratio of 1:1, 6:4 or 7:3 respectively. After extraction, the mixture was filtered, producing 50 mL of lignin-enriched extract with a solid content of ca. 10 mg/mL.

Preparation of O/W-miniemulsion stabilized by SMS derived bio-based surfactant

To prove the surface activity of the extraction products obtained by thermochemical pre-treatment they were used as surfactants to stabilize oil-in-water miniemulsions: After thermochemical pre-treatment (190°C, NaOH catalyzed), the slurry was filtered and the resulting extract was dried under reduced pressure. From the solid obtained, 50 mg was dissolved in 5 ml MilliQ water to yield a 10 mg/mL solution. 200 µL hexadecane was added and the mixture was sonicated (Branson Digital Sonifier W450-D, 1/2" tip, 70% amplitude, 3 min, 20 s ultrasound followed by 10 s pauses, 0°C) to form a miniemulsion. Afterward, the dispersion was stirred gently for at least 7 days. To investigate the impact of pH value or salt, the bio-based surfactant was dissolved in the respective aqueous NaOH (pH 11), HCl (pH 2) or NaCl (10 mg/mL, 100 mg/mL) solution instead of pure MilliQ water. Furthermore, the stability of the aqueous dispersions (at pH 7, without the addition of salt) at 50°C or 70°C was investigated.

Enzymatic degradation of SR-B loaded nanocarriers

0.3 mL of the laccase cocktail L371 was mixed with 1.7 mL glycine/sodium hydroxide buffer (pH 10.5) and 0.5 mL of a nanocarriers dispersion (solid content: 1.5 mg/mL). The degradation reaction proceeded for 24 h at room temperature under stirring while kept open to enrich the solution with oxygen. To determine the dye release, the nanocarriers were removed by centrifugation and the amount of SR-B in the supernatant was quantified by UV/Vis spectroscopy.

Synthesis

Polystyrene nanoparticles stabilized by an SMS derived bio-based surfactant

Carbohydrate-enriched fractions generated by the thermochemical pre-treatment were dried under reduced pressure. 240 mg of the obtained bio-based surfactant was dissolved in 24 mL MilliQ water. Afterward, 6 g styrene, 152 mg hexadecane and 102 mg of 2,2'-azobis(2-methylbutyronitrile) were added and the mixture was stirred vigorously for one hour. After sonication (Branson Digital Sonifier W450-D, 1/2" tip, 90% amplitude, 2 min, 20 s ultrasound followed by 10 s pauses, 0°C) the reaction was allowed to proceed at 70°C overnight. After the polymerization, the reaction mixture was filtered through a Kimtech wipe to remove any aggregates (typically no macroscopic aggregates were detected). For further purification, the dispersion was centrifuged for 45 min at 12k rpm and redispersed in MilliQ water (the solid content was adjusted to ca. 8 mg/mL).

Formation of nanocarriers from lignin-enriched Organosolv fractions

Lignin enriched extracts obtained from previous Organosolv treatment (EtOH-water 50:50) were dried under reduced pressure. The residue was dissolved in acetone and precipitated in water afterward. The solid was isolated by centrifugation and was dried at 50°C at reduced pressure. 40 mg of the fine brown powder was dissolved in 520 µL DMSO adding optionally 5 mg of sulforhodamine B. The solution was then mixed vigorously for 1 min at 20k rpm with a 1 wt% cyclohexane-PGPR solution using an IKA Ultraturrax disperser To form a pre-emulsion. Subsequently, the emulsion was treated with ultrasound for 3 min (Branson Digital Sonifier W450-D, 1/2" tip, 70% amplitude, 20 s ultrasound followed by 10 s pauses) cooled by water. A solution consisting of 2 g cyclohexane, 6 mg PGPR and 60 mg of TDI was added then dropwise and the reaction was allowed to proceed overnight at RT under stirring.

For solvent exchange, 400 µL of the dispersion was added slowly under vigorous shaking to 5 ml of a 1 mg/mL aqueous sodium dodecyl sulfate (SDS) solution. The mixture was sonicated for a further 3 min in a sonication bath (25 kHz) and finally stirred for 24 h with

an open cap To guarantee evaporation of the cyclohexane. For purification, the dispersions were centrifuged (30 min, 4k rpm), followed by solvent exchange and redispersion in aqueous SDS solution (0.1 wt%) afterward.

6.4 Results and Discussion

Compositional analysis of SMS

The substrate prepared specifically for growing mushrooms is a blend of natural products with high organic content. The major ingredients in the compost investigated in this study were wheat straw (62 wt%), gypsum (6 wt%), and poultry manure (30 wt%) as well as ammonium sulfate (0.6 wt%) as a nitrogen source. During the growth, the mycelium penetrated continuously the compost consuming carbohydrates, lignin, and nutrients. After the harvest, the spent mushroom substrate consisted mainly of water (> 60%), lignin, ash (25-35%), residual carbohydrates and fungal mycelium. The majority of the SMS dry matter (82-85%) was insoluble in water and was composed of ca. 30% lignin. Additionally, saccharides like glucan (8%) and xylan (4%), which are related to cellulose and hemicellulose respectively, were identified. Hence, SMS contains higher lignin amounts than agricultural residues like wheat straw (9-17%), corn stover (7-20%) or sugarcane bagasse (10-20%) but also than lignocellulosic feedstocks like oak, birch and poplar (with each ca. 25%) and is therefore considered as a particularly useful lignin source.[119]

Thermochemical treatment of SMS

The dried SMS was grounded with a mesh size of 6 mm and the moisture content was adjusted to improve processing and reproducibility. In spite of the presence of fungal enzymes (e.g. lignases, cellulases) and the mycelium penetration during the mushroom cultivation, which might lose the dense lignocellulose structure in the compost,[119] the spent mushroom substrate was found to be recalcitrant and demanding to process. To prevent clogging of the plug-flow reactor, the SMS was supplemented by wheat straw in a ratio of 4:6, which is another seasonal underutilized lignocellulosic feedstock.[120] The SMS (or the mixture with wheat straw) was treated at elevated temperatures in a pressure reactor with the addition of acid or base. Due to the recalcitrant structure of SMS and its buffering capacity, fractionation needed to be performed at high temperatures and with high catalyst concentrations. After the thermochemical treatment, the slurry was filtered, and the resulting filter cake was investigated separately from the liquid extract. To find optimal process conditions, the reaction temperature

was varied from 160°C to 190°C. SEC proved the extraction of a polydisperse mixture of oligomers, with molar masses slightly decreasing when the temperature of the process was increased, which indicates a more efficient fractionation of SMS under harsher conditions (SI: Figure 6.2). Independent of the temperature during the process, the monosaccharide xylose was the major exctracted compound, while glucose was solubilized always in lower amounts (Figure 6.1b, green). Respectively, the insoluble filter cake contained a large fraction of glucan, but significantly less xylan (Figure 6.1a, green). With increasing temperature, the concentration of xylose increased by the factor of three in the extract, and a reduced amount of xylan in the filter cake was detected. Additionally, arabinan was extracted, while in the filter cake it was only detected in small amounts. Interestingly, the amount of lignin, which was left in the solid, slightly increased comparing the processes at 160°C and 190°C, indicating more effective lignin solubilization at lower temperatures. However, from the ^{1}H NMR spectra of these extracts, mainly aliphatic species, i.e. carbohydrates were identified (Figure 6.1). Lignin and other aromatic compounds were extracted only in trace amounts. Phosphorylation of the extracted compounds allowed determination of aliphatic and aromatic hydroxyl groups, respectively, according to a literature protocol.[84] The extracts were reacted with 2-chloro-4,4,5,5-tetramethyl-1,3,2-dioxaphospholane and ^{31}P NMR spectra of the reaction products were recorded. The spectra indicated mainly signals of phosphorylated aliphatic alcohols, whereas almost no resonances belonging to phenolic compounds were detected (Figure 6.5B, black).

Alkaline catalysts promote the cleavages of ester linkages and glycosidic bonds in the cell walls, resulting in cellulose swelling and partial solubilization.[121] Particularly Na_2CO_3[122] and NaOH,[123] two inexpensive and abundant bases, showed high effectivity regarding the degradation of lignocellulosic biomass in previous studies.[29, 119, 124] Therefore, the influence of the catalysts on the thermochemical treatment of an SMS-wheat straw mixture was studied. Interestingly, the basic reaction conditions only reduced the amount of xylose in the extract, correlating with increasing xylan content in the respective filter cakes, but did not affect the amount of solubilized lignin or glucan (Figure 6.1, blue).

Moreover, H_2SO_4 is a commonly employed reagent to pretreat diverse biomass, as it effectively hydrolyzes hemicellulose to xylose, which then can be converted to furfural and derivatives.[125] In contrast to Na_2CO_3 and NaOH, the addition of the acid led to decreased yields of xylan in the filter cake but also to a reduction of xylose in the extract (Figure 6.1, red). Simultaneously, we found significantly increased concentrations of 5-HMF (745 mg L^{-1}, 250%) and furfural (1412 mg L^{-1}, 413%) in the extract, suggesting acidic degradation reactions of xylose.

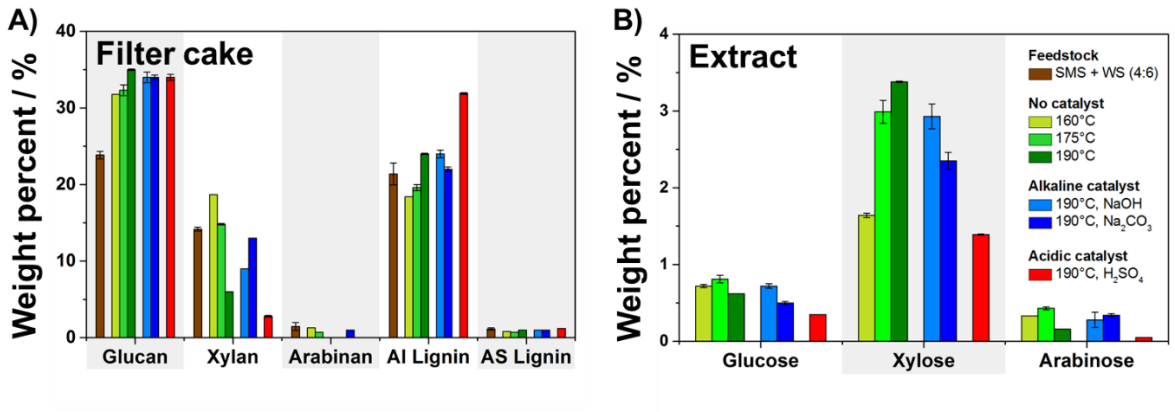

Figure 6.1: Compositional analysis of A) filter cake (weight percent refers to the dry mas of the filter cake; AI = acid insoluble, AS = acid soluble (Table 6.2). B) carbohydrate enrichted extract after thermochemical pre-treatment and filter press (Weight percent of liquid extract (Table 6.1)

Table 6.1: Compositional analysis of carbohydrate-enriched extracts obtained after thermochemical pretreatments of SMS/WS mixtures.

Temperature °C	**160**		**175**		**190**		**190**		**190**		**192**	
Residence time (min)	**10**		**10**		**10**		**10**		**10**		**10**	
Catalyst	**-**		**-**		**-**		**NaOH 4%**		**Na2CO3 4%**		**H2SO4 4%**	
Feedstock code	030/17-031/17		030/17-031/17		030/17-031/17		030/17-031/17		030/17-031/17		062/13+005/17	
Sample code	EXP2_LF		EXP3_LF		EXP4_LF		EXP8-LF		EXP12_LF		EXP5_LF	
g/L	Avg.	SD	Avg.	SD	Avg.	SD	Avg.	SD	Avg.	SD	Avg.	SD
Monomeric and oligomeric sugars												
Glucose	7,2	0,2	8,1	0,5	6,2	0,0	7,2	0,3	5,0	0,2	3,5	0,0
Xylose	16,4	0,3	29,9	1,5	33,8	0,1	29,3	1,6	23,5	1,1	13,9	0,1
Arabinose	3,3	0,0	4,3	0,2	1,6	0,0	2,8	0,1	3,4	0,2	0,5	0,0
Organic acids												
Succinic Acid	0,1	0,0	0,1	0,0	0,0	0,0	0,1	0,0	0,1	0,0	0,0	0,0
Lactico acid	0,2	0,0	0,5	0,0	0,8	0,0	1,2	0,0	0,4	0,0	0,1	0,0
Acetic acid	1,5	0,0	3,1	0,0	4,8	0,0	9,6	0,0	8,3	0,0	3,4	0,1
Levulinic acid	0,3	0,0	0,2	0,0	0,0	0,0	0,2	0,0	0,1	0,0	0,1	0,0
mg/L	**Avg.**	**SD**	**Avg.**	**SD**	**Avg.**	**SD**	**Avg.**	**SD**	**Avg.**	**SD**	**Avg.**	**SD**
5HMF	488,7	0,0	258,3	0,0	294,9	0,0	38,7	0,0	53,9	0,0	744,5	25,4
4-hydroxibenzoic	17,1	0,0	13,9	0,0	11,1	0,0	1,7	0,0	6,6	0,0	17,5	20,9
Vanillinic/syringic	71,1	0,0	83,3	0,0	63,7	0,0	54,2	0,0	69,9	0,0	99,7	4,4
p-Coumaric	24,5	0,0	14,8	0,0	6,0	0,0	12,9	0,0	7,7	0,0	7,9	0,7
Furfural	43,0	0,0	70,6	0,0	342,4	0,0	100,7	0,0	39,5	0,0	1411,7	15,0
Ferulic acid	6,5	0,0	10,7	0,0	16,4	0,0	4,4	0,0	12,5	0,0	11,7	1,2
Vainillin/syringaldehyde	40,1	0,0	42,9	0,0	56,0	0,0	20,2	0,0	24,4	0,0	90,1	3,8
5MethylFurfural	2,5	0,0	4,9	0,0	14,1	0,0	8,7	0,0	6,8	0,0	39,6	0,7
Phenol	0,0	0,0	0,0	0,0	12,2	0,0	0,0	0,0	0,0	0,0	0,0	0,0
Benzoic	0,0	0,0	0,0	0,0	0,0	0,0	29,9	0,0	51,8	0,0	0,0	0,0
Syringol	0,0	0,0	0,0	0,0	0,0	0,0	23,3	0,0	0,0	0,0	0,0	0,0
Guayacol	0,0	0,0	0,0	0,0	0,0	0,0	10,4	0,0	16,4	0,0	0,0	0,0
Benzaldehyde	0,0	0,0	0,0	0,0	0,0	0,0	0,0	0,0	0,0	0,0	0,0	0,0

Table 6.2: Compositional analysis of filter cake obtained after thermochemical pretreatments of SMS/WS mixtures.

Temperature °C	160		175		190		190		190		192	
Residence time (min)	10		10		10		10		10		10	
Catalyst	-		-		-		NaOH		Na2CO3		H2SO4 4%	
Feedstock code	030/17-031/17		030/17-031/17		030/17-031/17		0/17-031. 13/062		030/17-031/17		13/062+005/17	
Sample code	EXP2_SF		EXP3_SF		EXP4_SF		EXP8-SF		EXP12_SF		EXP5_SF	
%w/w	Avg.	SD	Avg.	SD	Avg.	SD	Avg.	SD	Avg.	SD	Avg.	SD
Moisture	7,7	0,0	8,6	0,0	8,7	0,1	10,5	0,1	9,8	0,1	59,3	0,3
Ashes	67,7	0,4	62,9	1,2	65,7	0,3	63,1	0,3	60,6	0,8	12,3	0,5
Insolubles												
Glucan	31,8	0,0	32,3	0,7	35,4	0,1	34,0	0,7	34,2	0,3	34,0	0,4
Xylan	18,7	0,0	14,8	0,1	6,2	0,0	8,8	0,0	13,3	0,0	2,8	0,1
Arabinan	1,3	0,0	0,7	0,0	0,2	0,0	0,3	0,0	0,6	0,0	0,0	0,0
AI Lignin	18,4	0,0	19,6	0,4	24,4	0,1	24,4	0,5	21,7	0,3	31,9	0,1
AS Lignin	0,8	0,0	0,7	0,0	0,9	0,0	1,2	0,0	0,8	0,0	1,2	0,0
AI Ash	1,8	0,0	2,0	0,1	2,4	0,0	2,6	0,0	2,1	0,1	3,0	0,1
Acetyl	10,3	0,0	8,5	1,0	3,9	0,4	2,0	0,0	1,7	0,4	1,3	0,2

AI: acid insoluble

AS: acido soluble

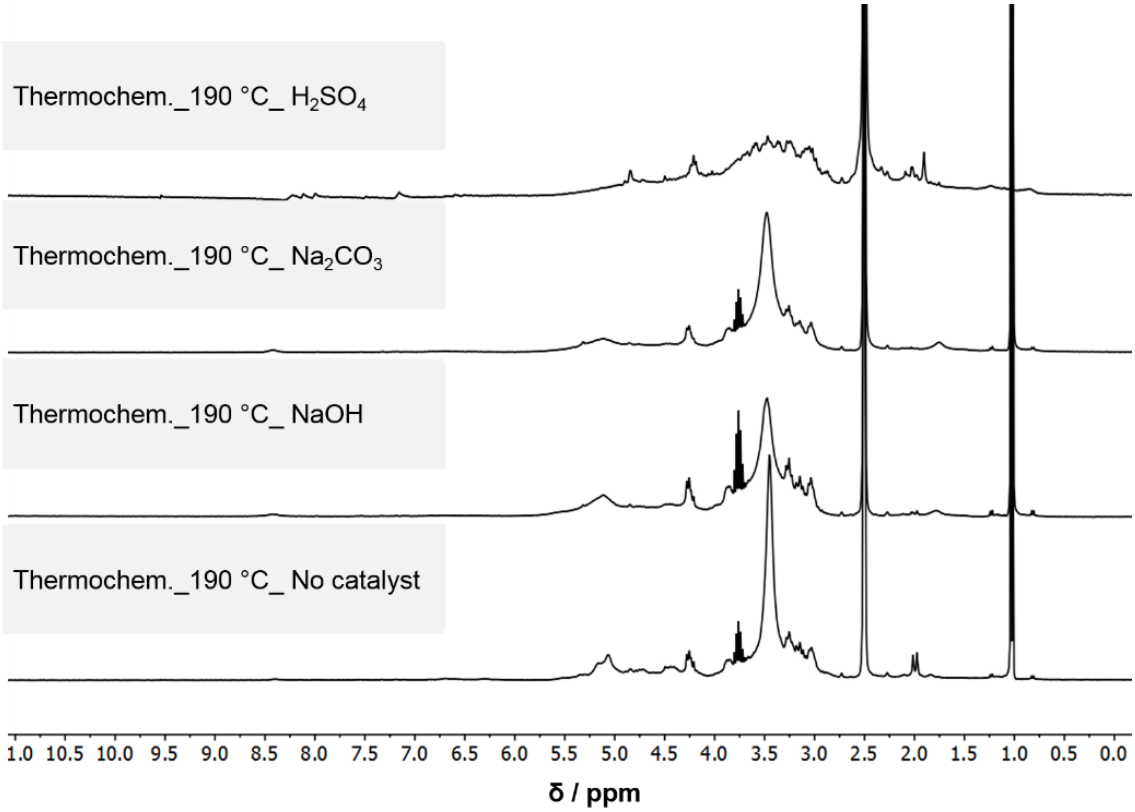

Figure 6.1: ^{1}H NMR spectra (DMSO-d_6, 25°C, 300 MHz) of SMS extracts obtained after thermochemical treatments.

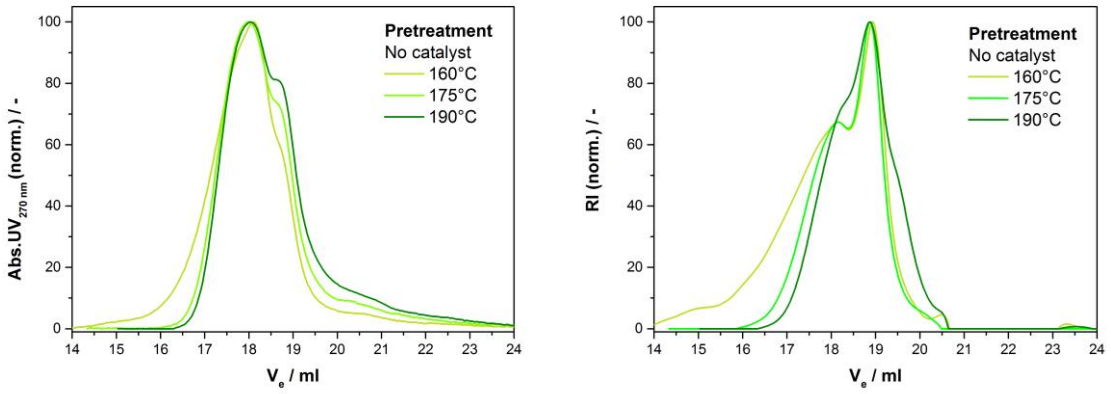

Figure 6.2: SEC elugrams using UV-detection (270 nm, left) or RI-detection (right) from extracts obtained from thermochemical pretreatments under 160°C, 175°C or 190°C without catalyst.

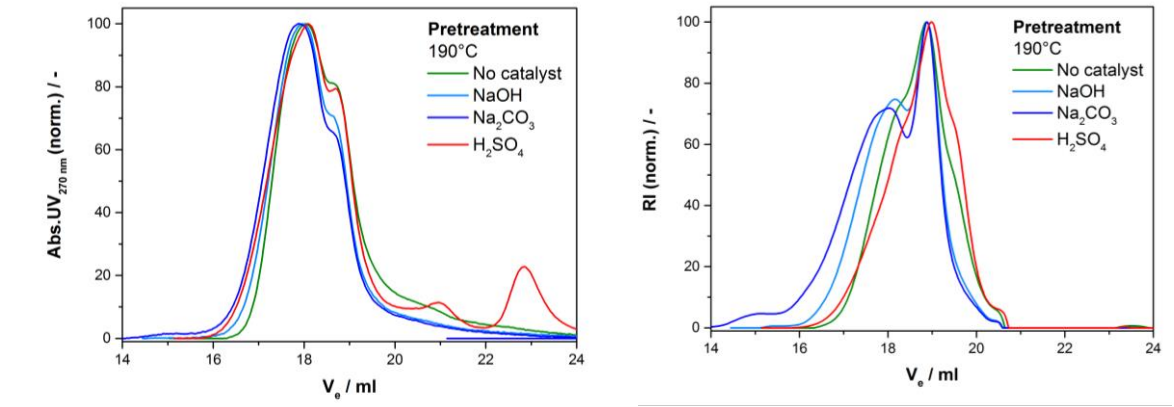

Figure 6.3: SEC elugrams using UV-detection (270 nm, left) or RI-detection (right) from extracts obtained from thermochemical pretreatments under 190°C using different catalysts.

Thus, all thermochemical treatments resulted in extracts enriched in a mixture of carbohydrates and carbohydrate derivatives. Independent on the catalyst, xylose was solubilized as the major compound, whereas lignin remained almost completely in the filter cake. In total, a carbohydrate yield of ca. 20% (Figure 6.8B) was reached, which is comparable to results already reported from SMS extractions in literature.[27, 115] In comparison, higher yields of carbohydrates were documented when fractionating lignocellulosic feedstocks like wheat straw, soybean straw,[128] spruce,[129] pine[130] under similar conditions (e.g. liquid hot water, acid or alkaline treatments) underlining the recalcitrancy of SMS.[29, 119] To further increase the carbohydrate yield, the recalcitrant filter cake could be treated additionally by enzymatic hydrolysis (e.g. cellulases) followed by an additional extraction step.[131]

Bio-based surfactants from carbohydrate-enriched SMS

Due to their versatile applicability such as in bioremediation, food, cosmetics, pharmaceuticals or nanotechnology, bio-based surfactants are expected to reach a market value of up to 2 billion USD by 2020.[132] Especially, regarding waste management and exploitation of renewable sources, surfactants produced from inexpensive waste feedstock are of growing interest.[132, 133]

The carbohydrate-enriched liquid fractions obtained after the thermochemical treatment of SMS were tested on their capacity to decrease the surface tension. The extracts, which had pH-values of 3.47 (for the H_2SO_4-treated SMS) and ca. 4.8 for all others, were lyophilized and added at different concentrations to water and the surface tension at the air-water interface was measured by a ring tensiometer. All extracts reduced the surface tension of pure water (with 72 mN m^{-1}); at concentrations of 3 g L^{-1}, extracts obtained by treatments using no or alkaline catalysts decreased the surface tension to ca. 57 mN m^{-1} proving their capability to be used as surfactants (Figure 6.4B). At the same weight concentration, the acidic extract only reduced the interfacial tension to ca. 62 mN m^{-1}, probably due to partial protonation of the compounds in the mixture resulting in lower interfacial activity. However, a further increase of the extracts (up to 50 g L^{-1}) still resulted in a steady decrease of the surface tension to values between 45-50 mN m^{-1}, indicating an incomplete surface coverage by surfactant molecules. A constant value for the surface tension was not reached, probably due to aggregates, which were detected by dynamic light scattering, contained in the SMS extract, which could not be separated by centrifugation or filtration. By further increasing the concentration of the extract, these aggregates were enriched steadily, leading to an additional surface on which the surfactant molecules can arrange, which led to a slight further decreased surface tension.[134]

Additionally, we determined the interfacial tension between chloroform and the aqueous SMS extracts (solid content of 10 mg mL^{-1}) with a spinning drop tensiometer. In accordance to our previous results, the interfacial tension between water and $CHCl_3$ was significantly reduced from 26.6 mN m^{-1} to 7.3 mN m^{-1} after the addition of the extract obtained from SMS treatments using no catalyst. Similar values of ca. 11 mN m^{-1} were measured for the other extracts (Table 6.3).

Table 6.3: Interfacial tension measured by spinning drop tensiometry between $CHCl_3$ and water at a concentration of 10.0 mg mL^{-1}.

Sampe code	Catalyst	Interfacial tension / Nm m^{-1}
030/17-031/17 Exp 4 LF		7.3 ± 0.45
030/17-031/17 Exp 8 LF	NaOH (4%)	10.00 ± 0.03
030/17-031/17 Exp 12 LF	Na2CO3 (4%)	11.11 ± 0.46
062/13-005/17 Exp 5 LF	H2SO4 (4%)	11.36 ± 0.01

The ability to decrease the interfacial tension suggests an extraction of amphiphilic hydrolysates from cellulose, hemicellulose, or lignin generated during the thermochemical treatment. As ^{1}H and ^{31}P NMR spectra (the latter after derivatization, Figure 6.5B) proved the solubilization of aromatic compounds only in minor extent, mainly UV-active oligomers were detected by SEC though (Figure 6.3) the extracts contained probably phenolic oligoglycosides. This correlates with slightly negative logD-values (distribution coefficient determined between water and octanol, Table 6.4) determined for all extracts and underlines the hydrophilic character of the amphiphilic oligosaccharides. Due to their amphiphilicity, such phenolic glycosides are interfacially active and can stabilize oil-in-water emulsions.

Table 6.4: Distribution coefficient between MilliQ water (pH7) and octanol at a concentration of 2.5 mg mL^{-1}.

Sampe code	Catalyst	LogD = $\log(c_{octanol})$-$\log(c_{water})$
030/17-031/17 Exp 4 LF		-0,42
030/17-031/17 Exp 8 LF	NaOH (4%)	-0,92
030/17-031/17 Exp 12 LF	Na2CO3 (4%)	-0,98
062/13-005/17 Exp 5 LF	H2SO4 (4%)	-0,66

The extracts were successfully used to stabilize oil-in-water miniemulsions - heterophase systems in which stable nanodroplets of one phase are dispersed in a second continuous phase.[135] In an oil-in-water miniemulsion, each nanodroplets of the oil can be considered as a nanoscopic, individual batch reactor that enables a variety of reactions, e.g. polymerizations and can be used to prepare various nanomaterials.[26] As an initial test for emulsion stabilization, 1 mL hexadecane (as dispersed phase) was dispersed into 25 mL of an aqueous SMS extract (catalyst: NaOH, 190°C) with a solid content of 1 wt%. After sonication, yellowish/ light-brown turbid dispersions were obtained which remained macroscopically stable for at least 7 days at room temperature. Phase separation was not observed when the dispersion was heated up to 70°C or after the addition of NaCl (100 mg/mL). Moreover, the dispersion did not undergo phase separation, when the pH of the

continuous phase was changed from 2 to 12, underlining the versatile applicability of the SMS-based surfactant.

As the results suggest that the carbohydrate-enriched fractions can stabilize oil-in-water droplets, we applied the extracts as stabilizers during a free radical miniemulsion polymerization of styrene to prepare polystyrene nanoparticles. A mixture of styrene, hexadecane (as costabilizer), and the initiator 2,2'-azobis(2-methylbutyronitrile) was emulsified in an aqueous SMS extract solution by vigorous stirring. After ultrasonication, a stable miniemulsion was obtained. The polymerization of styrene was carried out at 70°C for 15 h. After the reaction, a colloidally stable dispersion of PS-particles was obtained, independent which of the extracts was used for the stabilization. Dynamic light scattering (DLS) and electron microscopy proved the successful formation of spherical polystyrene particles (Figure 6.4A) with diameters between 500 and 1000 nm, which did not show any signs of aggregation for at least 5 months of storage at room temperature, proving the potential of SMS-derived extracts as bio-based surfactants.

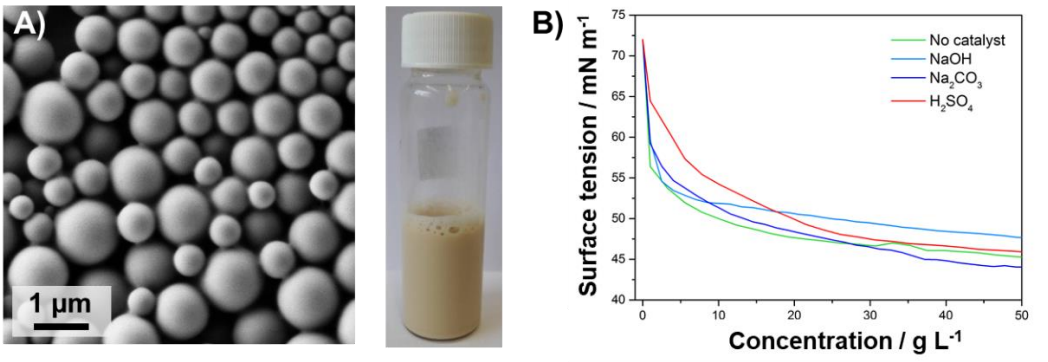

Figure 6.4: A) SEM image (left) and photo (right) of the polystyrene nanocarrier dispersion stabilized with the SMS-derived bio-based surfactant and B) Surface tension measurements of SMS-derived bio-based surfactants produced by thermochemical treatments at 190°C using different catalysts measured by ring-tensiometry.

Organosolv treatment of SMS

Organosolv is a pulping technique applied in paper industry that uses an organic solvent to solubilize lignin and hemicellulose.[136] As pure SMS is composed of ca. 30% lignin, it would be an ideal lignin feedstock. Therefore, we extracted SMS with different ethanol-water mixtures at 250°C in a batch reactor. Using a 50:50 ethanol-water mixture, the lignin amount in the solid residue was reduced by almost 40% (Figure 6.5A). By increasing the ethanol percentage from 50% to 70% the extracted lignin amount remained unchanged. Besides lignin, also glucan and hemicelluloses were extracted partially. However, ^{1}H NMR and ^{31}P NMR (after

derivatization) spectroscopy of the respective extracts showed mainly the for lignin typical signals (e.g.: ^{1}H: 6.0-8.0 ppm, aromatic protons; ^{31}P: 151-147 ppm aliphatic –OH, 146-139 ppm phenolic –OH) and hence lignin can be assumed as the major compound solubilized (Figure 6.5B, red; Figure 6.1). Fully in line with these results, FTIR spectra proved the presence of aromatic compounds by intense bands at 1609 cm^{-1} and 1457 cm^{-1} belonging to the vibration of the aromatic skeleton (Figure 6.4). Additionally, SEC analyses confirmed the presence of oligomeric and polymeric compounds in the extracts with relatively broad molar mass dispersity (with apparent M_n: ca. 800 g/mol, M_w: 3300 g/mol; $Đ$= 4.2; Figure 6.9).

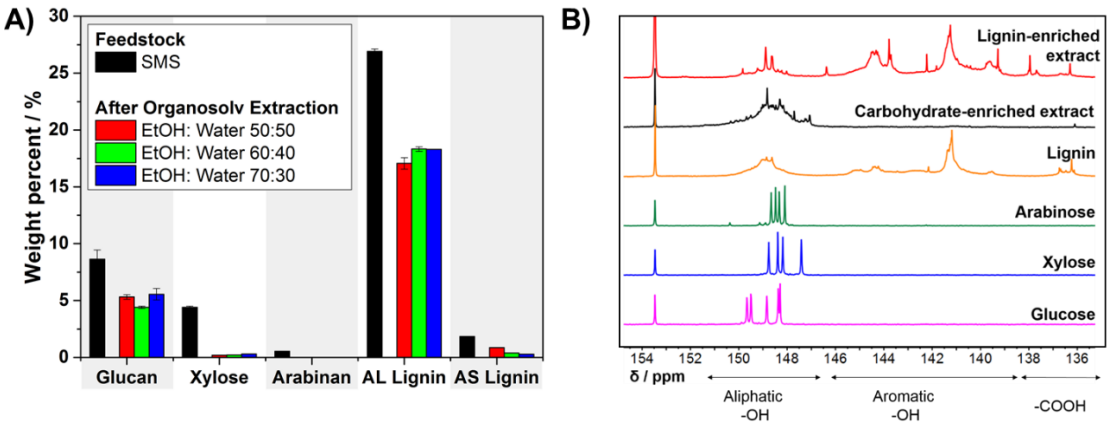

Figure 6.5: A) Compositional analysis of the filter cake left after extracting SMS with water-ethanol mixtures (Organosolv treatment). B) Comparison of the ^{31}P NMR spectra obtained from SMS-derived extracts and commercially available lignin as well as carbohydrates after phosphorylation.

Table 6.5: Compositional analysis of lignin enriched extracts obtained after Organosolv treatments of SMS alone or of a pretreated SMS-WS mixture.

Temperature (ºC) **Ethanol:H2O** **Solid content (%w/w)** **Code**	**SMS alone (before Organosolv) (015/18)**		**250 50:50 10 SMS_Ext26_R**		**250 60:40 10 SMS_EXT28_R**		**250 70:30 10 SMS_EXT28_R**	
	Avg.	SD	Avg.	SD	Avg.	SD	Avg.	SD
Glucan	8,2	0,8	5,3	0,2	4,4	0,1	5,6	0,5
Xylose	0,4	0,1	0,2	0,0	0,2	0,0	0,3	0,0
Arabinan	0,0	0,0	0,0	0,0	0,0	0,0	0,0	0,0
Al Lignin	27,0	0,0	17,1	0,5	18,3	0,2	18,3	0,0
AS Lignin	0,4	0,0	0,9	0,0	0,4	0,0	0,3	0,0
Al Ash	9,2	0,2	5,3	0,0	5,8	0,0	6,2	0,1
Acetyl	0,2	0,0	0,2	0,1	0,1	0,0	0,1	0,0

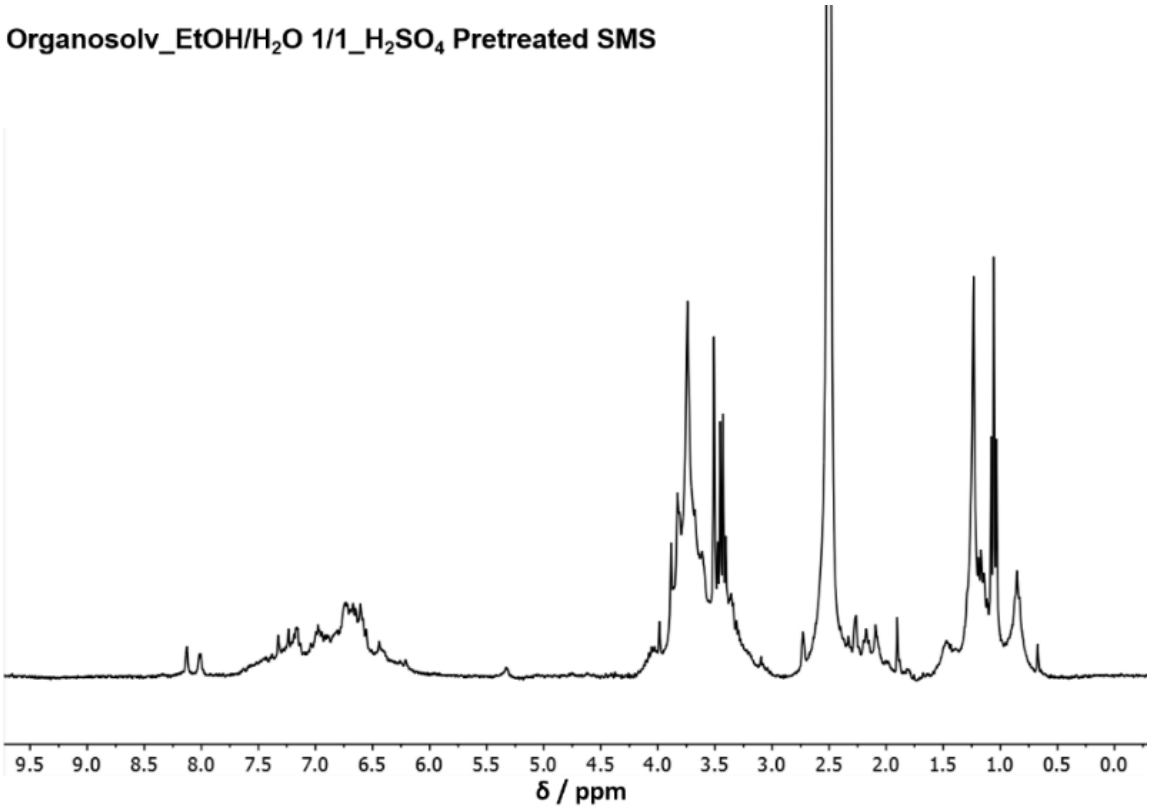

Figure 6.6: ^{1}H NMR spectra (DMSO-d_6, 25°C, 300 MHz) of SMS extracts obtained after Organosolv extraction.

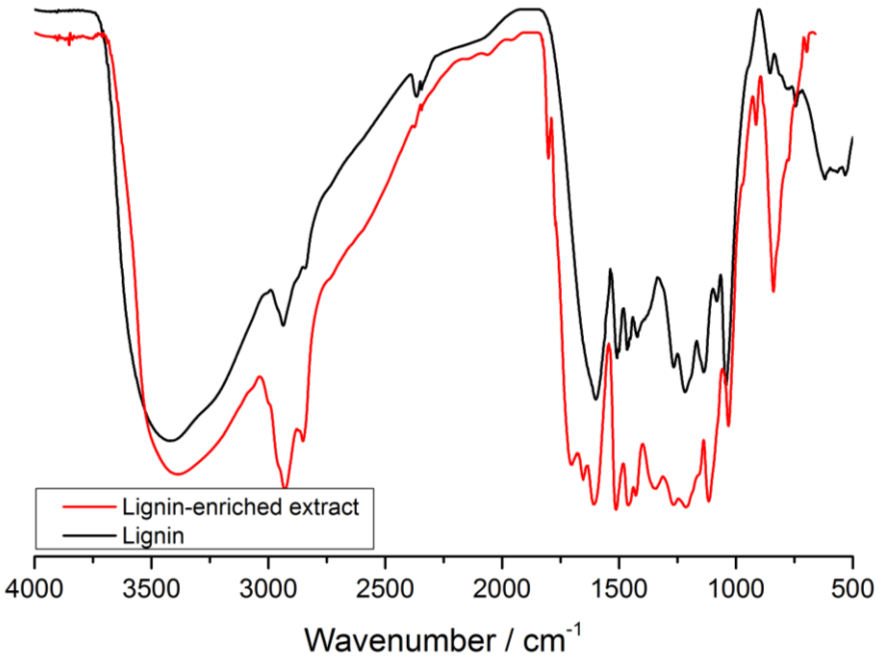

Figure 6.7: Overlay of FTIR (KBr) spectrum of lignin enriched SMS extracts obtained after Organosolv treatment (red) compared to a commercial lignin (black).

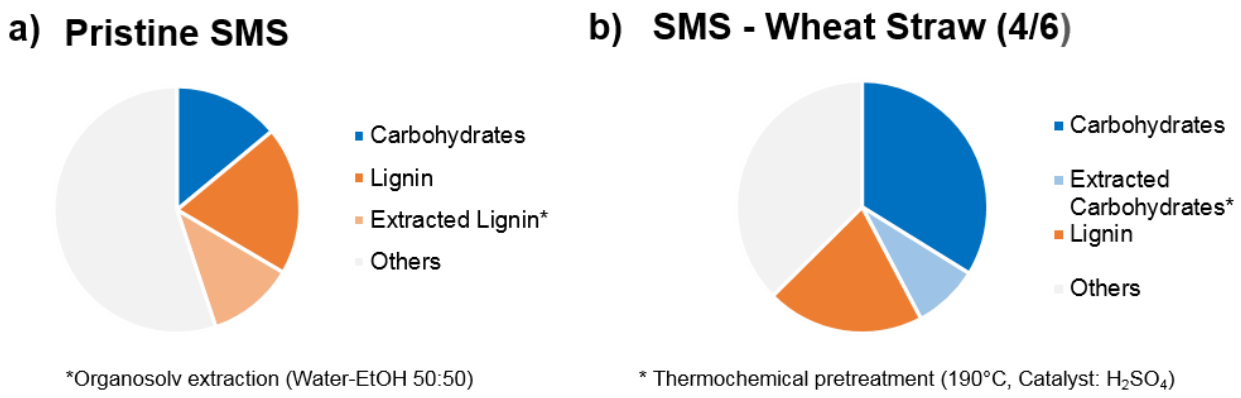

Figure 6.8: Composition of pristine SMS and a SMS-wheat straw mixture (ratio 4:6). All fractions are given in weight% of dry mass. The carbohydrates include glucan, xylan, arabinan, glucose, xylose and arabinose. Exemplarily, a) the amount of lignin isolated using Organosolv extraction (EtOH-Water 50:50) or b) the amount of isolated carbohydrates applying a thermochemical pretreatment (190°C, catalyst: H_2SO_4) is shown.

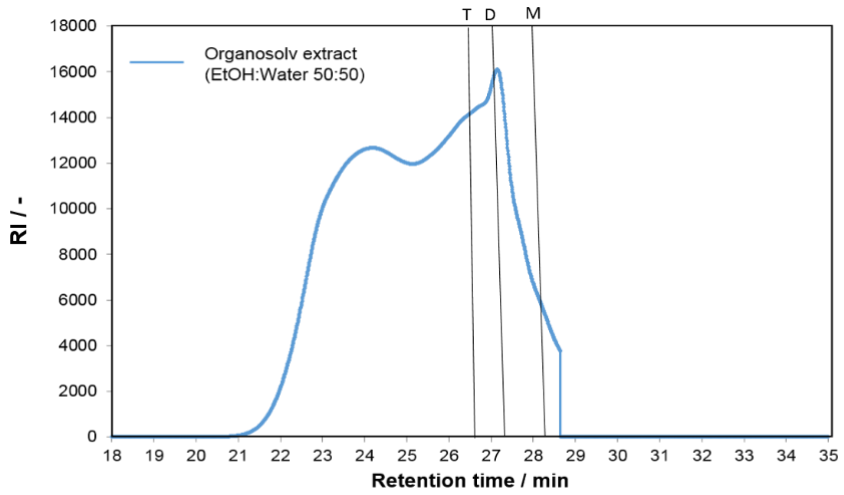

Figure 6.9: SEC elugram of "Organosolv extract" obtained after extraction with an EtOH-water mixture (50:50). (M = Monomer; D = Dimer; T = Trimer

Preparation of biodegradable nanocarriers from lignin-enriched fractions

In recent years, the exploitation of lignin was heavily researched particularly as a renewable feedstock for chemical syntheses and as fuel alternatives. However, the valorization to nanomaterials gained increasing interest recently.[29, 119, 127] Until now, solid or hollow particles with core-shell structures were prepared mainly by nano-precipitation, whereas only a few studies studied the preparation of chemically crosslinked lignin nanoparticles.[45] Herein, dye-loaded, biodegradable lignin nanocarriers were synthesized from lignin-enriched extracts

obtained after the Organosolv treatment. An interfacial polyaddition in inverse miniemulsion, similar to previously reported for commercial lignin, was adapted for the extracts.[9] For that, the solid was dissolved in DMSO and the dark-brown solution was dispersed in cyclohexane, containing the biocompatible and -degradable surfactant PGPR.[137] To further increase the sustainability of the process, bio-based solvents, e.g alcohols, could be used as a dispersed phase. To prove that the nanocarriers might be used to deliver drugs, sulforhodamine-B was encapsulated as a model cargo. The emulsion was sonicated to generate stable nanodroplets (DLS: 200-300 nm), which act as a template for the nanocarrier production. We used toluene-diisocyanate (TDI) as a cross-linker, as its isocyanate groups react with lignin's hydroxyl groups as well as with hydroxyl groups of carbohydrate residues at the droplet interface forming a cross-linked shell (Figure 6.10A). After the reaction, the solvent was exchanged by dispersing the product mixture into an aqueous 0.1 wt% sodium dodecyl sulfate solution and subsequent evaporation of cyclohexane. The resulting dispersion was centrifuged and re-suspended in fresh water. A stable aqueous dispersion of the SMS-based nanocarriers was obtained with diameters of ca. 290 nm (PDI 0.15) as determined by dynamic light scattering. After storage of 6 months at room temperature, no change in the particle size distribution was detected by DLS, proving the colloidal stability of the prepared nanocarrier dispersions. The morphology of the nanocarriers was a mixture of spherical core-shell and full particles. Previous studies with commercial lignin produced only core-shell structures under the same reaction conditions. The mixture of both core-shell and solid nanoparticles from the SMS-based lignin might be attributed to the diverse mixture of the Organosolv SMS-extract containing molecules of different hydrophilicity and reactivity so that the crosslinking with TDI occurred both at the interface and the inside of the DMSO droplets (Figure 6.10B). Despite the different morphologies of the nanocarriers, ca. 80% of the SR-B was determined inside of the nanocarriers after the transfer into an aqueous environment, proving that a DMSO-soluble cargo was effectively loaded into the SMS-based nanocarriers. The remaining 20% of SR-B were either not encapsulated or removed during the redispersion process. The aqueous dispersion could be stored at room temperature without any signs of degradation or leakage of the cargo during for at least four weeks.

As reported previously, lignin-based nanocarriers can be degraded enzymatically by laccases, which occur naturally in diverse fungi and catalyze the oxidation of phenolic compounds by simultaneous oxygen reduction.[36] To prove that also SMS-derived nanocarriers also undergo enzyme-triggered release of the cargo, we quantified the amount of free SR-B before and after addition of a laccase cocktail. After the addition of laccase to the dispersion, a 40% release of SR-B was determined after 24 h. As several pathogenic fungi segregate laccases,[138] the lignin-based nanocarriers might be applied as an enzyme-triggered drug delivery system, which could be of high interest to develop advanced fungal plant protection.

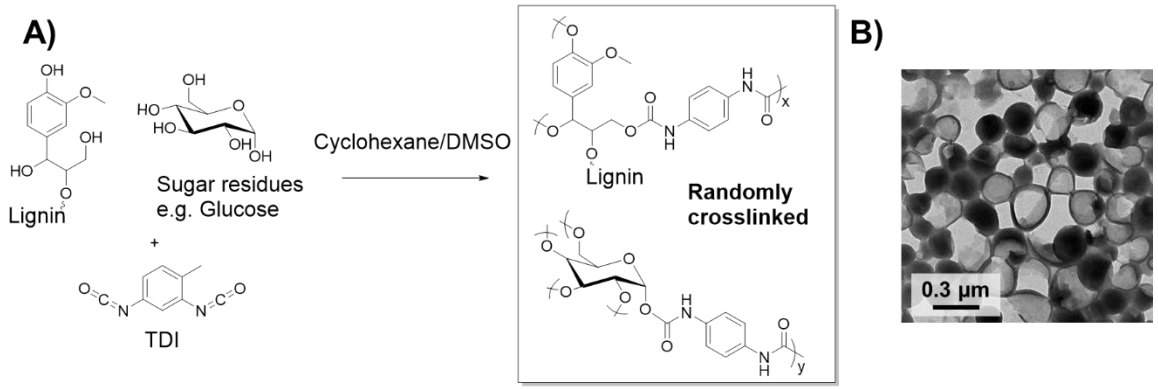

Figure 6.10: A) Possible reaction of Organosolv-SMS extract with TDI at the droplet interface of DMSO nanodroplets dispersed in cyclohexane.[9] B) TEM image of cross-linked Organosolv-SMS nanocarriers.

6.5 Conclusion

This work presents the valorization of the spent mushroom substrate (SMS) by two bio-refinery processes allowing the isolation of either carbohydrates (by a thermochemical treatment) or lignin (by an Organosolv extraction).

The obtained carbohydrate-enriched fractions contained xylose as the major compound whose concentration increased with rising temperature but decreased when using the alkaline catalysts Na_2CO_3 or NaOH. H_2SO_4 was found effective to solubilize xylan but resulted in low xylose concentrations due to following carbohydrate decomposition reactions. As the carbohydrate-enriched fractions significantly decrease the surface tension at a water-air interface, they are promising bio-based surfactants and were successfully used for miniemulsion polymerization.

Soluble lignin was obtained after extracting SMS with ethanol-water mixtures. The Organosolv-SMS (i.e. lignin-enriched fractions) were used as a raw material to generate loaded nanocarriers by an inverse miniemulsion approach. Due to their degradability by laccases, the nanocarriers are considered to be of high interest as bio-based drug delivery systems useful such as for sustainable plant protection.

7 Fungicide-loaded nanocarriers based on xylan

Sebastian J. Beckers, Luc Wetherbee, Jochen Fischer, Frederik R. Wurm

Unpublished data.

The nanocarrier preparation was performed together with Luc Wetherbee (intern student at MPIP in 2018) under scientific guidance of PD Dr. Frederik Wurm. The germination assay was performed by Dr. Jochen Fischer.

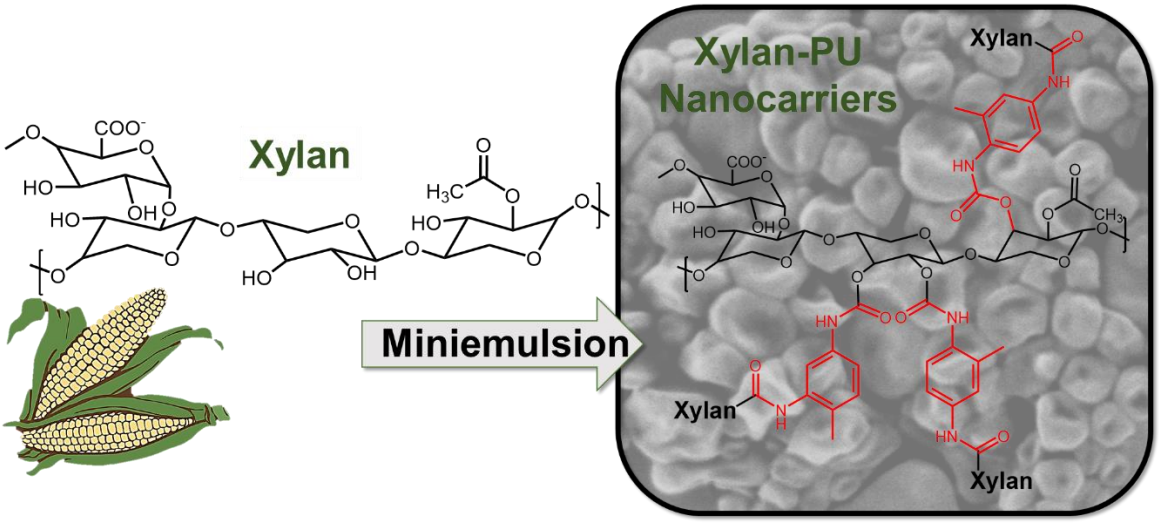

Keywords: *Hemicellulose, xylan, emulsion polymerization, nanocarrier, agriculture*

7.1 Abstract

Chapter 6 explained the preparation of hollow nanocarriers by interfacial polymerization of toluene diisocyanate (TDI) with lignin obtained after Organosolv extraction of spent mushroom substrate. Next to lignin, these extracts contained residual amounts of hemicellulose – a hetero-polysaccharide based on xylan. Exactly like lignin, hemicellulose is a renewable and abundant feedstock that might be of high interest as a bio-based carrier agent for agrochemical formulations. Therefore, this chapter describes how xylooligosaccharides extracted from corncobs can be used to produce loadable and degradable nanocarriers. The hollow nanocarriers were prepared by interfacial polyaddition in an inverse miniemulsion using TDI as a crosslinking agent. The degradability of the xylan-polyurethane nanocarriers was proven by a fungal germination assay and might be used as a trigger to release the encapsulated broad-spectrum fungicide pyraclostrobin.

7.2 Introduction

Xylan is the second most abundant plant polysaccharide on earth and can be extracted from lignocellulosic biomass, which is generated in billion tons as an industrial by-product of agriculture and forestry yearly.[139, 140] The biopolymer belongs to the class of hemicelluloses and is a major component (25-35% dry mass) of the plant cell wall. Naturally, hemicelluloses form together with lignin a branched matrix that embeds the cellulose nanofibrills. This natural composite material is referred as lignocellulose and is essential for the structure and toughness of the plant tissue.[140] Industrially, xylan is valorized mainly by the production of the low-calorie sugar replacement Xylit or it is used in various biorefineries for biofuel production without previous isolation from biomass.[139, 141, 142] Hence, in comparison to cellulose that finds numerous large-scale applications such as in the paper or in the tissue industry, hemicellulose and also xylan are significantly less used until now. The reasons might be the complex and heterogeneous molecular structure of the polysaccharides and the broad molecular weight distribution (10,000 - 40,000 g/mol) depending on the plant origin.[140] Structural characteristic for xylans is a β(1→4) glycosidically linked xylose backbone decorated with various amounts and types of side groups. Depending on the plant, the backbone can be acetylated or is functionalized partially with mono- and oligosaccharides composed of e.g. glucoronic acid and arabinofuranose. Likewise, linkages to lignin-derived moieties such as *p*-coumaryl, coniferyl, or sinapyl acid can occur. These side groups lead to an amorphous structure and strongly determine the solubility of the polymer.[140, 143, 144]

As xylan is a renewable, biocompatible and relative cheap feedstock, it is of high interest as carrier material for advanced drug delivery. Up to date, most investigations used xylan hydrogels to load drugs and only a very few studies dealt with the encapsulation of pharmaceuticals.[145-150] Next to applications in medicine, xylan is ideal as carrier agent in agrochemical formulations due to its plant origin. However, to the best of our knowledge, no studies have reported the formation of pesticide-loaded xylan nanocarriers yet.

A powerful tool to generated hollow nanocarriers is the interfacial polymerization of toluene diisocyanate (TDI) in an inverse miniemulsion.[151] As the stable nanodroplets act as a template where the crosslinker can react at the interface with various nucleophiles like hydroxyl groups or amines, core-shell structures are obtained that can be loaded with versatile active ingredients. Recently, our group produced TDI-crosslinked nanocarriers from lignin sulfonate or lignin-containing biomass extracts (see Chapter 6), which released the encapsulated drug only on-demand in the presence of lignin-degrading enzymes.[9, 100] This approach was extended herein to prepare xylan-polyurea/polyurethane nanocarriers for the encapsulation of the broad-spectrum fungicide pyraclostrobin (Figure 7.1). The nanocarrier dispersions obtained are based on a degradable and biomass-derived feedstock, we are convinced that the developed formulation is a powerful tool for the encapsulation of various agrochemicals (pesticides or fertilizers) which could help to increase the sustainability in plant protection.[144]

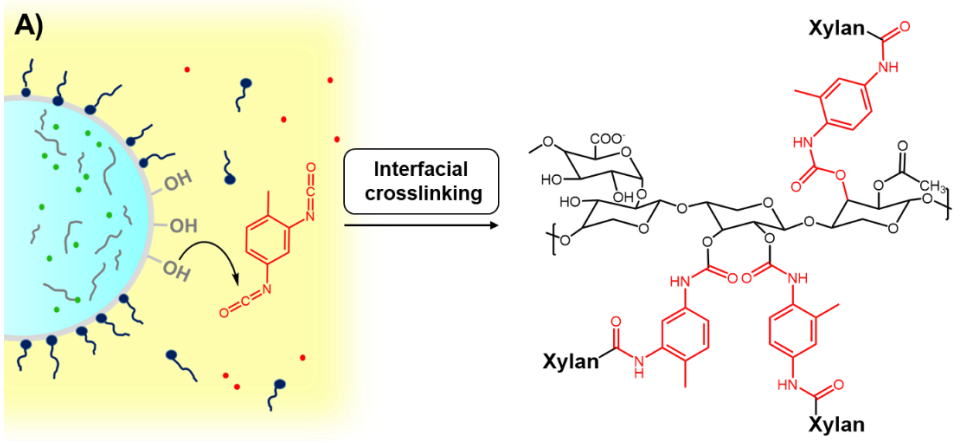

Figure 7.1: Crosslinking of xylan at the droplet interface to generate nanocarriers with core-shell structure.

7.3 Experimental section

Materials

Xylan from corncobs (Art. 8659.2) and beechwood (Art. 4414.2) was obtained from Carl Roth. Toluene diisocyanate (TDI), sodium dodecyl sulfate, 2-chloro-4,4,5,5-tetramethyl-1,3,2-dioxaphospholane and endo-N-hydroxy-5-norbornene-2,3-dicarboximide were purchased from Sigma Aldrich. Pyraclostrobin was bought from Toronto Research Chemicals. All materials were used without further purification.

Poly[(ethylene-*co*-butylene)-*b*-(ethylene oxide)] (= P(E/B-*b*-EO)) consisted of a poly(ethylene-*co*-butylene) block with a molecular weight of (M_w=3700 g/mol) and poly(ethylene oxide) block of (M_w = 3600 g/mol). The surfactant was synthesized according to the protocol of Schlaad *et al*.[152]

Methods

Nuclear magnetic resonance (NMR) spectroscopy

^{31}P NMR spectroscopy was performed at a Bruker AVANCE (USA) spectrometer at 300 MHz. Xylan's hydroxyl groups were quantified after derivatization with 2-chloro-4,4,5,5-tetramethyl-1,3,2-dioxaphospholane in a $CDCl_3$-pyridine-d_5 (4/6 v/v ratio) mixture in the presence of the internal standard endo-*N*-hydroxy-5-norbornene-2,3-dicarboximide and the relaxation agent Cr(III)acetylacetonate using the method of Balakshin *et al.*.[84]

Dynamic light scattering (DLS)

The hydrodynamic diameter of the nanocarriers was measured by DLS with a NICOMP 380 submicron particle sizer (Nicomp Particle Sizing systems, USA) at a fixed angle of 90° and a laser diode running at 635 nm. The sample was diluted to a concentration of 0.01 wt% with water or cyclohexane before measurement.

Fourier transform infrared (FTIR) spectroscopy

After crosslinking the dispersion was washed twice with cyclohexan and then dried *in vacuo*. The solid obtained was analyzed with a Nicolet iS10 FTIR spectrometer with Vertical ATR Accessory. Spectra were recorded between 600 and 4000 cm^{-1}.

Scanning electron microscopy (SEM)

The morphology of the nanocarriers was examined with a Gemini 1530 (Carl Zeiss AG, Oberkochem, Germany) scanning electron microscope (SEM) operating at 0.35 kV. The

samples were prepared by casting a diluted and purified nanocarrier dispersion on silicon wafers.

Size exclusion chromatography (SEC)

The molecular weight of the xylans was determined using a 0.07 M Na_2HPO_4 solution as an eluent. The measurement was performed at an Agilent 1100 Series (Agilent Technologies 1260 Infinity) as an integrated instrument, including a PSS Suprema linear XL column at 30°C, a RI detector at a flow rate of 1 mL/min.

Encapsulation efficiency

To quantify the amount of loaded cargo, the dispersion was transferred to water without prior purification and then filtered through an Amicon ultra centrifugation filter (MWCO: 3000 Da) to separate the nanocarriers from the aqueous supernatant. Pyraclostrobin was detected in the aqueous solution by HPLC.

Germination assay

Conidia of *Phaeomoniella chlamydospora* (Pch) and *Phaeoacremonium minimum* (Pmi) from 18-day-old agar plate cultures were harvested. After centrifugation at 4000 rpm for 10 minutes, the conidia were re-suspended in YMG-medium having a concentration of $1 \cdot 10^5$ spores per milliliter. The degradation test was carried out in 96-well microtiter plates (Greiner Bio-One GmbH, Frickenhausen). 1 µL of the nanocarrier dispersion (10 mg/mL; without loading, 1 wt% SDS solution as continuous phase) was then added to 200 µL MM1G medium containing 10.000 spores. After an incubation time of 72 hours at 27°C, the optical density was measured at a wavelength of 600 nm (Benchmark Plus Microplate reader, BioRad, Munich). Tests were conducted in triplicates. As references, the germination of Conidia in YMG medium (ideal growth conditions), in MM1G medium (minimal growth conditions) and the germination of spores in MM1G medium containing additionally 1 µL SDS solution were taken. The media had the following composition: YMG: 10.00 $g \cdot L^{-1}$ malt extract, 10.00 $g \cdot L^{-1}$ glucose, 4.00 $g \cdot L^{-1}$ yeast extract, pH 5.5; MM1G: 1 $g \cdot L^{-1}$ glucose, trace elements, pH 5.5.

Minimal inhibition concentration assay (Antifungal activity)

Pyricularia oryzae, Botrytis cinereal, Phaeomoniella chlamydospore, Phaeoacremonium aleophilum and *Neonectria ditissima* were used for the spore germination test. The nanocarrier dispersion was used in aliquots of 1, 5, 10, 25 and 50 µg/mL (active ingredient) per 96-well. The spores were diluted in YMG medium to a final concentration of 2000 spores/mL. 200 µL of the spore suspension was than added to the nanocarriers. The plates were incubated at 27°C and 120 rpm on an incubator and the optical density (OD) was measured every 24 hours at a wavelength of 600 nm. The antifungal activity was obtained by

comparing the OD after incubation of the samples treated with the positive control (just water is added), the negative control (plain fungicide is added) and the nanocarriers dispersion. The OD relative to the positive control is considered 100% of fungi growth.

Synthesis

Preparation of xylan nanocarriers

Xylan (156 mg, 2.85 mmol OH) extracted from corncobs, was dissolved at 60°C in 1.3 mL dimethyl sulfoxide (DMSO). To load the nanocarriers, pyraclostrobin (20 mg) was added additionally to the xylan solution. The mixture was then added to 9.6 mL cyclohexane containing 100 mg of the surfactant P(E/B-*b*-EO). To generate a miniemulsion, the two-phase mixture was ultrasonicated (Branson Digital Sonifier W450-D, 1/ 2″ tip, 70% amplitude, 3 min, 20 s ultrasound followed by 10 s pauses) while cooling with water. Subsequently, toluene diisocyanate (TDI, 123 µL, 0.86 mmol) was dissolved in a P(E/B-*b*-EO)-cyclohexane solution (57 mg in 6.4 mL) and was added dropwise to the miniemulsion under vigorous stirring (1000 rpm). The reaction was allowed to process for ca. 12 h at 25°C and 250 rpm. For solvent exchange, the nanocarriers were washed twice with cyclohexane and then added to a 0.1 wt% sodium dodecyl sulfate (SDS)-solution under sonication and shaking. The cyclohexane was evaporated by stirring overnight. The dispersions were characterized by DLS and SEM microscopy regarding their size distribution and morphology.

7.4 Results and discussion

To find a xylan feedstock that is suitable for nanocarrier preparation, we characterized two commercially available xylans isolated either from corncobs (Carl Roth, product number: 8659.2) or from beechwood (Carl Roth, product number: 4414.2). Both materials significantly differed in their solubility properties and in their molecular weight. When adding beechwood xylan to DMSO a yellowish, viscous gel was formed, whereas corncob xylan yielded a clear solution with comparably lower viscosity. As the latter carbohydrate had a lower molecular weight distribution according to SEC (Figure 7.2B), we assume that a less viscous solution was formed due to a limited ability to form chain entanglements. The emulsification of viscous solutions requires strong sonication or shear forces as the droplet break down needs a high-energy input. For this reason, corncob xylan was preferred as a starting material for the nanocarrier preparation. For further characterization, we quantified the hydroxyl groups of the carbohydrate with ^{31}P-NMR spectroscopy after derivatization with 2-chloro-4,4,5,5-

tetramethyl-1,3,2-dioxaphospholane according to the method of Balakshin *et al.* (Figure 7.2C).[84] The polymer had 18.3 mmol/g hydroxyl groups which allow further functionalization. As only signals between 153 and 145 ppm were detected, we assume that the herein used corncob xylan is purely carbohydrate-based containing no aromatic side like ferulic acid groups or lignin residues.

For nanocarrier preparation, a solution of DMSO and corncob xylan was added to a cyclohexane solution containing P(E/B-*b*-EO) as a surfactant. The two-phase mixture was stirred at 25°C and was then ultrasonicated to generate a miniemulsion. Finally, a cyclohexane solution containing P(E/B-*b*-EO) and toluene diisocyanate (TDI) was added dropwise via a cannula while stirring. The interfacial polyaddition reaction between xylans nucleophilic hydroxyl groups and the isocyanate groups of TDI was performed overnight at room temperature. The obtained dispersion did not phase separate for several weeks. The nanocarriers were analyzed regarding their size distribution and their morphology with DLS and SEM respectively. To remove excess P(E/B-*b*-EO), the dispersion was washed twice by repetitive centrifugation and resuspended in pure cyclohexane. A concentrated dispersion was then added dropwise to an aqueous solution containing the anionic surfactant sodium dodecyl sulfonate (SDS) under sonication and shaking. In the last step, cyclohexane was evaporated under vigorous stirring overnight to yield the final aqueous nanocarrier suspension.

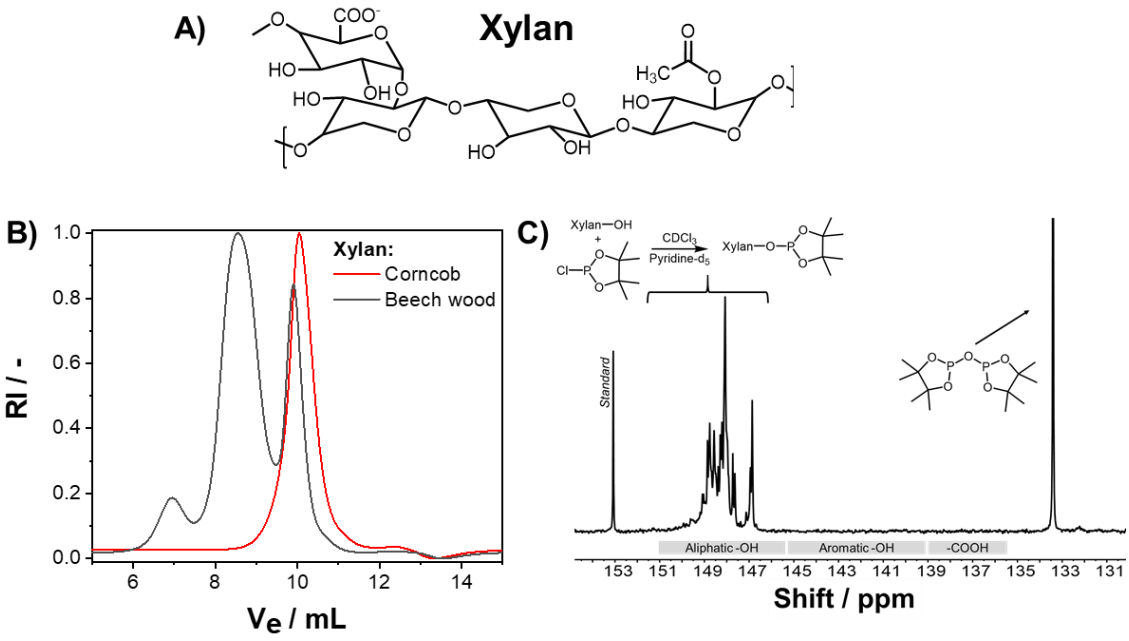

Figure 7.2: A) Molecular structure assumed for the herein used corncob xylooligosaccherides (Carl Roth, Product number: 8659.2). B) SEC elugram in 0.07 M Na_2HPO_4 solution of xylan isolated from corncob or from beechwood using polystyrene as a standard. C) ^{31}P-NMR of corncob xylan after phosphorylation according to the method of Balakshin *et al*..[84] The spectrum shows a purely aliphatic carbohydrate with 18.3 mmol/g hydroxyl groups.

To prove the interfacial crosslinking, SDS was removed by dialysis from the suspension and the nanocarriers were investigated as a solid by FTIR spectroscopy after lyophilization. In comparison to pristine xylan, a broad additional band between 1792 and 1623 cm^{-1} was monitored after crosslinking. The broad signal indicates the overlapping of three bands, which belong to the carbonyl stretching of urethane and urea linkages formed during the shell formation as well as the carbonyl stretching (1738 cm^{-1}) e.g. of O-acetyl side groups attached to the xylan backbone. Next to the addition of xylans hydroxyl groups to TDI forming a polyurethane capsule wall, the isocyanate can hydrolyze at the droplet interface by trace amount of water, which is dissolved in the DMSO phase. The formed amine can react with TDI's isocyanate groups and lead to a polyurea by-product.[9] Besides the carbonyl signals, we further monitored a strong band of aromatic skeletal vibrations at 1545 cm^{-1} as well as a reduced intensity of the OH stretching band at 1382 cm^{-1} and between 3700-3000 cm^{-1} in comparison to unmodified xylan. Both proved the formation of a covalently crosslinked xylan-polyurea/polyurethane shell.

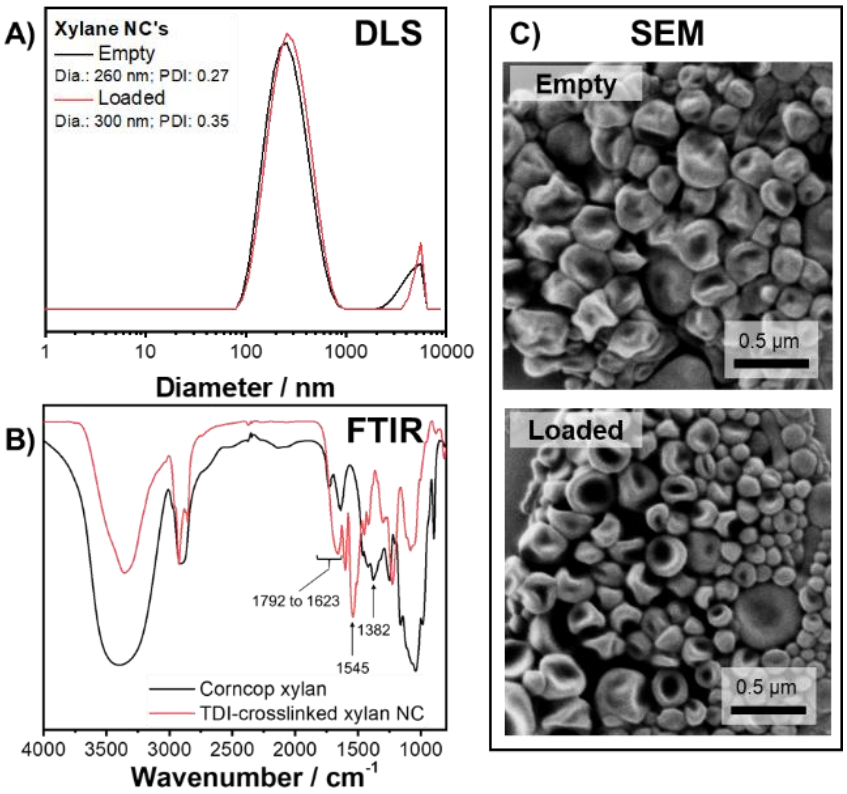

Figure 7.3: A) Size distribution of empty and pyraclostrobin-loaded nanocarrier dispersions measured by DLS. B) FTIR spectra of unmodified corncob xylan and xylan after interfacial crosslinking with TDI. C) SEM image showing the core-shell structure of loaded and empty xylan nanocarriers.

According to DLS, the generated xylan nanocarriers had a size distribution in cyclohexane and in water of 200-300 nm (PDI ca. 0.3, some larger aggregates might be formed). SEM showed hollow nanocarriers with a wall thickness of 10-20 nm, proving that xylan and TDI formed a dense shell surrounding the DMSO core during the crosslinking reaction. When reducing stepwise the ratio of hydroxyl to isocyanate groups from 1.65 over 1.29 to 0.86, no nanocarrier formation was observed by SEM. Hence, a monomer/crosslinker ratio of at least 1.65 is needed to form stable core-shell structures. To use the nanocarrier dispersion for drug delivery in agriculture, we added the broad-spectrum fungicide pyraclostrobin to the dispersed phase. Pyraclostrobin belongs to the class of strobilurines and inhibits the mitochondrial respiratory chain of numerous fungi.[153] It was used previously in our studies on lignin nanocarriers to treat the grapevine trunk disease Esca.[101] A fungicide loading of 8 wt% relative to the carrier material did not affect the nanocarrier morphology according to SEM, which proved the robustness of the method. Therefore, this approach might be extended to further pesticides to enable safer and easier handling of toxic agrochemicals. To quantify the amount of loaded cargo, the dispersion was transferred to water without prior purification and then filtered through an Amicon ultra centrifugation filter (MWCO: 3000 Da) to separate the nanocarriers from the aqueous supernatant. Only trace amounts of fungicide (< 0.01%) were detected in the aqueous solution by HPLC, proving n almost quantitative encapsulation. As pyraclostrobin has a very low solubility in water (ca. 1.9 mg/L), we assume no leakage when stored in an aqueous suspension similar to our previous findings to lignin nanocarriers.

At a solid content of < 1 - 10 mg/mL, the pyraclostrobin-loaded nanocarriers prevented the growth of several fungi (strains listed in Figure 7.4B), suggesting the feasibility of the formulation in plant protection. The enzymatic degradability of the carrier material was analyzed by quantifying the germination of spores belonging to the xylan-degrading fungi *Phaeomoniella chlamydospora* (Pch) or *Phaeoacremonium minimum* (Pmi) in the presence of only minimal amount of nutrition (Figure 7.4). More mycelium was formed in comparison to references containing SDS in equal concentration or the minimal medium alone, indicating that the incorporated xylan acted as a degradable breaking point which allowed the metabolization of the carrier material by the fungi. This mechanism might be applied to trigger the carrier degradation and by this the drug release in the presence of microorganisms.

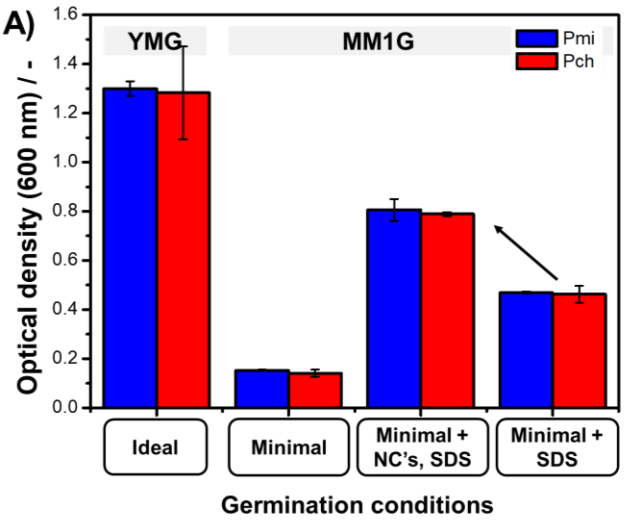

B)

Fungal strain	MIC / mg/mL
Pyricularia oryzae	< 1
Botrytis cinerea	< 5
Phaeomoniella chlamydospore	< 10
Phaeoacremonium aleophilum	< 10
Neonectria ditissima	< 10

Figure 7.4: Germination of fungal spores of Pmi and Pch quantified by optical density. The amount of mycelium formed depended on the growth conditions and the respective nutrition provided. B) Minimal inhibitory concentration (MIC) of pyracolstrobin-loaded xylan nanocarriers. Different fungal strains were tested.

7.5 Conclusion

This work describes the preparation of degradable xylan-based nanocarriers by interfacial crosslinking of corncob xylan with toluene diisocyanate in an inverse miniemulsion. Xylan extracted from corncobs was found to be a more suitable monomer than xylan from beechwood, as it forms a less viscous dispersed phase. The dispersions were colloidally stable as cyclohexane or aqueous dispersions for several weeks and contained nanomaterials with diameters between 200-300 nm and a core-shell structure. When adding the fungicide pyraclostrobin to the dispersed phase, the particle size distribution, the morphology and the stability of the dispersion did not change. As the nanocarriers could be degraded by fungi, the approach is considered a promising tool to generate bio-based nanoformulations which could help to increase sustainability in plant protection.

8 Synthetic Monolignol Dimers for the Preparation of Degradable Nanocarriers

Sebastian J. Beckers, Jochen Fischer, Frederik R. Wurm

Unpublished data.

The lignin segments and the nanocarrier preparation were performed by Sebastian Beckers under scientific guidance of PD Dr. Frederik Wurm. The germination assay was performed by Dr. Jochen Fischer.

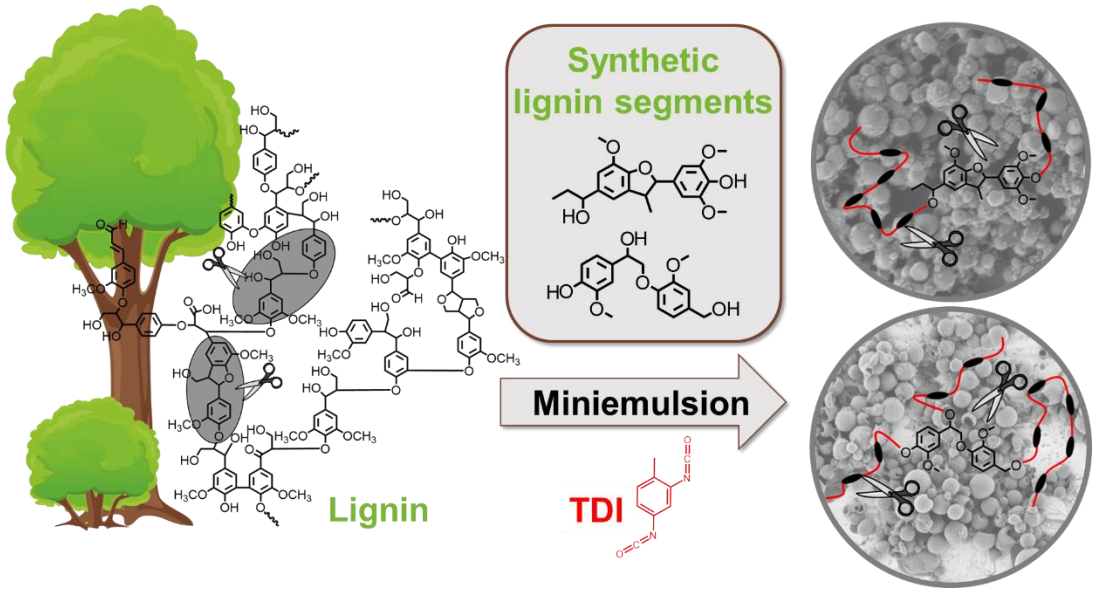

Keywords: *Lignin, polyurethanes, emulsion polymerization, nanocarriers*

8.1 Abstract

Lignin is a bio-based and biodegradable biopolymer with high structural diversity. Unlike many synthetic biodegradable polymers, such as polyesters, it is stable towards hydrolysis. However the ill-defined structure and batch to batch variations make its use often difficult. Therefore, two lignin monolignol dimers, phenylcoumaran and ß-O-4-aryl ether, were synthesized and used for the preparation of nanocarriers by interfacial crosslinking with toluene diisocyanate in an inverse miniemulsion. The nanocarriers had diameters between 200 and 400 nm and could be metabolized by lignin-degrading fungi. Therefore, the dispersions might be of interest as a degradable drug delivery system e.g. in advanced plant protection or as alternatives to natural lignin

8.2 Introduction

To overcome the increasing environmental pollution with plastic waste, next to innovative recycling strategies, the development of sustainable materials is required urgently.[154] For this reason, recently the lignocellulose component lignin got increasing attention as a sustainable and abundant feedstock for bio-based materials as several microorganisms such as fungi and bacteria can degrade it enzymatically but it is recalcitrant to hydrolysis.[27, 36, 155] In particular, peroxidases (lignin peroxidase, manganese peroxidases, versatile peroxidase) and laccases produced for example by white-rot basidiomycetes are known for their ability to break down the biopolymer efficiently leaving a whitish, cellulose-enriched material behind.[36]

Lignin is a complex and crosslinked aromatic polyether formed by radical polymerization during lignification in the cell wall of plants. Depending on plant type, age, and other natural factors, the polymer is composed of the monolignols *p*-coumaryl, coniferyl, and sinapyl alcohol in different ratios. The monomers are connected by various binding motifs, which can be obtained formally by radical dimerization reactions. The β-O-4-aryl ether is the most common binding motif in softwood (SW, 45-50%) or hardwood (HW, 60%) lignin. Likewise, the biphenyl linkage (SW: 20-25%, HW: 3-9%) but also phenylcoumaran (SW 9-12%, HW 3-11%) and pinoresinol (SW 2-6%, HW: 3-12%) were found in relatively high percentages.[27, 36]

Unlike other degradable polymers based on natural resources (like carbohydrates, e.g. starch, chitin, gelatin) or synthetic polymers (such as polyesters), lignin does not break down by hydrolysis but degrades selectively by lignase-producing micro-organisms.[154, 156] This

renders lignin an interesting feedstock for various applications, e.g as packaging or coating materials, where hydrolysis often impedes the applicability of “degradable polymers”. The degradation of bio-based lignin derivatives and several synthetic model compounds was studied and degradation mechanisms for each binding motif were postulated (Figure 8.1).[36]

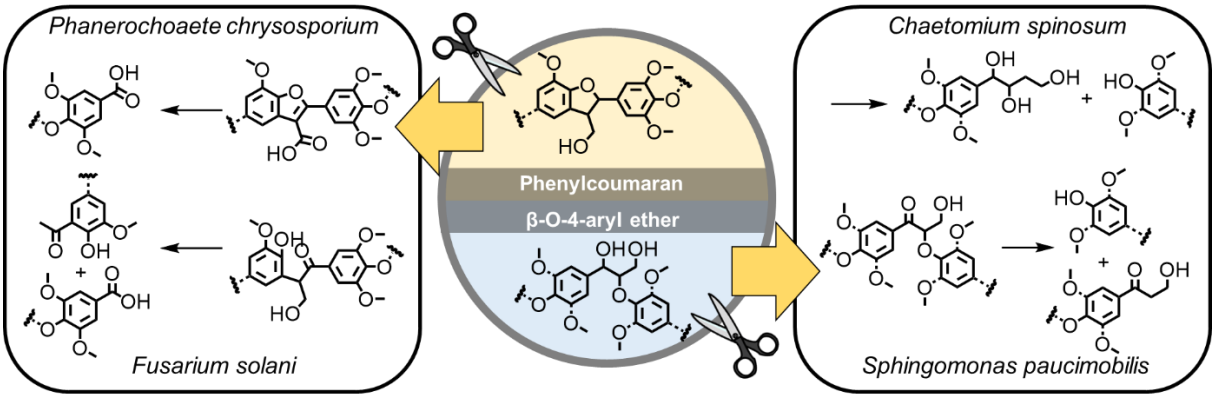

Figure 8.1: Examples for postulated degradation mechanisms of the lignin substructures phenylcoumaran and ß-O-4-aryl ether by microorganisms.[36, 157-160]

To date, lignin is used rarely as a molecular building block. This is mainly due to its heterogeneous molecular structure, which varies by source and batch and thus limits an application to processes, which do not rely on the very same molar structure or molar mass.[33] Challenging, for example, is the utilization of lignin as polyol in polyurethanes, as structural variations would result in different mechanical properties.[43] Another example is the preparation of biodegradable nanocarriers by crosslinking of lignin or lignin sulfonate in miniemulsion as shown by our group recently.[9, 100] Here, an oligomeric lignin derivative, which is susceptible to fungal degradation, combined with a certain degree of chemical functionality and solubility is essential. However, each lignin batch needs to be characterized and formulation conditions must adjusted respectively to keep a constant product quality. For many other applications, the diverse structure and molar mass inhibits lignin’s utilization and a synthetic alternative with defined molecular structure is required. However, artificial lignin oligomers with a defined molecular structure need elaborate multi-step syntheses, which makes them relatively unattractive for large-scale applications.[161-164] An alternative solution might be the polymerization of lignin-derived monomers, which are accessible in less synthetic steps. Very few studies used the β-O-4-aryl ether or pinoresinol binding motif to prepare synthetic “lignin-homopolymers”.[163, 165, 166]

Herein, we expand this strategy to new degradable lignin-related polymers. We prepared lignin monomers based on the β-O-4-aryl ether and the phenylcoumaran binding motif, respectively. Both were polymerized by interfacial polyaddition with toluene diisocyanate at the droplet interface of a miniemulsion to yield polyurethane nanoparticles. The resulting polymers were either linear or crosslinked and might be used after workup as polyurethanes or as biodegradable nanoformulation for drugs e.g. in plant protection (similar to native lignin). This approach will broaden the scope of lignin-derived polymers for applications in hydrolysis-stable but enzymatically degradable polymer materials for drug delivery and other materials science applications.

8.3 Experimental section

Materials

Carbonyldiimidazol, benzoic acid, acetovanillone, bromine and horseradish peroxidase were bought from Sigma Aldrich. Vanillin, isoeugenol and the $LiAlH_4$/THF solution (10%, ca. 2.5 mol/L) were obtained from TCI Chemicals. All materials were used without further purification.

Poly[(ethylene-*co*-butylene)-*b*-(ethylene oxide)] (P(E/B-*b*-EO)) consisted of a poly(ethylene-*co*-butylene) block with a molecular weight of (M_w=3700 g/mol) and poly(ethylene oxide) block of (M_w = 3600 g/mol). The surfactant was synthesized according to the protocol of Schlaad *et al*.[152]

Methods

Nuclear magnetic resonance (NMR) spectroscopy

^1H and ^{13}C nuclear magnetic resonance (NMR) spectroscopy was performed at a Bruker AVANCE (USA) system at 300 MHz. The NMR samples contained ca. 50 mg of the respective substance which was dissolved in 600 µL of either DMSO-d_6 or $CDCl_3$.

Dynamic Light Scattering (DLS)

The hydrodynamic diameters of the nanoparticles was measured by DLS with a NICOMP 380 submicron particle sizer (Nicomp Particle Sizing systems, USA) at a fixed angle of 90° and a laser diode running at 635 nm. The sample was diluted to a concentration of 0.01 wt% with water or cyclohexane before measurement.

Fourier transform infrared (FTIR) spectroscopy

To prove the covalent crosslinking of the nanocarriers, the washed dispersions were freeze dried and then analyzed with a Nicolet iS10 FTIR spectrometer with Vertical ATR Accessory. Spectra were recorded between 600 and 4000 cm^{-1}.

Scanning electron microscopy (SEM)

The nanocarrier morphologies were examined with a Gemini 1530 (Carl Zeiss AG, Oberkochem, Germany) scanning electron microscope (SEM) operating at 0.35 kV. The samples were prepared by casting diluted and purified nanocarrier dispersions on silicon wafers.

Germination assay

To prove that **4** and **6** are biodegradable, each monomer (25 mg) was dissolved in DMSO (5 mL). 20 mL of a 0.1 M HCl solution containing 1 mg/mL Lutensol AT50 was added dropwise over 30 min. Afterward, the suspension was dialyzed against MilliQ water (3 x 8 L for 12 h) to remove DMSO and HCl. The washed monomer particles were centrifuged at (4000 rpm, 30 min) and the clear supernatant was separated. To the pellet, a Lutensol AT50 solution (1 mg/mL) was added and the solid was resuspended. Each sample had a solid-content of 0.2 wt%.

Conidia of *Phaeomoniella chlamydospora* (Pch) and *Phaeoacremonium minimum* (Pmi) from 18-day-old agar plate cultures were harvested. After centrifugation at 4000 rpm for 10 minutes, the conidia were resuspended in YMG-medium to a concentration of $1 \cdot 10^5$ spores per milliliter. The degradation test was carried out in 96-well microtiter plates (Greiner Bio-One GmbH, Frickenhausen). 1 µL of the monomer dispersion (10 mg/mL) was then added to 200 µL MM1G medium containing 10.000 spores. After an incubation time of 72 hours at 27°C, the optical density was measured at a wavelength of 600 nm (Benchmark Plus Microplate reader, BioRad, Munich). Tests were conducted in triplicates. As references, the germination of Conidia in YMG medium (ideal growth conditions), in MM1G medium (minimal growth conditions) and the germination of spores in MM1G medium containing additionally 1 µL Lutensol (1 mg/mL) solution was taken.

The media had the following composition: YMG: 10.00 $g \cdot L^{-1}$ malt extract, 10.00 $g \cdot L^{-1}$ glucose, 4.00 $g \cdot L^{-1}$ yeast extract, pH 5.5; MM1G: 1 $g \cdot L^{-1}$ glucose, trace elements, pH 5.5.

Syntheses

4-acetyl-2-methoxyphenyl benzoate (1)

Carbonyldiimidazol (14.6 g, 90.3 mmol, 1 eq.) was dissolved in 100 mL tetrahydrofurane (THF). To the turbid solution, benzoic acid (11.0 g, 90.3 mmol, 1 eq.) was added under vigorous stirring while keeping the reaction vessel open to compensate for the fast increasing pressure due to the release of carbon dioxide. After the solution became clear, we added acetovanillone (15.0 g, 90.3 mmol, 1 eq.) and the reaction was allowed to proceed overnight at 50°C. 4-acetyl-2-methoxyphenyl benzoate was obtained as a white powder by precipitation in 500 mL water. The solid was filtered off and was dried at 40°C in a vacuum oven (21.6 g, 88%).

^{1}H NMR (300 MHz, 298 K, DMSO-d_6): δ 8.14-7.40 (m), 3.84 (s), 2.62 (s). **^{13}C NMR (300 MHz, 298 K, DMSO-d_6):** δ 196.97, 163.63, 151.02, 143.26, 135.84, 134.21, 129.86, 129.03, 123.24, 121.69, 111.67, 55.98, 26.73.

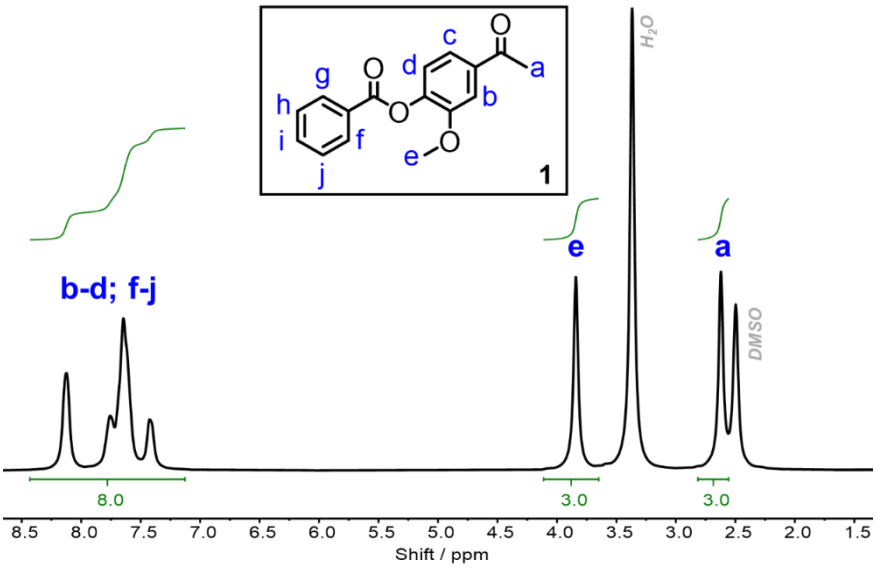

Figure 8.2: ^{1}H NMR (300 MHz, 298 K, DMSO-d_6) spectrum of 4-acetyl-2-methoxyphenyl benzoate **1** and the respective chemical shifts.

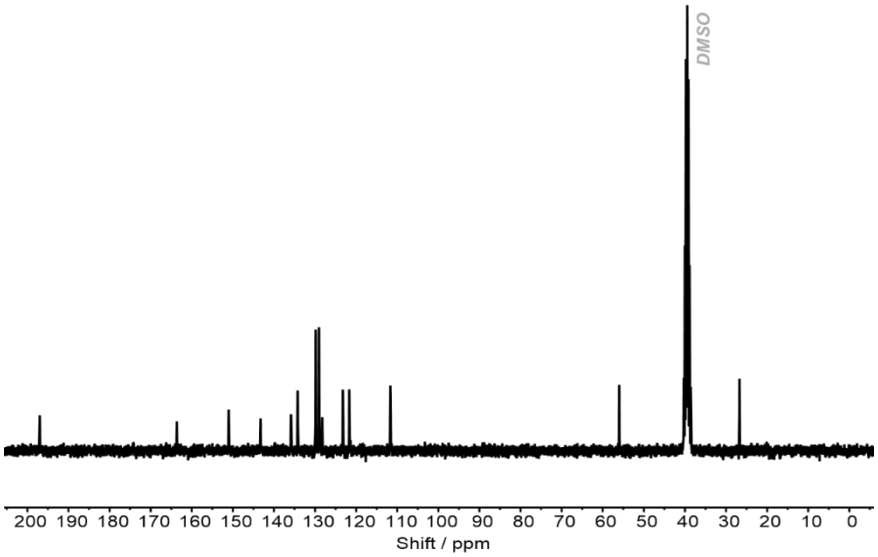

Figure 8.3: ^{13}C NMR (300 MHz, 298 K, DMSO-d_6) spectrum of 4-acetyl-2-methoxyphenyl benzoate **1** and the respective chemical shifts.

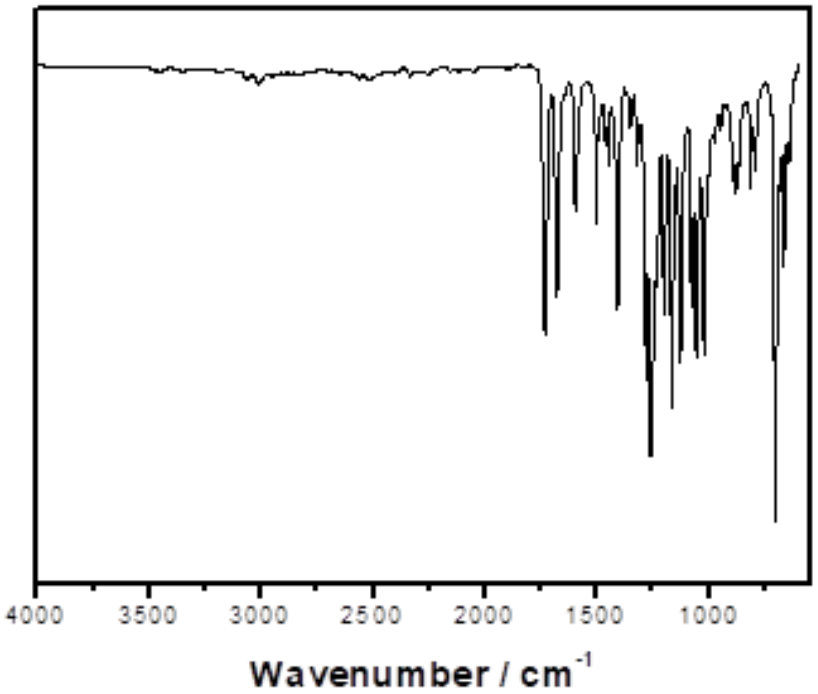

Figure 8.4: FTIR spectrum of 4-acetyl-2-methoxyphenyl benzoate **1**.

4-(2-bromoacetyl)-2-methoxyphenyl benzoate (2)

1 (16.2 g, 60.0 mmol, 1 eq.) was dissolved in a dioxane/diethyl ether mixture (dry, 3/4 vol.). Under an inert gas atmosphere, bromine (3.08 mL, 120.0 mmol, 2 eq.) was added dropwise via a syringe pump over 2 h under ice-cooling and vigorous stirring. The mixture was stirred for 60 min until 100 mL of diethyl ether was added. Subsequently, the solution was washed with ice-cold water (4 x 150 mL). In the last washing step, 4-(2-bromoacetyl)-2-methoxyphenyl benzoate precipitated as white solid, which was separated by filtration and finally dried at 40°C in a vacuum oven (10.7 g, 51%).

^{1}H NMR (300 MHz, 298 K, DMSO-d_6): δ 8.14-7.66 (m), 4.99 (s), 3.85 (s). **^{13}C NMR (300 MHz, 298 K, DMSO-d_6):** δ 190.82, 163.60, 151.18, 143.75, 134.29 132.97, 129.88, 129.07, 123.48, 122.21, 112.44, 56.14, 34.11.

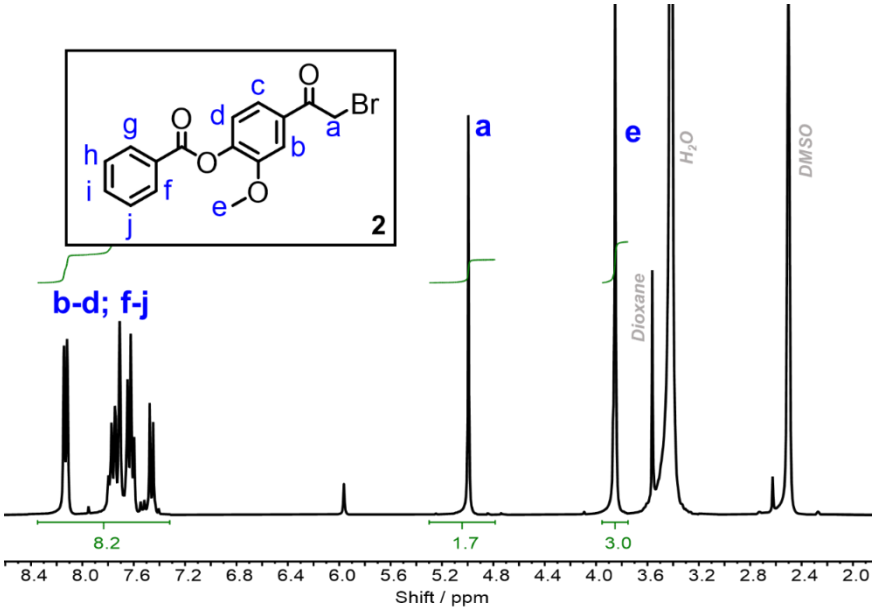

Figure 8.5: ^{1}H NMR (300 MHz, 298 K, DMSO-d_6) spectrum of 4-(2-bromoacetyl)-2-methoxyphenyl benzoate **2** and the respective chemical shifts.

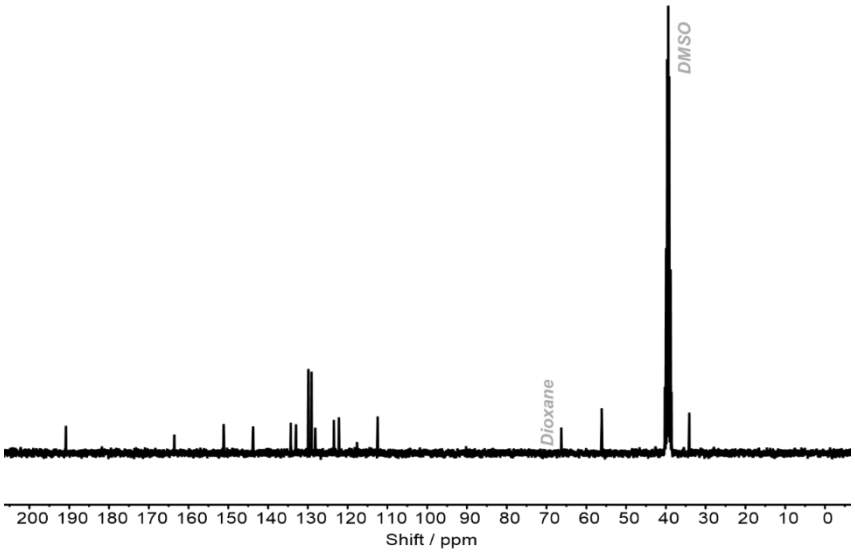

Figure 8.6: ^{13}C NMR (300 MHz, 298 K, DMSO-d_6) spectrum of 4-(2-bromoacetyl)-2-methoxyphenyl benzoate **2** and the respective chemical shifts.

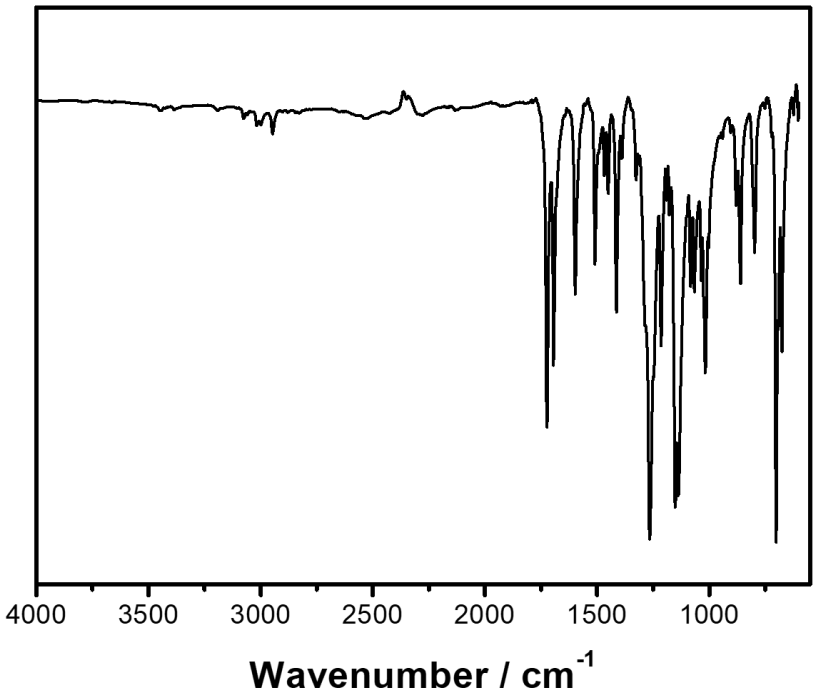

Figure 8.7: FTIR spectrum of 4-(2-bromoacetyl)-2-methoxyphenyl benzoate **2**.

4-(2-(4-formyl-2-methoxyphenoxy)acetyl)-2-methoxyphenyl benzoate (3)

To 30 mL dry THF, vanillin (2.2 g, 14.3 mmol, 1 eq.), potassium carbonate (3.0 g, 21.5 mmol, 1.5 eq.) and **2** (5.0 g, 14.3 mmol, 1 eq.) were added. The reaction was performed at 50°C under stirring and inter gas atmosphere. After two days, the formation of precipitate was observed and 50 mL water was added. The yellowish solid was separated by filtration and was washed with water (3 x 50 mL) to remove KBr and excess K_2CO_3. Impurities were removed from the crude product by column chromatography using at first pure dichloromethane (DCM) as an eluent. Finally, the column was flushed with a DCM methanol mixture (2 vol.%) to separate the product. The solutions were dried with $MgSO_4$ first, and the solvent was removed under reduced pressure to yield **3** as a yellowish powder (5.5 g, 92%).

^{1}H NMR (300 MHz, 298 K, DMSO-d_6): δ 9.84 (s), 8.15-7.11 (m) 5.81 (s), 3.89-3.87 (2s). **^{13}C NMR (300 MHz, 298 K, DMSO-d_6):** δ 192.84, 191.40, 163.64, 152.74, 149.15, 143.80, 133.12, 129.89, 129.07, 128.17, 125.52, 112.68, 111.72, 70.59, 56.14, 55.61.

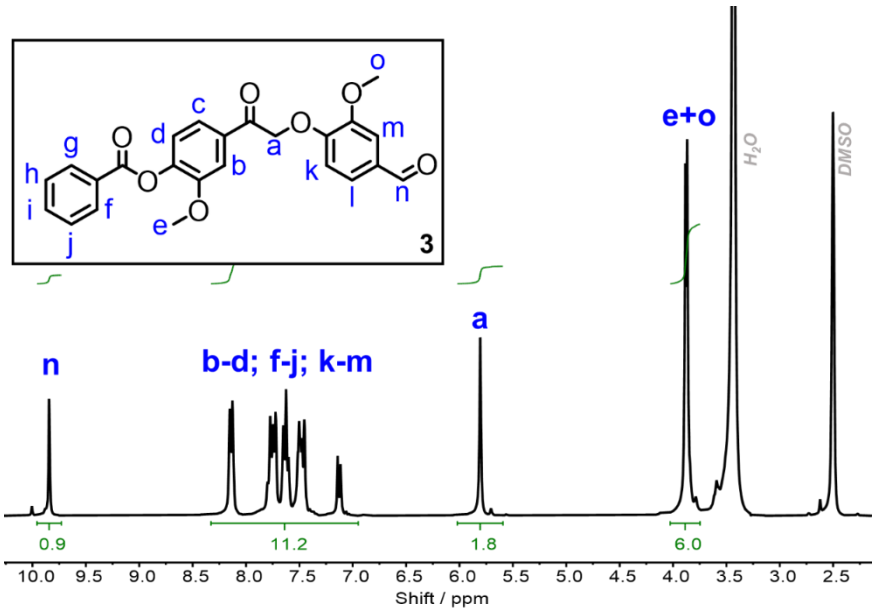

Figure 8.8: ^{1}H NMR (300 MHz, 298 K, DMSO-d_6) spectrum of 4-(2-(4-formyl-2-methoxyphenoxy)acetyl)-2-methoxyphenyl benzoate **3** and the respective chemical shifts.

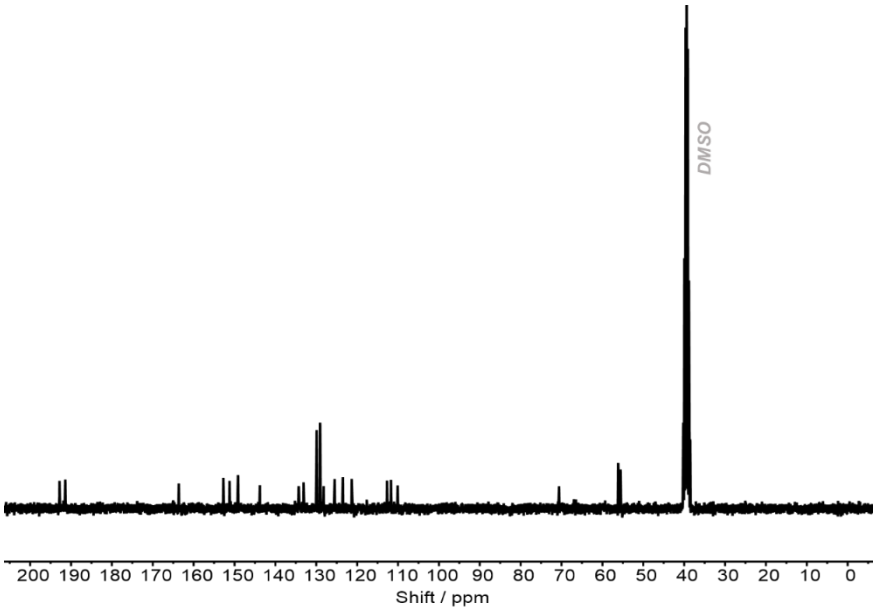

Figure 8.9: ^{13}C NMR (300 MHz, 298 K, DMSO-d_6) spectrum of 4-(2-(4-formyl-2-methoxyphenoxy)acetyl)-2-methoxyphenyl benzoate **3** and the respective chemical shifts.

4-(1-hydroxy-2-(4-(hydroxymethyl)-2-methoxyphenoxy)ethyl)-methoxyphenol (4)

To cleave the benzoyl protection moiety and to reduce the carbonyl groups, **3** (2.1 g, 5.0 mmol, 1 eq.) was dissolved in 90 mL THF and 13.75 mL of a $LiAlH_4$/THF solution (2.5 mol/L, 5.5 mmol, 1.1 eq.) was added dropwise while cooling with a water bath. After complete addition, the mixture was refluxed for 1 h at 70°C and then cooled down to room temperature under stirring overnight. Afterwards, ice was added to the solution until the evolution of gas stopped completely, leading to the formation of a gel-like solid. After having quenched unconverted $LiAlH_4$, 100 mL of a 10% H_2SO_4 solution was added and the mixture was washed with diethyl ether (3 x 100 mL). The combined organic phases were dried with $MgSO_4$ and were than evaporated under reduced pressure yielding a brownish oil. The crude product was dissolved in 200 mL of a saturated Na_2CO_3 solution and was then washed with diethyl ether (3 x 100 mL) to remove the benzyl alcohol. The aqueous phase was collected and was set with a 10% HCl solution to a pH of 3. Again, the mixture was washed with diethyl ether (3 x 200 mL). The organic phase was dried with $MgSO_4$ until **4** was obtained as a brownish oil under reduced pressure (0.85 g, 52%).

^{1}H NMR (300 MHz, 298 K, DMSO-d_6): δ 8.83 (s), 7.01-6.70 (m), 5.41(d), 5.06 (t), 4.80 (m), 4.40 (d), 3.98-3.86 (m), 3.75 (2s). **^{13}C NMR (300 MHz, 298 K, DMSO-d_6):** δ 148.84, 147.23, 146.94, 145.66, 135.33, 133.50, 118.65, 118.62, 114.92, 113.30, 110.92, 110.63, 74.31, 70.84, 62.77, 55.46.

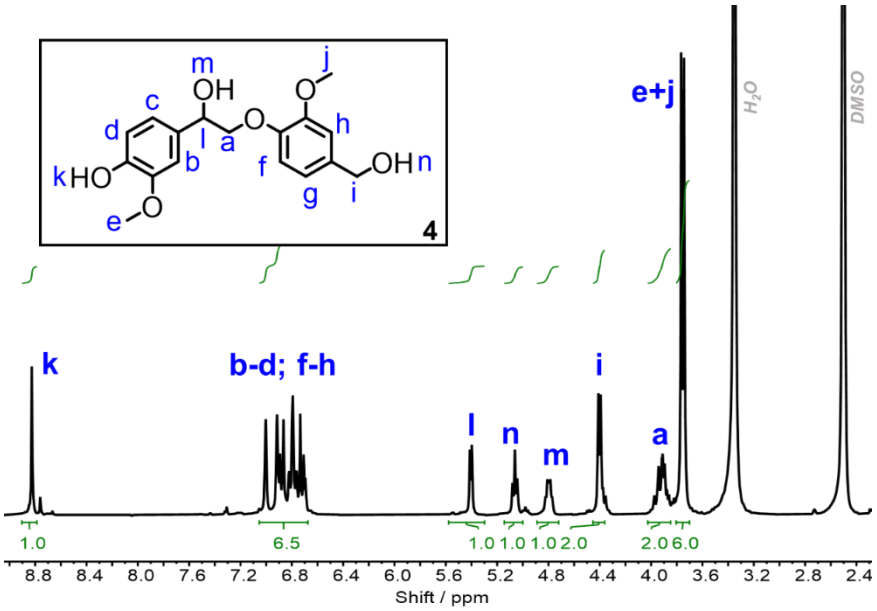

Figure 8.10: ^{1}H NMR (300 MHz, 298 K, DMSO-d_6) spectrum of 4-(1-hydroxy-2-(4-(hydroxymethyl)-2-methoxyphenoxy)ethyl)-methoxyphenol **4** and the respective chemical shifts.

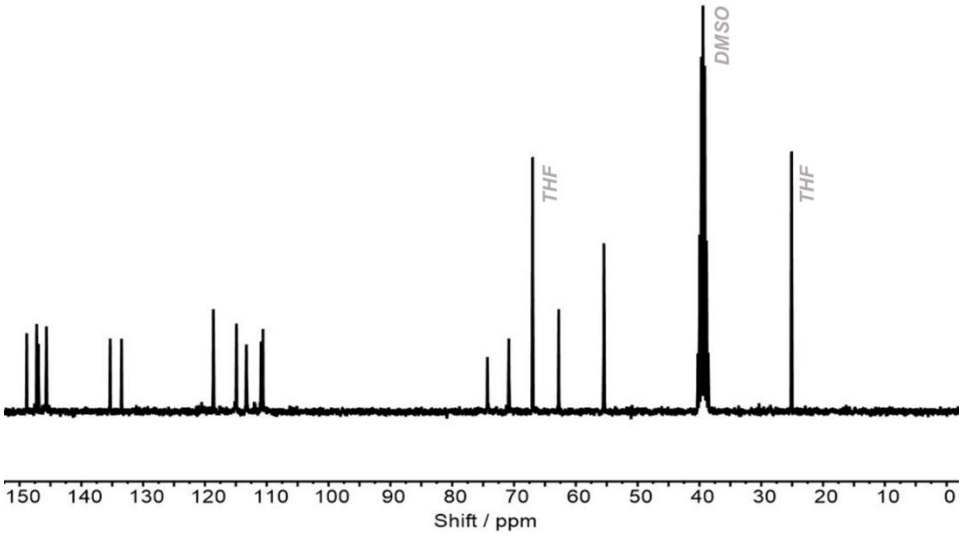

Figure 8.11: ^{13}C NMR (300 MHz, 298 K, DMSO-d_6) spectrum of 4-(1-hydroxy-2-(4-(hydroxymethyl)-2-methoxyphenoxy)ethyl)-methoxyphenol **4** and the respective chemical shifts.

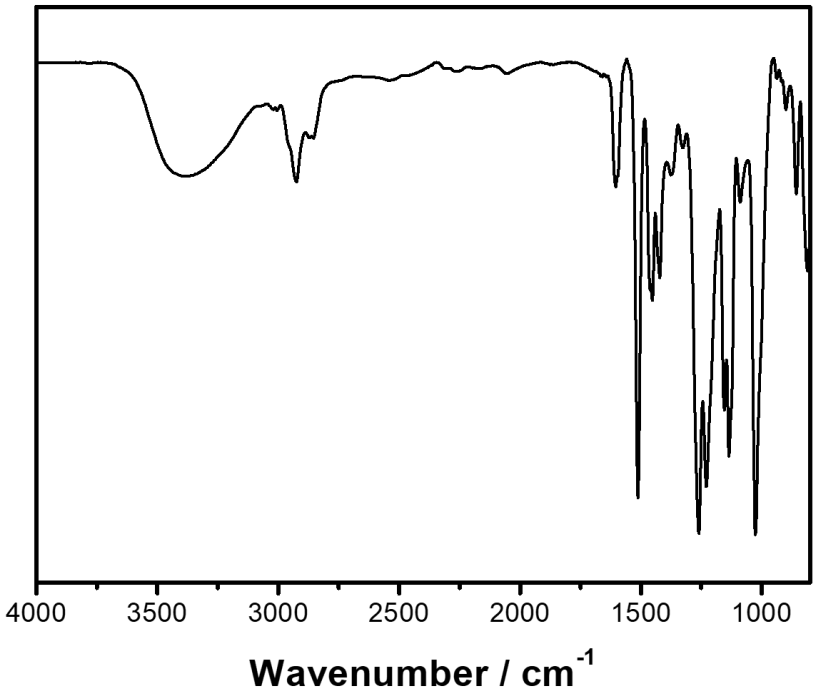

Figure 8.12: FTIR spectrum of 4-(1-hydroxy-2-(4-(hydroxymethyl)-2-methoxyphenoxy)ethyl)-methoxyphenol **4**.

(E)-2-methoxy-4-(7-methoxy-3-methyl-5-(prop-1-en-1-yl)-2,3-dihydrobenzofuran-2-yl)phenol (Dehydro-isoeugenol, 5)

Dehydro-isoeugenol was prepared by oxidative dimerization according to the method of Sarkanen *et al*.[167] Briefly, isoeugenol (5.0 g, 30.45 mmol) and horseradish peroxidase (10 mg) were dissolved in a mixture of acetone (125 mL) and water (200 mL). To initiate the reaction, a hydrogen peroxide solution (3.14%, 17.4 mL) was added over 45 min while cooling the vessel with a water bath. Afterwards, the mixture was stored at 4°C overnight to precipitate the product from the reaction mixture as slightly yellow crystals. The solid was filtered off and recrystallized in ethanol, yielding **5** as a white crystalline solid (3.4 g, 68%).

^{1}H NMR (300 MHz, 298 K, $CDCl_3$): δ 6.98-6.77 (m), 6.37 (d), 6.17-6.05 (m), 5.65 (s), 5.10 (d), 3.89 (2s), 3.50-3.40 (m), 1.89 (d), 1.38 (d). **^{13}C NMR (300 MHz, 298 K, $CDCl_3$):** δ 146.69, 146.59, 145.80, 144.17, 133.28, 132.21, 132.09, 130.94, 123.51, 119.99, 114.09, 113.32, 109.24, 108.94, 93.81, 45.64, 18.39, 17.57.

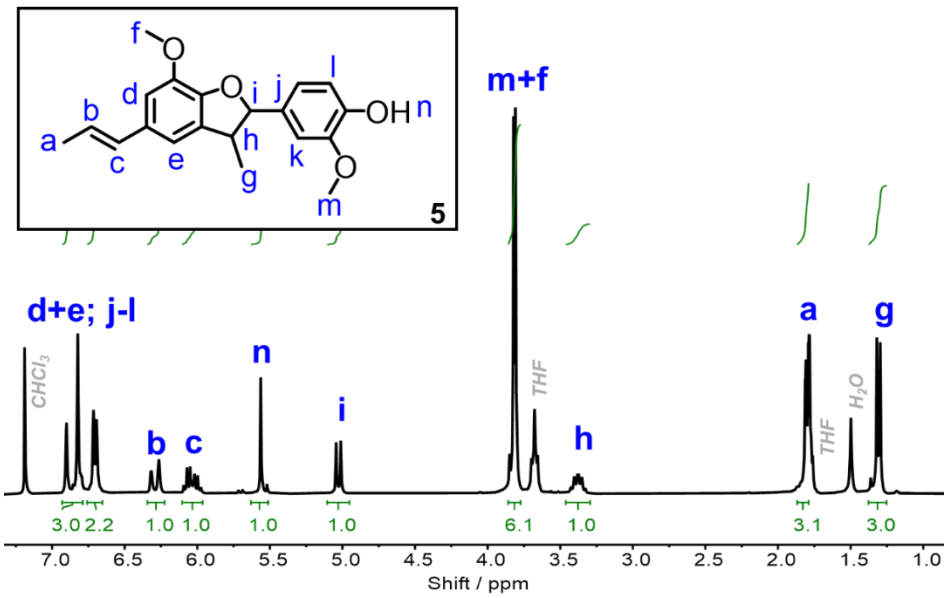

Figure 8.13: ^{1}H NMR (300 MHz, 298 K, $CDCl_3$) spectrum of (E)-2-methoxy-4-(7-methoxy-3-methyl-5-(prop-1-en-1-yl)-2,3-dihydrobenzofuran-2-yl)phenol (dehydro-isoeugenol, **5**) and the respective chemical shifts.

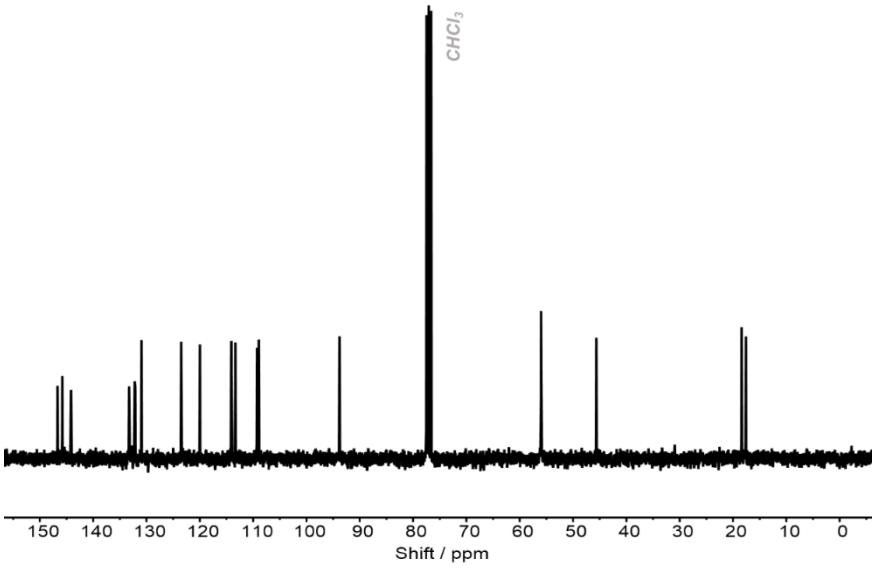

Figure 8.14: ^{13}C NMR (300 MHz, 298 K, $CDCl_3$) spectrum of (E)-2-methoxy-4-(7-methoxy-3-methyl-5-(prop-1-en-1-yl)-2,3-dihydrobenzofuran-2-yl)phenol (dehydro-isoeugenol, **5**) and the respective chemical shifts.

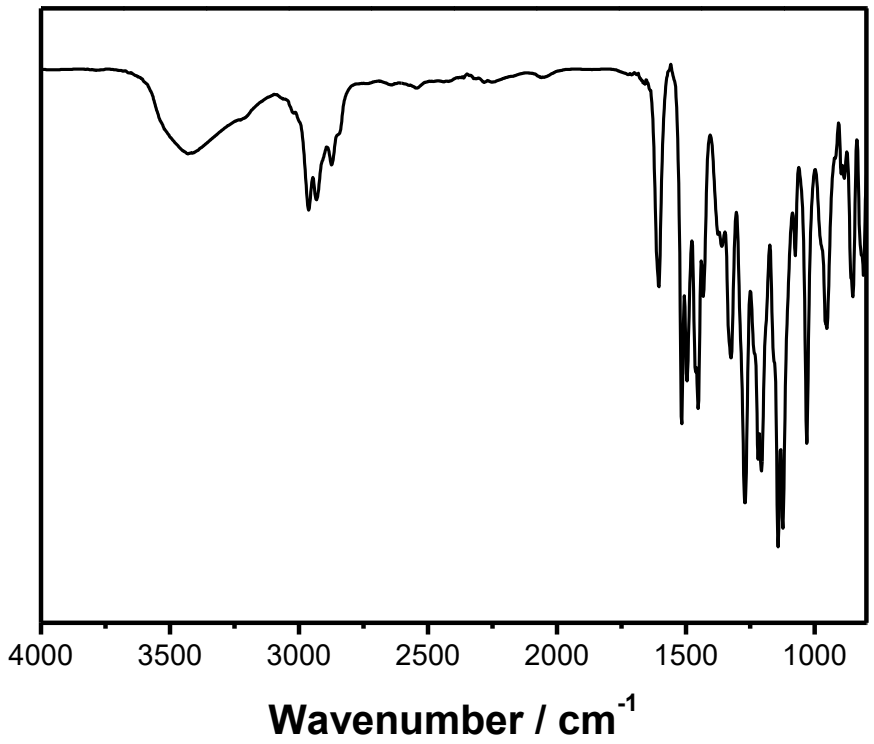

Figure 8.15: FTIR spectrum of (E)-2-methoxy-4-(7-methoxy-3-methyl-5-(prop-1-en-1-yl)-2,3-dihydrobenzofuran-2-yl)phenol **5**.

4-(5-(1-hydroxypropyl)-7-methoxy-3-methyl-2,3-dihydrobenzofuran-2-yl)-2-methoxyphenol (6)

To a solution of **5** (0.5 g in 5 mL THF, 1.53 mmol, 1 eq.) 9-borabicyclo[3.3.1]nonan (9-BBN, 0.5 M in THF, 6.12 mL, 3.1 mmol, 2 eq.) was added dropwise and the reaction was refluxed at 65°C for 4 h. Afterwards, sodium hydroxide (3.0 M in water, 0.77 mL, 2.3 mmol, 1.5 eq.) and then hydrogen peroxide (30%, 0.92 mL, 7.7 mmol, 5 eq.) was added to the mixture. After one hour, we diluted the solution with 20 mL brine and then extracted with ethyl acetate (3 x 30 mL). The crude product was isolated under reduced pressure from the organic phase and then purified by column chromatography using ethyl acetate and petrol ether (1:3) as eluent. Compound **5** had an R_f value of 0.68 whereas for **6** an R_f value of 0.15 was determined. After solvent evaporation, **6** was obtained as a yellowish solid (0.30 g, 60%).

^{1}H NMR (300 MHz, 298 K, $CDCl_3$): δ 6.90-6.68 (ml), 5.66 (s, n), 5.02 (d), 4.47 (t), 3.81 (2s), 3.38 (m), 1.72 (m), 1.30 (d), 0.86 (t). **^{13}C NMR (300 MHz, 298 K, $CDCl_3$):** δ 146.71, 145.80, 144.13, 144.09, 138.41, 133.11, 132.02, 119.96, 114.15, 113.36, 109.52, 109.90, 93.82, 76.34, 45.69, 32.06, 117.48, 10.41.

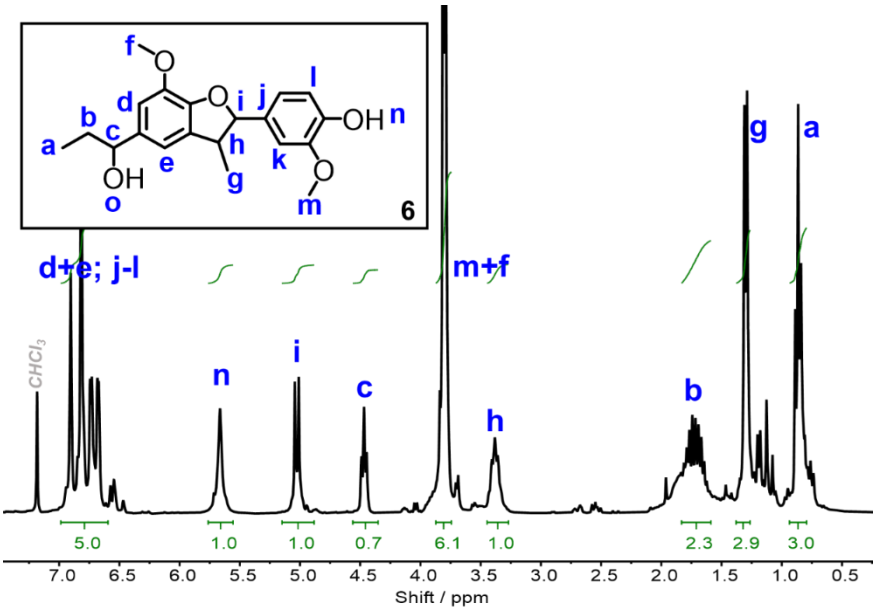

Figure 8.16: ^{1}H NMR (300 MHz, 298 K, $CDCl_3$) spectrum of 4-(5-(1-hydroxypropyl)-7-methoxy-3-methyl-2,3-dihydrobenzofuran-2-yl)-2-methoxyphenol **6** and the respective chemical shifts.

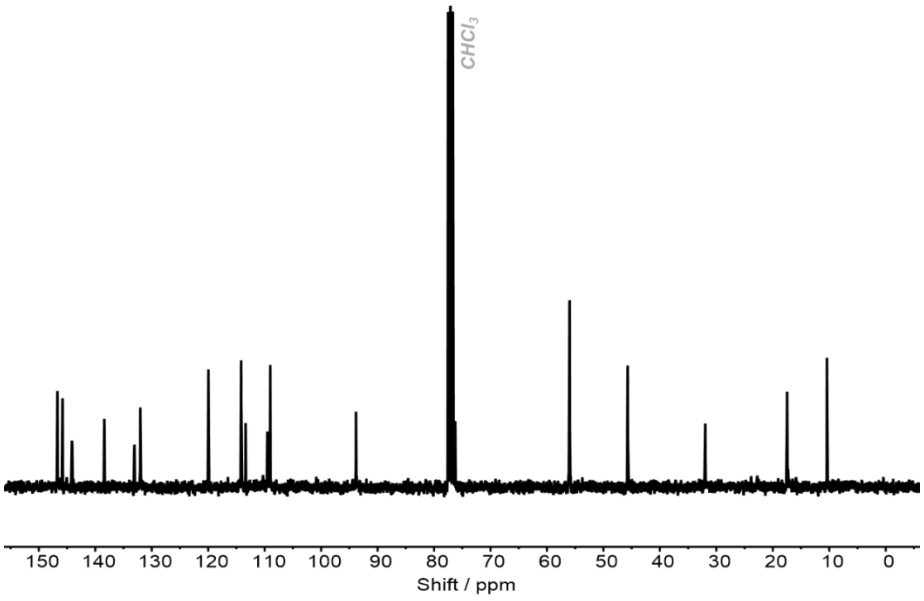

Figure 8.17: ^{13}C NMR (300 MHz, 298 K, $CDCl_3$) spectrum of 4-(5-(1-hydroxypropyl)-7-methoxy-3-methyl-2,3-dihydrobenzofuran-2-yl)-2-methoxyphenol **6** and the respective chemical shifts.

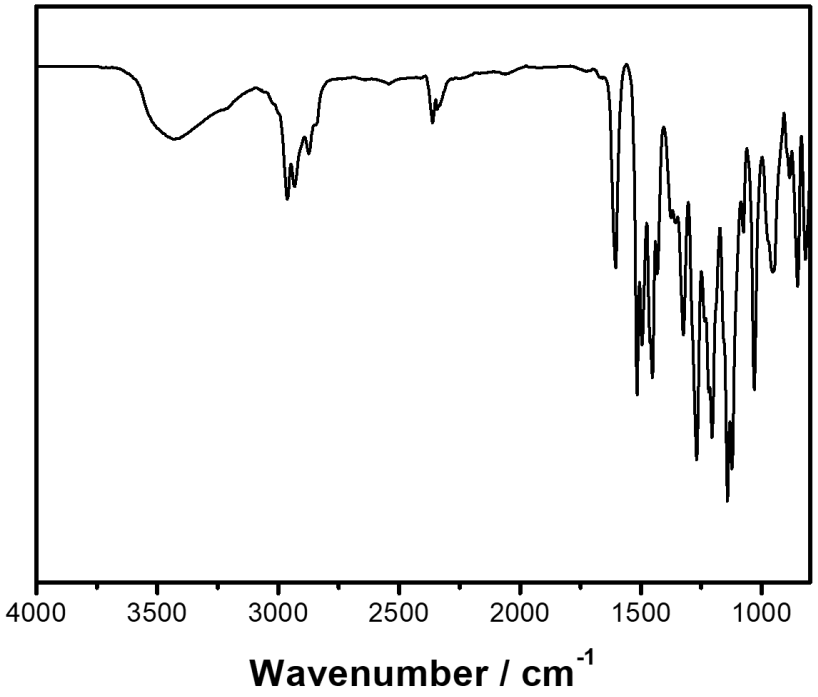

Figure 8.18: FTIR spectrum of 4-(5-(1-hydroxypropyl)-7-methoxy-3-methyl-2,3-dihydrobenzofuran-2-yl)-2-methoxyphenol **6**.

Preparation of nanocarrier dispersions

4 (0.1 g, 0.30 mmol) or **6** (0.1 g, 0.29 mmol) were dissolved separately in 1.5 mL DMSO and then added to each 9.6 mL cyclohexane containing 80 mg of the surfactant P(E/B-*b*-EO). To generate a miniemulsion, the two-phase mixture was ultrasonicated (Branson Digital Sonifier W450-D, 1/ 2″ tip, 70% amplitude, 3 min, 20 s ultrasound followed by 10 s pauses) while cooling with water. Afterwards, toluene diisocyanate (123 µL, 0.86 mmol) was dissolved in a P(E/B-*b*-EO)-cyclohexane solution (57 mg in 6.4 mL) and was added dropwise to the miniemulsion under vigorous stirring (1000 rpm). The reaction was allowed to process overnight at 30°C. For solvent exchange, the nanocarriers were washed twice with cyclohexane and then added to a 0.1 wt% SDS-solution under sonication and shaking. The cyclohexane was evaporated by stirring overnight. The dispersions were characterized by DLS and SEM microscopy.

8.4 Results and discussion

Lignin is abundant, cheap, and biodegradable but varies strongly from plant to plant or even from batch to batch. Therefore, we synthesized two monomers, derived from the monolignol dimers β-O-4-aryl ether and phenylcoumaran. All products were analyzed with ^{1}H and ^{13}C NMR spectroscopy and are based on starting materials occurring naturally in plants. Both monomers were used as degradable breaking points in the shell of polyurethane-based nanocarriers prepared by inverse miniemulsion. This approach shall combine degradability with reproducibility yielding lignin-related polymers:

(A) The β-O-4-monomer **4** was synthesized over four steps (Scheme 8.1). First, the phenolic hydroxyl group of acetovanillone, which has been isolated from a variety of plants, was protected by esterification with benzoic acid using carbonyldiimidazol (CDI) as a coupling agent. To activate the carboxyl group, benzoic acid was added to a supersaturated THF solution of CDI. Immediately, the development of gas was observed, indicating the elimination of carbon dioxide that was formed after the formation of the respective anhydride under imidazole cleavage. Without isolating the reaction product, acetovanillone was added to the yellowish, clear solution of the activated benzoic acid and the reaction was allowed to proceed overnight at 50°C. The benzoyl-protected acetovanillone **1** was obtained as a white powder after precipitation into water. Subsequently, the acetyl group of the reaction product was brominated with bromine in a solution of dioxane and diethyl ether at 0°C. The product was extracted and obtained as a yellowish solid. To a THF solution of **2** vanillin was added, which is produced in industrial scale from lignin sulfonates.[168] Vanillin was attached via a nucleophilic substitution under cleavage of hydrogen bromide to form an ether, which precipitated after two days at 50°C as yellowish solid. The crude product was washed twice with water and then purified by column chromatography. In the last step, reductive conditions were used to produce the β-O-4-monomer **4** as an off-white oil.

(B) Phenylcoumaran **5** was synthesized following the method of Sarkanen *et al.* by oxidative dimerization with hydrogen peroxide from isoeugenol in a water-acetone mixture using Horseradish peroxidase as a catalyst (Scheme 8.2).[167] To generate a di-functional monomer, the α_2,β_2-double bond was hydroborated using 9-borabicyclo[3.3.1]nonane (9-BBN) in a subsequent step (Scheme 8.2). For this purpose, phenylcoumaran and 9-BBN were refluxed in THF at 65°C to form an alkylborane. Afterwards, **5** was transformed by the addition of NaOH and hydrogen peroxide to generate the new monomer **6**, which was purified by column chromatography. ^{1}H NMR spectroscopy proved the conversion of the α_2,β_2-double bonds and the introduction of a hydroxyl group at $C\alpha_2$ e.g. by the triplet at 4.5 ppm.

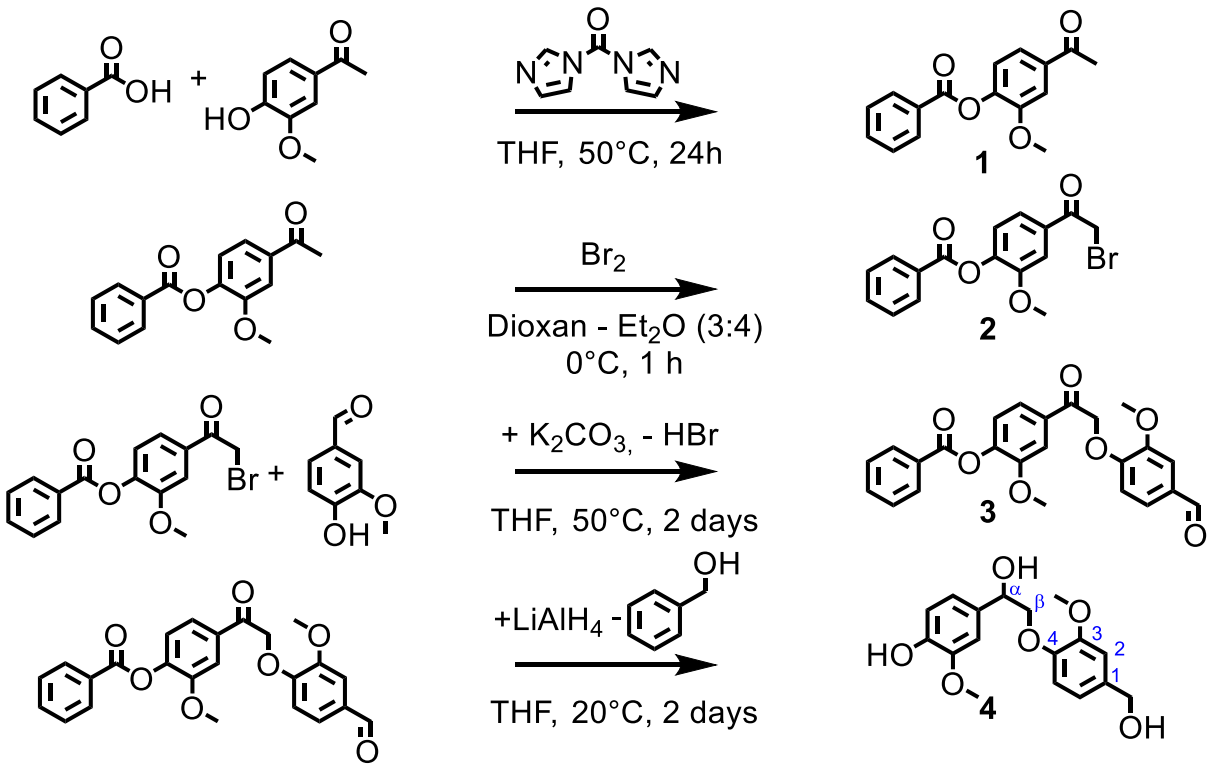

Scheme 8.1: Synthesis of monomer **4** over four steps from bio-based acetovanillone and vanillin. The monomer is related to lignin's β-O-4-aryl ether binding motif, which is the most common linkage in lignin.

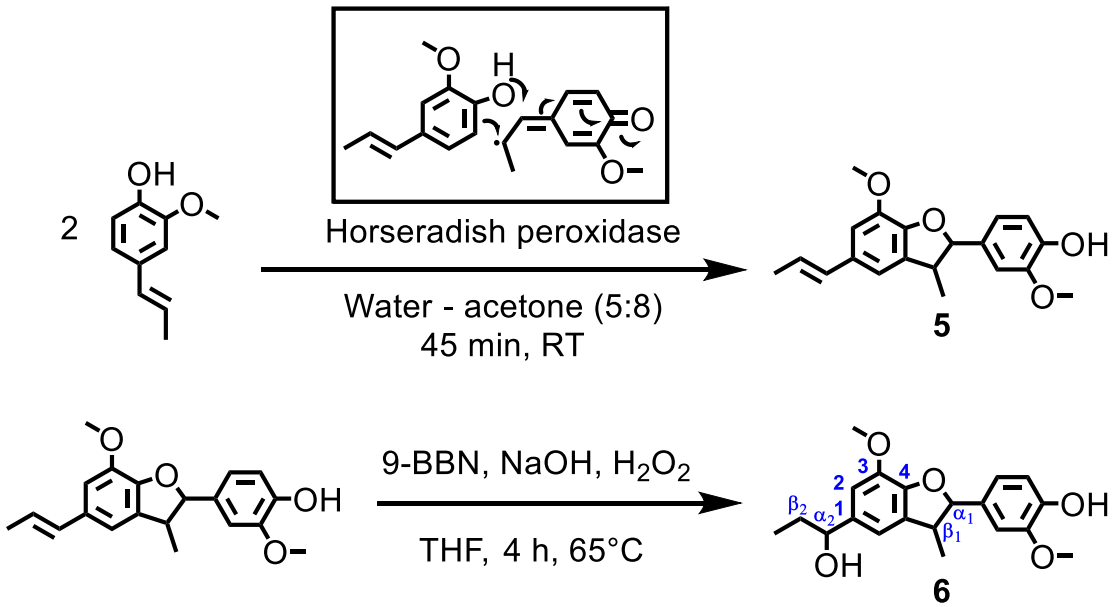

Scheme 8.2: Synthesis of phenylcoumaran according to the protocol of Sarakanen *et al.* and subsequent hydroboration to generate the new di-alcohol **6**.[167]

To prove that **4** and **6** can be degraded like the related natural lignin binding motifs phenylcoumaran and β-O-4-aryl ether, the monomers were dissolved in DMSO and subsequently precipitated in an aqueous solution containing the poly(ethylene glycol)-based surfactant Lutensol AT50. After the removal of DMSO by dialysis, a suspension was obtained that was stable for several hours containing surfactant stabilized aggregates with diameters in the micrometer range. The enzymatic degradability of **4** and **6** was analyzed by quantifying the germination of spores belonging to the lignin-degrading fungi *Phaeomoniella chlamydospora* (Pch) or *Phaeoacremonium minimum* (Pmi), which were cultured in a minimal amount of nutrition medium. As a reference, the germination was measured after the addition of a Lutensol AT50 solution to the medium, which had the same concentration as in the monomer suspensions. For Pch (blue, Figure 8.19), the fungal growth was equal when supplying exclusively Lutensol or additionally **4** and **6**. This indicates that the fungi were able to metabolize the surfactant indeed but that both monomers could not be degraded and used as an additional energy source. In contrast to this, Pch (red, Figure 8.19) showed increased mycelium growth of 24% for **4** and 11% for **6**. Hence, the synthetic lignin monomers can be degraded by certain fungal strains and might be used as microbial degradable breaking points in polymeric (nano-)materials.

.

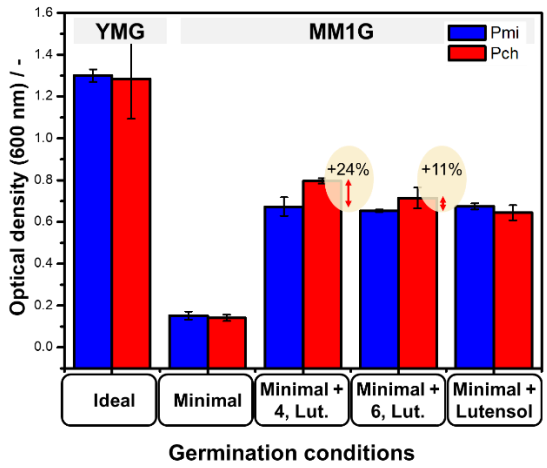

Figure 8.19: Germination of fungal spores of Pmi and Pch quantified by optical density. The amount of mycelium formed depended on the growth conditions and the respective nutrition provided. In a YMG medium the spores have ideal growth conditions whereas in MM1G only minimal amounts e.g. of glucose is available. An increased germination in comparison to the medium alone (“minimal”) proves that material was added which can be degraded by the fungi and supplied extra energy source.

The two monomers **4** and **6** were used to prepare polyurethane nanocarriers in an inverse miniemulsion with TDI as the comonomer (Scheme 8.3), similar to a protocol established by our group for lignin sulfonate.[9] The protocol was adjusted to the new synthetic lignin monomers; each monomer was dissolved in dimethyl sulfoxide (DMSO) and emulsified in cyclohexane containing the nonionic surfactant P(E/B-*b*-EO). To generate a stable miniemulsion, the two-phase mixture was ultrasonicated while cooling with a water bath. To initiate the crosslinking reaction, a solution of cyclohexane, P(E/B-*b*-EO), and TDI was added dropwise under vigorous stirring. The interfacial polyaddition was allowed to proceed overnight at 30°C while stirring at 1000 rpm.

The resulting dispersion was stable for several weeks without any phase separation. Dynamic light scattering (DLS) proved the formation of nanoparticles with an average diameter of 240 nm (PDI: 0.13) using **4** and 400 nm (PDI: 0.20) when adding **6** to the dispersed phase. Both dispersions contained nanoparticles with spherical or droplet-like shape according to SEM (Figure 8.21; Figure 8.22, Figure 8.3). Hence, in contrast to the lignin nanocarriers prepared from lignin sulfonate, no core-shell structures were observed.[9] We assume that the morphology differences, result mainly by the exchange of water against DMSO, as the latter solvent might have dissolved partially the polyurethane reaction products. To prove the interfacial crosslinking, the nanocarriers were washed to remove the surfactant and were then characterized via FTIR spectroscopy (Figure 8.21). In case of both monomers, an intense band of the urethane carbonyl bond at 1714 cm^{-1}, confirmed the successful polymerization. Additionally, a decrease of bands at 3400 cm^{-1}, 1271 cm^{-1} and 1034 cm^{-1}, which belong to the O-H stretching, the O-H bending and C-O stretching of hydroxyl groups, was detected. The FTIR spectra further indicated the presence of isocyanate groups with a band at 2275 cm^{-1}, which either might be used for further functionalization or will hydrolyze to amines in the presence of water. The polyurethane formed from phenylcoumaran **6** was soluble in different organic solvents, e.g. DMF; the GPC elugram proved an increased molecular weight after reaction with TDI (Figure 8.20). In contrast, the polymer obtained of monomer **4** resulted in crosslinked material and was insoluble in any common solvent.

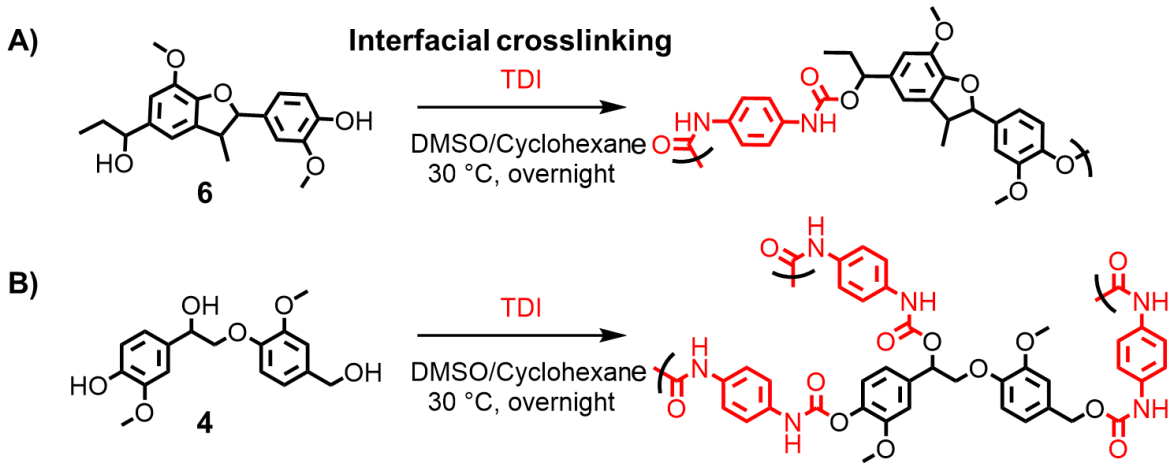

Scheme 8.3: Reactions scheme for the crosslinking of A) phenylcoumaran and B) β-O-4-aryl ether with toluene diisocyanate (TDI). Both are binding motifs that occur naturally in high percentages in the biopolymer lignin.

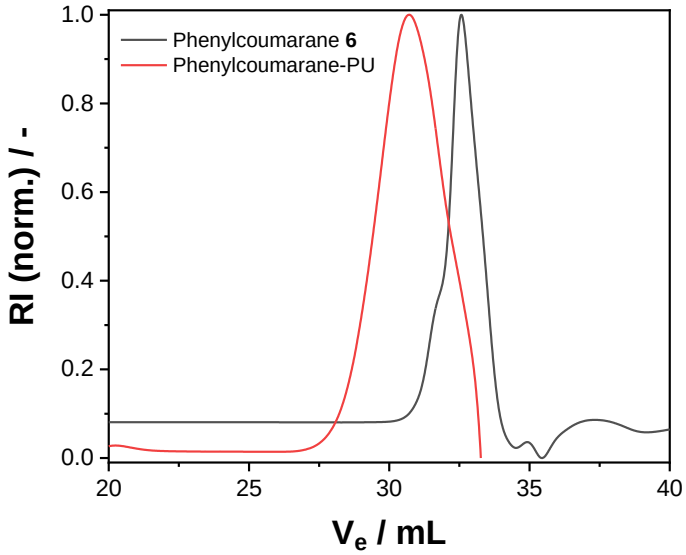

Figure 8.20: SEC elugram of **6** and phenylcoumaran-PU using DMF as eluent

To transfer the nanoparticles to water, excess P(E/B-*b*-EO) was removed from the dispersion by washing with fresh cyclohexane. The dispersion was added dropwise under sonication and shaking to a 0.1 wt% sodium dodecyl sulfate (SDS) solution in water. To evaporate the cyclohexane, the mixture was stirred overnight in an opened vial, yielding an aqueous dispersion. DLS remained relatively unchanged after transfer to water; visualization by SEM showed spherical and partially hollow particles for both polymers indicating interfacial crosslinking. The structural differences between images in cyclohexane and water, most likely can be explained by the exchange of DMSO against water as the dispersed phase. The DMSO might have acted as a softener which led to a deformation of the particle geometry during drop-

casting for SEM sample preparation. Unlike this, nanomaterials with an aqueous core were composed of a stiffer material and therefore had more homogenous, spherical structures during imaging.

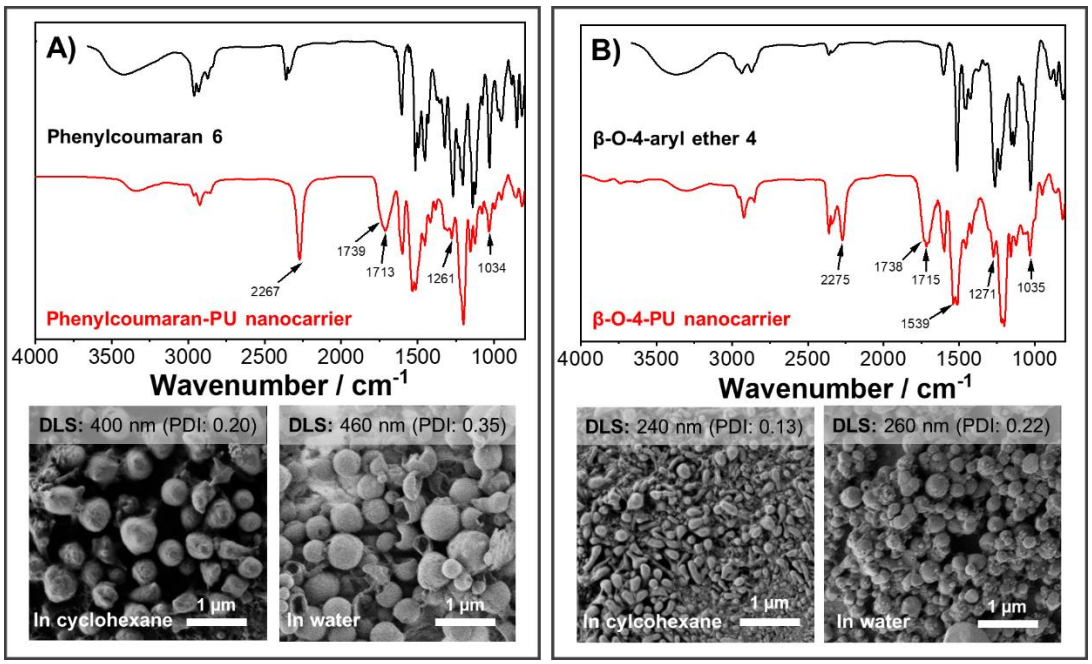

Figure 8.21: Characterization of polyurethane nanoparticles: FTIR spectra of the lignin monomers **6** A) and **4** B) before (black) and after crosslinking (red) with toluene diisocyanate. SEM images of the nanoparticles in cyclohexane or water, respectively; above the images, data from dynamic light scattering is summarized.

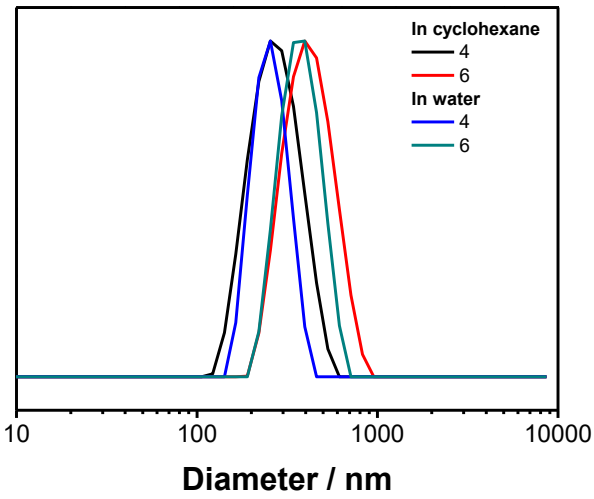

Figure 8.22: A: Diameters of PU-nanocarriers containing either monomer **4** or **6**. The measurement was performed in cyclohexane or after transfer two water in an aqueous solution.

8.5 Conclusion

In summary, this work presents the preparation of polyurethane nanoparticles that contain two new biodegradable building motifs of lignin. The β-aryl ether **4** was synthesized from a benzyl protected and brominated acetovanillone and vanillin. A subsequent reduction yielded a lignin-related monomer with three hydroxyl groups that allowed further functionalization. Phenylcoumaran **6** was obtained over a radical dimerization from isoeugenol which was hydroborinated to a di-alcohol subsequently. Both monomers were crosslinked at the interface of an inverse miniemulsion with TDI to yield hollow polyurethane nanocarriers. As **4** and **6** could be degraded by *Phaeomoniella chlamydospora*, the lignin-like monomers might act as “breaking points” in the polyurethane matrix. The degradable nanocarriers might be useful for example as a carrier agent for on-demand drug delivery in agricultural plant protection formulations.

9 Targeted drug delivery for sustainable crop protection: Transport and stability of polymeric nanocarriers in plants

Sebastian J. Beckers, Alexander H. J. Staal, Christine Rosenauer, Mangala Srinivas, Katharina Landfester, Frederik R. Wurm

Unpublished data.

This project was performed under the scientific guidance of PD Dr. Frederik Wurm and Katharina Landfester. Sebastian Beckers prepared the lignin as well as the polystyrene nanocarriers, characterized the wood saps, investigated the bio-nano-interactions and performed the *in planta*-studies. The “wood extracts” were provided by Dr. Jochen Fischer and characterized together with Christiane Grünewald. To localize the nanocarriers inside the grapevine plants, ^{19}F-MRI experiments were performed by Alexander H. J. Staal. The colloidal stability of the nanocarriers in wood extracts was investigated via dynamic light scattering by Christine Rosenauer.

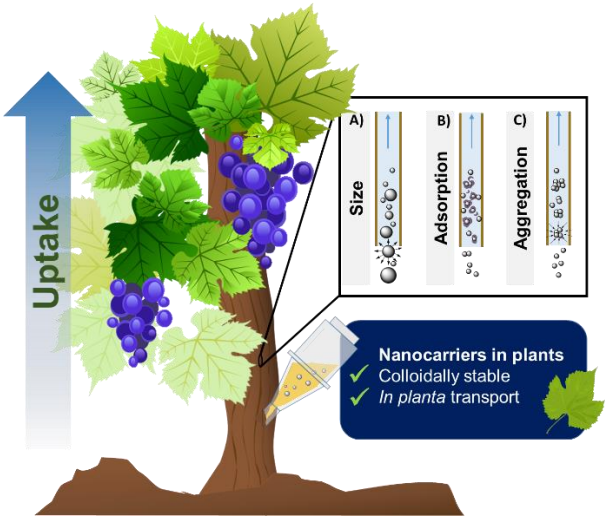

Keywords: *Nanocarriers, drug delivery, plant protection, in planta transport, miniemulsion*.

9.1 Abstract

The spraying of agrochemicals causes environmental pollution by toxic pesticides or fertilizers on a million-ton scale. A sustainable alternative is target-specific and on-demand drug delivery by polymeric nanocarriers. Several potential carrier systems have been presented in the last chapters. A trunk injection (as demonstrated in chapter 4) of an aqueous nanocarrier dispersion can overcome the biological size barriers of roots and leaves and allows the distribution of colloids larger than 100 nm through the vascular tissue of the plant. Essential for the development of new nanocarrier formulations is the understanding of the colloidal stability of the nanomaterials in the plant sap – the fluid transported in xylem and phloem containing water and nutrients - as this determines the distribution *in planta.* To date, the fate of polymeric nanocarriers inside a plant is unknown. We simulated the *in planta* conditions in young grapevine plants and studied the colloidal stabilitly of a systematic series of nanocarriers composed of polystyrene, lignin and polylactic-*co*-glycolic acid (PLGA) by a combination of different techniques. Despite the adsorption of carbohydrates and other biomolecules onto the nanocarriers' surface, they remained colloidally stable after incubation in the biological fluids, suggesting a potential transport via the xylem stream. The transport was tracked by fluoride- and ruthenium-labeled nanocarriers through the vascular tissue of grapevines cuttings by ^{19}F-MRI or ICP-OES. Both methods showed a fast carrier translocation in the plant and proved to be powerful tools to localize nanomaterials in plants. Hence, this study provides essential information for the design of nanocarriers for drug delivery inside of plants to a sustainable crop protection.

9.2 Introduction

Several million tons of agrochemicals are released in the environment every year.[1, 169] Sustainable delivery systems for crop protection and minimal drug dosage are urgently needed and cannot be obtained with conventional spraying.

One promising approach is the injection of drug-loaded nanocarriers for an 'on-demand' and target-specific release of pesticides or fertilizers.[6] Even if some *in planta* studies had been reported for trunk injections,[101, 170] neither the colloidal stability of the nano- or microcarriers inside of the plant nor the *in planta* transport after the injection are known. A detailed understanding of the behavior of polymeric nanocarriers *in planta* is essential to design new drug delivery systems for sustainable agriculture.

To date, agrochemicals are mainly distributed by the spraying of drug formulations onto the plants. Despite advanced formulations that enhance the adhesion to leaf surfaces[3] or the development of effective automated spraying devices,[171] spraying still is a potential risk for the environment and the farmer. Agrochemicals can be washed off by rain and wind and might accumulate in the soil or reach the groundwater.[1] Such contamination threatens insects, soil organisms and wild herbs, but might also contaminate crop and kettle and might be taken up by consumers.[1, 77] In addition, several devastating trunk diseases cannot be treated by spraying from the outside, as the pest is located inside of the trunk.[78, 172]

A sustainable alternative to conventional crop protection might be the utilization of nanotechnology, in analogy to human medicine.[51] Until now, in particular, inorganic metal nanoparticles (e.g. from gold, silver, zinc-, titanium- or copper oxide) have been studied due to their intrinsic toxicity for plant pathogens.[173] Besides, some more advanced drug delivery systems had been developed based on biopolymers such as chitosan,[120, 174] lignin,[100, 101] and alginate,[175] or from synthetic polymers such as poly(allyl amine) hydrochloride[176] or poly(ε-caprolactone).[174]

For optimal performance of a drug delivery vehicle *in planta*, successful translocation through a series of physiological and chemical barriers within the plant needs to be understood. Especially, size is considered one of the major restrictions for penetration into plant tissues.[177] Studies underlined that only relatively small nanomaterials are taken up by most roots (below 50 nm) or by penetration of leaf surfaces (below 10 nm).[178, 179] Hence, polymer-based nano- and microcarriers, which typically have diameters above 100 nm, cannot be taken up by the plants when sprayed. One promising alternative to overcome the size limitation is a trunk injection directly into the vascular tissue (Scheme 1A &B). A technique used until now only for pesticide solutions. When injected into the trunk, drug delivery vehicles should be transported via the vessels of the xylem or phloem, which have diameters of several micrometers.[101] Trunk injections can broaden significantly the scope for nano- and microcarrier-mediated drug delivery inside of plants.[177, 180] However, colloidal stability in the wood sap is crucial for the transport inside of the plant or for aggregation after injection, which had - to the best of our knowledge- not been studied yet. The colloidal stability inside of the plant is determined by the chemical design, surfactant, or surface charges that interact with the complex *in planta* conditions.

Herein, we report - for the first time - the behavior of polymeric nanocarriers in simulated wood saps and in *in planta* conditions by a set of experiments. First, we simulated the *in planta* conditions that a nanocarrier would encounter after trunk injection using wood extracts of commercially relevant fruiting plants (grapevine, apple, peach). A library of model-polystyrene nanocarriers (different surfactants, surface charges, and sizes, see Scheme 9.1C) was

investigated regarding their colloidal stability and surface modification after incubation in the respective biological fluids. Additionally, as biodegradable lignin and polylactic-*co*-glycolic acid (PLGA) nanocarriers have been considered as versatile drug delivery vehicles, we also tested these systems herein.[9, 100, 101, 181, 182] In spite of the formation of a bio-corona, all investigated nanocarriers remained macroscopically stable, however dynamic light scattering proved some aggregation for cationic nanocarriers. All nanocarriers were translocated in *in planta* studies, which was followed by tracing labeled nanocarriers either by ICP-OES (ruthenium-labeled) or by ^{19}F-MRI (fluoride-labeled).

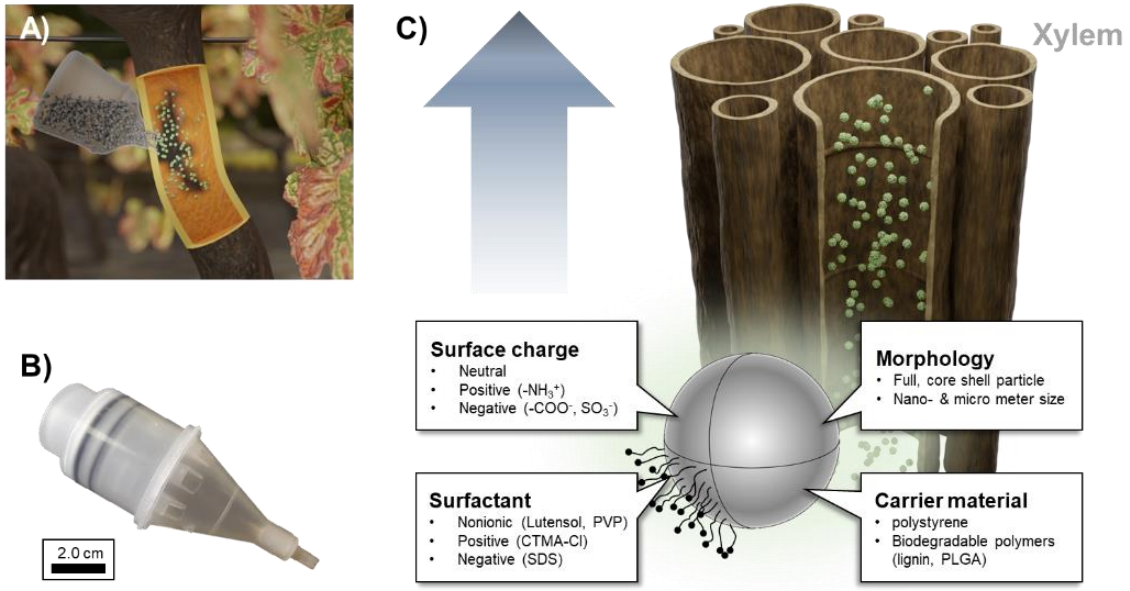

Scheme 9.1: A) Schematic illustration of a trunk injection of a nanocarrier dispersion. (B) Commercially available injector applicable for trunk injections supplied from Tree Tech Microinjection Systems (FL, US). C) Nanocarriers after injection into the xylem of plants and possible factors that influence nanocarrier stability and transport.

9.3 Experimental Section

Materials

The following materials were used: Anthrone, hexadecane, 2,2'-azobis(2-methylbutyronitrile) (V59), sodium dodecyl sulfate (SDS), cetyltrimethylammonium chloride solution (25 wt% in water, CTMA-Cl), acrylic acid, lignin sulfonic acid sodium salt (product number: 471038), Kraft lignin (product number: 370959), polyvinylpyrrolidone (PVP, 24 kg/mol), toluene diisocyanate (TDI) and 2,2'-(ethylenedioxy)bis(ethylamine) were obtained from Sigma Aldrich. 2-Aminoethyl methacrylate hydrochloride and ruthenocene were products

of Acros Organics and STEM chemicals, respectively. Lutensol AT50 was supplied from BASF SE. All chemicals were used without further purification. Polystyrene was obtained from Sigma Aldrich and was distilled before use. PFCE-loaded PLGA nanocarriers were prepared according to the protocol of Hoogendijk *et.al*. and were supplied by the Radboudumc (NL).

Vitis vinifera cv. 'Riesling' cuttings and plants were supplied by the DLR (Neustadt a. d. Weinstraße) and Antes Weinbau-Service GmbH (Heppenheim). Grafting wax prepared by W. Neudorff GmbH KG (Emmerthal, Germany) was used to seal the boreholes in the trunk. To mimic the *in planta* conditions after trunk injection, in February 2019, woodcut from the trunk of the following plants was collected: *Prunus persica* (Peach) cv. 'Red vineyard peach', *Malus domestica* (Apple) cv. 'Jonagold', *Vitis vinifera* (Grapevine) cv. 'Carbernet Sauvignon' and *Vitis vinifera* (Grapevine) cv. 'Riesling'.

Methods

Preparation of wood extracts

20 g of lyophilized wood chips (length: 1-3 cm; ca. 66 g wet mass) were blended for 1 min with 100 mL of MilliQ water. Afterward, the mixture was filtered through a paper filter to separate the solid. Before use, the extract was filtered through a 0.45 µm syringe filter. The solute concentration is assumed ca. 50% relative to *in planta* conditions.

High-performance anion exchange chromatography with pulsed amperometric detection (HPAEC-PAD)

Wood extracts were analyzed using high-performance anion-exchange chromatography. The solutes were separated as anions under high alkaline conditions (pH > 12), coupled with pulsed amperometric detection. HPAEC-PAD analysis was performed on a Shimadzu LC system equipped with two LC-10Ai pumps, a DGU-20A degassing unit, a SIL-10Ai autosampler, a CBM-20A controller and a CTO-20AC column oven. An analytical anion-exchange column of CarboPac MA1 (4 x 250 mm) in combination with a guard column of CarboPac MA1 (4 x 50 mm) at 20°C was used. A Dionex ED40 Electrochemical detector was used for the detection of carbohydrates and sugar alcohols in pulsed amperometric mode through standard quadruple waveform (t=0-0.40 s, p = 1.00 V; t = 0.41-0.42 s, p= -2.00 V; t = 0.43 s, p = 6.00 V; t = 0.44-0.50 s, p = -1.00 V). Eluent was prepared as the mobile phase, which consisted of 480 mM NaOH solution. Isocratic elution was performed at 0,4 mL/min. All the samples were filtrated through a 0,2 µm filter. Injection volume was 10 µL.

Gas chromatography with mass spectrometry detector (GC-MS)

The dry samples were derivatized with 10 µL of ethoxyamine hydrochloride solution in pyridine and 20 µL of pyridine for 90 min at 40°C. Subsequently, the samples were silylated for 50 min at 40°C with 70 µL MSTFA. The samples were analyzed with a Shimadzu GCMS-QP 2010 gas chromatograph coupled with a quadrupole mass analyzer. 1 µL aliquots of the samples were injected into a DB5-MS capillary column (30 m x 250 µm I.D., 0.25 µm film thickness, Phenomenex, Germany) in split mode (1:10) using an AOC20i autosampler. The temperature of the injection system was 250°C. The initial GC oven temperature was 70°C, 5 min after injection the GC oven temperature was increased with 5°C/min to 320°C and held for 5 min at 320°C. Helium was used as a carrier gas with a flow rate of 1 mL/min. Detection was achieved using MS detection in electron impact mode and full scan monitoring mode (m/z 15-800). The temperature of the ion source was set at 200°C and the transfer line at 275°C. Identification was carried out by comparing the mass spectra with the NIST spectral library.

Bio-corona formation in wood extracts

A dispersion (typically 1 wt%) with a calculated surface area of 0.05 m^2 was added to 0.5 mL of wood sap and incubated at 25°C for 1 h. Then, the dispersion was centrifuged (PS nanocarriers: 20k rpm, 30 min; Lignin nanocarriers: 10k rpm, 15 min) and the supernatant was replaced with MilliQ water. After resuspension of the pellet, the nanocarriers were washed by three further centrifugation steps and analyzed regarding surface modifications by ζ-potential measurements and anthrone- plus malate assays.

Anthrone 620 nm carbohydrate quantification assay

5 mg anthrone were dissolved in 1 mL of concentrated sulfuric acid. To 150 µL of the anthrone stock solution, 75 µL of a carbohydrate mixture was added. After incubation at 80°C for 10 min, the absorbance was measured at 620 nm with a Tecan Infinite M1000 plate reader. The evaluation was performed relative to a D-glucose calibration.

Pierce 660 nm protein quantification assay

The protein concentration of wood saps was determined using a Pierce 660 nm protein assay (Thermo Fisher, Germany) following the instructions from the manufacturer. The absorbance was measured at 660 nm with a Tecan infinite M1000 plate reader.

Malate and glycerol quantification assay

Malate was quantified enzymatically using Kit Nr. 10139068035 from R-biopharm. Kit Nr. 10148270035 from R-biopharm was used to quantify glycerol.

Dynamic light scattering (DLS)

All DLS experiments were performed on an ALV/CGS3 spectrometer (ALV GmbH, Germany) consisting of an electronically controlled goniometer and an ALV-5000 multiple tau full-digital correlator. As a light source, a helium-neon laser with a wavelength of 632.8 nm and output power of 25 mW (JDS Uniphase, USA, Type 1145P) was used. The measurement was performed in cylindrical quartz cuvettes (Inner diameter: 18 mm, Hellma, Germany) at room temperature for 5 times 30 s at 30°, 60°, 90°, 120° and 135°. Analysis of the autocorrelation function was using either using a CONTIN or a HDRC algorithm.

To determine the colloidal stability of nanocarrier dispersions after injection into a plant stem, the wood extract was filtered through a 0.45 µm Millex-LCR syringe filter. 50 µL was of a 1 wt% dispersion was then added to 150 µL of wood extract and incubated overnight at room temperature. Due to the negligible scattering contribution of wood saps from grapevine and apple, the data was evaluated using the CONTIN method, whereas extracts of peach wood, containing non-removable aggregates, needed evaluation with the HDRC algorithm.[85]

ζ-Potential measurements

To determine the ζ-potential, 20 µL of a 1 wt% dispersion was added to 2 mL of 1 mM KCl solution. 1 mL of the mixture was filled in a cuvette and analyzed using a Zetasizer NanoZ (Malvern).

Scanning electron microscopy (SEM)

SEM was performed on a Gemini 1530 (Carl Zeiss AG, Oberkochem, Germany) scanning electron microscope (SEM) operating at 0.35 kV. The samples were prepared by casting diluted nanocarrier dispersions on silicon wafers.

Particle charge detection (PCD)

The number of positive and negative surface charges was determined by titration of a 0.1 mg/mL nanocarrier dispersion on a particle charge detector PCD 02 (Mütek Gmbh, Germany) combined with a Titrino Automatic Titrator 702 SM (Metronohm AG, Switzerland). Positive or negative charges were titrated either against 0.001 N solutions of the anionic poly(ethylene sulfonate) or cationic poly(diallyl dimethylammonium chloride) respectively.

***In planta* studies – Nanocarrier uptake**

Two experimental setups to investigate the transport of nanocarriers inside of a plant were used:

(A) Nanocarrier uptake by transpirational pull over cutting edge: Cuttings (length 4 cm, diameter 0.8 cm) of *vitis vinifera* cv. ‘Riesling’ were grown for ca. 1.5 months in perlite until ca. 3-4 leaves were formed. The plants were placed in a vial with 5 mL of a 0.2 wt% nanocarrier

dispersion for 7 days at ca. 32°C (Figure 9.6A). Water was refilled regularly. Each experiment was performed in duplicates or triplicates (Table 9.2, Figure 9.8).

(B) Nanocarrier injections: V*itis vinifera* cv. 'Riesling' test plants (length: 25 - 30 cm, trunk diameter: 1.0 – 1.5 cm, one shoot with leaves: 30 – 40 cm) were grown in a pot with breeding ground until used (Figure 9.9B). To investigate the nanocarrier transport, 20 cm above the soil a 1-2 mm wide hole was drilled ca. 0.5 cm into the trunk and 0.2 µL of a 10 wt% PFCE-PLGA dispersion was injected with a 1 mL syringe attached to a metal extension with conus top (Figure 9.9C). The wound was sealed with grafting wax. The plant was kept for further days at ca. 32°C under regular addition of water until investigated by ^{19}F MRI.

Hydrolysis-resistance of PLGA nanocarriers *in planta*

The hydrolysis-resistance of the nanocarriers was tested before the measurement, by mixing 0.1 mL of 1 wt% dispersion with 0.4 mL of 'Riesling' wood extract (pH 5.3). After incubation for 7 days, the mixture was analyzed regarding size distribution and morphology by DLS and SEM. As both remained unchanged in comparison to the original nanocarriers, we assume no hydrolysis in the wood extracts.

Inductively coupled plasma emission spectroscopy (ICP-OES)

ICP-OES was performed at an Activa M spectrometer from Horiba to determine the metal content of "wood extracts", dispersions containing ruthenium-labeled nanocarriers and to localize the latter after uptake into grapevine cuttings. The samples were prepared as follows:

Before measurement, the wood extracts (0.5 mL) were diluted with (9.5 mL) MililQ water. The content of potassium (spectral line: 766 nm), sodium (spectral line: 590 nm), magnesium (spectral lines: 279 nm, 384 nm), calcium (spectral lines: 318 nm, 374 nm, 423 nm), sulfur (spectral lines: 182 nm, 213 nm) and phosphorus (spectral line: 178 nm) was determined subsequently by ICP-OES.

To determine the metal content of ruthenium-loaded polystyrene nanocarriers, 0.2 mL of a 1 wt% dispersion diluted with 9.8 mL MilliQ water. The amount of ruthenium was determined using spectral lines at 240 nm, 267 nm, and 273 nm.

To track ruthenium-loaded nanocarriers after uptake into grapevine cuttings (according to paragraph "Nanocarrier uptake by transpirational pull over cutting edge", the plants were cut into four 1 cm long segments. Wood and leaves were dried in an oven at 120°C and dissolved in 3 mL of a 1:1 mixture composed of hydrogen peroxide (30%) and concentrated sulfuric acid ("Piranha solution"). After the addition of further 7 mL MilliQ water, the ruthenium content was determined by ICP-OES (spectral lines: 240 nm, 267 nm, 273 nm). To quantify the amount of

nanocarriers, which were not taken up by the plant, the residual dispersion was analyzed in the same manner.

^{19}F MRI experiments

Image data was recorded on a Bruker BioSpec 117/16 11.7T horizontal bore MRI (Bruker, Germany) with a dual tuned ^{1}H/^{19}F bird cage coil with a length of 4 cm. For ^{19}F imaging, a 3D RARE sequence was used, imaging parameter: TR 1500ms, TE 6.62ms, turbo factor 44, 32 averages, matrix 64x64x16, field of view of 32x45x32mm, imaging time 12:48min. Excitation frequency 470,743 MHz. Co-registration of ^{1}H anatomical images was done with an unspoiled T1-weighted 2D FLASH, local shimming avoided artifacts in the low water content regions of the stem. Imaging parameters: TE 2.5 ms, TR 268 ms, FA 50deg, 2 averages, matrix 248x248 zero-filling to a 256x360 matrix, field of view 32x45mm, 40 1mm thick slices for an imaging time of 2:15 min. To obtain a sufficiently low ^{19}F detection threshold to visualize low concentrations of nanocarriers, a high-field small animal MRI system was used. The coil length did not allow for imaging of the entire stem and shoot simultaneously. Therefore, the length of the shoot was imaged in three separate images, anatomical landmarks, such as notches, allowed for the reconstruction of the entire stem and shoot.

Syntheses

Preparation of ruthenocene-loaded polystyrene nanocarriers

Polystyrene nanocarriers were produced by free-radical polymerization in miniemulsion using a modified literature protocol.[183, 184] For PS-SDS, hexadecane (8.3 mg, 0.036 mmol), V59 (3.3 mg, 0.017 mmol), and ruthenocene (6.6 mg, 0.029 mmol) were added to freshly distilled styrene (0.2 g 1.920 mmol). After addition of 0.8 mL of an aqueous 3 mg/mL SDS solution, the mixture was stirred with an IKA Ultraturrax to generate a pre-emulsion and then sonicated for 2 min (Branson Digital Sonifier W450-D, 1/4” tip, 70% amplitude) under ice-cooling. Afterward, the polymerization was allowed to proceed for 24 h at 72°C. Finally, the polystyrene dispersion was diluted with 5 mL MilliQ water and filtered through a KimWipe to remove macroscopic aggregates.

To exchange SDS against Lutensol AT50, a Lutensol solution (5 mg/mL) was added to the dispersion and the mixture was dialyzed (MWCO 1 kDa) against 500 mL MilliQ water for 3 h (this procedure was repeated five times) to yield PS-Lut.

To prepare CTMA-Cl-stabilized nanocarriers, a CTMA-Cl solution (5 mg/mL) was added to the previously prepared PS-Lut nanocarriers and the dispersion was dialyzed

(MWCO 25 kDa) against a 500 mL CTMA-Cl solution (5 mg/mL) for 3 h (this procedure was repeated five times) to obtain PS-CTMA.

Carboxyl-functionalized nanocarriers (PS-COOH) were prepared according to the above mentioned free-radical miniemulsion polymerization, adding additionally acrylic acid (4 mg, 0.056 mmol) to the dispersed phase prior sonication. For amino-functionalized nanocarriers (PS-NH_2), 2-aminoethyl methyacrylate hydrochloride (4 mg, 0.024 mmol) was dissolved in water instead. After addition of 0.8 mL of an aqueous 2.5 mg/mL Lutensol AT50 solution, the mixture was stirred with an IKA Ultraturrax and then sonicated for 2 min (Branson Digital Sonifier W450-D, 1/4" tip, 70% amplitude) at 0°C. The polymerization proceeded for 24 h at 72°C. Afterwards, 5 mL MilliQ water was added and the mixture was filtered through a KimWipe. To set the surfactant concentration to 5 mg/mL, the dispersion was dialyzed three times for 3 h against 500 mL of a Lutensol AT50 (5 mg/mL) solution with MWCO of 25 kDa. Finally, all dispersions were set to a concentration of 1 wt% with MilliQ water and characterized by DLS, SEM, ICP-OES and regarding their ζ-potential.

Preparation of ruthenocene-loaded polystyrene microcarriers

Polystyrene microcarriers were prepared by free-radical dispersion polymerization according to Jinhua *et al.*.[185] V59 (3.3 mg, 0.017 mmol) and ruthenocene (6.6 mg, 0.028 mmol) were mixed with freshly distilled styrene (0.196 g, 1.885 mmol). To the mixture, an ethanol solution of polyvinylpyrrolidone (40 mg in 1.76 g ethanol, 24 kg/mol) was added. After stirring at 250 rpm for 24 h at 72°C, the dispersion was centrifuged (30 min, 4000 rpm) and the supernatant was replaced with MilliQ water. For further purification, the beads were additionally washed twice with 5 mL water. The solid content was finally adjusted to 1 wt% by the addition of MilliQ water.

Preparation of lignin nanocarriers

Lignin nanocarriers were prepared according to our previously reported protocol by crosslinking methacrylated Kraft lignin in a direct miniemulsion.[101] Interfacial polyaddition in an inverse miniemulsion was used to prepare hollow lignin nanocarriers from lignin sulfonate sodium salt and toluene diisocyanate following our literature protocol.[9]

9.4 Results and Discussion

The colloidal stability of a nanocarrier dispersion inside of the plant determines the translocation through the vascular tissue of the plant. In general, two different scenarios are conceivable and should be studied in this paper:

(1) Depot: After injection into the trunk of the plant, the dispersion aggregates, which would probably lead to the formation of a “drug depot”. A sustained release of the drug by diffusion could occur. However, for a pathogen-induced drug release, the fungi or bacteria would need to penetrate the vascular system to reach the nanocarrier depot to initiate the drug release. Alternatively, the dispersion would need to be injected directly into the infected tissue.

(2) Transport: After injection into the trunk, the nanocarrier dispersion remains colloidally stable and can be transported through the plant reaching the place of infection. However, if the colloids move to the shoots or the leaves, they might be lost by pruning procedures or by shedding the leaves after summer, which might reduce the long-term protection.

Simulation of *in planta* conditions by wood saps

Characterization of wood saps: To understand the *in planta* conditions after nanocarrier injection, four different wood saps of relevant fruiting plants were used to simulate the *in planta* situation. Taking the global crop sizes of fruits into account, we chose to analyze the saps of *malus domestica* (apple, 89 Mio tons, rank 3 in 2016), *vitis vinifera* (grapes, 77 Mio tons, rank 4), and *prunus persica* (peach, 25 Mio tons, rank 10). The wood saps were produced by aqueous extraction of lyophilized wood chips and are mixtures of xylem and phloem saps. Wood extraction is a well-established method to isolate plant-based solutes e.g. for phytomedical applications.[173, 186, 187] According to the literature, wood sap is mainly composed of carbohydrates, organic acids, salts, and trace amounts of proteins as well as amino acids.[69, 70, 72] The wood saps were investigated regarding their chemical composition with HPLC, GC-MS, ICP-OES, and other assays (Figure 9.1). The quantification of carbohydrates by the Anthrone assay proved that with 30-70% carbohydrates are one of the major species in the sap. To a high extent, these originate from the phloem, in which carbohydrates are produced during photosynthesis and translocated throughout the plant. By HPLC, glucose, fructose, and sucrose were identified in all wood saps, whereas sorbitol was found only in the extracts of peach and apple (Figure 9.2). In accordance with literature, malate was found in remarkable amounts of up to 4.6% in all extracts. Further, tartaric acid was identified in extracts from ‘Riesling’ wood by GC-MS. Organic acids resulted not only in acid pH values of ca 5.5 but also affect the stability of colloids due to their ability to shield surface or surfactant charges. In contrast to nanocarrier-mediated drug delivery in blood for biomedical application, the risk of

protein adsorption and the resulting formation of aggregates is negligible in wood saps, as the protein amounts were below the detection limit of the Pierce assay. Further, potassium, sodium, magnesium, and calcium were quantified by ICP-OES. Considering the literature, we assume the respective counter ions like nitrate, chloride phosphate and sulfate are contained in the wood sap additionally.[72] The concentration was estimated by measuring the amount of phosphorus and sulfur by ICP-OES respectively.

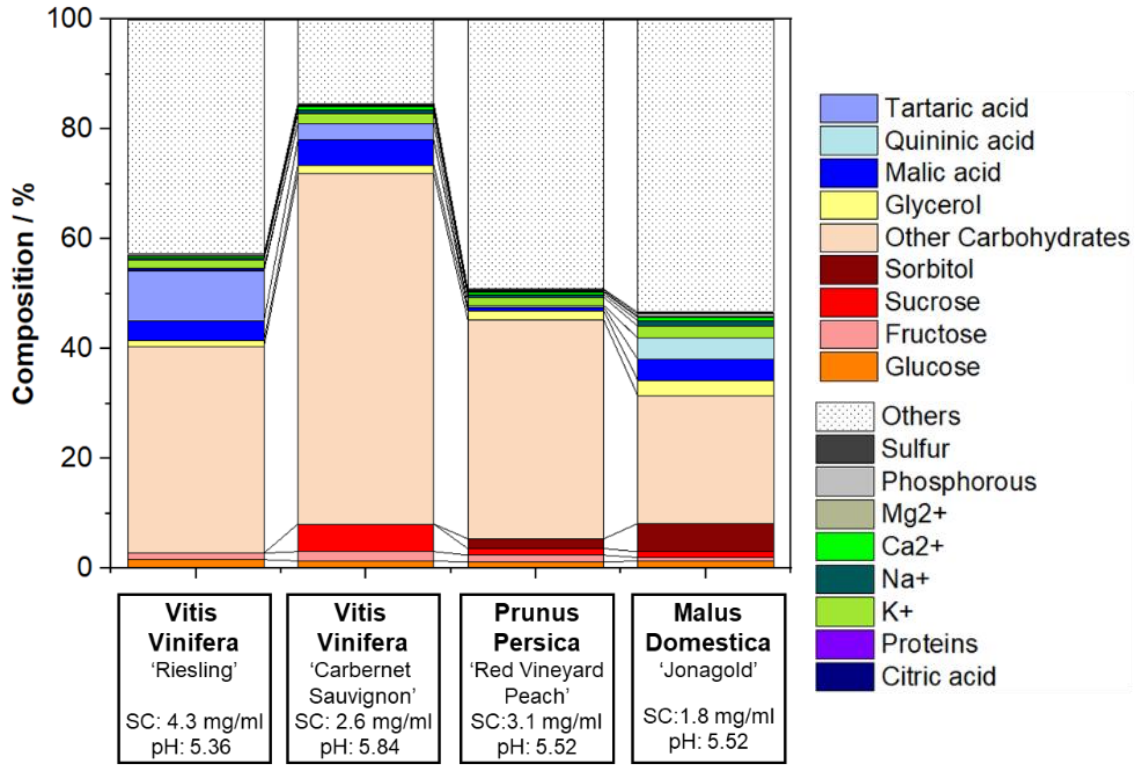

Figure 9.1: Composition of wood saps from four different commercially relevant fruiting plants (determined by HPLC, ICP-OES, GC-MS, Anthrone, and Pierce assay).

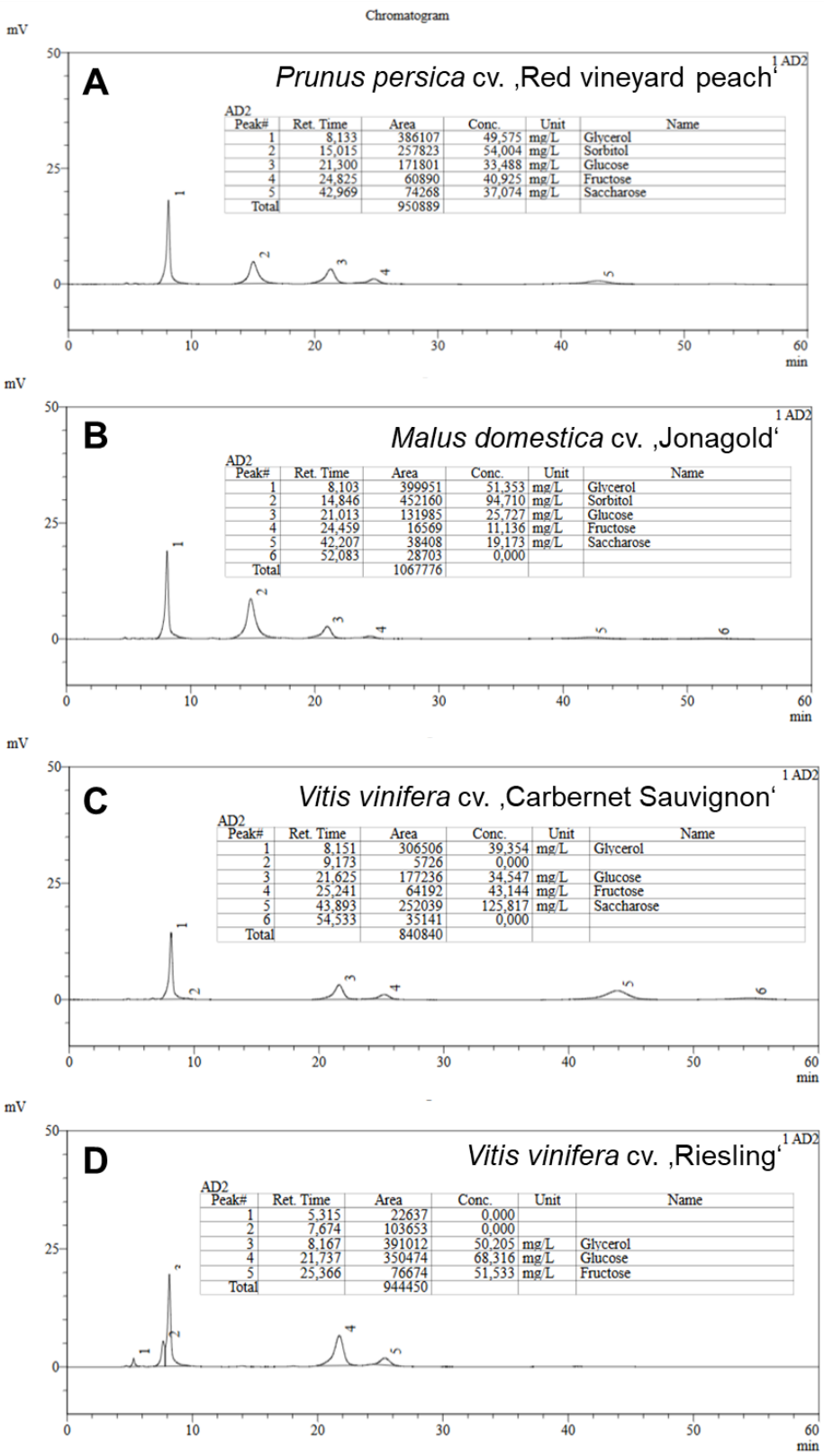

Figure 9.2: Elugrams measured by HPEAC-PAD of wood extracts from apple, peach and grapevine woodcut.

Nanocarrier library: We prepared a systematic library of nanocarriers and studied their colloidal stability in the wood saps. Nanocarriers based on different polymeric materials (polystyrene, lignin, and polyesters), stabilized with different surfactants, and different surface functionality, were prepared. Polystyrene nanocarriers are a well-established model to study interactions of nanocarriers with blood serum or plasma,[188] while to the best of our knowledge, nothing had been reported about colloidal stability of nanocarriers in wood saps. The model PS nanocarriers were stabilized either by the anionic surfactant SDS, the cationic CTMA-Cl, or by the nonionic surfactant Lutensol AT50. Additionally, we prepared copolymers of styrene with acrylic acid and 2-aminoeethyl methacrylate hydrochloride, which led to additional cationic or anionic charges on the nanocarriers. The ionic surface groups should mimic, for example, charged nanocarriers based on biopolymers, such as chitosan, lignin, or alginate, which might be interesting for *in planta* drug delivery. The characterization data of the PS-NP library is listed in Table 9.1 and Figure 9.3. Additionally, we prepared two biodegradable nanocarriers as closer models for *in planta* drug delivery, based on lignin and poly(lactide-*co*-glycolide) (PLGA). As both materials are bio-based and biodegradable, they are promising candidates for drug delivery and enzyme-triggered release in plant protection.[9, 101, 189, 190]

Lignin nanocarriers had been previously studied *in planta* for the treatment of the grapevine trunk disease Esca.[101] In our recent work, we injected aqueous nanocarrier dispersions into grapevine plants, in which lignase-producing fungi led to an ‘on-demand’ release of encapsulated pesticides.[9, 100, 101] However, the colloidal stability or transport inside of the plants had not been investigated. Herein, we studied two lignin nanocarriers, which differ next to their morphology in their chemical functionality and their surface charge: the above mentioned crosslinked lignin nanocarriers, which were prepared in a direct miniemulsion from methacrylated Kraft lignin allow the encapsulation of hydrophobic drugs. The nanocarriers had 0.9 anionic charges per nm^2 of particle surface and showed a negative ζ-potential of -20 mV, due to the negatively charged phenolate and carboxylate groups in lignin’s structure (Table 9.1). Additionally, lignin-nanocarriers were prepared by an inverse miniemulsion, which allows the encapsulation of more hydrophilic drugs. The crosslinking of a lignin sulfonate sodium salt with toluene diisocyanate at the interface resulted in nanocarriers with a core-shell structure and a ζ-potential of -28 mV because of phenolic units and sulfonic acid groups of the lignin sulfonate.

PLGA (lactide and glycolide in an equimolar ratio) nanocarriers were prepared by the method of Hoogendijk *et al.*. The nanocarriers were composed of a dense polymer matrix in which the MRI contrast agent perfluoro-15-crown-5-ether (PFCE) was embedded in domains of ca. 5 nm.[191] PLGA nanocarriers are heavily researched for biomedical applications as the (enzymatic) hydrolysis of its ester linkages not only allows a controlled release of encapsulated

cargo but also leads to the biocompatible degradation products lactic and glycolic acid.[181] Both compounds occur naturally in plants. Likewise, *in vitro* tests proved that PLGA nanocarriers are non-phytotoxic for plant cells (but was not tested herein).[192]

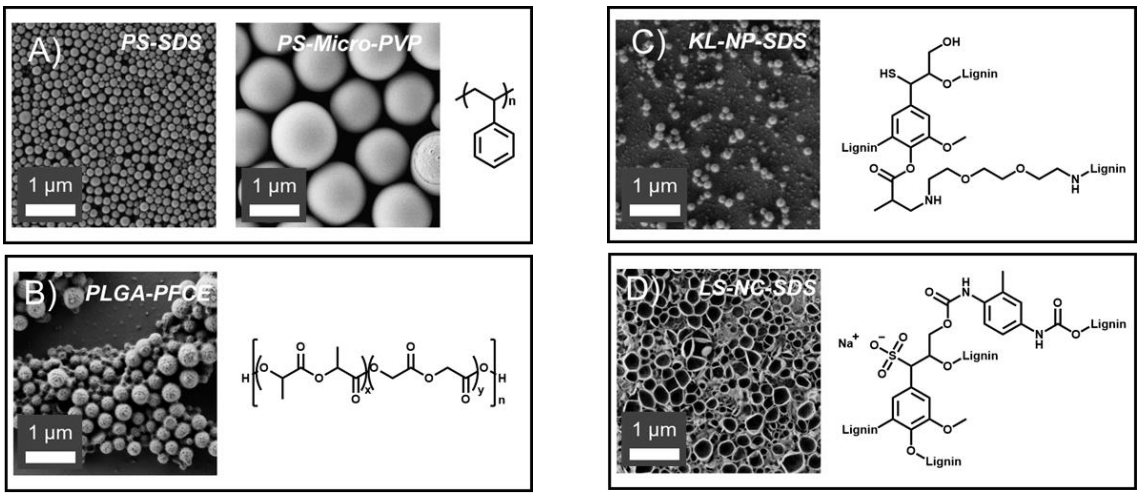

Figure 9.3: Scanning electron microscopy images showing the chemical structures and morphologies of (A) polystyrene, (B) PLGA, and (C and D) lignin nanocarriers**.**

Table 9.1: Characterization of PS, lignin and PLGA nanocarriers regarding particle size, PDI, ζ-potential and surface charge density.

Nanocarrier	R_h / nm	PDI / -	ζ-Pot. / mV	Groups / nm^{-1}
PS-SDS	90	0.002	-44 ± 1	-
PS-Lut.	110	0.005	-10 ± 2	-
PS-CTMA	120	0.048	+23 ± 1	-
PS-NH_2-Lut.	100	0.167	+7.0 ± 1	0.1
PS-COOH-Lut.	80	0.144	-34 ± 3	0.6
PS-Micro-PVP	1500*	-	-6.0 ± 2	-
KL-NP-SDS	90	0.256	-36 ± 3	-
LS-NC-SDS	150	0.416	-32 ± 1	-
KL-NP-Lut.	100	0.270	-20 ± 1	0.9
LS-NC-Lut.	160	0.407	-28 ± 1	-
PLGA-PFCE	220	0.381	-14 ± 1	-

*measured by SEM

Wood-sap nanocarrier interactions: The interactions of the different nanocarriers with the wood extracts of *Prunus persica* (peach) cv. 'Red vineyard peach', *Malus domestica*

(apple) cv. 'Jonagold', *Vitis vinifera* (grapevine, red grapes) cv. 'Carbernet Sauvignon' and *Vitis vinifera* (grapevine, white grapes) cv. 'Riesling' were studied. The nanocarriers were incubated in the wood sabs to mimic the *in planta* conditions after the injection into a plant and the ζ-potentials were measured, which indicated the adsorption of charged compounds on the nanocarriers' surface. In general, the ζ-potentials decreased for non-ionic (PS-Lut) and positively charged nanocarriers (PS-NH_3^+-Lut) indicating the adsorption of organic acids and other anions (e.g. phosphate, nitrate, and sulfate or interfacially active compounds), whereas the ζ-potential remained relatively constant in the case of all nanocarriers with an originally negative ζ-potential (PS-COO^--Lut, KL-NP-Lut and LS-NC-Lut, Figure 9.4 A and B). The amount of surface-adsorbed carbohydrates was quantified by the Anthrone assay and found to be ca. 0.5 – 3.0 mg·m^{-2}, which means a surface coverage of 1 - 8% after the applied procedure (considering an area of 0.78 nm^2 for a single glucose molecule (Figure 9.4 C & D).

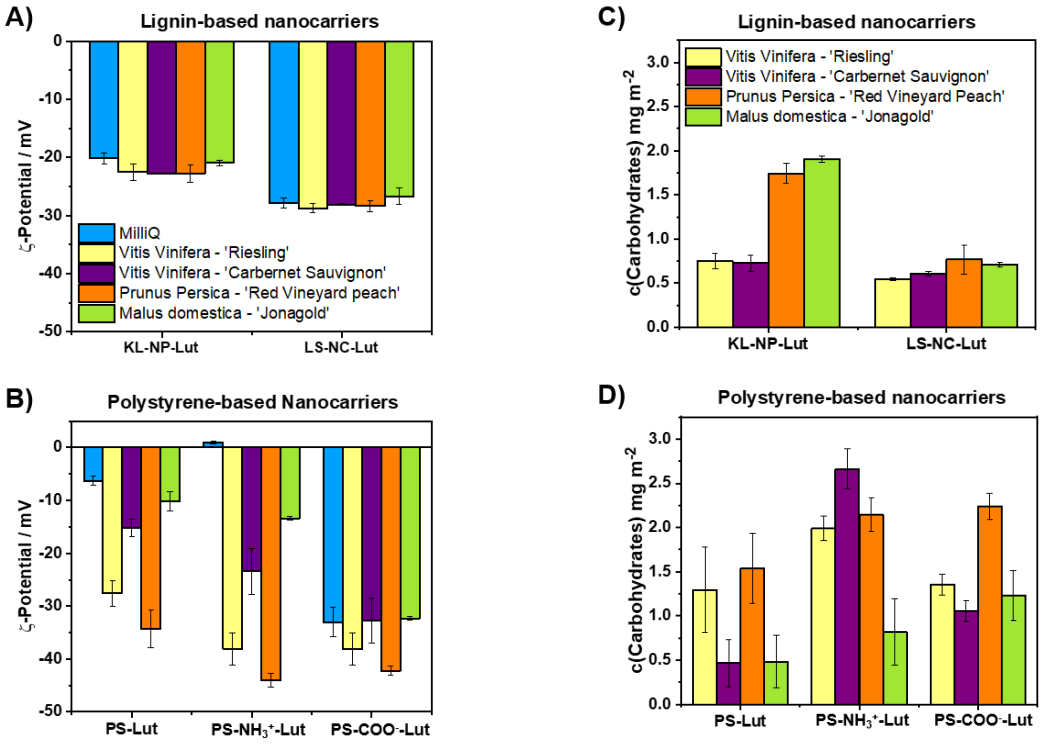

Figure 9.4: Nanocarriers incubated in wood saps: ζ-potentials (A & B) and carbohydrate adsorption (C & D) (after 1 h incubation at RT). All nanocarriers were stabilized with the nonionic surfactant Lutensol AT50.

Colloidal stability of nanocarriers in wood sap. Dynamic light scattering was used to monitor the colloidal stability of the nanocarrier dispersions after incubation in the wood saps. For nanocarriers in wood saps from grapevines and apple, a bi-exponential fit for the evaluation

was used, as the wood saps did not contain additional scattering (Equation 9.1). In contrast, extracts from peach wood exhibited strong scattering also without the addition of nanocarriers (max 0.8% of scattering; removal by centrifugation or filtration impossible). To evaluate the colloidal stability of the nanocarriers in peach extract, we used the protocol of Rausch *et al.* for data evaluation, which was previously used to analyze the colloidal stability of nanocarriers in blood serum.[85] Herein, we expanded this method to wood saps for the first time, proving the technique's versatile fields of application. Briefly, the autocorrelation function of the biological fluid (Equation 9.2) is described as a sum of three exponentials where a_i is the amplitude and $\tau_i = 1/(q^2 D_i)$ is the decay time containing the scattering vector q and the Brownian diffusion coefficient D_i.

Equation 9.1

$$g_{1,NP} = a_{1,NP} \cdot e^{-\frac{t}{\tau_{1,NP}}} + a_{2,NP} \cdot e^{-\frac{t}{\tau_{2,NP}}}$$

Equation 9.2

$$g_{1,WS} = a_{1,WS} \cdot e^{-\frac{t}{\tau_{1,WS}}} + a_{2,WS} \cdot e^{-\frac{t}{\tau_{2,WS}}} + a_{3,WS} \cdot e^{-\frac{t}{\tau_{3,WS}}}$$

After determining both scattering profiles separately, a mixture of nanocarriers and wood sap was analyzed. If the nanocarriers stay colloidal stable, the corresponding autocorrelation function can be fitted as a sum of $g_{1,NP}$ and $g_{1,WS}$ (Equation 9.3). However, a sufficient fitting is impossible in case of aggregation and an additional exponential term, describing the scattering of the new species must be added (Equation 9.4).

Equation 9.3

$$g_{1,Mix} = f_{NP}\, g_{1,NP} + f_{WS}\, g_{1,WS}$$

Equation 9.4

$$g_{1,Mix} = f_{NP}\, g_{1,NP} + f_{WS}\, g_{1,WS} + f_{Agg}\, g_{1,Agg}$$

Almost all nanocarrier dispersions remained stable after incubation in the wood extract. Despite the varying compositions for grapevine, apple, and peach, only marginal changes regarding the size distribution of each dispersion were observed. We therefore assume that these nanocarriers also remain colloidally stable inside of a plant and can be distributed through the vascular plant tissue. The only exception was CTMA-Cl stabilized PS-particles, which agglomerated and formed macroscopic aggregates due to shielding of CTMA's positive charges by anionic solutes from the wood sap. If the aggregates get larger than the micrometer-sized channels of the vascular tissue the transport might be hindered and a depot could be formed.

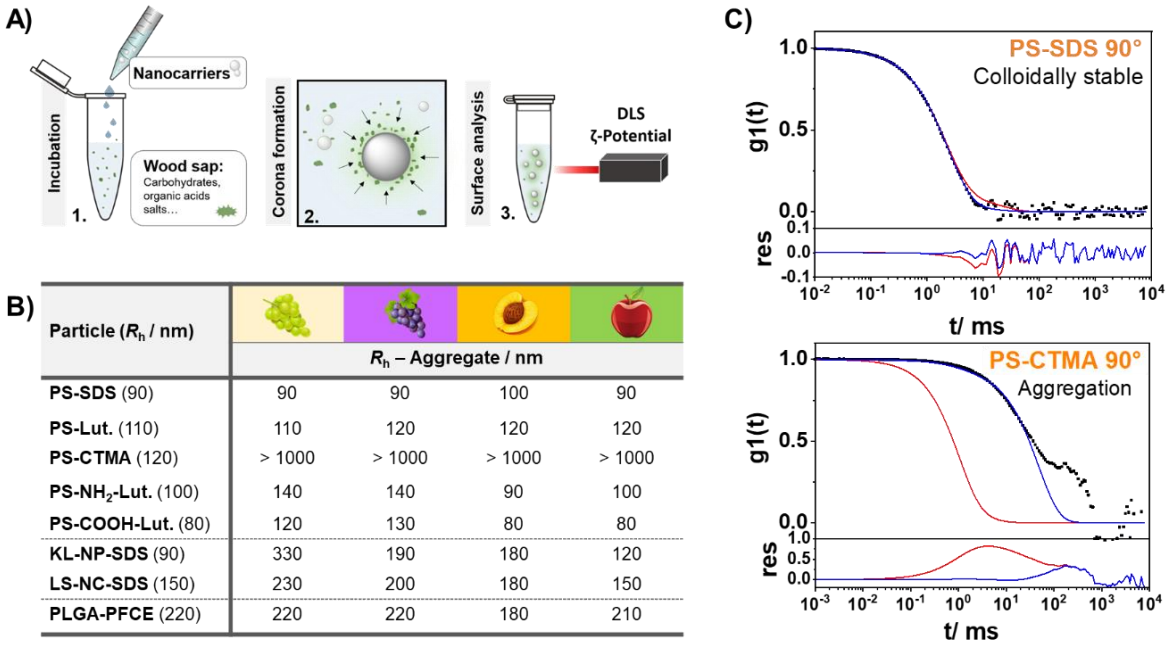

B)

Particle (R_h / nm)	R_h – Aggregate / nm			
PS-SDS (90)	90	90	100	90
PS-Lut. (110)	110	120	120	120
PS-CTMA (120)	> 1000	> 1000	> 1000	> 1000
PS-NH_2-Lut. (100)	140	140	90	100
PS-COOH-Lut. (80)	120	130	80	80
KL-NP-SDS (90)	330	190	180	120
LS-NC-SDS (150)	230	200	180	150
PLGA-PFCE (220)	220	220	180	210

Figure 9.5: Colloidal stability of nanocarriers in wood saps. A) Procedure to investigate interactions of wood saps and nanocarriers. B) Colloidal stability of nanocarriers after 24 h incubation in different wood saps mimicking the *in planta* conditions, measured by dynamic light scattering (DLS). C) Two examples showing the autocorrelation function of colloidally stable nanocarriers (PS-SDS) and the formation of aggregates after incubation in 'Riesling' sap (PS-CTMA).

***In planta* bio-distribution**

The transpiration stream generated by the evaporation of water over the leaf surface enables the plant to transport water and nutrients through the vascular tissue in the trunk. To understand if this mechanism can be used for the distribution of nanocarriers *in planta*, we monitored the transport of labeled nanocarriers either by inductively coupled plasma emission spectroscopy (ICP-OES) or by ^{19}F magnetic resonance imaging (MRI):

1. Elemental analysis by ICP-OES. The bio-distribution of a systematic library of ruthenium-loaded PS model nanocarriers and biodegradable lignin nanocarriers in grapevine cuttings (*Vitis vinifera* cv. 'Riesling'; length: 4 cm, diameter: 0.8 cm) was studied by elemental analysis. PS model nanocarriers allowed a systematically variation of surfactant, surface charge, and diameter, while lignin nanocarriers represent a promising formulation for sustainable plant protection. During the miniemulsion polymerization, we loaded ruthenocene into the nanocarriers, which acted as an ICP-probe for the biodistribution. The plants were immersed into a nanocarrier dispersion and after seven days, the stem of each plant was cut into 1 cm long pieces (Figure 9.6A). Each piece of wood was dissolved in a mixture of hydrogen

peroxide and concentrated sulfuric acid (“piranha solution”) and the ruthenium amount was analyzed by ICP-OES.

The amount of the ruthenium correlated with the trunk height of each segment and yielded a nanocarrier-specific ruthenium transport profile: In all cases, the ruthenium content was high for segments located at lower parts of the trunk and decreased up to the leaves, where no or only trace amounts were detected. However, in almost all wooden segments ruthenium was detected, indicating a transport through the trunk. Surfactant, surface charge, or size influenced the transport kinetics only slightly. Figure 9.6B shows the transport profiles for PS nanocarriers, stabilized with nonionic, anionic, and cationic surfactants: CTMA-Cl stabilized nanocarriers exhibited the lowest transport of this series. This correlates with the formation of aggregates after the incubation in wood sap observed by DLS. Nanocarriers stabilized with the anionic SDS indicated slightly higher amounts of ruthenium in higher parts of the cutting, followed by the nonionic nanocarriers that exhibited the highest values for ruthenium. Very similar transport profiles were observed when nanocarriers without, or with positive or negative surface charges were analyzed (all stabilized by nonionic surfactant), indicating a slightly lower transport of ruthenium for ionically charged nanocarriers, compared to the nonionic analogs (Figure 9.6D). Likewise, the anionic lignin nanocarriers did not significantly differ from PS-based dispersion regarding their ruthenium distribution profile (SI: Figure 9.7), suggesting that various nanocarriers are applicable for drug delivery in plants. Moreover, we compared the bio-distribution of polystyrene nanocarriers (Ø 200 nm) prepared by the miniemulsion approach with polystyrene microcarriers (Ø 1500 nm) synthesized by a simple dispersion polymerization (Figure 9.6B). Although differing in size, for both carrier-types an almost identical ruthenium profile was detected, which correlated with microscopy images showing diameters of ca. 20 µm for the xylem vessels of the herein used test plants. We assume that controlled drug delivery inside of plants is possible when the drug delivery vehicle is significantly smaller than the diameter of the plant’s transport vessels and aggregation is avoided.

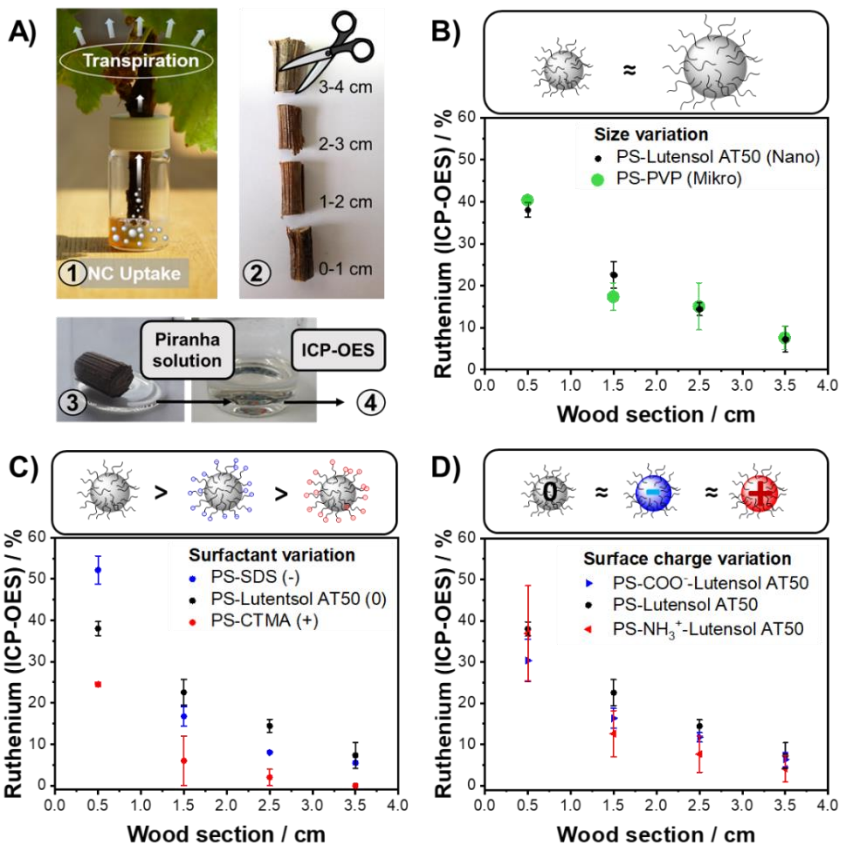

Figure 9.6: Uptake and transport of ruthenium-labeled nanocarriers through Riesling cuttings: A) Experimental setup to follow the transport: 1. Uptake and distribution for 7 days. 2. Cutting into four segments. 3. Dissolution in 'Piranha solution'. 4. Quantification of ruthenium. Distribution profile of ruthenium-labeled polystyrene nanocarriers monitored by ICP-OES depending on B) size, C) surfactant, D) surface charge.

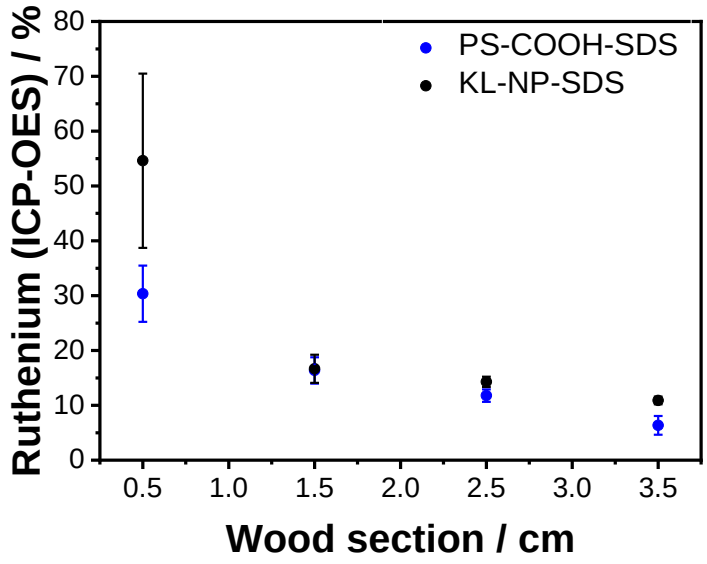

Figure 9.7: Distribution profile of ruthenium-labeled lignin nanocarriers (KL-NP-SDS) in comparison to polystyrene-based nanocarriers (PS-COOH-SDS) after uptake into the trunk of a Riesling cutting. The plants were immersed in a nanocarrier dispersion for 7 days. Ruthenium was quantified by ICP-OES.

Table 9.2: Ruthenium amounts quantified by ICP-OES in wood segments of 'Riesling' cuttings after uptake of ruthenocene-loaded polystyrene nanocarriers.

Sample ID	Plant segment:	1	2	3	4	Res. Disp.
PS-SDS-1	c(Ru-ICP)	1.55	0.46	0.26	0.16	0.75
	Ru%	48.74	14.47	8.18	5.03	23.58
PS-SDS-2	c(Ru-ICP)	1.69	0.58	0.24	0.18	0.35
	Ru%	55.59	19.08	7.89	5.92	11.51
	Average	**52**	**17**	**8**	**5**	**18**
	Error	**3.42**	**2.31**	**0.14**	**0.44**	**6.04**
PS-Lut-1	c(Ru-ICP)	0.98	0.68	0.38	0.15	0.52
	Ru%	36.16	25.09	14.02	5.54	19.19
PS-Lut-2	c(Ru-ICP)	1.00	0.65	0.44	0.31	0.26
	Ru%	37.59	24.44	16.54	11.65	9.77
PS-Lut-3	c(Ru-ICP)	1.20	0.54	0.38	0.14	0.72
	Ru%	40.27	18.12	12.75	4.70	24.16
	Average	**38**	**23**	**14**	**7**	**18**
	Error	**1.70**	**3.14**	**1.57**	**3.10**	**5.97**
PS-CTMA-1	c(Ru-ICP)	0.05	0.00	0.00	0.00	0.15
	Ru%	25.00	0.00	0.00	0.00	75.00
PS-CTMA-2	c(Ru-ICP)	0.06	0.03	0.01	0.00	0.15
	Ru%	24.00	12.00	4.00	0.00	60.00
	Average	**25**	**6**	**2**	**0**	**68**
	Error	**0.50**	**6.00**	**2.00**	**0.00**	**7.50**
PS-COOH-1	c(Ru-ICP)	0.56	0.36	0.25	0.10	1.14
	Ru%	23.24	14.94	10.37	4.15	47.30
PS-COOH-2	c(Ru-ICP)	0.75	0.33	0.27	0.15	0.79
	Ru%	32.75	14.41	11.79	6.55	34.50
PS-COOH-3	c(Ru-ICP)	0.80	0.45	0.30	0.19	0.54
	Ru%	35.09	19.74	13.16	8.33	23.68
	Average	**30**	**16**	**12**	**6**	**35**
	Error	**5.13**	**2.40**	**1.14**	**1.71**	**9.65**
PS-NH2-1	c(Ru-ICP)	0.95	0.30	0.17	0.07	0.42
	Ru%	49.74	15.71	8.90	3.66	21.99
PS-NH2-2	c(Ru-ICP)	0.50	0.11	0.04	0.01	1.63
	Ru%	21.83	4.80	1.75	0.44	71.18
PS-NH2-3	c(Ru-ICP)	0.86	0.38	0.27	0.18	0.47
	Ru%	39.81	17.59	12.50	8.33	21.76
	Average	**37**	**13**	**8**	**4**	**38**
	Error	**11.55**	**5.64**	**4.47**	**3.24**	**23.24**
PS-Mikro-1	c(Ru-ICP)	0.08	0.04	0.04	0.02	0.02
	Ru%	41.03	20.51	20.51	10.26	7.69
PS-Mikro-2	c(Ru-ICP)	0.17	0.06	0.04	0.02	0.14
	Ru%	39.53	13.95	9.30	4.65	32.56
	Average	**40**	**17**	**15**	**7**	**20**
	Error	**0.75**	**3.28**	**5.61**	**2.80**	**12.43**

2. Imaging by ^{19}F MRI. To visualize the transport of the nanocarriers through the vascular tissue of grapevine cuttings, we utilized perfluoro-15-crown-5-ether (PFCE) loaded PLGA nanocarriers, which were traced by ^{19}F MRI. The fluoride-containing cargo acts as a contrast agent and allows a specific and quantitative localization by ^{19}F MRI, as plant tissue is almost free of fluoride.[193] According to SEM and DLS, the morphology of the nanocarriers does not change in acidic 'Riesling' wood sap (pH of 5.4), which proves the stability of the PLGA-matrix against hydrolysis under these conditions. Grapevine shoots were immersed into dispersions of PFCE-loaded PLGA nanocarriers (*Vitis vinifera* cv. 'Riesling'; length: 4 cm, diameter: 0.8 cm; as shown in Figure 9.6A) or a nanocarrier dispersion was injected with a syringe into the trunk of potted grapevine plants (*Vitis vinifera* cv. 'Riesling'; length: 25 - 30 cm, diameter: 0.8 – 1.0 cm; Figure 9.9B). The transport of the nanocarriers was visualized after 2, 7, and 30 days:

Figure 9.8: *Vitis vinifera* cv. 'Riesling' plants used for *in planta* studies. Into the plants on the left the nanocarriers were injected, while the grapevine cuttings on the right were immersed into a nanocarrier dispersion

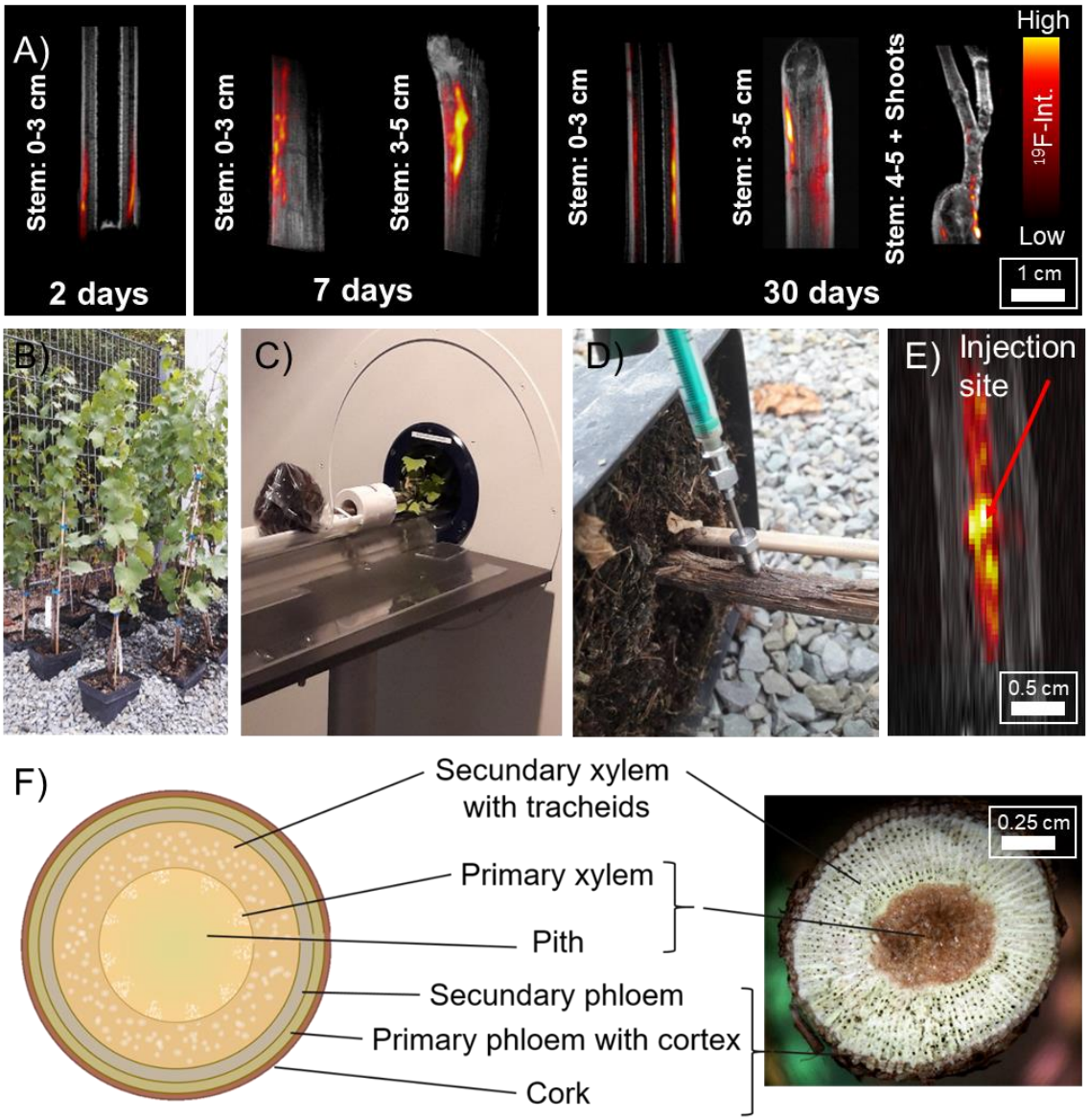

Figure 9.9: A) ^{19}F-^{1}H overlay MRI images of grapevine cuttings 2, 7, and 30 days after uptake of perfluoro-15-crown-5-ether (PFCE) loaded PLGA nanocarriers via the transpiration stream. For uptake, the cuttings were immersed in nanocarriers dispersion as shown in Figure 9.6A. PFCE allows the localization of the nanocarriers within the plant. The concentration of fluoride is shown in yellow (high), red (low), black/grey (none). B) Potted 'Riesling' test plants. C) grapevine test plant in MRI. (D) Injection of a concentrated nanocarrier dispersion into the trunk of a potted grapevine test plant. (E) ^{19}F-^{1}H overlay MRI image showing the injection profile after an injection of 0.2 µL of a 10 wt% PFCE-PLGA dispersion via syringe. No further transport was observed 7 days after the treatment. (F) Schematic illustration and photo of a cross-section of a grapevine shoot used to study the nanocarrier uptake.

When immersing the Riesling cuttings into a PFCE-loaded nanocarrier dispersion, a high ^{19}F resonance signal was detected especially in tissue with strong sapflow (trunk side from which the leaf was grown). This signal was located mainly between bark and pith, which suggests that xylem transport was used as a primary distribution mechanism. After two days, a ^{19}F MRI signal was detected at a trunk height of 1.5 cm proving translocation of the

nanocarriers (Figure 9.9A, left image). 5 days later, a strong ^{19}F MRI resonance signal was detectable in the complete shoot (Figure 9.9A, middle image), which extended after 30 days also to the fine stems of the leaves, proving a fast distribution of the nanocarriers inside of the cutting (Figure 9.9A, right image). In correlation with the results obtained from ICP-OES analysis, no fluoride signal was detected in the leaves. We assume that the nanocarriers remain in wooden trunk tissue.

When the nanocarrier dispersion was injected into a trunk of potted Riesling plants, an intense ^{19}F MRI signal was detected in the pith (Figure 9.9D). The signal reached ca. 4 cm above and 6 cm below the point of injection showing that the nanocarriers were pressed through plant tissue. After a week, the fluoride distribution profile showed a slight increase of fluoride at higher parts of the plant, but the major signal remained at the point of the injection, which most likely is due to the weaker sapflow in the pith (Figure 9.9E, Figure 9.10).

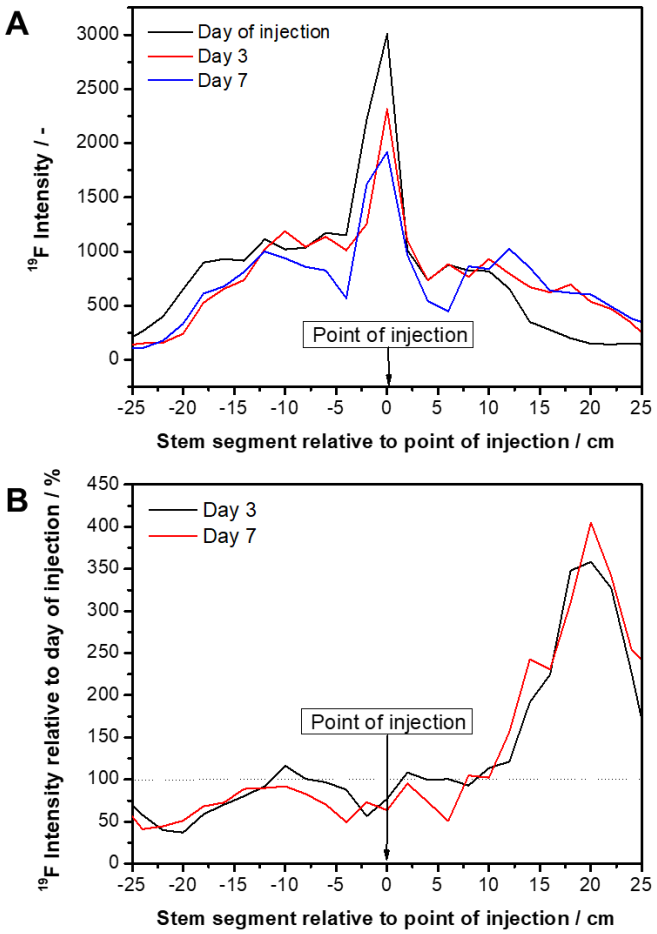

Figure 9.10: Distribution profile of PFCE-loaded nanocarriers in the trunk of potted Riesling plants after injection with a syringe**.** A) ^{19}F Intensity relative to point of injection after 0 and 3 days and after a week. B) ^{19}F Intensity related to intensity measured directly after injection (day 0). A slight movement of upwards the stem was observed.

9.5 Conclusion

This work presents the first investigation of the stability and the transport of polymeric nanocarriers in plants: wood saps proved to be suitable to simulate real *in planta* conditions. Most investigated nanocarriers did not aggregate significantly when incubated in the extracts of grapevine, apple, or peach and might be suitable as drug delivery vehicles in plants. To visualize the transport in living plants, we used Riesling cuttings or young potted Riesling plants. We developed two techniques based on elemental mapping (by ICP-OES) or imaging (by ^{19}F MRI). Chemical composition, size, surface charge, or surfactant of the nanocarriers were varied systematically and in all cases, transport through the vascular tissue of our test plants was detected. The surface charges seemed to play a minor role in transport efficiency when Riesling cuttings were incubated in nanocarrier dispersions. Injection in potted Riesling plants was slower, compared to incubation of cuttings directly in nanocarrier dispersions but effective transport of nanocarriers was visualized in both cases. To conclude, polymeric nano- and microcarriers are a versatile strategy to develop targeted drug delivery inside of plants and will allow the development of sustainable delivery of agrochemicals in the future.

.

10 Conclusion

Nanocarrier-mediated drug delivery is a powerful tool not only in medicine but also in agriculture. Enzyme-responsive lignin nanocarriers were designed that release an encapsulated fungicide only in presence of lignolytic fungi associated to the grapevine trunk disease Esca. As a carrier material, methacrylated Kraft lignin was used which can be produced safely and cost-efficient on a large-scale. A single injection of a lignin nanocarrier dispersion into the trunk of Esca-infected grapevine plants was applied successfully as curative treatment using only a minimal pesticide dose. We are therefore convinced that targeted drug delivery by nanocarrier injections should be further established in plant protection and can contribute to the reduction of environmental effects from the pollution of agrochemicals.

The methacrylation of lignin is not limited to Kraft lignin but can be extended to Organosolv lignin and lignin sulfonates. However, the functionalized lignins differ strongly in their chemical properties such as solubility. Hence, exchange within the nanocarrier production process is not possible, without adjusting the preparation protocol. Therefore, in the case of the hydrophilic lignin sulfonate, the crosslinking was performed at the droplet interface instead of inside the oil droplets as done with methacrylated Kraft lignin.

Hydrophilic drugs can be encapsulated by interfacial polymerization of toluene diisocyanate with lignin sulfonate in an inverse miniemulsion. This approach was found very robust and enabled the preparation of nanocarriers from Organosolv lignin, which was extracted from spent mushroom substrate, and from xylan extracted from corncobs. The Challenge of both materials is their structural heterogeneity depending on the biomass origin. An alternative strategy is the application of synthetic monomers based on the lignin substructures β-O-4-aryl ether and phenylcoumaran. Both might combine degradability with constant chemical properties and act as “breaking points” when incorporated in the polyurethane shell of a nanocarrier.

The nanocarriers developed in this thesis might be useful as eco-friendly formulations for targeted drug delivery of pesticides in agriculture. To overcome the biological size barriers of the plant, the nanocarriers should be injected directly into the vascular tissue of the trunk. Inside the plant, solutes (e.g. carbohydrate) of the wood sap adsorb on the nanocarrier surface. Nevertheless, most nanocarriers remain colloidally stable and distribute via the xylem tissue of the plant.

Hence, this thesis proves the great potential of nanotechnology to increase sustainability in agriculture. Especially the miniemulsion approach revealed itself as a versatile tool to prepare lignocellulose-based nanocarrier dispersions. Although the technique shows many advantages, it has been not established for the preparation of formulations in plant

protection yet. Therefore, the testing of less elaborated methods e.g. in macroemulsion might be of interest. The nanomaterials were produced from “green” resources like lignin or hemicellulose, which are still mostly considered as low-value side products of paper industry or agriculture due to their structural complexity. With progress in biomass processing and analytics, these waste streams offer promisingrenewable alternatives to replace petroleum-based feedstock being not in concurrence with food production. Next to different preparation methods, we could show that nanocarriers can be applied as a curative, protective and efficient treatment against Esca and demonstrated first results revealing the fate after injection into the trunk of grapevines. However, the biology of plants and pests is complex and the interaction with nanomaterials still not investigated in detail. For optimal performance, further understanding especially of the pathogen-induced nanocarrier degradation as well as the long-term fate inside the plant and in the environment is necessary. We are convinced that this thesis is a first step into a bright future of controlled drug delivery in plant protection and that the concept can be extended to many plants and pathogens.

References

1. Fenner, K.; Canonica, S.; Wackett, L. P.; Elsner, M., Evaluating Pesticide Degradation in the Environment: Blind Spots and Emerging Opportunities. *Science* **2013,** *341*, 752-758.
2. ECHA https://echa.europa.eu/de/registry-of-restriction-intentions/-/dislist/details/0b0236e18244cd73 (accessed 29.02.2020).
3. Yusoff, S. N. M.; Kamari, A.; Aljafree, N. F. A., A review of materials used as carrier agents in pesticide formulations. *Int. J. Environ. Sci. Technol.* **2016,** *13*, 2977–2994.
4. ALCA https://www.azlca.com/uploads/documents/corechpt4_pesticideformulations1.pdf (accessed 21.06.2020).
5. Wicki, A.; Witzigmann, D.; Balasubramanian, V.; Huwyler, J., Nanomedicine in cancer therapy: Challenges, opportunities, and clinical applications., J. Control. Release **2015,** *200*, 138-157.
6. Wang, P.; Lombi, E.; Zhao, F. J.; Kopittke, P. M., Nanotechnology: A New Opportunity in Plant Sciences. *Trends Plant Sci.* **2016,** *21*, 699-712.
7. Yiamsawas, D.; Beckers, S. J.; Lu, H.; Landfester, K.; Wurm, F. R., Morphology-Controlled Synthesis of Lignin Nanocarriers for Drug Delivery and Carbon Materials. ACS Biomater. Sci. Eng. **2017,** *3*, 2375-2383.
8. Frederik Wurm, K. L., Doungporn Yiamsawas, Eckhard Thines, Jochen Fischer Lignin biomaterial as agricultural drug carrier, WO2017134308A1, 2017.
9. Yiamsawas, D.; Baier, G.; Thines, E.; Landfester, K.; Wurm, F. R., Biodegradable lignin nanocontainers. *RSC Adv.* **2014,** *4* (23), 11661.
10. Delidovich, I.; Hausoul, P. J. C.; Deng, L.; Pfützenreuter, R.; Rose, M.; Palkovits, R., Alternative Monomers Based on Lignocellulose and Their Use for Polymer Production. *Chemical Reviews* **2016,** *116*, 1540-1599.
11. Lauth G. J., Kowalczyk J., Einführung in die Physik und Chemie der Grenzflächen und Kolloide. Springer-Verlag: Berlin Heidelberg, 2016.
12. Sharma, M. K.; Shah, D. O., Introduction to Macro- and Microemulsions. In *Macro- and Microemulsions*, American Chemical Society: 1985; Vol. 272, pp 1-18.
13. Schubert, H., Einführung in die Emulgiertechnik. In *Emulgiertechnik: Grundlagen, Verahren und Anwendungen*, Behr's Verlag: Hamburg, 2012; Vol. 1, pp 1-15.
14. B. Freudig, S. T., Tropfenzerkleinerung in Hochdruckhomogenisatoren. In *Emulgiertechnik: Grundlagen, Verfahren und Anwendungen*, Behr's Verlag: Hamburg, 2012; Vol. 1, pp 343-366.
15. Microfluidics http://de.microfluidicscorp.com/microfluidizer%C2%AE-prozessoren/labormaschinen/lm10/ (accessed 29.02.2020).
16. Behrend, O., Emulgieren mit Ultraschall. In *Emulgiertechnik: Grundlagen, Verfahren und Anwendungen*, Behr's Verlag: Hamburg; 2012; Vol. 1, pp 299-339.
17. Timmermann, F., Emulgatoren: Aufbau und Wirkungsweise. In *Emugliertechnik: Grundlagen, Verfahren und Anwendungen,* Behr's Verlag: Hamburg, 2012; Vol. 1, pp 19-42.
18. BASF https://www.homecare-and-i-and-i.basf.com/products/products-detail/Lutensol-AT%2050%20Powder/30043970 (accessed 29.02.2020).
19. Butt H.-J., Kappel M., *Surface and Interfacial Forces*, Wiley-VCH: Weinheim, 2010; Vol. 1.
20. Pohl, M., Grenzflächeneigenschaften. In *Emulgiertechnik: Grundlagen, Verfahren und Anwendungen*, Verlag, B. s., Ed. Hamburg, 2012.
21. Danner, T., Grundlagen der Tropfenkoaleszenz. In *Emulgiertechnik: Grundlagen, Verfahren und Anwendungen*, Behr's Verlag: Hamburg, 2012; Vol. 1, pp 233-245.
22. Schubert, H., Physikalisch-chemische Grundlagen der Stabilität von O/W-Emulsion. In *Emulgiertechnik: Grundlagen, Verfahren und Anwendungen*, Behr's Verlag: Hamburg, 2012; Vol. 1, pp 207-230.

23. Landfester, K., Synthesis of colloidal particles in miniemulsion. *Annual Review of Materials Research* **2006,** *36*, 231-279.
24. Antonietti, M.; Landfester, K., Polyreactions in miniemulsions. *Prog. Polym. Sci.* **2002,** *27*, 689-757.
25. Landfester, K., Anwendungen von Miniemulsion. In *Emulgiertechnik: Grundlagen, Verfahren und Andwendungen*, Behr's Verlag: Hamburg, 2012; Vol. 1, pp 667-685.
26. Landfester, K., Miniemulsions for Nanoparticle Synthesis. *Top Curr Chem* **2003,** *227*, 75-123.
27. Rinaldi, R.; Jastrzebski, R.; Clough, M. T.; Ralph, J.; Kennema, M.; Bruijnincx, P. C. A.; Weckhuysen, B. M., Wege zur Verwertung von Lignin: Fortschritte in der Biotechnik, der Bioraffination und der Katalyse. *Angew. Chem..* **2016,** *128*, 8296-8354.
28. Behr, A.; Seidensticker, T., Der "Holzstoff". In *Einführung in die Chemie nachwachsender Rohstoffe*, Springer-Verlag: Berlin, Heidelberg, 2018. Vol. 1, pp 201-216.
29. Schutyser, W.; Renders, T.; Van den Bosch, S.; Koelewijn, S. F.; Beckham, G. T.; Sels, B. F., Chemicals from lignin: an interplay of lignocellulose fractionation, depolymerisation, and upgrading. *Chem. Soc. Rev.* **2018,** *47*, 852-908.
30. McCarthy, J. L.; Islam, A., Lignin Chemistry, Technology, and Utilization: A Brief History. In *Lignin: Historical, Biological, and Materials Perspectives*, American Chemical Society: 1999; Vol. 742, pp 2-99.
31. Yuan, T.-Q.; Sun, S.-N.; Xu, F.; Sun, R.-C., Characterization of Lignin Structures and Lignin–Carbohydrate Complex (LCC) Linkages by Quantitative 13C and 2D HSQC NMR Spectroscopy. *J. Agric. Food Chem*., **2011,** *59*, 10604-10614.
32. Marjamaa, K.; Kukkola, E. M.; Fagerstedt, K. V., The role of xylem class III peroxidases in lignification. *J. Exp. Bot.* **2009,** *60*, 367-76.
33. Tao, J.; Li, S.; Ye, F.; Zhou, Y.; Lei, L.; Zhao, G., Lignin – An underutilized, renewable and valuable material for food industry. *Critical Reviews in Food Science and Nutrition* **2019**, 1-23.
34. Tribot, A.; Amer, G.; Abdou Alio, M.; de Baynast, H.; Delattre, C.; Pons, A.; Mathias, J.-D.; Callois, J.-M.; Vial, C.; Michaud, P.; Dussap, C.-G., Wood-lignin: Supply, extraction processes and use as bio-based material. *Eur. Polym. J*.. **2019,** *112*, 228-240.
35. Kai, D.; Tan, M. J.; Chee, P. L.; Chua, Y. K.; Yap, Y. L.; Loh, X. J., Towards lignin-based functional materials in a sustainable world. *Green Chem.* **2016,** *18*, 1175-1200.
36. Bugg, T. D. H.; Ahmad, M.; Hardiman, E. M.; Rahmanpour, R., Pathways for degradation of lignin in bacteria and fungi. *Nat. Prod. Rep.* **2011,** *28*, 1883-1896.
37. Pollegioni, L.; Tonin, F.; Rosini, E., Lignin-degrading enzymes. *The FEBS Journal* **2015,** *282*, 1190-1213.
38. Christopher, L. P.; Yao, B.; Ji, Y., Lignin Biodegradation with Laccase-Mediator Systems. *Frontiers in Energy Research* **2014,** *2, 1-13*.
39. Zerva, A.; Simić, S.; Topakas, E.; Nikodinovic-Runic, J., Applications of Microbial Laccases: Patent Review of the Past Decade (2009–2019). *Catalysts* **2019,** *9*, 1-25.
40. Higuchi, T., Microbial degradation of lignin: Role of lignin peroxidase, manganese peroxidase, and laccase. *Proc. Jpn. Acad. B Phys. Biol. Sci.,* **2004,** *80*, 204-214.
41. Munk, L.; Sitarz, A. K.; Kalyani, D. C.; Mikkelsen, J. D.; Meyer, A. S., Can laccases catalyze bond cleavage in lignin? *Biotechnology Advances* **2015,** *33*, 13-24.
42. Chen, Y. R.; Sarkanen, S.; Wang, Y. Y., Lignin-degrading enzyme activities. *Methods Mol Biol* **2012,** *908*, 251-68.
43. Calvo-Flores, F. G.; Dobado, J. A., Lignin as renewable raw material. *ChemSusChem* **2010,** *3*, 1227-1235.
44. Ren, T.; Qi, W.; Su, R.; He, Z., Promising Techniques for Depolymerization of Lignin into Value-added Chemicals. *ChemCatChem* **2019,** *11*, 639-654.
45. Beisl, S.; Miltner, A.; Friedl, A., Lignin from Micro- to Nanosize: Production Methods. *Int. J. Mol. Sci.* **2017,** *18*, 31.

46. Tian, D.; Hu, J.; Chandra, R. P.; Saddler, J. N.; Lu, C., Valorizing Recalcitrant Cellulolytic Enzyme Lignin via Lignin Nanoparticles Fabrication in an Integrated Biorefinery. *ACS Sustain. Chem. Eng.* **2017,** *5*, 2702-2710.
47. Frangville, C.; Rutkevičius, M.; Richter, A. P.; Velev, O. D.; Stoyanov, S. D.; Paunov, V. N., Fabrication of Environmentally Biodegradable Lignin Nanoparticles. *ChemPhysChem* **2012,** *13*, 4235-4243.
48. Ago, M.; Huan, S.; Borghei, M.; Raula, J.; Kauppinen, E. I.; Rojas, O. J., High-Throughput Synthesis of Lignin Particles (~30 nm to ~2 μm) via Aerosol Flow Reactor: Size Fractionation and Utilization in Pickering Emulsions. *ACS Appl. Mater. Interfaces* **2016,** *8*, 23302-23310.
49. Chen, N.; Dempere, L. A.; Tong, Z., Synthesis of pH-Responsive Lignin-Based Nanocapsules for Controlled Release of Hydrophobic Molecules. *ACS Sustain. Chem. Eng.* **2016,** *4*, 5204-5211.
50. Sanzari, I.; Leone, A.; Ambrosone, A., Nanotechnology in Plant Science: To Make a Long Story Short. *Front. Bioeng. Biotech.* **2019,** *7, 1-12*.
51. Prasad, R.; Bhattacharyya, A.; Nguyen, Q. D., Nanotechnology in Sustainable Agriculture: Recent Developments, Challenges, and Perspectives. *Front. Microbiol.* **2017,** *8*, 13.
52. Kim, S. W.; Jung, J. H.; Lamsal, K.; Kim, Y. S.; Min, J. S.; Lee, Y. S., Antifungal Effects of Silver Nanoparticles (AgNPs) against Various Plant Pathogenic Fungi. *Mycobiology* **2012,** *40*, 53-58.
53. Yamamoto, O., Influence of particle size on the antibacterial activity of zinc oxide. *International J.Inorg. Mater.* **2001,** *3*, 643-646.
54. Kah, M.; Hofmann, T., Nanopesticide research: Current trends and future priorities. *Environ. Int.* **2014,** *63*, 224-235.
55. Tong, Y.; Wu, Y.; Zhao, C.; Xu, Y.; Lu, J.; Xiang, S.; Zong, F.; Wu, X., Polymeric Nanoparticles as a Metolachlor Carrier: Water-Based Formulation for Hydrophobic Pesticides and Absorption by Plants. *J. Agric. Food Chem.* **2017,** *65*, 7371-7378.
56. Campos, E. V. R.; de Oliveira, J. L.; Fraceto, L. F.; Singh, B., Polysaccharides as safer release systems for agrochemicals. *Agron Sustain Dev*. **2015,** *35*, 47-66.
57. Behr, A.; Seidensticker, T., Der "Holzstoff". In *Einführung in die Chemie nachwachsender Rohstoffe*, Springer-Verlag: Berlin, Heidelberg, 2018. Vol. 1, pp 201-216.
58. Kashyap, P. L.; Xiang, X.; Heiden, P., Chitosan nanoparticle based delivery systems for sustainable agriculture. *Int. J. Biol. Macromol.* **2015,** *77*, 36-51.
59. Liang, W.; Yu, A.; Wang, G.; Zheng, F.; Jia, J.; Xu, H., Chitosan-based nanoparticles of avermectin to control pine wood nematodes. *Int. J. Biol. Macromol.* **2018,** *112*, 258-263.
60. Kumar, S.; Chauhan, N.; Gopal, M.; Kumar, R.; Dilbaghi, N., Development and evaluation of alginate–chitosan nanocapsules for controlled release of acetamiprid. *Int. J. Biol. Macromol.* **2015,** *81*, 631-637.
61. Fernández-Pérez, M.; González-Pradas, E.; Villafranca-Sánchez, M.; Flores-Céspedes, F., Mobility of isoproturon from an alginate–bentonite controlled release formulation in layered soil. *Chemosphere* **2000,** *41*, 1495-1501.
62. Guan, H.; Chi, D.; Yu, J.; Li, H., Encapsulated ecdysone by internal gelation of alginate microspheres for controlling its release and photostability. *Chem. Eng. J.* **2011,** *168*, 94-101.
63. Garrido, J.; Cagide, F.; Melle-Franco, M.; Borges, F.; Garrido, E. M., Microencapsulation of herbicide MCPA with native β-cyclodextrin and its methyl and hydroxypropyl derivatives: An experimental and theoretical investigation. *J. Mol.* **2014,** *1061*, 76-81.
64. Barik, T. K.; Sahu, B.; Swain, V., Nanosilica—from medicine to pest control. *Parasitol. Res.* **2008,** *103*, 253.
65. Chen, J.; Wang, W.; Xu, Y.; Zhang, X., Slow-Release Formulation of a New Biological Pesticide, Pyoluteorin, with Mesoporous Silica. *J. Agric. Food Chem*. **2011,** *59*, 307-311.

66. Li, Z.-Z.; Xu, S.-A.; Wen, L.-X.; Liu, F.; Liu, A.-Q.; Wang, Q.; Sun, H.-Y.; Yu, W.; Chen, J.-F., Controlled release of avermectin from porous hollow silica nanoparticles: Influence of shell thickness on loading efficiency, UV-shielding property and release. *J. Controlled Release* **2006,** *111*, 81-88.
67. Cao, L.; Zhang, H.; Cao, C.; Zhang, J.; Li, F.; Huang, Q., Quaternized Chitosan-Capped Mesoporous Silica Nanoparticles as Nanocarriers for Controlled Pesticide Release. *Nanomaterials* **2016,** *6*, 1-13.
68. Sipponen, M. H.; Lange, H.; Crestini, C.; Henn, A.; Österberg, M., Lignin for Nano- and Microscaled Carrier Systems: Applications, Trends, and Challenges. *ChemSusChem* **2019,** *12*, 2039-2054.
69. Su, Y.; Ashworth, V.; Kim, C.; Adeleye, A. S.; Rolshausen, P.; Roper, C.; White, J.; Jassby, D., Delivery, uptake, fate, and transport of engineered nanoparticles in plants: a critical review and data analysis. *Environ. Sci. Nano* **2019,** *6*, 2311-2331.
70. E.J. Jäger, S. N., E. Ohmann, *Botanik*. Spektrum Akademischer Verlag: Heidelberg, 2009; Vol. 5.
71. Stroock, A. D.; Pagay, V. V.; Zwieniecki, M. A.; Holbrook, N. M., The Physicochemical Hydrodynamics of Vascular Plants. *Annu. Rev. Fluid Mech.* **2014,** *46*, 615-642.
72. Keller, M., *The Science of Grapevines*; Academic Press: New York, 2010; Vol. 2.
73. Behzadi, S.; Serpooshan, V.; Tao, W.; Hamaly, M. A.; Alkawareek, M. Y.; Dreaden, E. C.; Brown, D.; Alkilany, A. M.; Farokhzad, O. C.; Mahmoudi, M., Cellular uptake of nanoparticles: journey inside the cell. *Chem. Soc. Rev.* **2017,** *46*, 4218-4244.
74. Sun, T.; Zhang, Y. S.; Pang, B.; Hyun, D. C.; Yang, M.; Xia, Y., Engineered Nanoparticles for Drug Delivery in Cancer Therapy. *Angew. Chem. Int. Ed.* **2014,** *53*, 12320-12364.
75. Peer, D.; Karp, J. M.; Hong, S.; Farokhzad, O. C.; Margalit, R.; Langer, R., Nanocarriers as an emerging platform for cancer therapy. *Nat. Nanotechnol* **2007,** *2*, 751.
76. Hu, Q.; Katti, P. S.; Gu, Z., Enzyme-responsive nanomaterials for controlled drug delivery. *Nanoscale* **2014,** *6*, 12273-12286.
77. Arias-Estévez, M.; López-Periago, E.; Martínez-Carballo, E.; Simal-Gándara, J.; Mejuto, J.-C.; García-Río, L., The mobility and degradation of pesticides in soils and the pollution of groundwater resources. *Agric. Ecosyst. Environ.* **2008,** *123*, 247-260.
78. Bertsch, C.; Ramírez-Suero, M.; Magnin-Robert, M.; Larignon, P.; Chong, J.; Abou-Mansour, E.; Spagnolo, A.; Clément, C.; Fontaine, F., Grapevine trunk diseases: complex and still poorly understood. *Plant Pathol.* **2013,** *62*, 243-265.
79. Graniti, A.; Surico, G.; Mugnai, L., Esca of Grapevine : A Disease Complex or a Complex of Diseases. *Phytopathol. Mediterr* **2006,** *39*, 16-20.
80. Chiarappa, L., Wood decay of the Grapevine and its relationship with black measles disease. *Phytopathology* **1959,** *49*, 510-519.
81. Mugnai, L.; Graniti, A.; Surico, G., Esca (Black measles) and brown wood-streaking: Two old and elusive diseases of grapevines. *Phytopathol. Mediterr* **1999,** *83*, 404-418.
82. Khan, A.; Eskalen, A.; Gubler, W. D., Rootstock Susceptibility to «Phaeomoniella chlamydospora» and «Phaeoacremonium» spp. *Phytopathol. Mediterr* **2001,** *40, 433-438*.
83. Piradashvili, K.; Alexandrino, E. M.; Wurm, F. R.; Landfester, K., Reactions and Polymerizations at the Liquid-Liquid Interface. *Chem. Rev.* **2016,** *116*, 2141-2169.
84. Balakshin, M.; Capanema, E., On the Quantification of Lignin Hydroxyl Groups With31P and13C NMR Spectroscopy. *J. Wood Chem. Technol.* **2015,** *35*, 220-237.
85. Rausch, K.; Reuter, A.; Fischer, K.; Schmidt, M., Evaluation of Nanoparticle Aggregation in Human Blood Serum. *Biomacromolecules* **2010,** *11*, 2836-2839.
86. Kettering, M.; Valdivia, C.; Sterner, O.; Anke, H.; Thines, E., Heptemerones A∼G, Seven Novel Diterpenoids from Coprinus heptemerus: Producing Organism, Fermentation, Isolation and Biological Activities. *J. Antibiot.* **2005,** *58*, 390-396.

87. Bruno, G.; Sparapano, L., Effects of three esca-associated fungi on Vitis vinifera L.: V. Changes in the chemical and biological profile of xylem sap from diseased cv. Sangiovese vines. *Physiol. Mol. Plant Pat.* **2007,** *71*, 210-229.
88. Gómez, P.; Báidez, A. G.; Ortuño, A.; Del Río, J. A., Grapevine xylem response to fungi involved in trunk diseases. *Ann. Appl. Biol.* **2016,** *169*, 116-124.
89. Grosman, D. M.; Clarke, S. R.; Upton, W. W., Efficacy of two systemic insecticides injected into loblolly pine for protection against southern pine bark beetles (Coleoptera: Curculionidae). *J. econ. entomol.* **2009,** *102*, 1062-1069.
90. Percival, G. C.; Boyle, S., Evaluation of microcapsule trunk injections for the control of apple scab and powdery mildew. *Ann. Appl. Biol.* **2005,** *147*, 119-127.
91. Úrbez-Torres, J. R.; Haag, P.; Bowen, P.; O'Gorman, D. T., Grapevine Trunk Diseases in British Columbia: Incidence and Characterization of the Fungal Pathogens Associated with Esca and Petri Diseases of Grapevine. *Plant Dis.* **2013,** *98*, 469-482.
92. Lorrain, B.; Pasquier, G.; Jourdes, M.; Dubrana, A.; Geny, L.; Rey, P.; Doneche, B.; Teissdere, P.-L., Effect of Esca disease on the phenolic and sensory attributes of Cabernet Sauvignon grapes, musts and wines. *Aust. J. Grape Wine Res.* **2012,** *18*, 64-72.
93. Murolo, S.; Romanazzi, G., Effects of grapevine cultivar, rootstock and clone on esca disease. *Australasian Plant Pathol.* **2014,** *43*, 215–221.
94. Lecomte, P., Darrieutort, G., Pieri, P., Rey, P., Fermaud, M., Esca en France : progression et causes probables. *Union Girondine des Vins de Bordeaux* **2013**, 34-38.
95. Mutawila, C.; Fourie, P. H.; Halleen, F.; Mostert, L., Histo-pathology study of the growth of <I>Trichoderma harzianum</I>, Phaeomoniella chlamydospora</I> and <I>Eutypa lata</I> on grapevine pruning wounds. *Phytopathol. Mediterr.* **2011,** *50*, 46-60.
96. DLR http://www.dlr.rlp.de/Internet/global/themen.nsf/Web_P_WB_Rebschutz_XP/0213F4E9F3596261C12580AC0056E34A/$FILE/Rebschutz%202017_03.pdf. (accessed 29.02.2020)
97. Angioni, A.; Dedola, F.; Garau, V. L.; Schirra, M.; Caboni, P., Fate of Iprovalicarb, Indoxacarb, and Boscalid Residues in Grapes and Wine by GC–ITMS Analysis. *J. Agric. Food Chem.* **2011,** *59*, 6806-6812.
98. Garcia-Cazorla, J.; Xirau-Vayreda, M., Persistence of Dicarboximidic Fungicide Residues in Grapes, Must, and Wine. *Am. J. Enol. Vitic.* **1994,** *45*, 338-340.
99. Taverna, M. E.; Busatto, C. A.; Lescano, M. R.; Nicolau, V. V.; Zalazar, C. S.; Meira, G. R.; Estenoz, D. A., Microparticles based on ionic and organosolv lignins for the controlled release of atrazine. *J. Hazardous* **2018,** *359*, 139-147.
100. Beckers, S. J.; Dallo, I. A.; del Campo, I.; Rosenauer, C.; Klein, K.; Wurm, F. R., From Compost to Colloids—Valorization of Spent Mushroom Substrate. *Sustain. Chem. Eng.* **2019,** *7*, 6991-6998.
101. Fischer, J.; Beckers, S. J.; Yiamsawas, D.; Thines, E.; Landfester, K.; Wurm, F. R., Targeted Drug Delivery in Plants: Enzyme-Responsive Lignin Nanocarriers for the Curative Treatment of the Worldwide Grapevine Trunk Disease Esca. *Adv. Sci. 0*, 1802315.
102. Hodásová Ľudmila, J. M., Škulcová Andrea, Ház Aleš, Lignin, potential products and their market value. *Wood Res.* **2015,** *60*, 973-986
103. BVL, Beistoffe in zugelassenen Pflanzenschutzmitteln. Lebensmittelsicherheit, B. f. V. u., Ed. 2018.
104. IFA http://gestis.itrust.de/nxt/gateway.dll/gestis_de/018390.xml?f=templates$fn=default.htm$3.0. (accessed 29.02.2020)
105. Reyes-Rivera, J.; Terrazas, T., Lignin Analysis by HPLC and FTIR. In *Methods Mol Biol*, **2017,** *1544*, 193-211.
106. Infochampi http://www.infochampi.eu/production-figures/. (accessed 11.3.2019).

107. Infochampi http://www.infochampi.eu/international-flows/fresh-mushroom-flows-country-list/eu28-fresh-mushroom-flows/. (accessed 11.03.2019).
108. Eurostat www.ec.europa.eu/eurostat/. (accessed 21.03.2017).
109. Lau, K. L.; Tsang, Y. Y.; Chiu, S. W., Use of spent mushroom compost to bioremediate PAH-contaminated samples. *Chemosphere* **2003,** *52*, 1539-1546.
110. Phan, C.-W.; Sabaratnam, V., Potential uses of spent mushroom substrate and its associated lignocellulosic enzymes. *Appl. Microbiol. Biotechnol.* **2012,** *96*, 863-873.
111. Jordan, S. N.; Mullen, G. J.; Murphy, M. C., Composition variability of spent mushroom compost in Ireland. *Bioresour. Technol.* **2008,** *99*, 411-418.
112. Hanafi, M.; Hafifah, F.; Rezania, S.; Mat Taib, S.; Md Din, M. F.; Yamauchi, M.; Sakamoto, M.; Hara, H.; Park, J.; Ebrahimi, S. S., Environmentally sustainable applications of agro-based spent mushroom substrate (SMS): an overview. *J. Mater. Cycles Waste Manage.* **2018,** *20*, 1383-1396.
113. Ko, H. G.; Park, S. H.; Kim, S. H.; Park, H. G.; Park, W. M., Detection and recovery of hydrolytic enzymes from spent compost of four mushroom species. *Folia Microbiol.* **2005,** *50*, 103-106.
114. Gadd, G. M., *Fungi in Bioremediation*. Cambridge University Press: Cambridge, 2001.
115. Zhu, H.; Sheng, K.; Yan, E.; Qiao, J.; Lv, F., Extraction, purification and antibacterial activities of a polysaccharide from spent mushroom substrate. *Int. J. Biol. Macromol.* **2012,** *50*, 840-843.
116. Balan, V.; da Costa Sousa, L.; Chundawat, S. P. S.; Vismeh, R.; Jones, A. D.; Dale, B. E., Mushroom spent straw: a potential substrate for an ethanol-based biorefinery. *J. Ind. Microbiol. Biotechnol.* **2008,** *35*, 293-301.
117. Zhu, Y.; Chang, Y.; Guan, J.; Shanguan, G.; Xin, F., Butanol production from organosolv treated spent mushroom substrate integrated with in situ biodiesel extraction. *Renewable Energy* **2016,** *96*, 656-661.
118. Kang, B.; Opatz, T.; Landfester, K.; Wurm, F. R., Carbohydrate nanocarriers in biomedical applications: functionalization and construction. *Chem. Soc. Rev.* **2015,** *44*, 8301-8325.
119. Karimi, K., *Lignocellulose-based Bioproducts*. Springer-Verlag: Cham, 2015; Vol. 1, pp 1-36.
120. Jin, Q.; Yang, L.; Poe, N.; Huang, H., Integrated processing of plant-derived waste to produce value-added products based on the biorefinery concept. *Trends Food Sci. Technol.* **2018,** *74*, 119-131.
121. Cheng, Y. S.; Zheng, Y.; Yu, C. W.; Dooley, T. M.; Jenkins, B. M.; VanderGheynst, J. S., Evaluation of high solids alkaline pretreatment of rice straw. *Appl. Biochem. Biotechnol.* **2010,** *162*, 1768-84.
122. Kim, I.; Rehman, M. S. U.; Han, J.-I., Enhanced glucose yield and structural characterization of corn stover by sodium carbonate pretreatment. *Bioresour. Technol.* **2014,** *152*, 316-320.
123. Kim, I.; Han, J.-I., Optimization of alkaline pretreatment conditions for enhancing glucose yield of rice straw by response surface methodology. *Biomass Bioenergy* **2012,** *46*, 210-217.
124. Mosier, N.; Wyman, C.; Dale, B.; Elander, R.; Lee, Y. Y.; Holtzapple, M.; Ladisch, M., Features of promising technologies for pretreatment of lignocellulosic biomass. *Bioresour. Technol.* **2005,** *96*, 673-686.
125. Lavarack, B. P.; Griffin, G. J.; Rodman, D., The acid hydrolysis of sugarcane bagasse hemicellulose to produce xylose, arabinose, glucose and other products. *Biomass Bioenerg.* **2002,** *23*, 367-380.
126. Saeman, J. F., Kinetics of Wood Saccharification - Hydrolysis of Cellulose and Decomposition of Sugars in Dilute Acid at High Temperature. *Ind. Eng. Chem.* **1945,** *37*, 43-52.
127. Chen, H., *Lignocellulose Biorefinery Engineering*. Elsevier Ltd.: Amsterdam, 2015.
128. Wan, C.; Zhou, Y.; Li, Y., Liquid hot water and alkaline pretreatment of soybean straw for improving cellulose digestibility. *Bioresour. Technol.* **2011,** *102*, 6254-6259.

129. Shuai, L.; Yang, Q.; Zhu, J. Y.; Lu, F. C.; Weimer, P. J.; Ralph, J.; Pan, X. J., Comparative study of SPORL and dilute-acid pretreatments of spruce for cellulosic ethanol production. *Bioresour. Technol.* **2010,** *101*, 3106-3114.
130. Lim, W.-S.; Lee, J.-W., Influence of pretreatment condition on the fermentable sugar production and enzymatic hydrolysis of dilute acid-pretreated mixed softwood. *Bioresour. Technol.* **2013,** *140*, 306-311.
131. Alvarez, C.; Reyes-Sosa, F. M.; Diez, B., Enzymatic hydrolysis of biomass from wood. *Microb. Biotechnol.* **2016,** *9*, 149-56.
132. Sarubbo L.A., L. J. M., Rufino R.D., Production of a Low-cost Biosurfactant for Application in the Remediation of Sea water Contaminated with Petroleum Derivates. *Mech. Chem. Eng. Trans.* **2016,** *49*, 523-528.
133. Sachdev, D. P.; Cameotra, S. S., Biosurfactants in agriculture. *Appl. Microbiol. Biotechnol.* **2013,** *97*, 1005-16.
134. Aveyard, R.; Binks, B. P.; Chen, J.; Esquena, J.; Fletcher, P. D. I.; Buscall, R.; Davies, S., Surface and Colloid Chemistry of Systems Containing Pure Sugar Surfactant. *Langmuir* **1998,** *14*, 4699-4709.
135. Crespy, D.; Landfester, K., Miniemulsion polymerization as a versatile tool for the synthesis of functionalized polymers. *Beilstein journal of organic chemistry* **2010,** *6*, 1132-1148.
136. Johansson, A.; Aaltonen, O.; Ylinen, P., Organosolv pulping — methods and pulp properties. *Biomass* **1987,** *13*, 45-65.
137. Kunduru, K. R.; Basu, A.; Haim Zada, M.; Domb, A. J., Castor Oil-Based Biodegradable Polyesters. *Biomacromolecules* **2015,** *16*, 2572-2587.
138. Brijwani, K.; Rigdon, A.; Vadlani, P. V., Fungal Laccases: Production, Function, and Applications in Food Processing. *Enzyme Res.* **2010,** *2010*, 1-10.
139. Naidu, D. S.; Hlangothi, S. P.; John, M. J., Bio-based products from xylan: A review. *Carbohydr. Polym.* **2018,** *179*, 28-41.
140. Deutschmann, R.; Dekker, R. F. H., From plant biomass to bio-based chemicals: Latest developments in xylan research. *Biotech. Adv.* **2012,** *30*, 1627-1640.
141. Mäkinen, K. K., The Rocky Road of Xylitol to its Clinical Application. *J. Dent. Res.* **2000,** *79*, 1352-1355.
142. Sharma, H. K.; Xu, C.; Qin, W., Biological Pretreatment of Lignocellulosic Biomass for Biofuels and Bioproducts: An Overview. *Waste and Biomass Valori.* **2017,** *10*, 235-251.
143. Smith, P. J.; Wang, H.-T.; York, W. S.; Peña, M. J.; Urbanowicz, B. R., Designer biomass for next-generation biorefineries: leveraging recent insights into xylan structure and biosynthesis. *Biotechnol. Biofuels* **2017,** *10*, 286.
144. Nuruzzaman, M.; Rahman, M. M.; Liu, Y.; Naidu, R., Nanoencapsulation, Nano-guard for Pesticides: A New Window for Safe Application. *J. Agric. Food Chem.* **2016,** *64*, 1447-1483.
145. Daus, S.; Heinze, T., Xylan-Based Nanoparticles: Prodrugs for Ibuprofen Release. *Macromol. Biosci.* **2010,** *10*, 211-220.
146. Cartaxo da Costa Urtiga, S.; Aquino Azevedo de Lucena Gabi, C.; Rodrigues de Araújo Eleamen, G.; Santos Souza, B.; Pessôa, H. d. L. F.; Marcelino, H. R.; Afonso de Moura Mendonça, E.; Egito, E. S. T. d.; Oliveira, E. E., Preparation and characterization of safe microparticles based on xylan. *Drug Dev. Ind. Pharm.* **2017,** *43*, 1601-1609.
147. Sauraj; Kumar, S. U.; Kumar, V.; Priyadarshi, R.; Gopinath, P.; Negi, Y. S., pH-responsive prodrug nanoparticles based on xylan-curcumin conjugate for the efficient delivery of curcumin in cancer therapy. *Carbohyd. Polym.* **2018,** *188*, 252-259.
148. Marcelino, H.; da Silva, A.; Gomes, M.; Oliveira, E.; Nagashima-Junior, T.; Pinheiro, G.; da Silva, A.; Timoteo, A.; Agnez-Lima, L.; Ayala, A.; Oliveira, A.; do Egito, E., Leads from Physical, Chemical, and Thermal Characterization on Cytotoxic Effects of Xylan-Based Microparticles. *Polymers* **2015,** *7*, 2304-2315.
149. Silva, A. E.; Oliveira, E. E.; Gomes, M. C. S.; Marcelino, H. R.; Silva, K. C. H.; Souza, B. S.; Nagashima, T.; Ayala, A. P.; Oliveira, A. G.; Egito, E. S. T. d.,

Producing xylan/Eudragit® S100-based microparticles by chemical and physico-mechanical approaches as carriers for 5-aminosalicylic acid. *J. Microencapsul.* **2013,** *30*, 787-795.
150. Chang, M.; Liu, X.; Meng, L.; Wang, X.; Ren, J., Xylan-Based Hydrogels as a Potential Carrier for Drug Delivery: Effect of Pore-Forming Agents. *Pharmaceutics* **2018,** *10, 1-13*.
151. Crespy, D.; Stark, M.; Hoffmann-Richter, C.; Ziener, U.; Landfester, K., Polymeric Nanoreactors for Hydrophilic Reagents Synthesized by Interfacial Polycondensation on Miniemulsion Droplets. *Macromolecules* **2007,** *40*, 3122-3135.
152. Schlaad, H.; Kukula, H.; Rudloff, J.; Below, I., Synthesis of α,ω-Heterobifunctional Poly(ethylene glycol)s by Metal-Free Anionic Ring-Opening Polymerization. *Macromolecules* **2001,** *34*, 4302-4304.
153. Krämer W.; Schimer, U.; Jeschke P.; Witschel M.; *Modern Crop Protection Compounds.* Wiley-VCH Verlag GmbH & Co. KGaA: Hamburg, 2011; Vol.3.
154. Haider, T. P.; Völker, C.; Kramm, J.; Landfester, K.; Wurm, F. R., Plastics of the Future? The Impact of Biodegradable Polymers on the Environment and on Society. *Angew. Chem. Int. Ed.* **2019,** *58*, 50-62.
155. Bugg, T. D. H.; Rahmanpour, R., Enzymatic conversion of lignin into renewable chemicals. *Curr. Opin. Chem. Biol.* **2015,** *29*, 10-17.
156. Vroman, I.; Tighzert, L., Biodegradable Polymers. *Materials* **2009,** *2*, 307-344.
157. Picart, P.; Domínguez de María, P.; Schallmey, A., From gene to biorefinery: microbial β-etherases as promising biocatalysts for lignin valorization. *Front. Microbiol.* **2015,** *6,* 1-8.
158. Reiter, J.; Strittmatter, H.; Wiemann, L. O.; Schieder, D.; Sieber, V., Enzymatic cleavage of lignin β-O-4 aryl ether bonds via net internal hydrogen transfer. *Green Chem.* **2013,** *15*, 1373-1381.
159. Nakatsubo, F.; Kirk, T. K.; Shimada, M.; Higuchi, T., Metabolism of a phenylcoumaran substructure lignin model compound in ligninolytic cultures of Phanerochaete chrysosporium. *Arch. Microbiol.* **1981,** *128*, 416-420.
160. Ohta, M.; Higuchi, T.; Iwahara, S., Microbial degradation of dehydrodiconiferyl alcohol, a lignin substructure model. *Arch. Microbiol.* **1979,** *121*, 23-28.
161. Lancefield, C. S.; Westwood, N. J., The synthesis and analysis of advanced lignin model polymers. *Green Chem.* **2015,** *17*, 4980-4990.
162. Forsythe, W. G.; Garrett, M. D.; Hardacre, C.; Nieuwenhuyzen, M.; Sheldrake, G. N., An efficient and flexible synthesis of model lignin oligomers. *Green Chem.* **2013,** *15*, 3031-3038.
163. Kishimoto, T.; Uraki, Y.; Ubukata, M., Easy synthesis of β-O-4 type lignin related polymers. *Org. Biomol. Chem.* **2005,** *3*, 1067-1073.
164. Kishimoto, T.; Uraki, Y.; Ubukata, M., Synthesis of β-O-4-type artificial lignin polymers and their analysis by NMR spectroscopy. *Org. Biomol. Chem.* **2008,** *6*, 2982-2987.
165. Marine, J.; Louis, H.; Samad, J. A.; Miguel, P.; Raphaël, M.; Marina, G.; Johnny, B.; Patrick, B.; Paul-Henri, D.; Florent, A., Syringaresinol: A Renewable and Safer Alternative to Bisphenol A for Epoxy-Amine Resins. *ChemSusChem* **2017,** *10*, 738-746.
166. Hollande, L.; Jaufurally, A. S.; Ducrot, P.-H.; Allais, F., ADMET polymerization of bio-based monomers deriving from syringaresinol. *RSC Adv.* **2016,** *6*, 44297-44304.
167. Sarkanen, K. V.; Wallis, A. F. A., Oxidative dimerizations of (E)- and (Z)-isoeugenol (2-methoxy-4-pro-penylphenol) and (E)- and (Z)-2,6-dimethoxy-4-propenylphenol. **J.** *Chem. Soc. Perkin Trans. I,* ***1973,*** *24,* 1869-1878.
168. Fache, M.; Boutevin, B.; Caillol, S., Vanillin Production from Lignin and Its Use as a Renewable Chemical. *ACS Sustain. Chem. Eng.* **2016,** *4*, 35-46.
169. Smith, A. M.; Gilbertson, L. M., Rational Ligand Design To Improve Agrochemical Delivery Efficiency and Advance Agriculture Sustainability. *ACS Sustain. Chem. Eng.* **2018,** *6*, 13599-13610.

170. Berger, C.; Laurent, F., Trunk injection of plant protection products to protect trees from pests and diseases. *Crop Prot.* **2019,** *124*, 104831.
171. Rowe, D. E.; Malone, S.; Yates, Q. L., Automated greenhouse spray system for i ncreased safety and flexibility. *Crop Science* **2000,** *40*, 1176-1179.
172. Janse J. D., Obradivic A., Xylella Fastidiosa its Biology, Diagnosis, control and risks *J. Plant Path.* **2010,** *92, 35-48*.
173. Malairajan, P.; Gopalakrishnan, G.; Narasimhan, S.; Veni, K. J. K.; Kavimani, S., Anti-ulcer activity of crude alcoholic extract of Toona ciliata Roemer (heart wood). *J. Ethnopharmacol.* **2007,** *110*, 348-351.
174. Grillo, R.; Pereira, A. E. S.; Nishisaka, C. S.; de Lima, R.; Oehlke, K.; Greiner, R.; Fraceto, L. F., Chitosan/tripolyphosphate nanoparticles loaded with paraquat herbicide: An environmentally safer alternative for weed control. *J. Hazard* **2014,** *278*, 163-171.
175. Patel, S.; Bajpai, J.; Saini, R.; Bajpai, A. K.; Acharya, S., Sustained release of pesticide (Cypermethrin) from nanocarriers: An effective technique for environmental and crop protection. *Process Saf. Environ.* **2018,** *117*, 315-325.
176. Meurer, R. A.; Kemper, S.; Knopp, S.; Eichert, T.; Jakob, F.; Goldbach, H. E.; Schwaneberg, U.; Pich, A., Biofunctional Microgel-Based Fertilizers for Controlled Foliar Delivery of Nutrients to Plants. *Angew. Chem. Int. Ed.* **2017,** *56*, 7380-7386.
177. Pérez-de-Luque, A., Interaction of Nanomaterials with Plants: What Do We Need for Real Applications in Agriculture? *Front. Environ. Sci.* **2017,** *5, 1-7*.
178. Kole, C.; Kumar, D. S.; Khodakovskaya, M. V., *Plant Nanotechnology - Principles and Practices, Springer-Verlag: Berlin Heidelberg*; 2016.
179. Nair, R.; Varghese, S. H.; Nair, B. G.; Maekawa, T.; Yoshida, Y.; Kumar, D. S., Nanoparticulate material delivery to plants. *Plant Sci.* **2010,** *179*, 154-163.
180. Rosell, J. A.; Olson, M. E.; Anfodillo, T., Scaling of Xylem Vessel Diameter with Plant Size: Causes, Predictions, and Outstanding Questions. *Curr. For. Rep.* **2017,** *3*, 46-59.
181. Makadia, H. K.; Siegel, S. J., Poly Lactic-co-Glycolic Acid (PLGA) as Biodegradable Controlled Drug Delivery Carrier. *Polymers* **2011,** *3*, 1377-1397.
182. Fredenberg, S.; Wahlgren, M.; Reslow, M.; Axelsson, A., The mechanisms of drug release in poly(lactic-co-glycolic acid)-based drug delivery systems—A review. *Int. J. Pharm.* **2011,** *415*, 34-52.
183. Holzapfel, V.; Musyanovych, A.; Landfester, K.; Lorenz, M. R.; Mailänder, V., Preparation of Fluorescent Carboxyl and Amino Functionalized Polystyrene Particles by Miniemulsion Polymerization as Markers for Cells. *Macromol. Chem. Phys.* **2005,** *206*, 2440-2449.
184. Mohr, K., Aggregation Behavior of Polystyrene-Nanoparticles in Human Blood Serum and its Impact on the in vivo Distribution in Mice. *J. Nanomed. Nanotechnol.* **2014,** *5,* 1-10.
185. Jinhua, L.; Guangyuan, Z., Polystyrene Microbeads by Dispersion Polymerization: Effect of Solvent on Particle Morphology. *Int. J. Poly. Sci.* **2014,** *2014*, 1-4.
186. Uhlenbrock, L.; Sixt, M.; Tegtmeier, M.; Schulz, H.; Hagels, H.; Ditz, R.; Strube, J., Natural Products Extraction of the Future—Sustainable Manufacturing Solutions for Societal Needs. *Processes* **2018,** *6* (10).
187. Halabalaki M.; Bertrand S.; Stefanou A.; Gindro K.; Kostidis S.; Micros, E.; Skaltsounis L. A.; Wolfender J.; Sample Preparation Issues in NMR-basedPlant Metabolomics: Optimisation forVitisWood Samples. *Phytochem. Anal.* **2014,** *25*, 350-356.
188. Loos, C.; Syrovets, T.; Musyanovych, A.; Mailander, V.; Landfester, K.; Nienhaus, G. U.; Simmet, T., Functionalized polystyrene nanoparticles as a platform for studying bio-nano interactions. *Beilstein J. Nanotechnol.* **2014,** *5*, 2403-12.
189. Fortunati, E.; Rescignano, N.; Botticella, E.; La Fiandra, D.; Renzi, M.; Mazzaglia, A.; Torre, L.; Kenny, J. M.; Balestra, G. M., Effect of poly(dl-lactide-co-glycolide) nanoparticles or cellulose nanocrystals-based formulations on Pseudomonas

syringae pv. tomato (Pst) and tomato plant development. *J. Plant Dis. Prot.* **2016,** *123* 301-310.
190. Liang, Z.; Xu, J.-P.; Meng, X.-L.; Lu, W.; Wang, J.; Xia, H., Improve bioavailability of Harpin protein on plant use PLGA based nanoparticle. *J. Biotechnol.* **2009,** *143*, 296-301.
191. Koshkina, O.; Lajoinie, G.; Baldelli Bombelli, F.; Swider, E.; Cruz, L. J.; White, P. B.; Schweins, R.; Dolen, Y.; van Dinther, E. A. W.; van Riessen, N. K.; Rogers, S. E.; Fokkink, R.; Voets, I. K.; van Eck, E. R. H.; Heerschap, A.; Versluis, M.; de Korte, C. L.; Figdor, C. G.; de Vries, I. J. M.; Srinivas, M., Multicore Liquid Perfluorocarbon-Loaded Multimodal Nanoparticles for Stable Ultrasound and 19F MRI Applied to In Vivo Cell Tracking. *Adv. Funct. Mate.* **2019,** *29*, 1806485.
192. Ulusoy, E.; Derman, S.; Erişen, S., The Cellular Uptake, Distribution and Toxicity of Poly (lactic-co-glycolic) Acid Nanoparticles in Medicago sativa Suspension Culture. *Rom. Biotechn. Let.* **2019**.
193. Baunthiyal, M.; Ranghar, S., Accumulation of Fluoride by Plants: Potential for Phytoremediation. *CLEAN – Soil Air Water* **2015,** *43,* 127-132.